Answers Research Journal 14 (2021): 303–415.
www.answersingenesis.org/arj/v14/bright_angel_tonto_group_grand_canyon.pdf

ARJ

The Petrology of the Bright Angel Formation, Tonto Group, Grand Canyon, Arizona

Andrew A. Snelling, Answers in Genesis, PO Box 510, Hebron, Kentucky, 41048.

Abstract

Investigation of the nature of the folding of the Cambrian Tonto Group strata in Grand Canyon necessitates first investigating the petrology of those strata. The Cambrian Bright Angel Formation is a 82–137 m (325–450 ft) thick slope-forming unit that recessively outcrops in the middle of the Tonto Group along ~500 km of the walls of Grand Canyon and beyond. Erosion of the underlying Precambrian basement rocks produced the Great Unconformity on which the Tonto Group was deposited as part of the fining upwards Sauk megasequence that blankets North America and other continents. The Bright Angel Formation consists of ~40% green, strongly laminated shales, ~30% crumbly and well-laminated siltstones, and ~30% sandstone beds. The latter are often hard and ledge-forming, some are conglomeratic, and most are variously cross-laminated, indicative of high-energy water transport. Trilobites, brachiopods, and other invertebrates, as well as shell fragment "hash" are found fossilized in the Bright Angel Formation, along with abundant tracks and traces left by trilobites and other invertebrates, and cryptospores of land plants and algae, but not marine algae. U-Pb dated detrital zircon grains from the underlying Tapeats Sandstone coupled with biostratigraphic trilobite faunal zones correlated globally have constrained the conventional age of the Bright Angel Formation to 502–507 Ma. Detrital zircon U-Pb ages from the formation identify the primary source of the sediments as the locally underlying Precambrian crystalline basement. The uniformitarian interpreted depositional environments for the Bright Angel Formation are intertidal to subtidal shallow-marine environments, yet it has been described as "one of the most dramatic global marine transgressions in Earth history." While quartz is dominant, K-feldspar content ranges from 11.0% to 46.9%, various carbonates are present up to 32.4% and illite is ubiquitous, indicative of glauconite and of the detrital muscovite flakes that are wedged between the other grains. The shales consist of alternating thin illite-dominated laminae interstratified with thin laminae of siltstone. Grains are angular to sub-rounded, and the fabric is cemented by silica as quartz overgrowths. The strongly cross-laminated sandstone beds and the laminated siltstones and shales are consistent with rapid deposition by high-energy storm-like surges, with spontaneous stratification of the heterogranular sediment mixture and of mud floccules. There is no evidence, macroscopic or microscopic, of any metamorphic changes to the detrital mineral grains or textures. Instead, the mineralogical content, textural features, sedimentary structures, continental-scale deposition, and even the tracks and traces of transitory invertebrates, all indicate rapid burial. Furthermore, all are consistent with the catastrophic erosion of the Great Unconformity near the initiation of the global Genesis Flood cataclysm only about 4350 years ago, and the subsequent hurricane- and tsunami-driven rapid short-distance transport and deposition of the Bright Angel Formation, likely in the first few days or weeks of that year-long event.

Keywords: Bright Angel Formation, Grand Canyon, Cambrian, Tonto Group, stratigraphy, fossils, sedimentary structures, U-Pb detrital zircon ages, provenance, depositional environment, quartz, K-feldspar, detrital muscovite, glauconite, silica cement, global Flood cataclysm

Introduction

The Cambrian Bright Angel Formation is a 82–137 m (325–450 ft) thick slope-forming unit that recessively outcrops in the middle of the Tonto Group, overlying the prominent cliff-forming Tapeats Sandstone, and near the base of the Paleozoic sequence of flat-lying sedimentary layers making up the walls of Grand Canyon for ~500 km through the Canyon and beyond. It consists of interbedded relatively thin alternating layers of fine-grained sandstone, siltstone and shale containing quartz with large amounts of K-feldspar and minor detrital muscovite, both eroded from the underlying Precambrian basement rocks, primarily granites and schists, and with frequently dominating glauconite, iron oxides and some carbonate minerals. Bedding is very well developed, the green shales being fissile, and the sandstone beds are sometimes variously cross-laminated and contain significant amount of brachiopod shell fragments. The Bright Angel Formation was deposited as part of the fining upwards Sauk megasequence that blankets North America and has been traced across other continents.

Many structures in sedimentary rock layers result from the primary depositional processes, such as graded bedding and cross-bedding (Boggs 1995). On the other hand, soft-sediment deformation structures or penecontemporaneous structures are so called because they develop at the time of deposition or shortly thereafter, during the early stages of the

sediment's consolidation and before full lithification. This is because the sediments need to be unsolidified or "liquid-like" for such deformation to occur (Boggs 1995).

However, other structures in sedimentary rocks are caused by deformation long after lithification and diagenesis have occurred. Rocks buried deep in the earth may be under sufficient prolonged confining pressures or stress and temperatures to deform plastically. In other words, incremental strain over a long period. This also is believed to be able to fold rock layers. These types of behavior are called ductile deformation. It is the ability of a rock to accumulate strain (folding) on a mesoscopic scale. Under the confining pressures and accompanying elevated temperatures, the rock grains may recrystallize and/or the minerals undergo metamorphism, some new minerals such as micas growing perpendicular to the stress to accommodate it. Hand and thin section analysis should be able to determine if rocks have experienced ductile deformation. The Paleozoic rocks, including the Bright Angel Formation of Grand Canyon most likely were not buried deep enough to experience ductile deformation as they were well above the brittle-ductile transition zone. Incremental strain over sustained periods of time is harder to differentiate. As noted above, it can also result in ductile deformation.

On the other hand, under some near surface conditions, rock layers may remain coherent because the grains and/or layers within them can facilitate the folding. This type of deformation is most common in near surface rocks and is a type of brittle deformation. Most near surface rock layers undergo brittle fracturing and faulting, leaving the rock's grains fractured. Some coherent units may slide past one another along bedding planes as the rocks are folded. This helps accommodate folding through flexural slip. Tell-tale signs of this should be thus clearly evident in outcrops and from microscope examination of the rock fabric and the sediment grains.

There are several prominent locations in the Grand Canyon where the Paleozoic sedimentary rock layers are folded, sometimes in conjunction with faulting. And there apparently are unresolved questions as to whether the folding represents soft-sediment deformation folding or later tectonic folding (ductile or brittle) after the whole strata sequence was deposited. In most instances the folding is usually claimed to be the result of ductile (plastic) behavior of the lithified sedimentary rocks under prolonged stress due to Late Mesozoic-Early Cenozoic deformation during the Laramide Orogeny, hundreds of millions of years after the whole Paleozoic strata sequence was deposited (Huntoon 2003; Karlstrom and Timmins 2012). However, the macroscopic fabric of the Cambrian Tonto Group sedimentary rock layers involved in these folds should be able to determine if the folding was instead due to soft-sediment deformation. Any soft-sediment deformation should have occurred soon after deposition of these sedimentary units in the Cambrian (499–508Ma) (Karlstrom et al. 2020), and well before the tectonic activity of the Laramide Orogeny in the terminal Mesozoic and earliest Cenozoic (60–70Ma). This poses an apparent dilemma that obviously needs resolving, and thus a focused study was designed to determine the timing and nature of this folding, beginning with a thorough investigation of the petrology of each of these rock units, and subsequent detailed examination of these rock units in folds.

One of the folds in question is the deformation of the Cambrian Tapeats Sandstone upwards into, and against the Butte Fault at the synclinal hinge of the East Kaibab Monocline in eastern Grand Canyon during the Laramide Orogeny (Huntoon 2003; Karlstrom and Timmins 2012). The best exposed fold along this system is in Carbon Canyon at river mile 65 (figs. 1 and 2). Hill and Moshier (2009) claim that evidence from field studies and rock deformation experiments demonstrate that these solid rocks behaved in a ductile manner as the sandstone strata were deformed slowly under great stress, and that the strata thus were "bent" by microscopic re-orientations of mineral grains and by changes in bedding thickness along the fold. They then reference Huntoon (2003) to state that these tight folds in beds of the Tapeats Sandstone in Carbon Canyon can be explained by mechanical crowding at the synclinal hinge of the East Kaibab Monocline during slow deformation under stress of the solid sandstone in a ductile manner.

However, Hill and Moshier (2009) offer no supporting evidence of these claims. They provide no documentation of the quoted rock deformation studies, nor any evidence from any thin section examination of the Tapeats Sandstone from these folds of the claimed microscopic re-orientations of mineral grains. And the only documentation they provide of any field studies is a single photograph of the vertical beds of the Tapeats Sandstone at the Carbon Canyon location, but not of the folded beds showing the mechanical crowding. For that they refer to Huntoon (2003), but his field photograph, while showing the bent beds of the Tapeats Sandstone at the location in question, is incorrectly labeled as the south wall of Chuar Canyon, when it is in fact the south wall of Carbon Canyon. Furthermore, Huntoon (2003) did not provide any thin section evidence for any re-orientation of mineral grains.

Subsequently, Tapp and Wolgemuth (2016) similarly discussed the Carbon Canyon fold. They showed a photo of the fold (their fig. 12-13, 125),

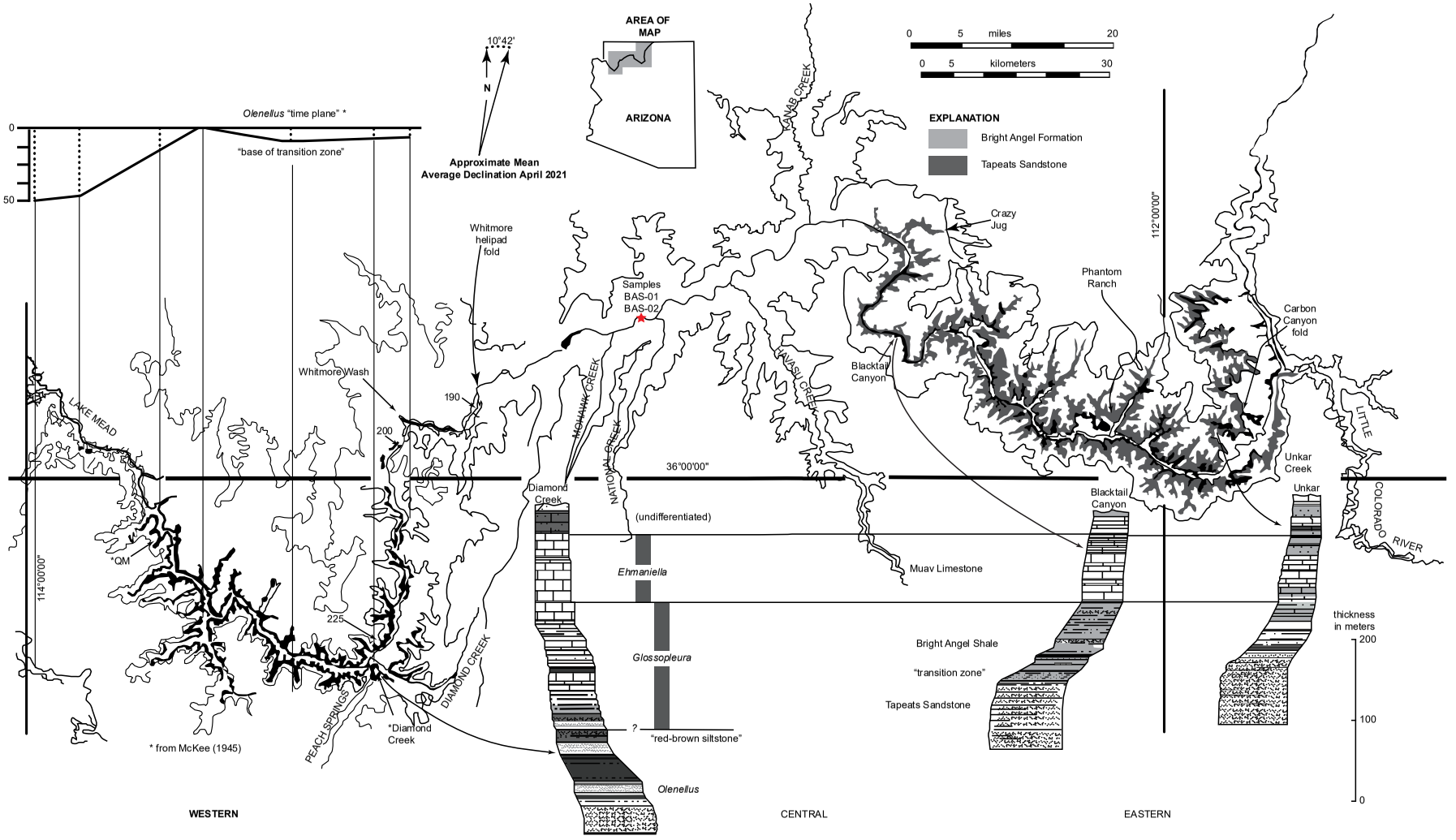

Fig. 1. Map of Grand Canyon showing the extent of exposure of the siliciclastic components of the Tonto Group, the Tapeats Sandstone and the overlying Bright Angel Formation (after Rose, 2006, 225, fig. 1). Below the map are three representative stratigraphic sections shown in stylized profile of geomorphic expression. These three sections are provided in detail in Appendix A (Unkar), B (Blacktail Canyon), and C (Diamond Creek), available online in the Supplementary material. The inset in the upper left is the basis for the time-transgressive model proposed by McKee (1945). The datum was compiled from the reported height (in meters) at which McKee reported collecting *Olenellus* fossils from seven sites above the "base of the transition zone" in the western Grand Canyon.

Fig. 2. The Carbon Canyon fold in which beds of the Tapeats Sandstone have been folded (bent) through 90° adjacent to the Butte Fault. Carbon Canyon is a side canyon to the Colorado River corridor at river mile 65 and the fold is exposed best in the southern wall of the canyon about 2 km (about 1.2 mi) from the river. The man who is ~1.8 m (6 ft) tall standing on the fold provides the scale.

describing it as compressional folding in the Tapeats Sandstone. On an overlay they traced some of the sandstone beds through the fold, some of the fractures, and the apparent changing direction of the fold noses, which they claimed to be due to flexural slippage. They claimed that the bending resulted in numerous fractures in each sandstone bed that did not heal (reseal). They then illustrated what flexural slippage would look like in two hypothetical folds (in their fig. 12–14, 125), describing how flexural slippage creates gaps in the fold noses that may be filled in later with weathered material or weaker rock units may deform into the spaces. Either way, the layering in the fold hinges would likely be thickened relative to the widths of the sandstone beds along the fold limbs. They claimed that neither of these features would be present if this fold had occurred due to soft-sediment deformation. However, their photo of the fold shows no such thickening of the sandstone beds in the fold hinges, and they fail to discuss alternate explanations for the fractures, such as due to contraction horizontally within the beds during dewatering and lithification. Additionally, there is no evidence of thickening of shale-rich beds in the Bright Angel Formation where they are folded, as would be expected.

There is a second location in Grand Canyon where there is similar folding, but in exposed Bright Angel Formation at river mile 187.4, known as the Whitmore helipad fold (figs. 1 and 3). The fold is river left above the banks of the Colorado River, clearly visible, and thus easily accessible from the nearby beach. It is a very tight fold with very little mechanical crowding of the constituent relatively thin shale and sandstone beds in the Bright Angel Formation, but there is some small offsetting along two fault lines associated with the two hinge zones. Again, the folding and faulting are claimed to have occurred during the Laramide Orogeny (Karlstrom and Timmins 2012), a very long time after the Cambrian deposition of the Bright Angel Formation, yet the character of the shale and sandstone beds also appear to be consistent with soft-sediment deformation soon after deposition. Neither Hill and Moshier (2009) nor Tapp and Wolgemuth

Fig. 3. The Whitmore helipad fold in which thin shale and sandstone beds of the Bright Angel Formation have been folded (bent), as seen in the cliff above the banks of the Colorado River, river left at river mile 187.4. The locations of the samples collected are marked by the labeled spots of orange tape, and the ladder provides scale.

(2016) make any mention of the Whitmore helipad fold.

It has been extensively documented that lithified rocks which have suffered ductile deformation will exhibit outcrop evidence of bedding plane slip and attenuation, such as flexural slippage (Ramsay 1967). However, field examination of these specific folds is insufficient to determine whether they were due to such ductile behavior of the lithified rocks under much later prolonged stress or due to soft-sediment deformation soon after deposition. Detailed microscopic examination is thus absolutely necessary to document the character of the sandstone, specifically, the textural relationships between the constituent grains and the timing of the formation of the cement (lithification). Telltale microscopic textures would be evident, such as grain-boundary sliding, the preferred orientation and recrystallization of the original detrital grains, as well as deformation lamellae and undulose extinction in those grains, and the original sedimentary cement between them would be absent or metamorphosed. Such textural features would be absent if the folding was due to soft-sediment deformation, as the original detrital grains and the cement binding them together in the sandstone in the folds would be essentially identical to those in the same sandstone distant from the folds.

It appears that none of these earlier investigators have done any thin section investigations of the shale and sandstone beds in the Bright Angel Formation to substantiate their claims of ductile deformation in such folds. Obviously, more detailed field and laboratory studies (especially intensive microscope examination) are needed to resolve the questions of what condition the shale and sandstone beds were in when they were deformed into this fold, and thus how soon after their deposition the deformation occurred, before or after lithification of the shale and sandstone. Any field and laboratory study of the Bright Angel Formation in the Whitmore helipad fold should thus also include a field and laboratory study of the Bright Angel Formation in other locations distant from this fold. This would enable observations and conclusions at the one location to be confirmed in the studies at the other locations. The evidence seen in thin section examination of the shale and sandstone beds in this fold should be different from that in the distant Bright Angel Formation shale and sandstone samples if the folding was due to ductile behavior under the stress of deformation of the lithified shale and sandstone, whereas the microscope evidence should be nearly

identical in all samples if the folding was due to soft-sediment deformation.

Therefore, on a research and sampling trip through the Grand Canyon with National Park Service approval, some 12 samples of the Bright Angel Formation were collected, ten samples from the Whitmore helipad fold, with permission from the Hualapai nation, and two samples from a similar stratigraphic position within the formation at a sufficient distance away from this fold so as to provide comparative control samples for the subsequent detailed thin section examination (figs. 1 and 3). Thus, the purpose of this paper is to review extensively what is already known about the petrology of the Bright Angel Formation as the context for then reporting the detailed microscope observations made on the collected samples. From the mineralogy and textures of these samples, inferences can then be drawn about the sediment source, its transport and deposition, and the formation's subsequent history, providing the documentation that can be referred to and built on in a subsequent paper focused on the timing of lithification (cementation) of the Bright Angel Formation in the Whitmore helipad fold before or after the folding occurred, that is, soft-sediment deformation or ductile deformation, respectively.

Past Investigations of the Tonto Group

The earliest conventional scientific explanations for deposition of the lower Paleozoic strata of Grand Canyon region were offered by some of the most prominent North American geologists. Indeed, the Cambrian of Grand Canyon is regarded as one of the classic sedimentary rock sequences exposed in North America. These strata crop out in the lower cliff sections of Grand Canyon, along a prominent, essentially horizontal surface known as the Tonto Platform in the central part of the Canyon, and near the banks of the Colorado River in western areas of the Canyon (figs. 1 and 4). The surface of the Tonto Platform roughly coincides with the top of the lowermost Cambrian unit, the Tapeats Sandstone. Above the Tapeats, a series of small cliffs are separated by thicker intervals of slopes composed of alternating beds of finer-grained deposits of shale, siltstone and sandstone of the Bright Angel Formation. These, in turn, are overlain by cliffs of resistant carbonates of the Muav Formation and then the Frenchman Mountain Dolostone (formerly the "unclassified dolomites"), the topmost units of the Tonto Group.

The Tonto Group forms the base of the kilometers-thick succession of generally flat-lying sedimentary strata that make up the Colorado Plateau. As described above, it straddles the conspicuous slope in the classic Grand Canyon cliff-slope profile known as the Tonto Platform (fig. 4). This geomorphic profile is consistent throughout the eastern exposures of Grand Canyon, which are much more visited, photographed, and familiar to most people. However, there is a great gap in exposed outcrops which separates the distinct eastern and western exposures of the Tonto Group (fig. 1). Only the uppermost cliff-forming carbonates of the Muav Formation are continuously traceable across the ~50 km (31 mi) gap between these exposures, and the stratigraphy of the less familiar western exposures differs in important ways from that of the eastern exposures. For one, the quality of Tonto Group exposure is poorer in the western canyon due to several faults complicating the traceability of marker beds. Secondly, it is covered by lava or rubble across several tens of kilometers. Lastly, the inaccessible sheer cliffs impede close inspection.

The Tonto Group was first defined by Gilbert (1875, his figure 82) and Powell (1876, 60) and then recognized to be Cambrian by Walcott (1895, 317). The conventional model of shelf deposition for the Tonto Group on a passive continental margin can be traced from Powell (1891) through Gilbert (1875), Walcott (1910), and Noble (1914, 1922), to McKee (1945). It is now a textbook example of a marine transgressive sequence to which Sloss (1963) applied the term "Sauk sequence."

McKee (1945) provided the most comprehensive account of Tonto Group deposition. He proposed a time-transgressive, "deepening seas" model which has endured as the classic model of passive margin sedimentation and a landward advance of a wave-worn shoreline. His "deepening seas model" described the major threefold division of the Tonto Group as:

(1) a nearshore, high-energy regime represented by the Tapeats Sandstone,
(2) an offshore, low-energy regime represented by the Bright Angel Shale (now the Bright Angel Formation), and
(3) an even more distal low-energy carbonate buildup as "a chemical precipitate," represented by the Muav Limestone (now the Muav Formation).

Unlike his predecessors McKee (1945) claimed that all three units, including the Bright Angel Formation, were deposited below wave base. That conclusion was necessitated by the presence of the phyllosilicate glauconite in the upper portion of the Tapeats Sandstone and in shales of the Bright Angel Formation. Glauconite has long been accepted as a necessary indicator of low oxygen conditions in a deep marine setting, but this is no longer the case (McRae 1972). Other facies characteristics that are contrary to deep marine deposition were only minimally discussed by McKee (1945) in general terms of minor regressions or other temporarily exceptional

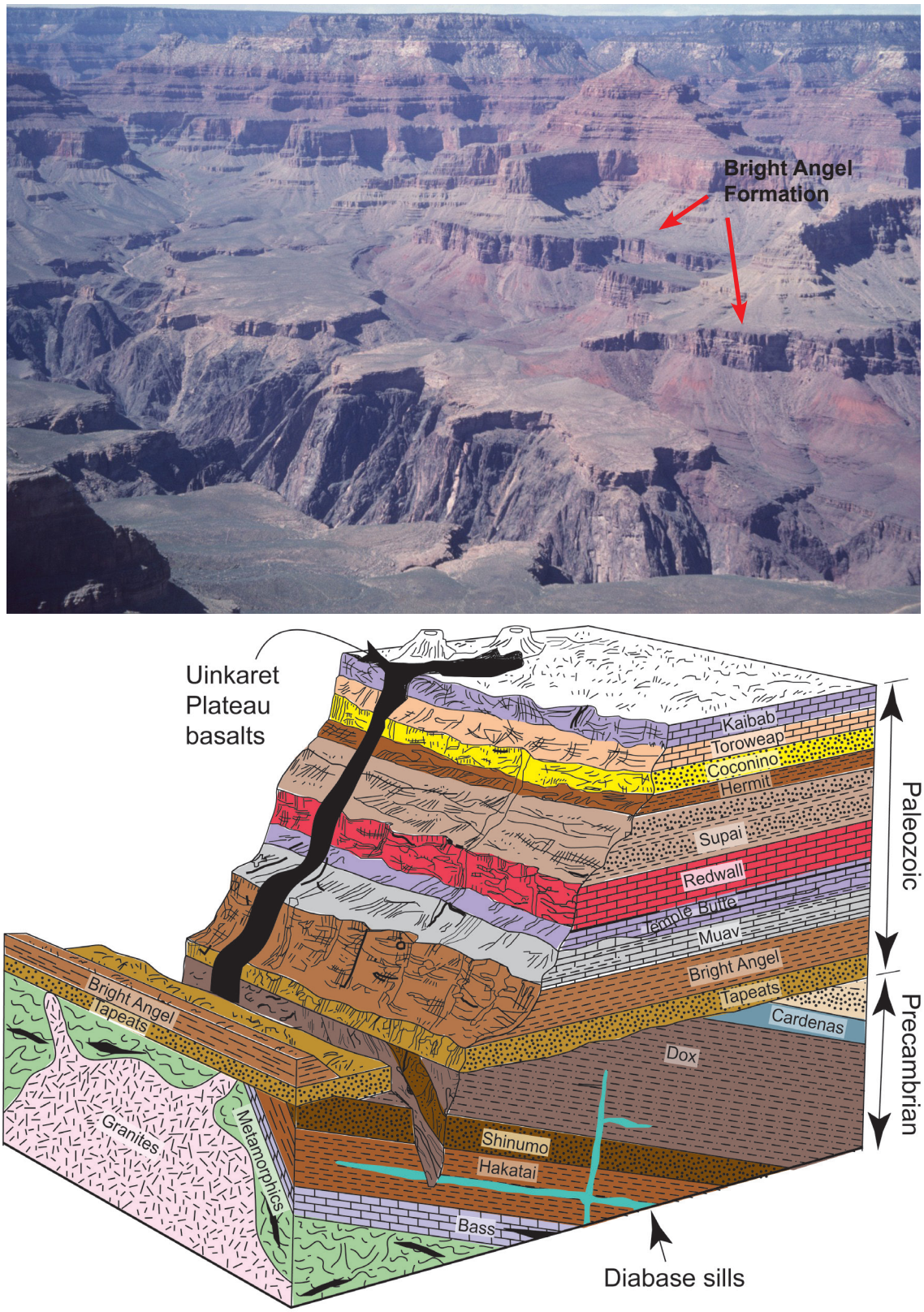

Fig. 4. The strata of the Grand Canyon. (a) The view of the Grand Canyon from the South Rim overlooks. From the skyline looking down are the horizontal sedimentary layers making up the walls of the Canyon. The small "capping" on the cliff near the foreground, below which is the inner gorge consisting of schists intruded by granites, is the Tapeats Sandstone. The extensive wide almost flat areas above the Tapeats Sandstone in the middle foreground is the Tonto Platform. In the distance to the left above the Tapeats Sandstone in the slope is the overlying Bright Angel Formation (arrowed). (b) A block diagram of the Grand Canyon strata corresponding to the vista seen in (a), except for the basalts that are found in the western Canyon (after Austin 1994, 13, fig.2.5).

conditions. This simple and elegant explanation for the intact layer-cake stratigraphy of the Grand Canyon's Tonto Group was thus settled on early and generally has not been revisited.

An important consideration in the development of the "deepening seas" model of time-transgressive shoreline retreat is that McKee (1945) worked his way eastward from the thicker basin-ward exposures of western Grand Canyon, starting at Grand Wash Cliffs, to the region of central Grand Canyon reported previously by Noble (1914, 1922). Comparatively little early stratigraphic work was done on the eastern exposures, so McKee (1945) depended on the single generalized measured section of Wheeler and Kerr (1936) to characterize the stratigraphy of the eastern exposures. In so doing he applied Noble's solely lithologic facies criteria for subdividing the Tonto Group to the western exposures and as a result placed the Bright Angel Formation–Muav Formation contact some 150 m (492 ft) below what it would be if lithologic contacts were followed instead (Huntoon 1989). This quirk in nomenclature provided the impression that the Muav and Bright Angel Formations crossed time boundaries with reference to biostratigraphically defined "time planes" (fig. 5).

Conventional chronostratigraphic control within the Tonto Group is provided by sparse and poorly preserved trilobite fragments and rare articulated trilobites but is complicated by numerous misidentifications by Resser (1945), subsequent taxonomic revisions (for example, Sundberg 1999), and the probability of mixed samples among poorly recorded collection sites. Nevertheless, McKee (1945) portrayed the biostratigraphy as thorough and precise, indicating uniform convergence of "thin fossil zones" with definite lithologic boundaries lower in the section as they are traced from west to east (fig. 5).

The classic work of McKee (1945) and Resser (1945) has endured as the most comprehensive study of the Cambrian system in the Grand Canyon. These Cambrian strata occur throughout the Rocky Mountains and have since become the classic (textbook) example of a transgressive fining-upwards sequence of sandstone, mudstone and limestone that accumulated on the slowly subsiding Cordilleran miogeosyncline and adjacent craton (Lochman-Balk 1970, 1971; Stewart 1972; Stewart and Suczek 1977). It is thus postulated that during the early and middle Cambrian, a north-south trending strandline migrated progressively eastward across the craton. This shoreline was characterized by numerous embayments and offshore islands that affected sedimentation in nearshore areas. Shoreline migration was mostly eastward, resulting in deposition of coarse clastics in shallow water areas to the east and finer clastics and carbonates in the more offshore areas to the west. Numerous regressive phases apparently interrupted this overall eastward transgression resulting in complicated facies interactions.

However, limited subsequent research on Tonto Group strata has not kept pace with conventional developments in the last fifty years of the dynamics of modern nearshore and shelf depositional systems (for example, Nummedal 1991), failing to apply them to the uniformitarian explanation for the deposition of these rock units. Only a few studies have attempted to carefully document the lateral and vertical facies associations, including in the Bright Angel Formation (Blakey and Middleton 2012; Elston 1989; Hagadorn et al. 2011; Hereford 1977; Martin 1985; Martin, Middleton, and Elliott 1986; Middleton 1989; Middleton and Elliott 2003; Rose, Middleton, and Elliott 1998; Rose 2003, 2006, 2011, Wanless 1973a).

Wanless (1973a, b, 1975, 1981) presented the first challenge to the "deepening seas" model in demonstrating the petrographic similarity between modern intertidal carbonates and the Muav Formation facies that McKee (1945) interpreted as the most distal and deepest of the Tonto Group units. Wanless (1973a, b, 1981) further suggested that the whole of the Tonto Group deposition was in extremely shallow water. On the basis of detailed stratigraphic, sedimentologic and paleontologic studies of measured sections of the Bright Angel Formation in eastern Grand Canyon, Martin (1985) and Martin, Middleton, and Elliott (1986) maintained that deposition of the transgressive succession was in a subtidal marine environment influenced by tidal and meteorologic currents, including those due to storms.

Elston (1989) built on the "classic work" of McKee (1945) by taking his measured sections, and those of Noble (1922) and Wheeler and Kerr (1936) and recompiling them carefully with the same lithologies but adding some measured sections of his own in eastern Grand Canyon. His correlations and his revised nomenclature are depicted in fig. 6. His proposed correlations indicated that following deposition of the massive sandstone member of the Tapeats Sandstone in western Grand Canyon, an eastward transgression of the epicontinental sea across the central and eastern Grand Canyon occurred at or near the *Olenellus* horizon, which lies a few feet above the top of the massive sandstone member. The overlying red brown sandstone member in the west traces into the upper part of the Tapeats Sandstone in the central and eastern Grand Canyon, and the underlying shaly interval in the west passes into parallel-bedded, cross-laminated sandstone eastwards into the central Canyon. Correlations above the Tapeats Sandstone indicated that a series of marker beds, identified as members of the Bright

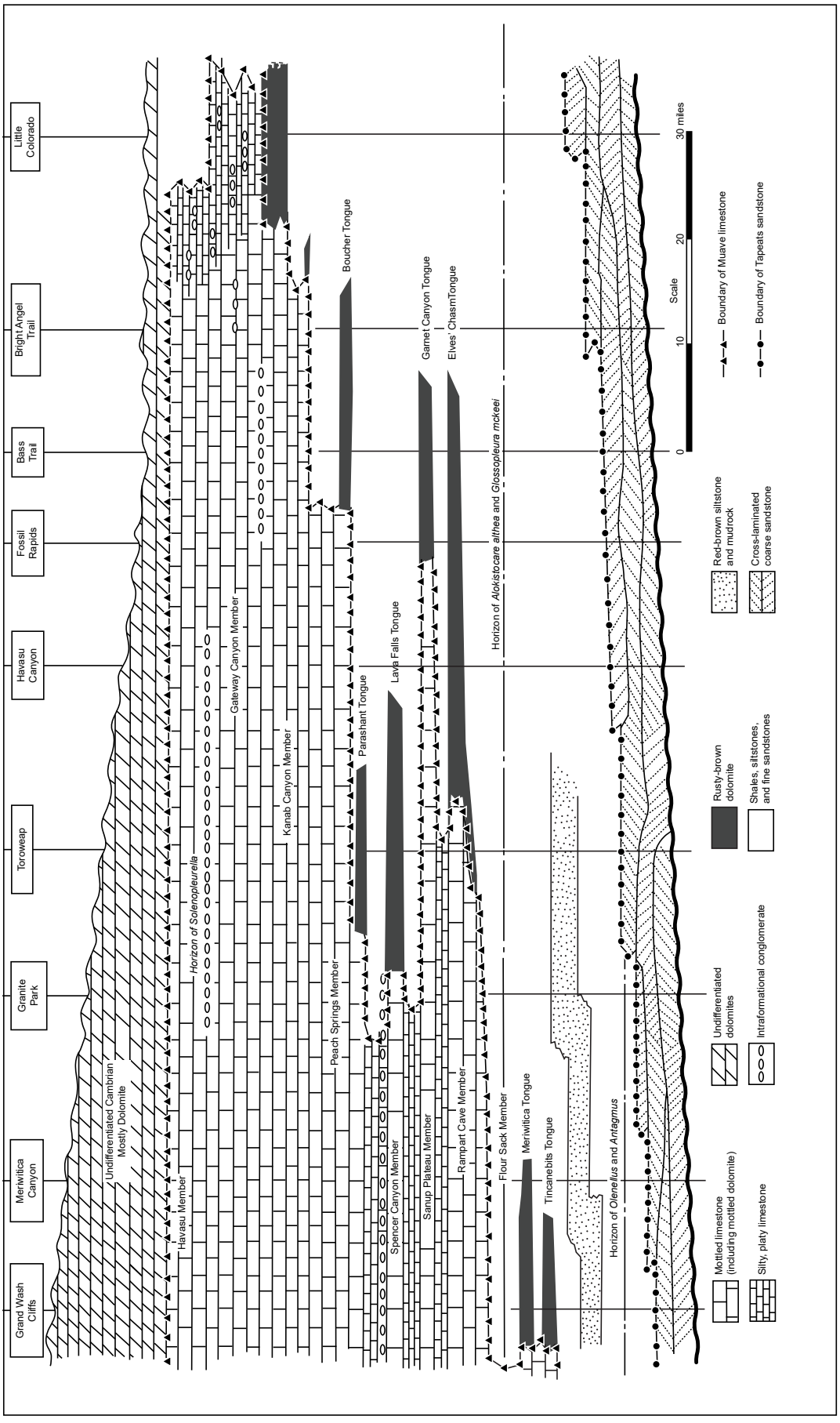

Fig. 5. The diagrammatic section of McKee (1945, 14, fig.1) of the Cambrian deposits in the Grand Canyon, showing stages in transgression and regression and distribution of facies from east to west. His time planes are horizontal, and the actual thickness varies from 1500 ft (about 460 m) in the west to 800 ft (about 245 m) in the east.

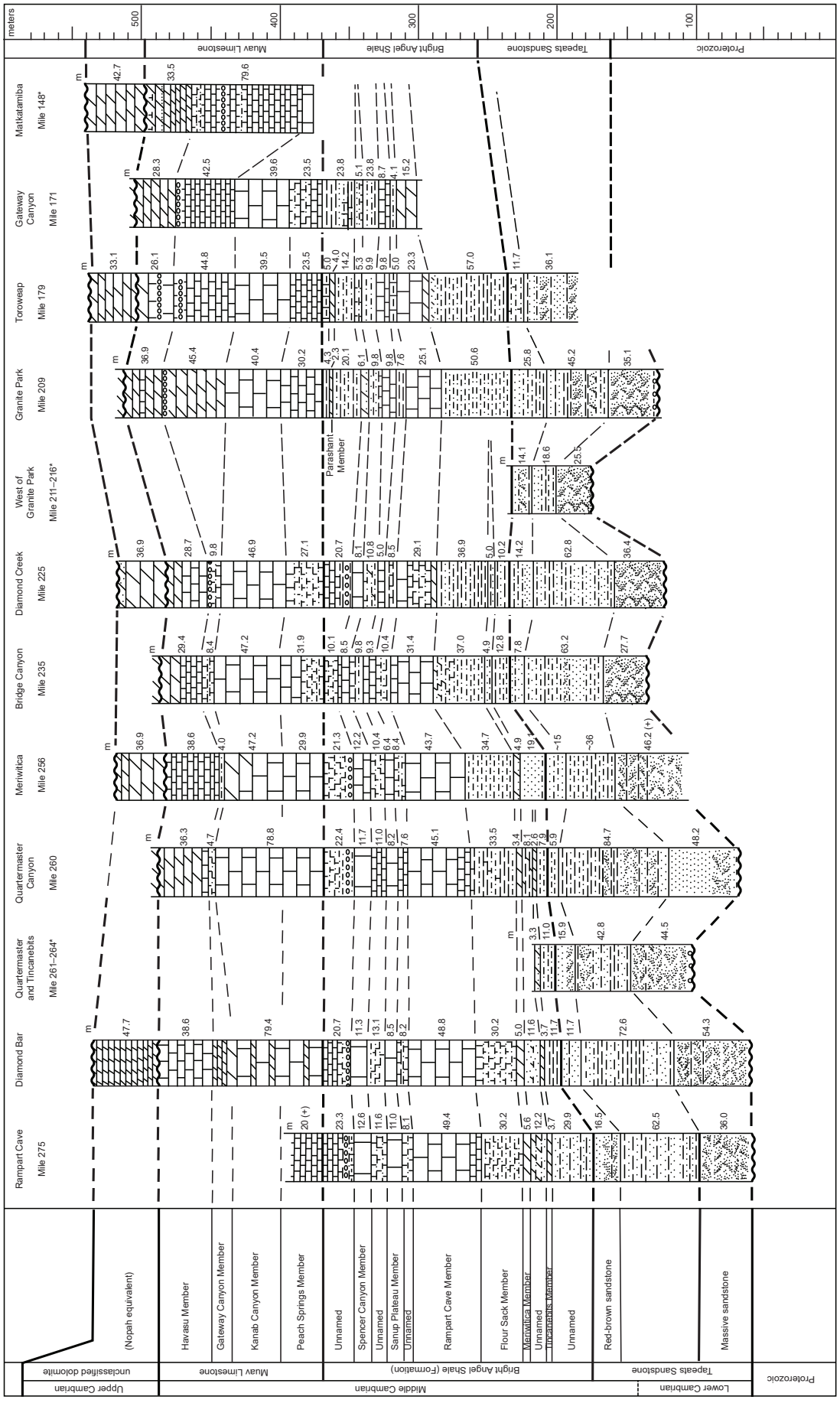
meters
500
400
300
200
100
Muav Limestone
Bright Angel Shale
Tapeats Sandstone
Proterozoic
Rampart Cave Mile 275
Diamond Bar
Quartermaster and Tincanebits Mile 261–264*
Quartermaster Canyon Mile 260
Meriwitica Mile 256
Bridge Canyon Mile 235
Diamond Creek Mile 225
West of Granite Park Mile 211–216*
Granite Park Mile 209
Toroweap Mile 179
Gateway Canyon Mile 171
Matkatamba Mile 148*
Parashant Member
Upper Cambrian
Middle Cambrian
Lower Cambrian
Proterozoic
unclassified dolomite
(Nopah equivalent)
Muav Limestone
Bright Angel Shale (Formation)
Tapeats Sandstone
Havasu Member
Gateway Canyon Member
Kanab Canyon Member
Peach Springs Member
Unnamed
Spencer Canyon Member
Unnamed
Sanup Plateau Member
Unnamed
Rampart Cave Member
Flour Sack Member
Meriwitica Member
Unnamed
Tincanebits Member
Unnamed
Red-brown sandstone
Massive sandstone

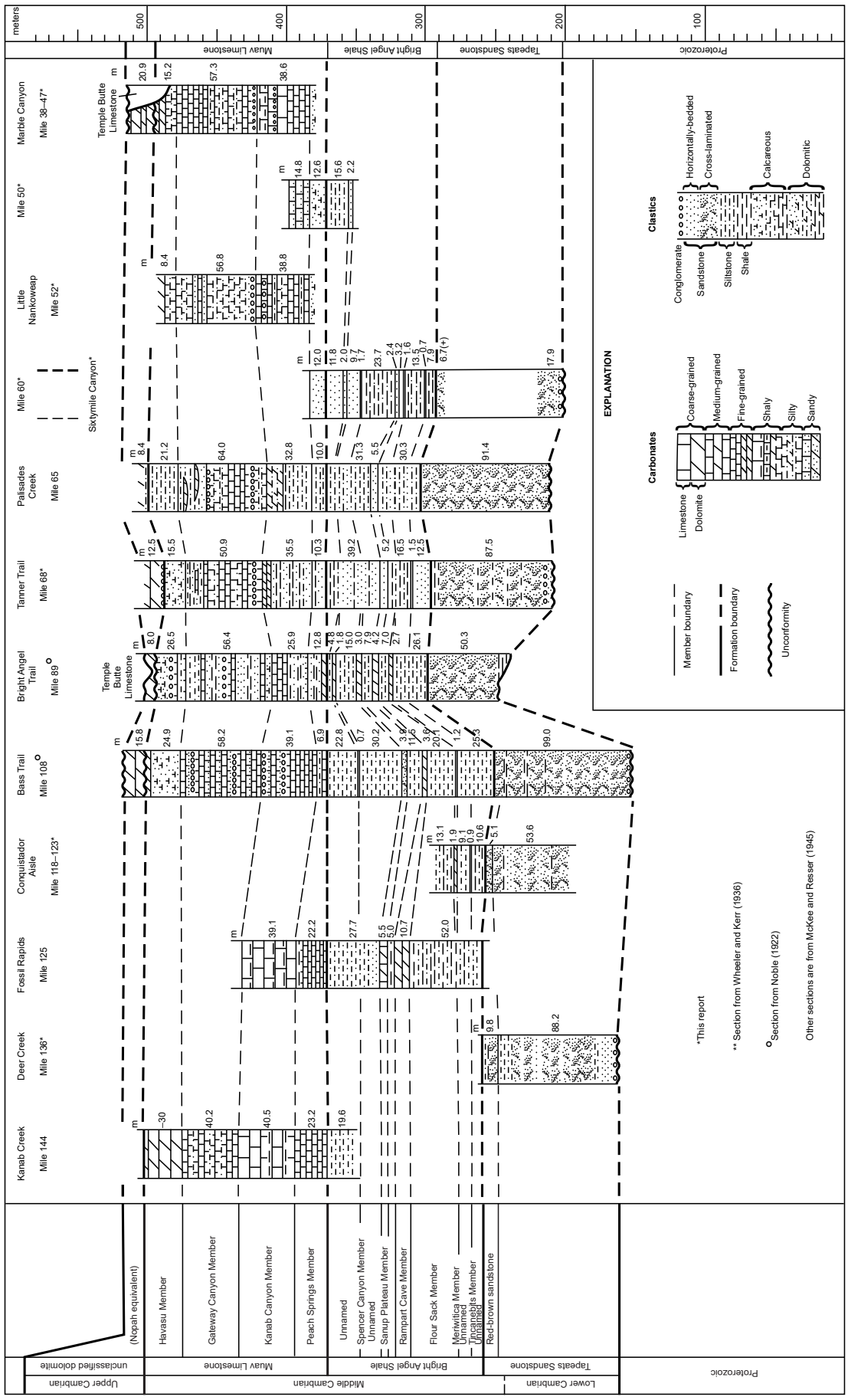

Fig. 6 (pages 312 and 313). The diagrammatic sections of Elston (1989, 134–135, figs. 15a,b) showing the correlation of the Cambrian Tonto Group deposits in the Grand Canyon and the facies changes based on McKee (1945), Noble (1922) and Wheeler and Kerr (1936) but with his revised nomenclature. (a) The western half of the Grand Canyon, Rampart Cave (river mile 275) to Matkatamiba Canyon (river mile 150). (b) The eastern half of the Grand Canyon, Kanab Creek (river mile 144) to Marble Canyon (river miles 38-47).

Angel Formation, record facies changes reflecting slight shifts in environments of marine deposition rather than major transgressions and regressions of the epeiric sea as concluded by McKee (1945).

Subsequently, Middleton and Elliott (2003) summarized the available data to describe the depositional systems of the Tonto Group presumed to have existed during the Cambrian history of northern Arizona, using both sedimentologic and ichnologic data. Rose (2003, 2006, 2011) provided new stratigraphic data and sedimentologic evidence from his 29 measured complete and partial sections to support Wanless' (1973a, b) claim and detailed the depositional, geochemical, and biological characterization of his proposed extensive, pervasively shallow paleoenvironment responsible for the Tonto Group. Finally, Blakey and Middleton (2012) briefly reviewed the interpreted paleogeography and geologic history of the Cambrian system's record in Grand Canyon within the overall tectonic setting of southwestern North America.

Most recently, Karlstrom et al. (2018, 2020) have redefined the Tonto Group and Sauk megasequence in Grand Canyon region. They concluded that the Sixtymile Formation is Cambrian and therefore locally the base of the Tonto Group, conformably overlain by the Tapeats Sandstone and the Bright Angel Formation. Similarly, they concluded the Frenchman Mountain Dolostone is conformable above the Muav Formation. It extends across the Grand Canyon as the Undifferentiated Dolomites (McKee 1945) whose name it now replaces and is thus the topmost part of the Tonto Group and the Sauk megasequence transgression.

Regional Stratigraphic Relationships of the Tonto Group

As now proposed, the Tonto Group in the Grand Canyon region comprises five formations that are, in ascending order, the Sixtymile Formation, Tapeats Sandstone, Bright Angel Formation (primarily shale), Muav Formation (primarily limestone), and the Frenchman Mountain Dolostone (Karlstrom et al. 2020). The term "Tonto Group" was first used by Gilbert (1874, 1875) to describe the Tapeats-Bright Angel-Muav fining-upwards sandstone-shale-limestone sequence, although he considered these rock units to be Silurian. Subsequent stratigraphic and paleontologic work by Walcott (1890, 1895) established that the Tonto Group is Cambrian, and Noble (1914) introduced these three formation names during his mapping of the Shinumo Quadrangle in the Grand Canyon.

Strata of the Tonto Group also crop out along the Grand Wash Cliffs in western Arizona and further west at Frenchman Mountain just outside Las Vegas, Nevada, where the Muav Formation is overlain conformably by the Frenchman Mountain Dolostone. To the east, the Tonto Group also crops out in the Juniper Mountains and Black Hills in west-central Arizona (Middleton and Elliott 2003). In those areas the Tapeats Sandstone is overlain disconformably by the Devonian Martin Formation, or the Chino Valley Formation of uncertain age designation (Hereford 1975). It is presumed that the Bright Angel and Muav Formations were removed by extensive pre-Devonian erosion (Middleton and Elliott 2003). In central Arizona scattered outcrops of the Tapeats Sandstone occur along the East Verde River and in the Sierra Ancha Range north of Young, Arizona. Tonto Group equivalents in southeastern Arizona include the Bolsa Quartzite and part of the overlying Abrigo Formation (Hayes and Cone 1975; Middleton 1989).

These Cambrian strata overlie a variety of Precambrian lithologies throughout the Grand Canyon. In the eastern Canyon and in some central areas, the Tonto Group rests on tilted beds of the Precambrian Grand Canyon Supergroup, which consists of the Unkar and Chuar Groups, whereas in the western areas and other central places the Tonto Group nonconformably overlies various older Precambrian granite plutons that intrude schists of the Granite Gorge Metamorphic Suite (figs. 4 and 7). This major unconformity between the Precambrian and Tonto Group strata, which has been long recognized, is called the Great Unconformity due to its visual prominence and continental (and global) extent (Peters and Gaines 2012). Traditionally, it has been thought to represent either a considerable period of time during which there were episodes of slow mountain-building and extensive weathering and erosion, or a very short and intense period of catastrophic uplift and erosion. Walcott (1910) applied the name "Lipalian interval" to the period of uniformitarian time represented by this unconformity. Since the Tonto Group is Cambrian (~500 Ma) where it sits on the crystalline basement granites and metamorphic schists (fig. 7b) that are generally dated at 1.6–1.7 Ga (Karlstrom et al. 2003) the time interval at the Great Unconformity is about 1.1 Ga. In contrast, where the Tonto Group sits on the tilted Grand Canyon Supergroup sedimentary strata (fig. 7a) it has been harder to date those sedimentary rocks, so their ages have been variously estimated based on the 1.1 Ga Rb-Sr age for the Cardenas Basalt lavas that are sandwiched between the Unkar Group and Chuar Group sedimentary strata (Elston and McKee 1982; Larson, Patterson, and Mutschler 1994). Thus, the time interval at the Great Unconformity with the Grand Canyon Supergroup sedimentary strata is <500 Ma.

Fig. 7. The Great Unconformity as exposed throughout the Grand Canyon (a) View from the edge of Horseshoe Mesa of the tilted Precambrian Unkar Group sedimentary strata with the Grand Canyon Supergroup eroded across at the Great Unconformity with the Tapeats Sandstone deposited on it, overlain by the Bright Angel Formation. (b) The Great Unconformity is just below the cliff of Tapeats Sandstone on the near horizon and consists of the eroded surface of the Ruby Pluton (a hornblende-biotite granodiorite intruded by later large granitic veins) at about river mile 105. The Bright Angel Formation is barely visible in the slope overlying the Tapeats Sandstone.

However, recent radiometric dating results have further constrained the time interval represented by the Great Unconformity. A U-Pb age of 742Ma was obtained for zircons within a thin tuff bed at the top of the Walcott Member of the Kwagunt Formation (Chuar Group) just below the Great Unconformity (Karlstrom et al. 2000). Subsequently, an Ar-Ar age of 764Ma was obtained for authigenic K-feldspar within early diagenetic marcasite nodules in the underlying Awatubi Member of the Kwagunt Formation (Dehler et al. 2017), and a U-Pb age of 729Ma was obtained for zircons from the same thin tuff bed at the top of the overlying Walcott member (Rooney et al. 2018), both in the upper Chuar Group of the uppermost Grand Canyon Supergroup in eastern Grand Canyon. Furthermore, in eastern Grand Canyon a small wedge of sedimentary strata known as the Sixtymile Formation is sandwiched between the Grand Canyon Supergroup and the Tonto Group. Hithertofore they have been regarded as Precambrian and thus below the Great Unconformity. However, Karlstrom et al. (2018, 2020) have convincingly demonstrated that the Sixtymile Formation contains detrital zircons with the youngest U-Pb ages of 505–527Ma and is thus Cambrian. It is therefore now regarded as being above the Great Unconformity, and thus represents the onset of the transgression that deposited the rest of overlying Tonto Group. So, the time interval at the Great Unconformity could be about 200Ma.

The surface on which the Tonto Group accumulated was fairly irregular, though it is also flat at many locations. Where irregular it was characterized by a rolling topography of resistant bedrock "hills" (often Unkar Group Shinumo Quartzite) and "lowlands." The Precambrian bedrock appears to have been extensively weathered in places and eroded during the claimed prolonged period of subaerial exposure. Walcott (1880) and Noble (1914) were first to recognize that the Precambrian surface represented an apparent paleotopography and that Tonto Group sedimentation patterns were influenced by the relief and lithologies of those "hills." Others likewise documented the influence of the Precambrian topography on Cambrian sedimentation in other areas of the Rocky Mountains and in the midcontinent (Middleton and Elliott 2003). There are numerous places in the Canyon where the Tapeats Sandstone thins across or pinches out against those Precambrian highs. Where the Tapeats Sandstone pinches out, the Bright Angel Formation directly overlies the Precambrian surface.

A claimed apparently highly weathered horizon occurs on top of the Precambrian surface in several places in the Canyon. The only effort to understand the genesis of that claimed horizon is that of Sharp (1940). His study suggested that extensive chemical weathering of Precambrian rocks occurred prior to deposition of Cambrian sediments. In places that apparently highly weathered surface or potential regolith is up to 15.3m (50ft) thick, but elsewhere is generally less than 3.1m (10ft) thick. Sharp (1940) speculated that where the Tapeats Sandstone sits on unaltered Precambrian basement, that regolith was probably removed by the wave erosion associated with the initial Cambrian transgression. Sharp (1940) and McKee (1945) suggested that the presence of such a thick, apparently weathered horizon indicated that dominantly humid conditions existed during the earliest Paleozoic prior to deposition of the Tonto Group. However, there have been no petrologic and geochemical studies that could substantiate that hypothesis. Furthermore, from a uniformitarian perspective during the ~200 million years represented at the Great Unconformity, the climate could have changed numerous times prior to deposition of the Tonto Group, and in the presumed absence of terrestrial vegetation weathering processes in soils would have been different (Basu 1981), so a humid climate interpretation is quite tenuous.

At the continental scale, Sloss (1963) recognized that the Great Unconformity and the overlying Tonto Group could be correlated across North America, the latter representing the first of six major sequences of rock-stratigraphic units which he named the Sauk megasequence. Peters and Gaines (2012) further documented that the Great Unconformity is a well-recognized, globally-occurring stratigraphic surface, which in most regions across the globe separates continental crystalline basement rocks from much younger Cambrian shallow marine sedimentary deposits, that is, the Sauk megasequence. Using stratigraphic and lithologic data for 21,521 rock units from 830 geographic locations in North America they demonstrated that the Tapeats Sandstone correlates with very similar basal Sauk sandstones right across North America (fig. 8), such as the Flathead Sandstone in Wind River Canyon, Wyoming, the Mt. Simon Sandstone in a drill-hole in northern Illinois, and the Sawatch Formation near Manitou Springs, Colorado. Similarly, Clarey and Werner (2018) constructed over 1500 local stratigraphic columns across North America, South America, Africa, and the Middle East recording the detailed lithologic information and the Sloss megasequence boundaries at each site. From these data they created a detailed 3-D lithology model for each continent using the local columns, and also constructed maps of the basal lithology for each megasequence. They thus demonstrated the continuity of the basal Sauk sandstone layer (the Tapeats Sandstone, the Bright Angel Formation and their equivalents) across the North American continent, across North Africa and the Middle East,

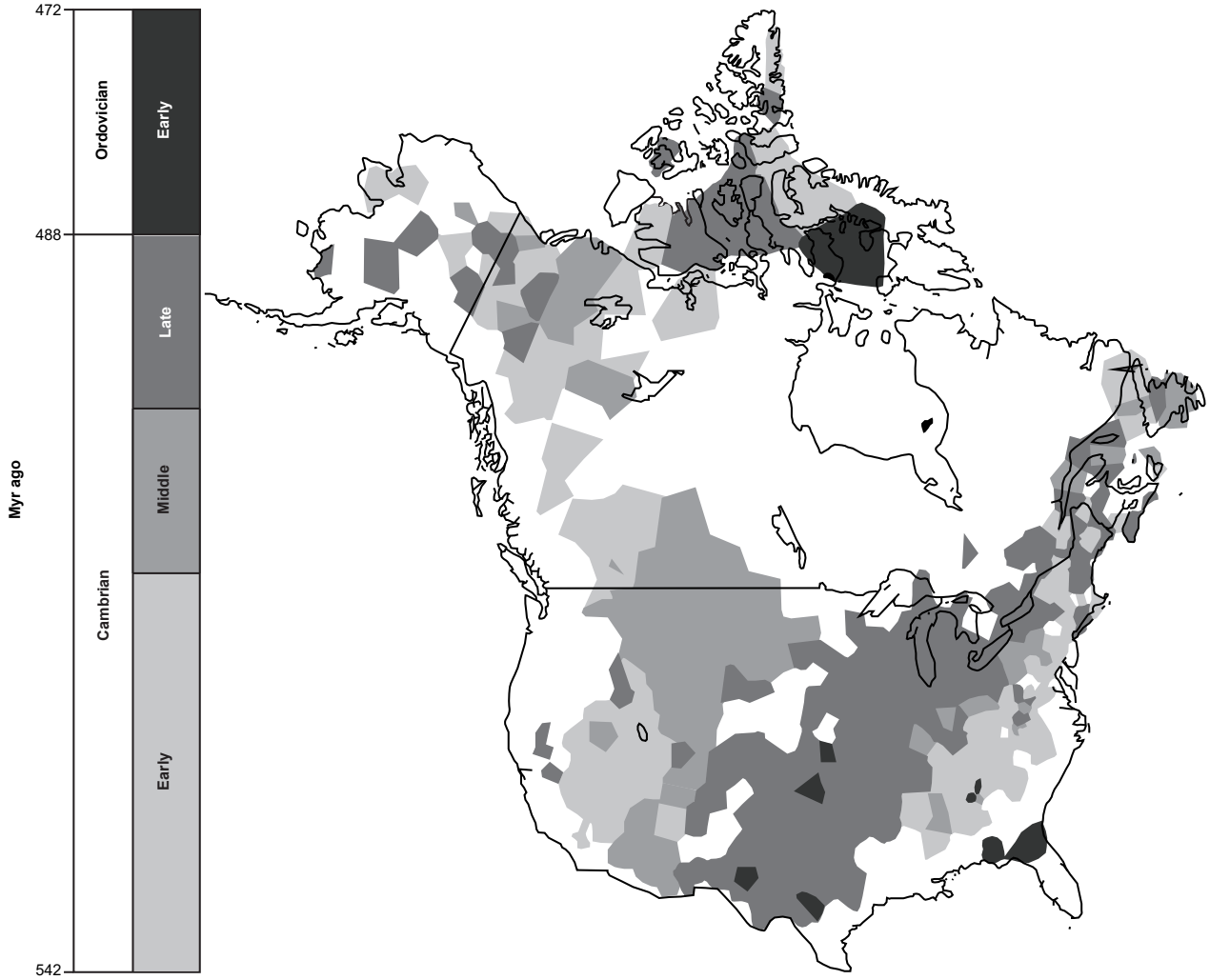

Fig. 8. The distribution and age of the Sauk megasequence, the oldest Phanerozoic sedimentary rocks of North America (after Peters and Gaines 2012, 363, fig. 1). Not only were the basal Tapeats sandstone and its equivalents, as well as the overlying Bright Angel Formation, deposited continent-wide, but the Great Unconformity beneath it was also eroded continent-wide and beyond (globally).

and across South America where the Sauk is only found within portions of Peru, Bolivia and northern Argentina. Furthermore, in many locations the basal Sauk megasequence is also coincident with the Great Unconformity.

The Stratigraphy of the Bright Angel Formation

The Bright Angel Formation is probably the least-studied formation in the Grand Canyon. It was first described by Newberry (1861), who examined it in the canyon of Diamond Creek. It was named by Noble (1914) for exposures of slope-forming, interbedded, fine-grained sandstone, siltstone and shale just above the Tonto Platform along Bright Angel Creek. Conglomerates and coarse-grained sandstones of the Bright Angel Formation contain quartz, minor amounts of K-feldspar and sedimentary rock fragments, and glauconite (Middleton and Elliott 2003). The latter is responsible for giving the green color to many of the siltstones and sandstones. In contrast, a number of the sandstones and siltstones contain a high percentage of hematitic ooids and iron oxide cements which impart a reddish-brown coloration. The dominant lithology of the formation is greenish shale composed largely of illitic clay with varying amounts of chlorite and kaolinite. Inarticulate brachiopods, trilobites and *Hyolithes* of the Lophophorata clade are locally abundant, while trace fossils are extremely abundant and varied (see below).

The Bright Angel Formation is over 450 ft (137 m) thick in western Grand Canyon, only 270 ft (82 m) at Toroweap in the central canyon, and 325 ft (99 m) along Bright Angel Creek (McKee 1945). This variability in thickness is due to the complex intertonguing relationships with the Muav Formation (figs. 5 and 9). The Bright Angel Formation thins toward the south and is only a few feet thick in the Juniper Mountains north of Prescott, Arizona (Middleton and Elliott 2003). South and east of the Black Hills,

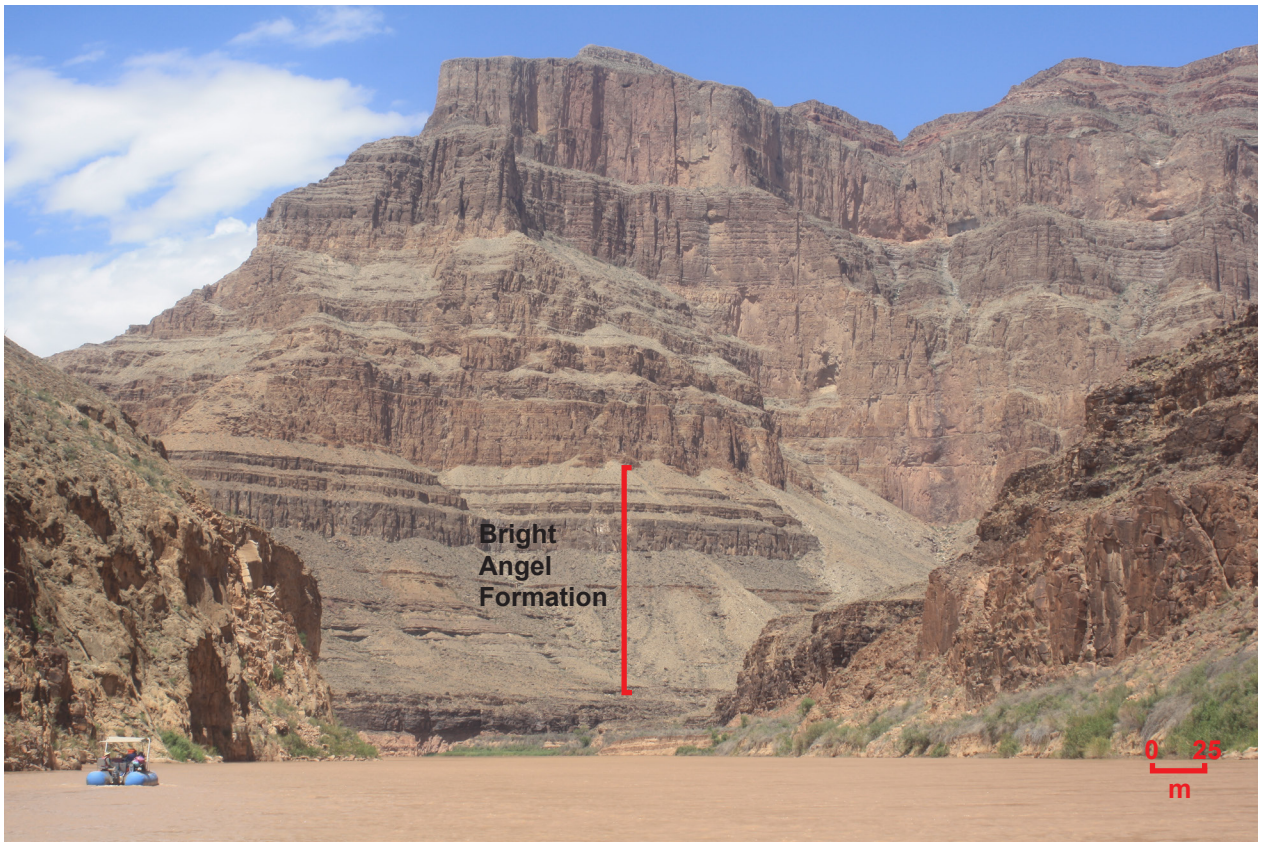

Fig. 9. Apparent complex intertonguing relationships in the western Grand Canyon (river mile 257.5) between the Bright Angel Formation (in the slope above the first small "cliff" at river level in the distance) and the overlying Muav Formation (the prominent cliffs above the slope). At the top of that slope are three small stepped cliffs representing hard carbonate beds compared to the softer shale beds between them that have more easily eroded. Those three small cliff-forming carbonate beds were initially mapped as tongues of Muav lithology within the Bright Angel Formation (fig. 5, McKee 1945), but are now included in the Bright Angel Formation (Elston 1989). Scale as indicated.

Arizona, the formation is absent, presumably the result of extensive erosion.

McKee (1945) found there were no sharp bounding surfaces between the Bright Angel Formation and the formations above and below it (figs. 5 and 9). The gradational nature of its contact with the underlying Tapeats Sandstone was first described by Schuchert (1918), who also referred to its transition to the overlying Muav Formation (primarily limestone). The boundaries between these formations are thus somewhat arbitrary, the lower limit of the Bright Angel Formation being placed above the highest bed of Tapeats-like coarse sandstone, and the upper limit being placed at the base of the lowest bed of massive, mottled limestone.

McKee (1945) described the Bright Angel Formation as composed of numerous lithologies which are somewhat gradational. He found it difficult to plot the distribution of each lithology because of their numerous alternations and recurrences, and because of poor exposures. Green shale, brown-spotted siltstone and micaceous grey siltstone occur throughout the Grand Canyon area, but certain other lithologies are restricted to the eastern or western Canyon (figs. 10–12).

McKee (1945) determined that the basal part of the Bright Angel Formation consists of three principal lithologies which occur in varying proportions but are similar in character and in relation to one another:

(1) a green fissile shale, which is paper thin, locally micaceous and responsible for slope development,
(2) a greenish-buff, crumbly siltstone and sandstone, which is poorly sorted, lacks lamination structures and tends to form weak ledges, and
(3) a dark brown or purple quartzitic sandstone, which is hard and ledge-forming.

Each of these lithologies is repeated many times in the zone immediately above the transition section of the Tapeats Sandstone. This basal Bright Angel Formation zone is 30–50 ft (9–15 m) thick in the western Grand Canyon but is considerably thicker in eastern Grand Canyon.

Immediately above this basal zone of the Bright Angel Formation are a series of red-brown siltstones and shales that are prominently developed in western Grand Canyon (McKee 1945). These "red-brown beds"

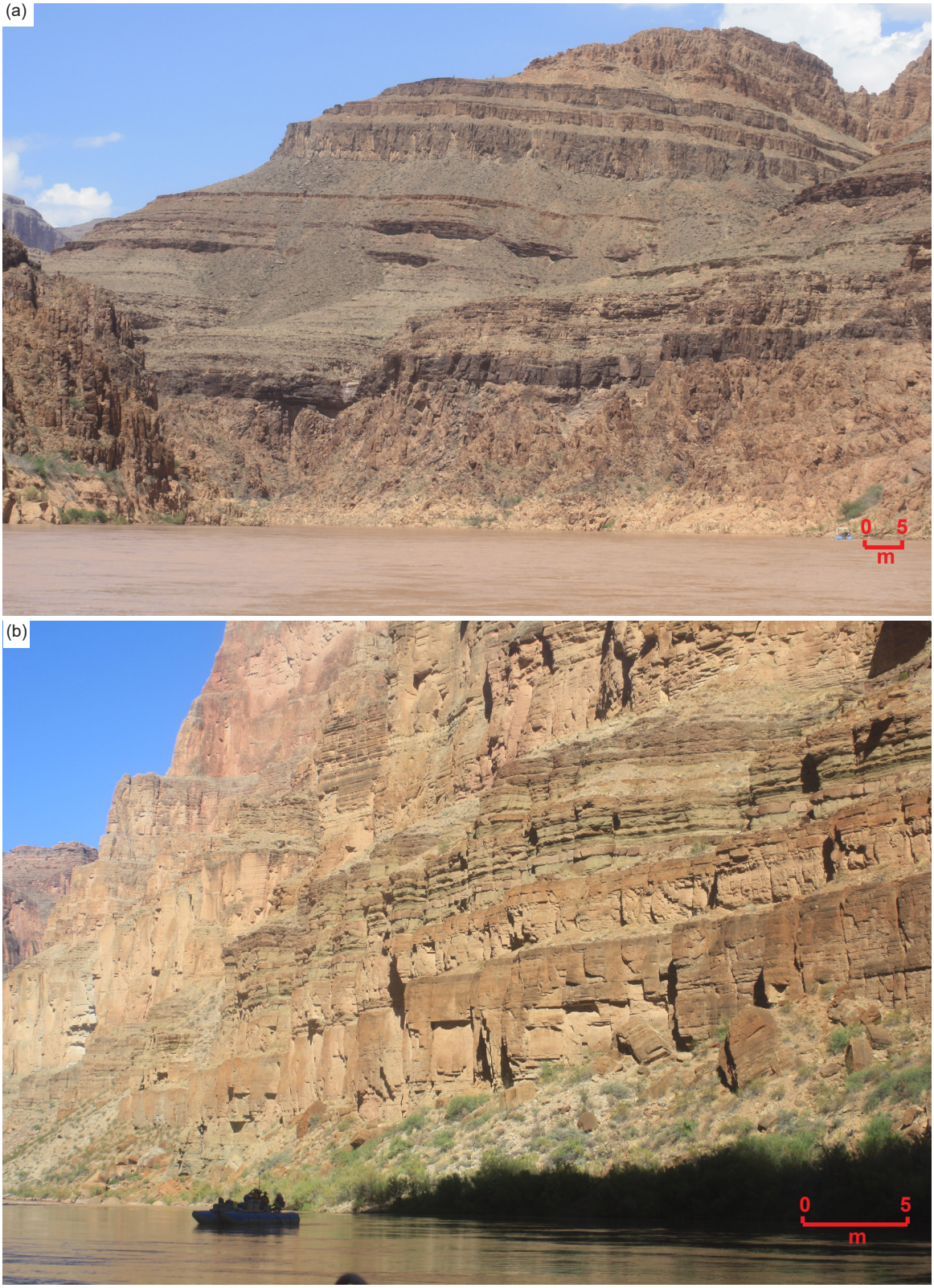

Fig. 10. Typical cliff profiles of the Bright Angel Formation. The scale bar to the right in each view is ~5 m (~16.5 ft). (a) From river level up is granitic basement in the cliff with a small thickness of the unconformably overlying Tapeats Sandstone capping it. The full thickness of the Bright Angel Formation can be seen in the slope above with harder sandstone and carbonate beds (lower and higher in the section, respectively) forming small stepped cliffs with eroded shales and siltstones forming slopes between them (river mile 257). (b) The upper section of the Bright Angel Formation showing the harder hematitic colored sandstone beds with interbedded gray siltstones and green shales (river mile 170).

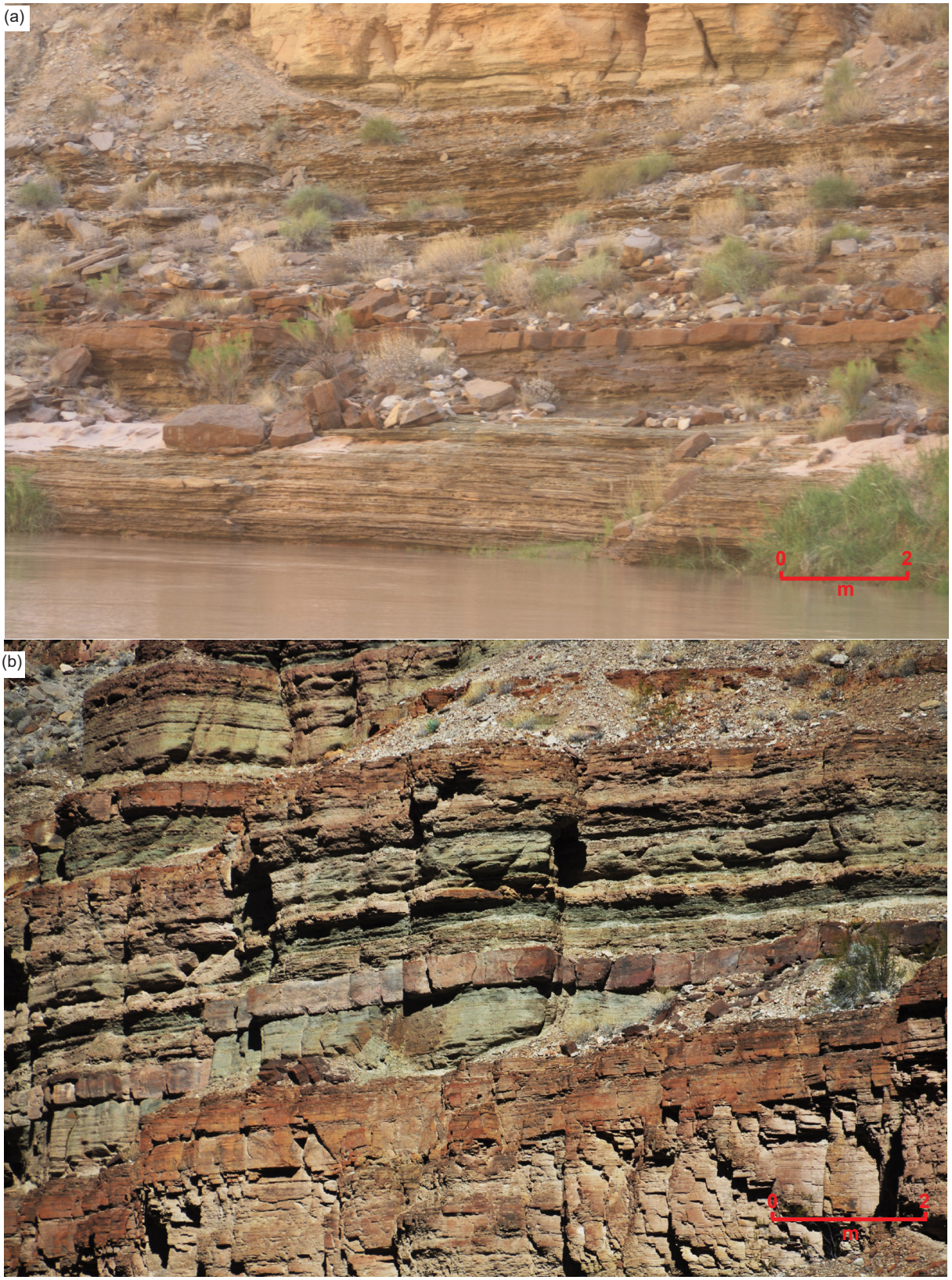

Fig. 11. Lithologies within the Bright Angel Formation in the central Grand Canyon. The scale bar to the right in each view is ~2 m (~6.5 ft). (a) Interbedded thin beds and laminae of alternating siltstone and shale (mudstone) with the occasional thicker more resistant (harder) red-brown sandstone beds forming ledges (river mile 168). (b) Closer view of greenish laminated shale and siltstone beds alternating with red-brown sandstone and siltstone beds (river mile 170).

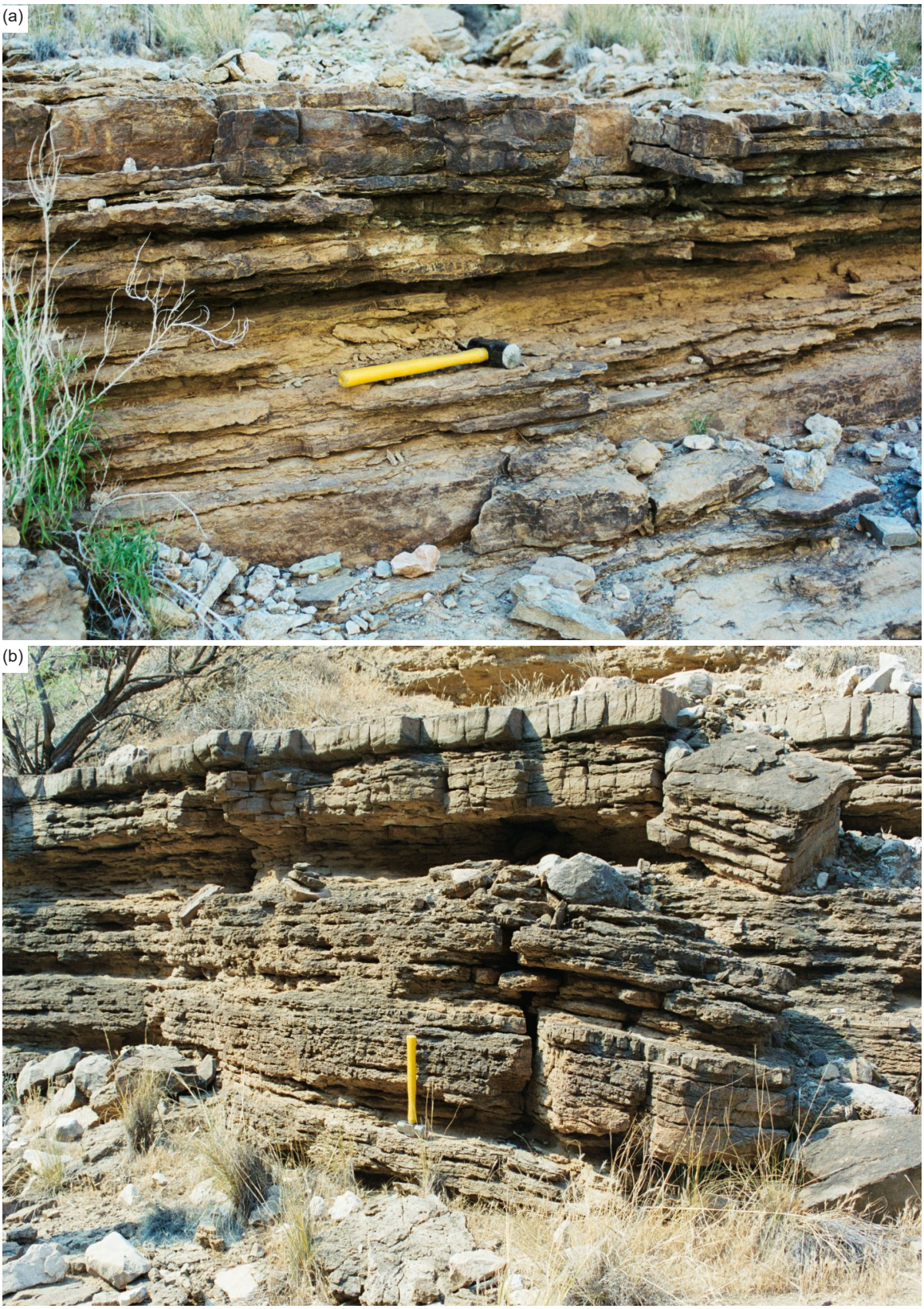

Fig. 12. Lithologies within the Bright Angel Formation in the eastern Grand Canyon. The large hammer and handle (~0.36 m or ~1.2 ft long) in each view provides the scale. (a) Alternating hard sandstone and siltstone beds at the top of the formation, with fossilized worm trails evident on the tops of some siltstone beds. This outcrop probably represents the red-brown sandstone capping a fining-upward sequence (Martin 1985) or parasequence (Rose 2003) (river mile 48.5). (b) Another outcrop of alternating hard calcareous sandstone and siltstone beds, the uppermost thicker sandstone bed capping a fining-upward sequence or parasequence (river mile 55.5).

consist of fissile shale, mudstone and siltstone, both flat-bedded and weakly cross-laminated (fig. 11). The deep color of these beds, plus some of them form a fairly prominent cliff about midway in the Bright Angel Formation, causes them to be conspicuous. No body fossils have been found in them, but small trace fossils and ripple marks are common, and locally muscovite flakes are abundant. In the same stratigraphic position in eastern Grand Canyon these "red-brown beds" are absent and in their place are mainly fairly massive beds from a few inches to a few feet (c.10 cm–1 m) in thickness which Noble (1922) called "magenta sandstones." These sandstones form weak but fairly prominent ledges in many places, especially in the upper part of the formation (fig. 12). They have a relatively coarse texture and consist largely of quartz grains with a ferruginous cement, but also contain ferruginous mud and hematite. Cross-lamination is locally well-developed, and small brachiopod shells showing signs of grinding and attrition are abundant in some of these beds.

Above the "red-brown beds" of western Grand Canyon and high up stratigraphically in eastern Grand Canyon is a laminated, quartzitic siltstone which is characterized by brown spots throughout a gray to buff rock (McKee 1945). The siltstone laminae range from 1/16 to ½ in (1.6–13 mm) thick and in a few places up to 2½ in (63.5 mm) thick. The brown spots, which are mostly between 1/16 and ¼ in (1.6 and 6 mm) in diameter, appear to be caused by local addition of ferruginous material. For the most part these brown spots are fairly evenly distributed through the rock, but they vary greatly in the total amount of space they occupy from 10 to nearly 90% of the rock.

McKee (1945) recognized one member in the Bright Angel Formation which he called the Flour Sack Member (fig. 5). It consists of shale, siltstone and limestone and forms the uppermost part of the formation in western Grand Canyon (fig. 10a). Limestone decreases in abundance toward the east until the entire member is shale at its easternmost outcrop near Quartermaster Canyon. Still another persistent lithology McKee (1945) described in the Bright Angel Shale is a laminated micaceous siltstone of uniform brown or greenish-grey color (figs. 10b and 11b). It forms the top part of the formation in western Grand Canyon and is part of all tongues that project from the east into the Muav Formation. It grades westward into laminated silty limestones that are assigned to the Muav, and eastward into green fissile shales. Tongues of hard dolomite which weather into conspicuous, rusty-colored cliffs in various parts of Grand Canyon are also included in the Bright Angel Formation (fig. 9). These dolomite tongues merge westward into massive limestones of the Muav Formation.

Like the rest of the Cambrian strata of Grand Canyon, the Bright Angel Formation crosses time-lines, becoming younger toward the east because deposition started in the west and progressed eastward. In the western part of Grand Canyon, the base of the formation lies below the *Ollenellus-Antagmus* assemblage zone that forms an event horizon (fig. 5). Therefore, the base of the Bright Angel Formation there is late Early Cambrian (Middleton and Elliott 2003), whereas in eastern Grand Canyon the lower third of the formation lies below the Middle Cambrian *Alokistocare-Glossopleura* assemblage zone event horizon (fig. 5).

Whereas McKee (1945) worked primarily in western Grand Canyon, starting at Grand Wash Cliffs, to the central Grand Canyon area reported previously by Noble (1914, 1922), he did comparatively little work on the eastern exposures, depending on the single generalized measured section of Wheeler and Kerr (1936) to characterize the stratigraphy of the eastern exposures. And yet, those few who have subsequently investigated the Bright Angel Formation have added little to describing and defining its stratigraphy.

Martin (1985) focused his work on the eastern exposures of the Bright Angel Formation, measuring six stratigraphic sections from Boucher Canyon (river mile 97) to Tanner Canyon (river mile 69). In these sections he recognized three predominant facies sequences that were repeated numerous times in the formation's stratigraphy, each characterized by its lithologies, sedimentary structures and ichnofaunal assemblages—coarsening-upward (fig. 13), cross-stratified (fig. 14), and fining-upward (fig. 15). The lithologies he identified consisted of mudstones, mottled siltstones, sandstones of various types (conglomeratic, massive bioturbated, hematitic oolitic, horizontally-stratified and cross-stratified, the latter either planar-tabular, trough, herringbone or hummocky). He also designated units of what he called heterolithics, which essentially are mixtures of lithologies, primarily minor sandstone within mudstone or sometimes siltstone, that are either lenticular and sometimes wavy or flaser bedded, or continuously interbedded. The coarsening-upward sequences are usually mudstone transitioning upward into siltstone, though sometimes further upward to sandstone, whereas the fining-upward sequences are almost exclusively within sandstones.

Elston (1989) and several of his associates measured five stratigraphic sections of the Tonto Group throughout Grand Canyon intermediate to those measured and compiled by McKee (1945), but also added four more stratigraphic sections of the far eastern exposures beyond Palisades Creek (river mile 66) as far as Marble Canyon (river miles 38-

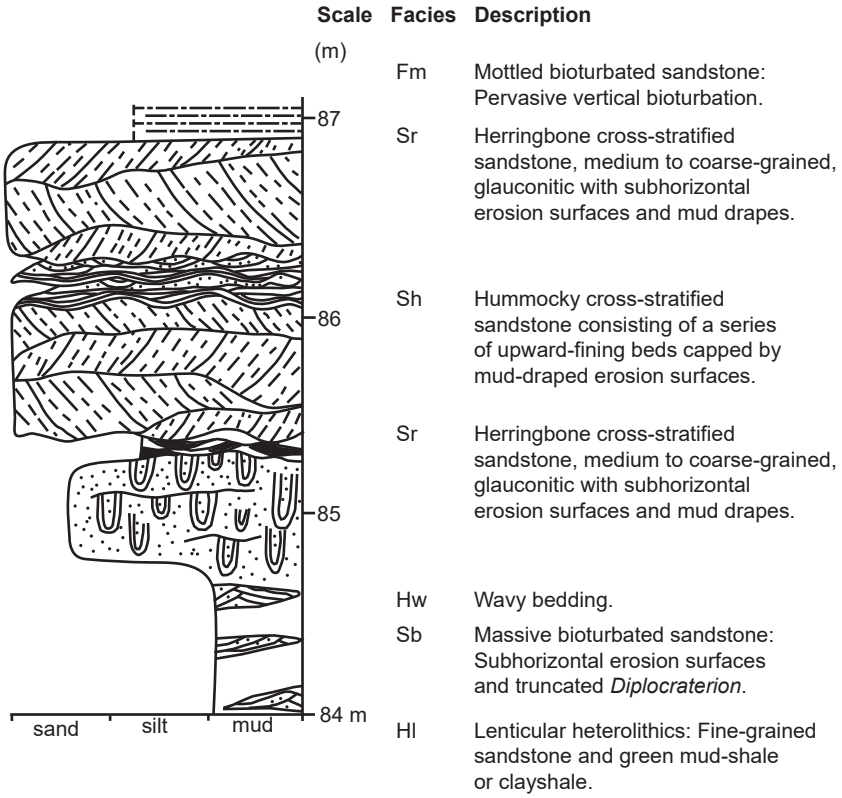

Fig. 13. Diagrammatic stratigraphic section at Horn Creek (river mile 90.8) of an idealized coarsening-upward sequence as described (after Martin 1985, 210, fig. 51a). The horizontal scale shows the grain sizes and the vertical scale is thickness in meters.

47), though two of those sections did not contain any Bright Angel Formation (see fig. 6 where his added stratigraphic sections are marked). In referring to the lithology correlation diagram of McKee (1945) showing the several distinctive units within the Bright Angel Formation (fig. 16), Elston (1989) noted that near the Grand Wash Cliffs to the west the Bright Angel Formation is dominated by limestone units and the proportion of shale increases in an easterly direction (figs. 6a and 16). Furthermore, the limestone beds in the west pass laterally into dolostone beds in central Grand Canyon, and these in turn become glauconitic sandstone beds in eastern Grand Canyon (figs. 6 and 16). In fact, exposed at river level along miles 50–60 the Bright Angel Formation consists dominantly of silty sandstone, and intervals of slightly more resistant, magenta-colored, glauconitic sandstone are seen to be distributed across the sandstone section (fig. 6b), similar to the distribution of dolostone and sandy dolostone units in the Bright Angel Formation to the west (fig. 6a).

Therefore, Elston (1989) proposed the provisional correlations shown in fig. 6. As documented by McKee (1945), the facies changes in the Bright Angel Formation are evident in the east-to-west direction. Elston (1989) determined that the purplish or magenta-colored sandstone beds of the Bright Angel Formation in eastern Grand Canyon appear to correlate with beds that become yellowish-brown to reddish-brown dolostone beds in central Grand Canyon, and these dolostones then grade laterally into limestone members of the Bright Angel Formation to the west. A thickness increase also accompanies these facies changes westward in the Bright Angel Formation, and sandstone and mudstone-siltstone decrease as limestone increases. Furthermore, in western Grand Canyon between the Peach Springs Member of the Muav Formation and the Flour Sack member of the Bright Angel Formation, McKee (1945) had identified four members or tongues which he had assigned to the Muav Formation (figs. 5 and 16). Later, Elston (1989) assigned them to the Bright Angel Formation instead of the Muav Formation (fig. 6). This assignment and the lateral continuity of the members thus removed the need for the upward shingling or intertonguing at the base of the Muav Formation as suggested by McKee (1945) in his lithology-based nomenclature (fig. 5).

Middleton (1989) summarized the stratigraphy of the Bright Angel Formation based on the work of McKee (1945) and Martin (1985). The formation is over 135 m (443 ft) thick in western Grand Canyon, thinning markedly towards the east, and also younging towards the east. In western Grand

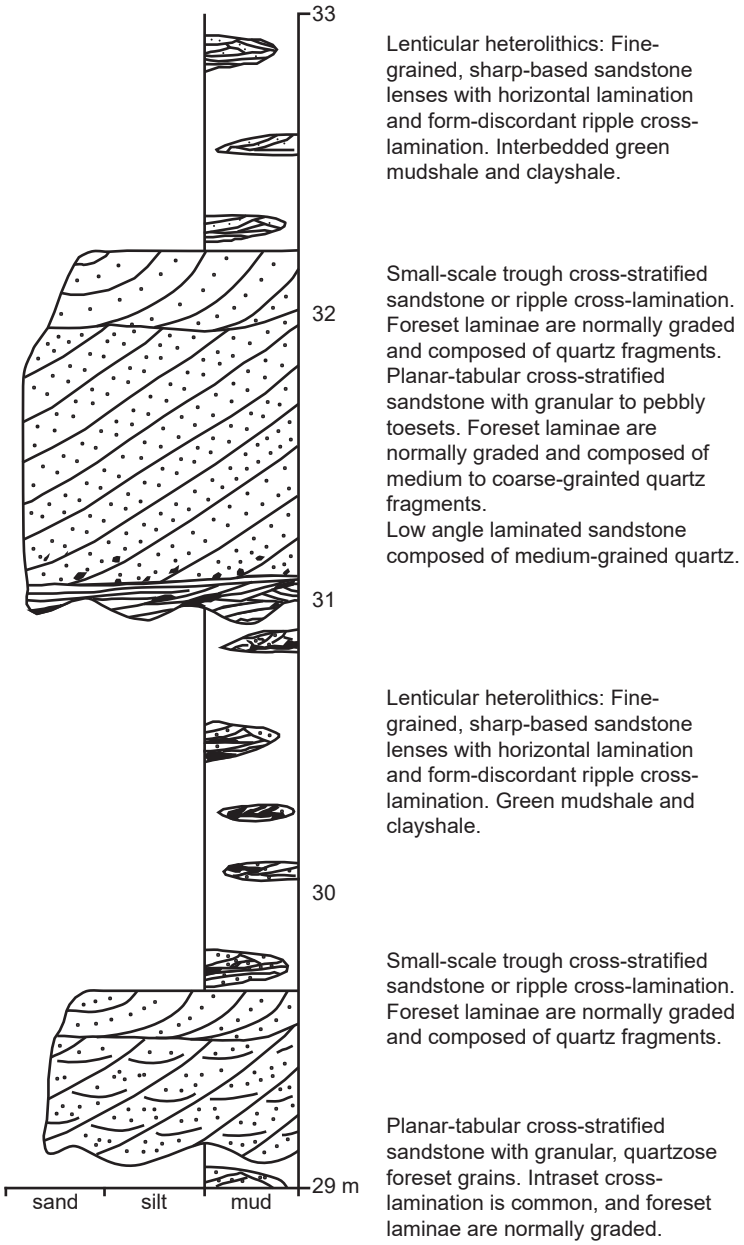

Fig. 14. Diagrammatic stratigraphic section at Tanner Canyon (river mile 69) illustrating the various cross-stratified sandstone beds in a sequence with interbedded lenticular heterolithics as described (after Martin 1985, 215, fig. 54). The horizontal scale shows the grain sizes and the vertical scale is thickness in meters.

Canyon, the base of the formation lies below the *Olenellus-Antagmus* fossil assemblage zone and hence is designated as late Early Cambrian, whereas in eastern Grand Canyon the upper two-thirds of the formation lies above the *Alokistocare-Glossopleura* fossil assemblage zone and thus is designated as Middle Cambrian. Although the formation typically overlies the Tapeats Sandstone, the Bright Angel Formation unconformably and directly rests on Precambrian rocks where the basement relief is extreme. It primarily consists of shale, siltstone and sandstone, the latter being more common near the formation's base, although sandstones occur at several horizons within the formation. And in addition to sand- and silt-sized grains of quartz, feldspar and sedimentary rock fragments, glauconitic grains and hematitic ooids are also common.

Rose (2003) collected stratigraphic data from 29 representative full and partial measured sections at sites throughout the western, central, and eastern Grand Canyon. He recognized the same problem that Elston (1989) did with McKee's (1945) placement of the boundary between the Bright Angel and Muav Formations in the western Grand Canyon. Furthermore, Rose (2006, 2011) remarked that no type section yet exists for the Tonto Group or any of its constituent units, even though the section described by Noble (1922) along the Bass Trail has

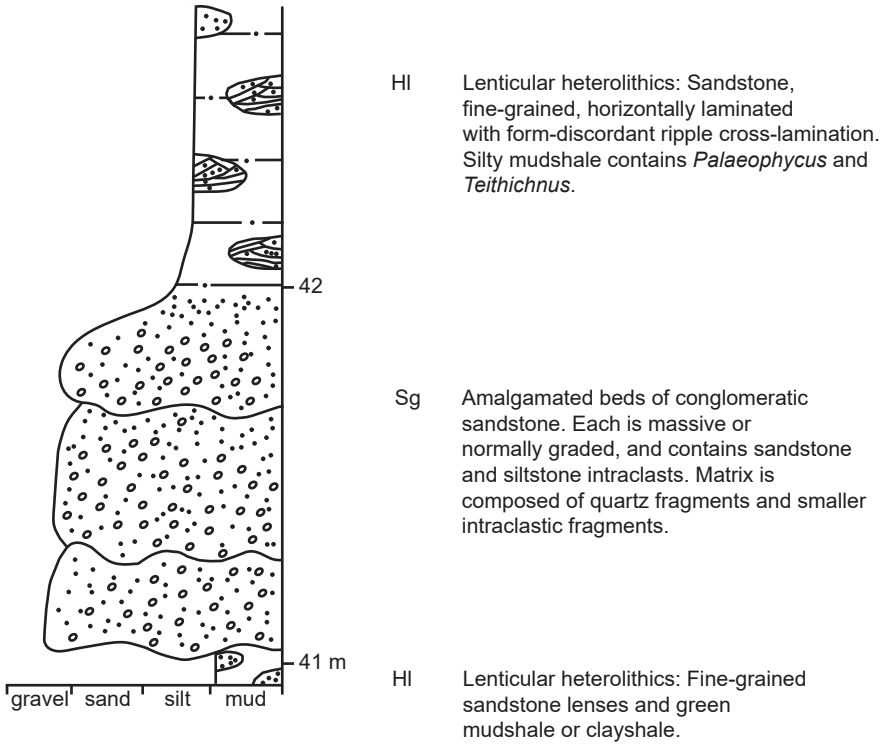

Fig. 15. Diagrammatic stratigraphic section at Horn Creek (river mile 90.8) of an idealized fining-upward sequence consisting of amalgamated conglomeratic sandstone beds that are normally graded and then grade upwards into lenticular heterolithics (after Martin 1985, 176, fig. 28c). The horizontal scale shows the grain sizes and the vertical scale is thickness in meters.

served as a *de facto* type section. McKee (1945) had used the Bright Angel Creek section only for defining and naming the Bright Angel Formation. Rose (2003) proposed his measured section at Blacktail Canyon (river mile 120.5) as a suitable formal type section (fig. 1, and Appendix B in the Supplementary material), because it is accessible from the Colorado River, and because it is between two long straight stretches of the river, which provides a clear view in both directions of the continuity of marker beds and the cliff-slope profile that help define unit boundaries (Rose 2011). However, Rose (2003) provided extra details of his measured section through the Bright Angel Formation at the location he called Crazy Jug (fig. 17), which is close to the Tapeats Creek area only about 11 miles (~18 km) to the north of his Blacktail Canyon measured section proposed as the Tonto Group type section (fig. 1 and Appendix B in the Supplementary material). Yet the differences in the detailed stratigraphy of the Bright Angel Formation over such a short distance are readily evident from a comparison between the Crazy Jug and Blacktail Canyon stratigraphic sections (figs. 17 and 18).

Rose (2003) described some four facies within the Bright Angel Formation. Chief in abundance is a green fissile shale, which is predominantly interbedded at centimeter scale with a well-sorted pale pinkish-tan fine quartz sandstone, but which can take on other colors ranging from dark reddish-brown to pale yellowish gray, medium greenish gray and medium gray (depending on its glauconite, hematite or other mineral content). Dark reddish-brown colors are not nearly as common as grayish green colors and are loosely coincident with increasing thickness and/or abundance of sandstone layers, especially those that are arkosic or hematite-stained. McKee (1945) had recognized brown spotted sandstone beds as a distinct facies, but Rose (2003) concluded such were just an intermediate step to the fully hematite-stained sandstones. Rose (2003) noted that the thicknesses of interbedded sandstone layers vary from a few millimeters to tens of centimeters (~0.2-inch to16 or more inches) and are usually consistent in thickness, or may gradationally thicken or thin up-section, even in bundled trends for up to five cycles. Martin (1985) had denoted these green fissile shales with the interbedded sandstones as heterolithics.

Rose's (2003) second facies is green crumbly siltstone, the same as McKee (1945), but comparable to the mottled siltstone of Martin (1985). This green crumbly siltstone is a highly bioturbated, variously micaceous, glauconitic and /or hematitic admixture of the more abundant mudstone-sandstone interbeds with which it commonly overlies in gradational contact. His third facies is glauconite-rich horizons which occur most commonly in

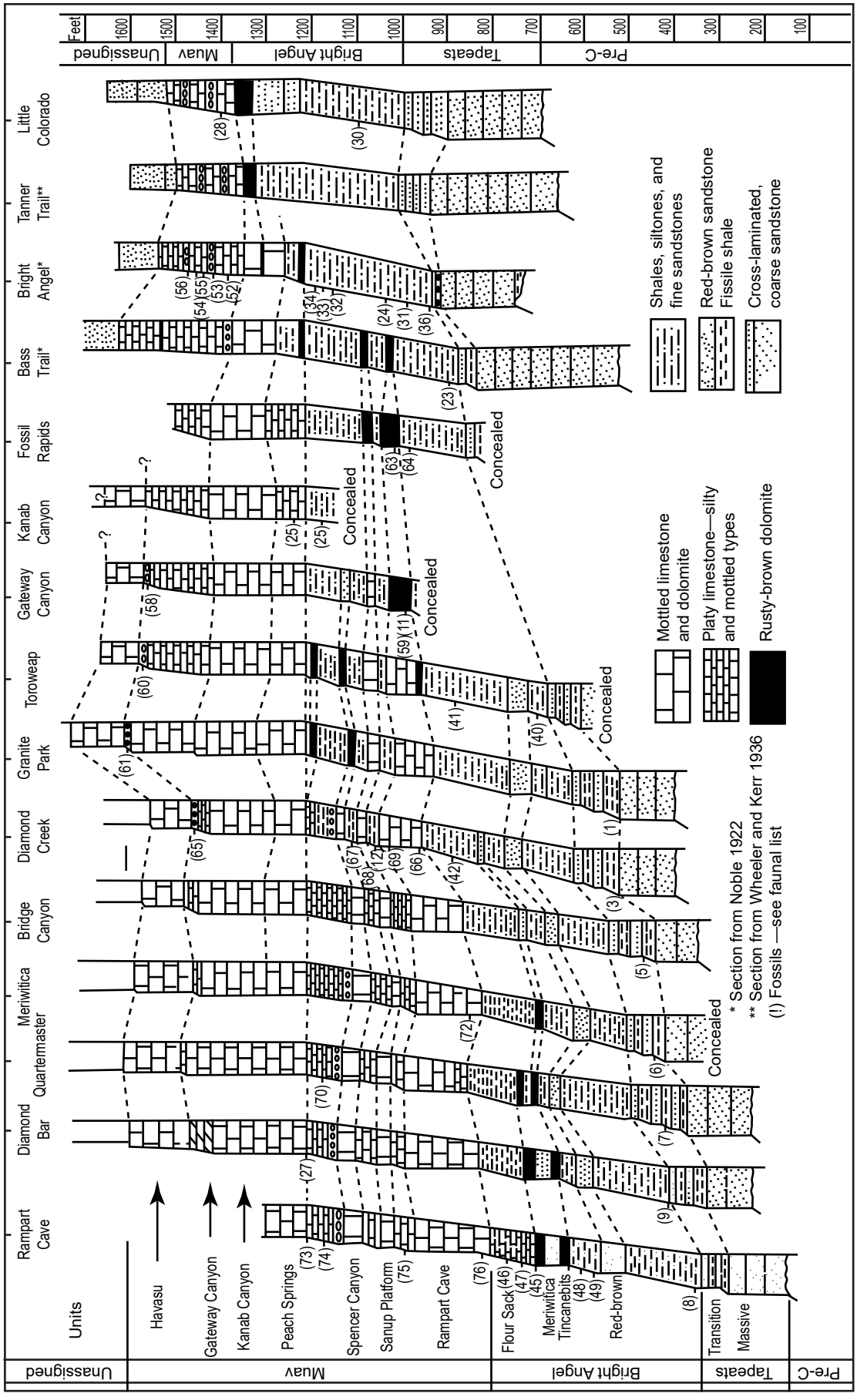

Fig. 16. The McKee (1945, 19, fig. 2b) correlation of the Tonto Group units and formations based on lithologies (after Elston 1989, 132, fig. 15.1).

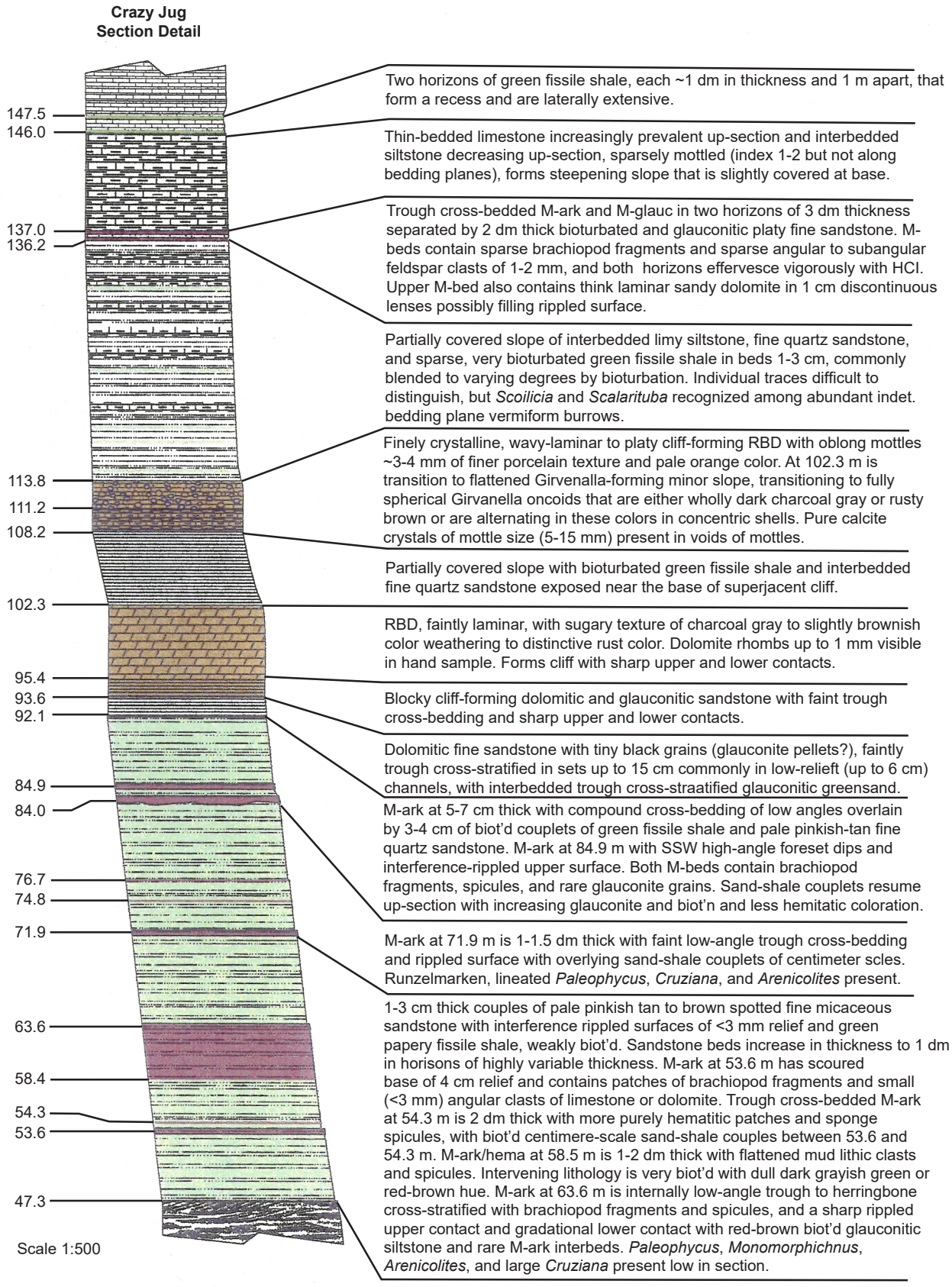

Fig. 17. Detailed measured stratigraphic section of the Bright Angel Formation at the Crazy Jug location marked on fig. 1 (after Rose 2003, 246; Rose 2011, 94, fig.5).

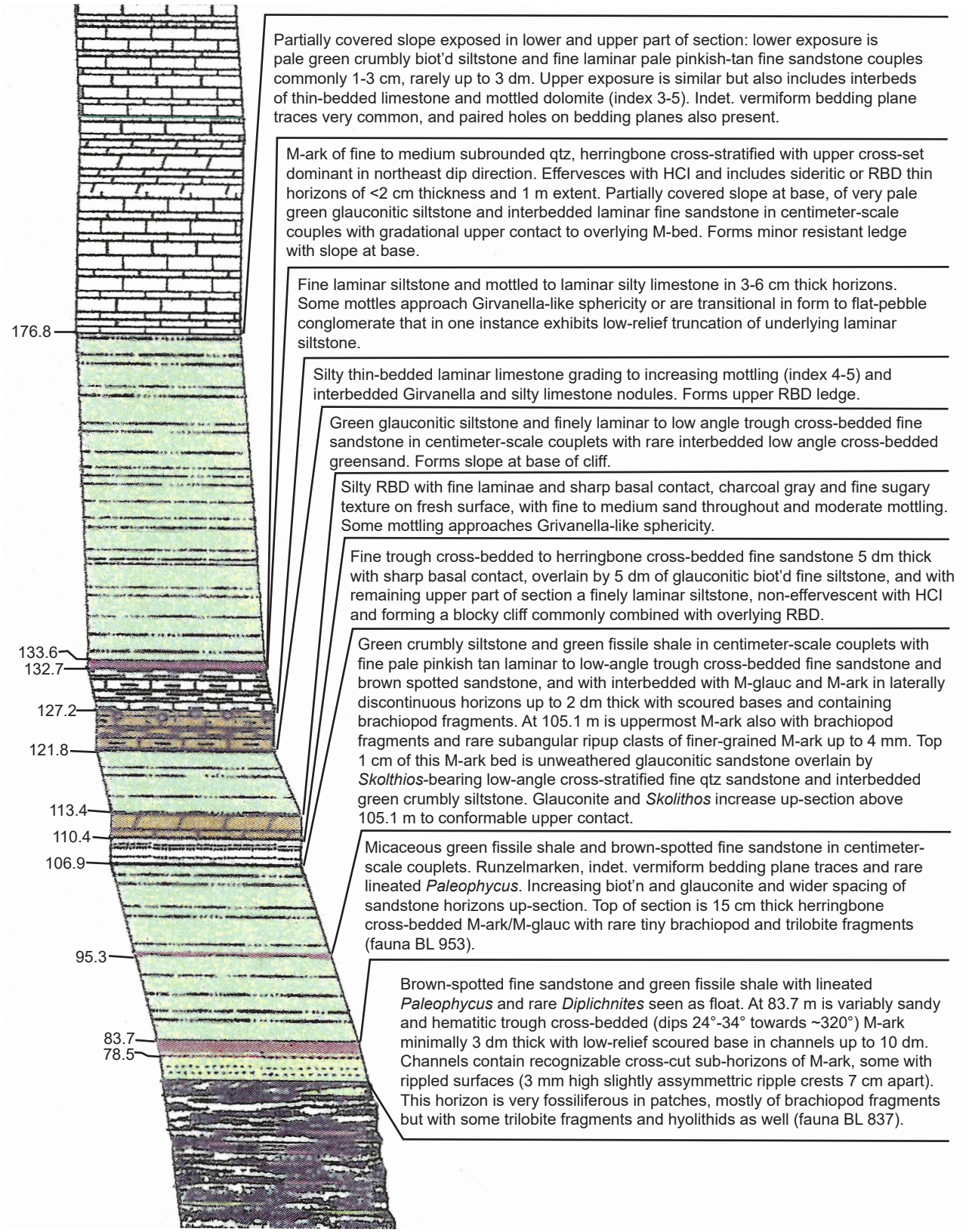

Fig. 18. Detailed measured stratigraphic section of the Bright Angel Formation at the Blacktail Canyon (river mile 120.5) location marked on fig. 1 (after Rose 2003, 242; Rose 2011, 95, fig. 6).

association with the green crumbly siltstone facies. The concentration of glauconite varies from a few widely distributed individual grains to greensands of over 40% glauconite in diffuse horizons a few centimeters to several decimeters (~1in to ~1.5ft) in thickness.

Rose's (2003) fourth facies is magenta-colored sandstones, the resistant iron-rich maroon to red-brown sandstones also recognized by Noble (1922) and McKee (1945). Rose (2003) designated three type lithologies in this facies—hematitic magenta sandstones (the least prevalent), glauconitic magenta sandstones and arkosic magenta sandstones (the most prevalent). These lithologies are highly variable, showing various gradations between one another and with unaltered greensands and green crumbly siltstone. The hematitic and glauconitic magenta sandstone beds are typically 10–50cm (~4in to ~1.6ft), whereas the arkosic magenta sandstone beds range from a few millimeters (~0.2in) in thickness to prominent resistant cliffs a few meters (up to ~16ft) in height. Some arkosic magenta sandstone beds are poorly sorted and include a very coarse component in which unaltered angular feldspar clasts may reach small-pebble size of 4–10mm (~0.15–0.4in). Sub-rounded clasts of similarly hematite-cemented arkosic sandstones may also be present with the coarse component in sizes commonly as large as 4–14cm (~1.6–5.5in) and are commonly irregular blade-like or oblate in shape. A few of these beds have also yielded identifiable fossil fragments, but local concentrations of shelly material are dominated by a "hash" of unidentifiable weathered and eroded fossil fragments.

Rose (2006, 2011) added little to his above description of the lithologies within the Bright Angel Formation but emphasized that exposed slope-forming sections of the formation consist of a dominant heterolithic lithology of cm-scale pale pinkish-tan sandstone and green fissile shale couplets. These couplets occur as the basal part of typical facies stacking patterns and define an apparent overall architecture of stacked parasequences. Rose (2003) had recognized two such stacking patterns in the Bright Angel Formation—a magenta arkosic sandstone capping parasequence (fig. 19), and a carbonate capping parasequence (fig. 20). In both parasequences the green fissile shales coarsen upwards into green crumbly siltstone. This stacking pattern occurs at a scale of several meters to tens of meters as apparent bioturbation becomes more infaunal than epifaunal up the stack, with the result that layers are disrupted and homogenized with an apparently increasing amount of added glauconite. This is the same as the green crumbly siltstone facies of McKee (1945), which typically is in recess-forming beds exposed below capping ferruginous (magenta) sandstone layers that occur in apparent sharp, eroded channels cut within the underlying siltstone (fig. 19). Such ferruginous sandstone layers form prominent resistant marker beds that are traceable laterally for several tens of meters or more. Nevertheless, the lateral variations in lithologies within the Bright Angel Formation and the lack of consistent laterally extensive marker beds, as seen by comparing detailed measured sections only miles apart (figs. 17 and 18), makes defining a type section difficult. The exception are the tongues or members originally mapped by McKee (1945) (fig. 5) and confirmed by Elston (1989) (fig. 6).

Paleontology of the Bright Angel Formation

McKee (1945) noted that fossils are locally very common in the Bright Angel Formation, but in general, determinable forms are difficult to find. However, well-preserved trilobites and some brachiopods are in some of the green fissile shales (fig. 21) and in brown-spotted laminated siltstones. Furthermore, shells of linguloid brachiopods are abundant in some of the magenta and also buff sandstones. But as noted by Rose (2003), local concentrations of shelly material are dominated by a "hash" of unidentifiable weathered and eroded fossil fragments. Almost everywhere in the formation are abundant trails, what McKee (1932) called fucoid-like casts, and vertical borings of worms. Resser (1945) provided a detailed cataloging of all fossils collected from 74 listed localities by numerous workers including Walcott, Noble, Wheeler and McKee, 35 of which were in the Bright Angel Formation, and systematic descriptions of all species.

Since that early work by McKee (1945) and Resser (1945) there has been virtually no work done on the taxonomy and biostratigraphy of Cambrian strata in the Grand Canyon (Middleton and Elliott 2003). Indeed, Foster (2011) agreed that very little more has been learned about the paleofaunal record of the Bright Angel Formation in Grand Canyon since 1945. Thus, the systematics of the invertebrate fauna buried in the Bright Angel Formation remain the same.

Invertebrates

Despite the paucity of well-preserved invertebrate fossils, analysis of the fauna has provided information on the biostratigraphic zonation of the Tonto Group (Middleton and Elliott 2003). Trilobites and brachiopods are the most abundant fossils reported from the Tonto Group, though most specimens are poorly preserved. Fragments of sponges, "primitive" mollusks, echinoderms, and algae occur in the Bright Angel Formation, but these fossils are not very abundant.

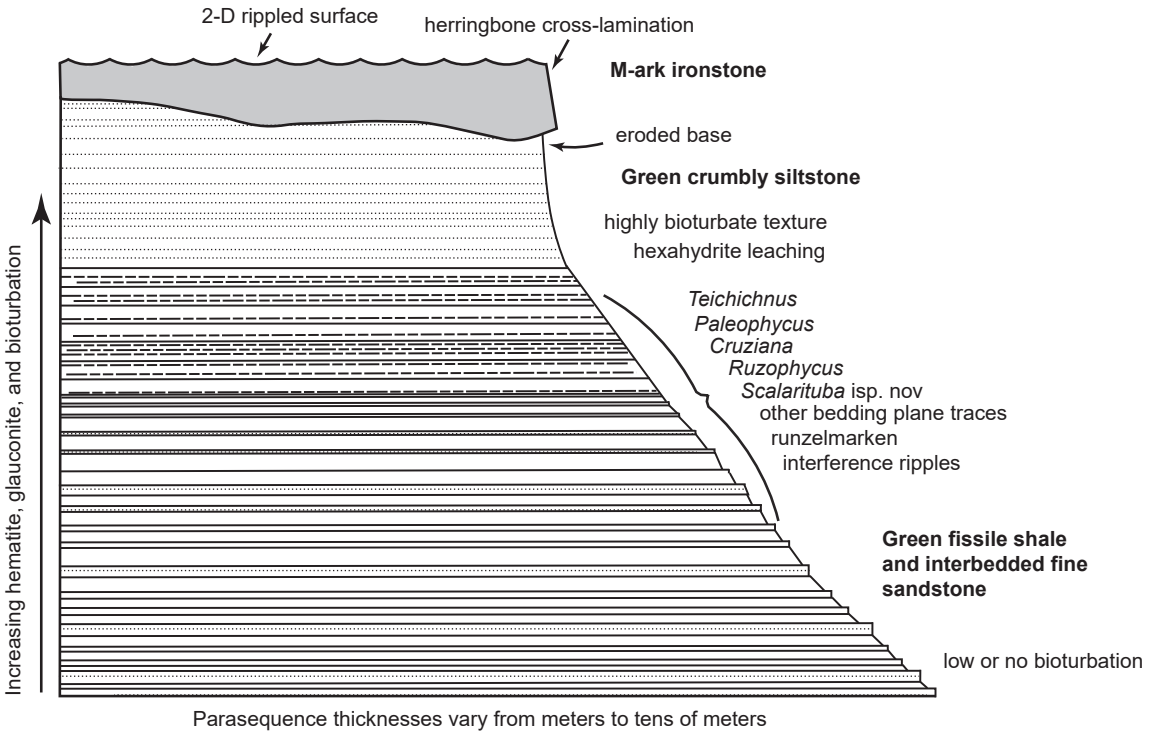

Fig. 19. A generalized diagrammatic representation of a magenta (hematitic) sandstone bed capped parasequence in the Bright Angel Formation (after Rose 2003, 85, fig. 57a). This shale-siltstone-sandstone fining-upward sequence is similar to those recognized by Martin (1985). Thicknesses vary from meters to tens of meters. Note the contact of the sandstone bed scoured into the underlying laminated crumbly siltstone.

Trilobites are the most abundant fossils in the Tonto Group generally, and common genera include *Olenellus*, *Antagmus*, *Zacanthoides*, *Albertella*, *Kootenia*, *Glossopleura*, and *Bolaspis*. Most specimens are poorly preserved, occurring in the coarser-grained sandstones and also in the green fissile shales of the Bright Angel Formation (fig. 21). Resser (1945) reported 47 species of trilobites from the Tonto Group and suggested that these arthropods were to some degree facies-specific.

More than thirty body fossil localities are known in the Bright Angel Formation within Grand Canyon National Park (Foster 2011). The middle Cambrian part of the Bright Angel Formation overall contains a respectable diversity of species (table 1), including at least four genera of brachiopods, one of hyoliths, and four genera of possible bradoriid arthropods, along with fifteen species of trilobites, and two species of eocrinoids. Most sites are in levels within the *Glossopleura walcotti* zone of the Delamaran Stage, Lincolnian Series. Two quarries in the Bright Angel Formation on the Tonto Platform near the South Rim have produced, together, at least 630 specimens and 8 species of hyolithids, brachiopods, trilobites, and eocrinoids.

In 1911, Cameron worked a site in the Bright Angel Formation in eastern Grand Canyon, on the Tonto Platform not far from Indian Garden below the South Rim, where he found several trilobite specimens. He eventually sent some of the specimens to Walcott at the Smithsonian Institution, who published illustrations of some of them (Walcott 1916a, b, 1924, 1925). In 1915, Walcott dug at the same site for a day or so. In 1930, McKee worked at the site and also made a significant collection, consisting of about 100 specimens and at least eight taxa (Foster 2011). The site is approximately 41 m (~135 ft) above the base of Bright Angel Shale Formation and is in a light green, slightly silty shale (fig. 22).

The second site is also near Indian Garden. It may have been found originally by Wheeler and Kerr in 1935, but it is known that it was worked at least in 1936 by McKee. Original records show that this McKee Quarry site is not far from the Cameron-Walcott Quarry, but they are distinct. Even though McKee worked this quarry in 1936, records show McKee collected more than 200 partial and complete trilobite specimens at this site in 1930 (Foster (2009). The McKee Quarry was relocated in 2009 (Foster 2011), when several brachiopod shells and trace fossils (*Rusophycus*) were found there. The McKee Quarry site occurs in a green to greenish-gray shale, about 25 m (~82 ft) above the lower contact of the Bright Angel Formation with the Tapeats Sandstone (fig. 22). This site may be the same as locality 31 in McKee (1945) and Resser (1945), but this is uncertain

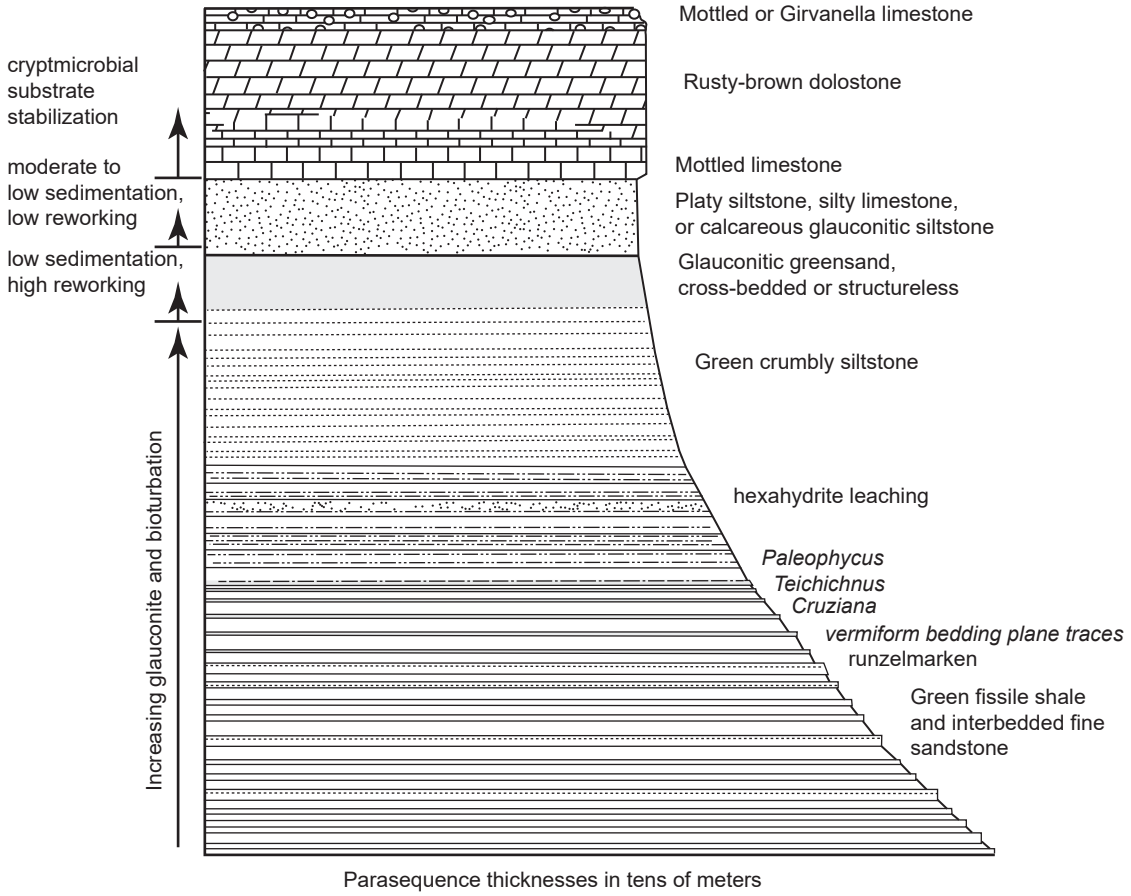

Fig. 20. A generalized diagrammatic representation of a rusty-brown (hematitic) dolostone (RBD) bed capped parasequence in the Bright Angel Formation (after Rose 2003, 87, fig.58a). Thicknesses vary from meters to tens of meters. Note the sharp contact between the darker colored dolostone cap and the underlying bioturbated crumbly siltstone.

(Foster 2011). The taxa listed are similar, the worker dates appear mostly compatible, and the description of the location is very roughly compatible.

Trilobites are the most numerous and diverse taxa, and one of the quarries has yielded several type specimens (Foster 2011). Among the trilobites are:

Fig. 21. Trilobite fossil, probably *Anoria tontoensis* (Walcott 1916b), from green fissile shale within the Bright Angel Formation, Grand Canyon. This specimen was on display in an exhibit at Yavapai Point on the South Rim and likely came from one of the two quarries worked for fossils below the South Rim, probably the Cameron-Walcott quarry (see text). Scale bar is ~5 cm (~2 in).

(1) an indeterminate species of *Amecephalus*, probably either *A. packi* or possibly *A. piochensis*;
(2) several well-preserved specimens of *Amecephalus althea*;
(3) *Kootenia*, rare in the Bright Angel Formation;
(4) relatively abundant specimens of *Glossopleura boccar*;
(5) rare specimens of *G. walcotti*?; and
(6) numerous specimens of "*Anoria*" *tontoensis* (fig. 21).

Most characters used to distinguish *Glossopleura* and "*Anoria*" prove to be non-diagnostic, but they were retained as separate genera by Foster (2011). Preservation of trilobite skeletal elements at these sites suggests that both contain a relatively high percentage of complete specimens, although this ratio is probably inflated to some degree by collecting bias.

The trilobite samples from the McKee Quarry and the Cameron-Walcott Quarry number just over 500 specimens and 100 specimens, respectively (fig. 23) (Foster 2011). The McKee Quarry is dominated by the dolichometopids *Glossopleura boccar* and "*Anoria*" *tontoensis* which are graphed together here due to their similarity, especially among isolated

Table 1. Faunal list for the middle Cambrian part of the Bright Angel Formation in Grand Canyon, mostly the *Glossopleura walcotti* zone but including some biostratigraphically higher taxa. This was compiled and modified from McKee (1945) and Resser (1945) and also based in part on data from Foster (2011), so taxonomic identification of some species may have changed since McKee's (1945) and Resser's (1945) listing. This listing is mostly from the Flour Sack Member of the Bright Angel Formation and lower, although some stratigraphically higher species are included. *Indicates species known from the McKee Quarry and/or Cameron-Walcott Quarry (after Foster 2011, 100).

Brachiopoda	**Trilobita**
Paterina superba	**Corynexochida**
Dictyonina arizonaensis	*Zacanthoides walapai*
D. crenistria	*Albertella schenki*
Lingulella euglypha	*Ptarmigania* sp.
*L. chuarensis**	*Clavaspidella* sp.
L. spatula	*G. mckeei* (= *G. boccar*)*
L. lineolata	*"Anoria" tontoensis**
L. zetus	*Glyphaspis* sp.
L. themis	*Kootenia* sp.*
*L. mckeei**	**Ptychopariida**
Nisusia obscura	*Amecephalus althea**
Hyolitha	*Amecephalus* sp. cf. *A. packi**
Hyolithes sp.*	*Acrocephalops ?arizonaensis*
Arthropoda	*Parehmania tontoensis*
Bradoriida?	*Elrathia nitens*
"*Bradoria tontoensis*"	*Pachyaspis fonticola*
Dielymella appressa	*Spencia tontoensis*
D. dorsalis	**Echinodermata**
D. nasuta	**Eocrinoidea**
D. recticardinalis	*Gogia multibrachiatus**
Indianites curtus	*Gogia? longidactylus**
Indianites impressus	
Walcotella apicalis Walcottella spp. (12 additional species from one site)	

pygidia. Together they make up about 27% of the sample. Ptychopariids constitute 15% of the sample at the McKee Quarry, and among these are at least eight complete, articulated *Amecephalus althea*. There are six specimens in the sample, identified as *Amecephalus* sp. on the graph, that are clearly different species from *A. althea* and that probably contain *A.* cf. *packi* and possibly *A. piochensis*. The Cameron-Walcott Quarry is dominated by "*Anoria*" *tontoensis* but also contains a significant component of *Glossopleura*, mostly *G. boccar* but also with at least two *G.*? *walcotti*. *Kootenia* is also present but rare at this site. *Amecephalus* sp. is less abundant here than at the McKee Quarry, and it is unclear what species these specimens represent.

Relative abundances of trilobite elements are shown for the two quarries (fig. 24) (Foster 2011). There is an abundance of isolated pygidia and an odd lack of isolated thoracic segments and other sclerites at the Cameron-Walcott Quarry. Such elements constitute nearly 30% of the sample at the McKee Quarry. Foster (2011) suggested that the absence of isolated sclerites at the Cameron-Walcott Quarry may be a result of a much smaller sample size not having picked up this component, or it may have to do with different collecting styles between the different collecting crews, the earlier workers possibly having left unidentifiable trilobite remains and single elements in the field.

The number of complete, articulated trilobite molts and skeletons (including those missing only the librigenae) is high at both sites, compared to isolated trilobite elements, at about 17–20% (fig. 24). Although this probably reflects a real trend of greater articulation percentage at these sites than in many other formations in the Cambrian of western North America, the degree of articulation was probably inflated by collecting bias in favor of well-preserved specimens. The true degree of articulation at these two Bright Angel Formation sites in Grand Canyon

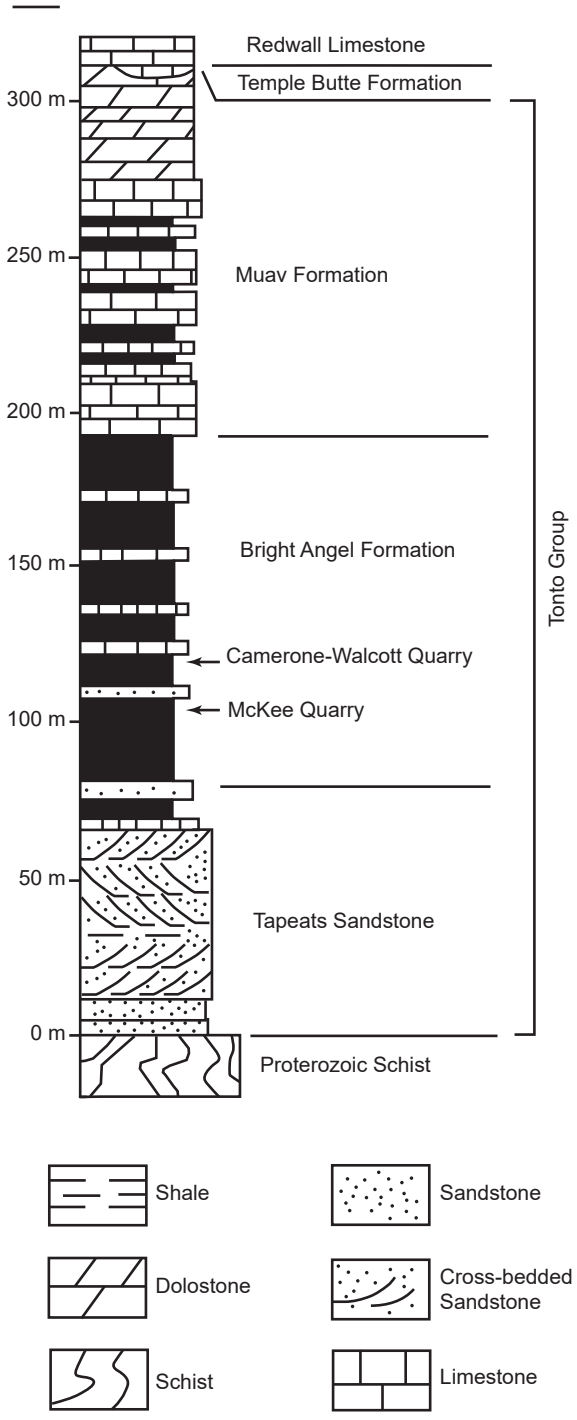

Fig. 22. Generalized stratigraphic section of the Tonto Group in the Grand Canyon showing the stratigraphic positions of the Cameron-Walcott Quarry and the McKee Quarry, as taken from the notes of E. D. McKee in Grand Canyon museum collections records (after Foster 2011, 104, fig.3.2).

is probably lower than seen in these two quarries (Fig. 24). In both Bright Angel Formation quarries, the high ratio of complete specimens, pygidia, and cranial elements to rarer isolated thoracic segments and to hypostomes suggests winnowing or some other taphonomic filter.

Orientation data were taken by Foster (2009, 2011) on nineteen slabs of shale from the McKee Quarry, each containing from three to fourteen trilobite specimens ranging from isolated pygidia to complete specimens. Although the *in situ* up-down orientation of the slabs in outcrop had not been recorded, the sclerites appear in individual slabs to have preferred orientations. The ratios range from 3:3 ("up" versus "down", as preserved within-slab) up to 10:0. Even the slab with the most specimens on it has a ratio of 13:1. Nearly half the slabs have preferred up-down sclerite ratios with binomial probabilities significant at the 95% level (for example, ratios of 13:1, 10:0, 9:1, 9:0, 8:0), and the chance probability of several of the slab ratios is <0.001. The average ratio for the nineteen slabs from the McKee Quarry is 85.6% one orientation over the other (Foster 2009, 2011). This is a higher ratio than at the Cameron-Walcott Quarry, which has a per-slab average of 71.5% one orientation over the other (twelve slabs with 9–26 cranidia each in ratios 5:4 to 17:1).

Unfortunately, the Bright Angel Formation slabs studied by Foster (2009, 2011) contain no ripple marks or other potential post-collection indicators of original-up. He concluded that it is therefore impossible to know based on these data if the average preferred orientation from the McKee Quarry slabs reflects the true orientation of the full sample in the outcrop. The data do at least hint at a strong trend in up-down orientation of *Glossopleura* and *Amecephalus* sclerites, suggesting that biostratinomic characteristics of the material may have been directly influenced by external factors to a higher degree than within the Cameron- Walcott Quarry. The sclerites do not seem to have become extensively fragmented. These combinations of characters seemed to suggest to Foster (2009, 2011) relatively rapid burial and some current activity, but the fine-grained nature of the sediments and apparently low level of fragmentation of the material indicated that the site was possibly not in a particularly high-energy environment.

Brachiopods are locally abundant in the coarser-grained sandstones of the Bright Angel Formation (Middleton and Elliott 2003). The most common genera are *Lingulella*, *Paterina*, and *Nisusia*. Martin (1985) commented that whole shells average 0.75 cm (0.3 inches) long, and while whole specimens are occasionally preserved, they are not in the common bed-perpendicular life position. In general, the brachiopods tend to occur in beds containing few other invertebrate taxa, the majority being fragmented and stratified in the sandstone beds (Martin 1985), although Foster (2011) also reported the few brachiopod fossils found in the green fissile shales in the Cameron-Walcott and McKee Quarries. Disarticulated shells of *Lingulella chuarensis* (Resser

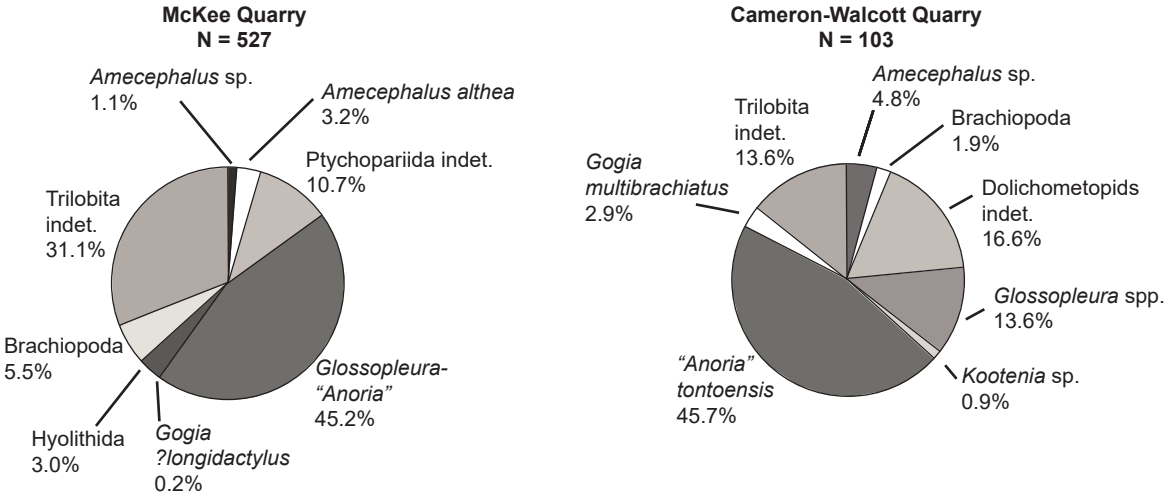

Fig. 23. Pie charts showing fossil taxa and relative abundances preserved at the McKee Quarry and the Cameron-Walcott Quarry in the Bright Angel Formation, Grand Canyon (after Foster 2011, 116, fig.12).

1945, 189, plate 17, figs. 17–21 and plate 18 figs. 22, 23; Walcott 1898, 399; Walcott 1901, 691) occur at both sites – two shells from the Cameron-Walcott Quarry and at least 25 from the McKee Quarry. Specimens of *Lingulella mckeei* (Walcott 1898, 399; Walcott 1901, 691) were also found. However, Foster (2011) noted that its difference in shell shape with *Lingulella chuarensis* is modest and certainly less than that between either species or several others of *Lingulella* known from the Bright Angel Formation so that they may not be separate species.

Paleontologists have reported a number of species of "primitive" mollusks (Conchostraca) from the coarser-grained, hematitic sandstone of the Bright Angel Formation (Middleton and Elliott 2003). The association of these fossils in coarser-grained sandstones led Resser (1945) to speculate that these mollusks occupied shallow-water habitats, but documentation of this possible environmental zonation is unsubstantiated.

Middleton and Elliott (2003) recorded that echinoderms and gastropods have been described from the Tonto Group, though they certainly are the rarest taxa. They reported two well-preserved specimens of the echinoderm *Eocrinus* from the Bright Angel Formation. Their excellent preservation might suggest relatively quiet water environments, or more likely rapid burial.

Foster (2011) reported the two partial specimens, each with part and counterpart molds, and the single partial specimen of the echinoderm *Eocrinus multibrachiatus* (Kirk 1945, 185–187, plate 16, figs. 1–5) found in the Cameron-Walcott Quarry. The calyx and brachioles of each specimen are well-preserved and there appear to be close to 40 brachioles in this species. Also, a partial calyx and stalk of *Eocrinus longidactylus* (Walcott 1886, 820, plate 5, fig. 3, and plate 6, figs. 1, 1a–1c) was found in the McKee Quarry. The species *E. longidactylus* appears to have had approximately twenty brachioles (Kirk 1945).

The clade Lophophorata is represented by several well-preserved species from the Bright Angel Formation of *Hyolithes*. Foster (2011) reported that indeterminate hyolithids are represented by 16 conchs from the McKee Quarry. At least one of

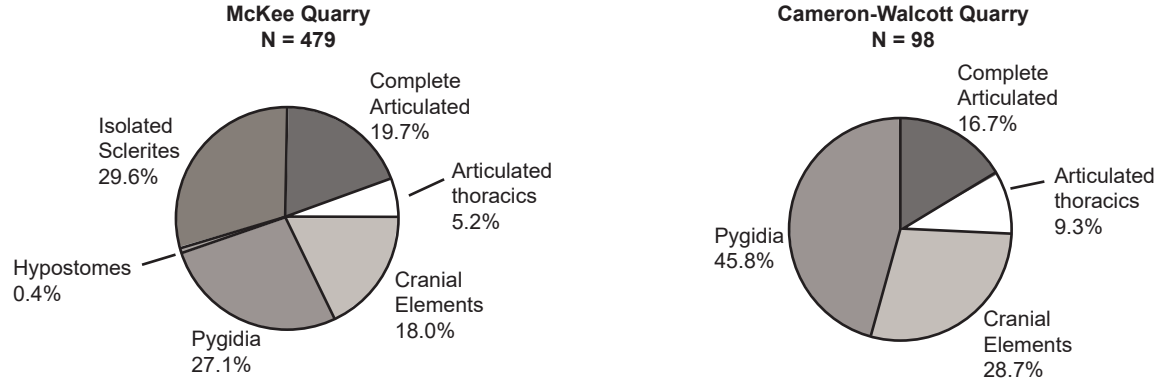

Fig. 24. Pie charts showing relative abundances of elements of trilobites preserved at the McKee Quarry and the Cameron-Walcott Quarry in the Bright Angel Formation, Grand Canyon (after Foster 2011, 117, fig.13).

these has an articulated operculum preserved as well. There are nearly thirty specimens that may be hyolithid opercula also, but these could not be distinguished from possible brachiopod shells or fragmentary trilobite sclerites due to the preservative put on the specimens in the field. Most hyolithid specimens in the Bright Angel Formation were referred to *Hyolithes* sp. by Resser (1945), but their preservation prevents more detailed identification.

Elliott and Martin (1987a) described six-rayed sclerites which they assigned to the genus *Chancelloria* from the Bright Angel Formation along Horn Creek in the central Grand Canyon. Although Walcott (1920) considered *Chancelloria* to be a sponge (Phylum Porifera), Rigby (1976) and Elliott and Martin (1987a) questioned the assignment of this genus to that phylum and suggested that *Chancelloria* represents a separate, yet unknown, phylum.

Cryptospores

Middleton and Elliott (2003) noted that algae had been reported from the Tonto Group but did not specify where. However, the green fissile shales within the transition zone to the Bright Angel Formation at the top of the Tapeats Sandstone (Rose 2006), and above that interval in the basal section of the Bright Angel Formation itself, have yielded abundant cryptospores (Strother 2000; Strother and Beck 2000; Strother et al. 2004a). These organic-walled microfossils include spores of probable land plants and terrestrial algae, but rather surprisingly, no spores of marine algae, in addition to cuticle fragments and probable egg cases of metazoans. Strother et al. (2004a) noted that palynomorph preservation degraded where apparently there had been increased bioturbation.

Baldwin et al. (2004) examined stratigraphic sections through the Bright Angel Formation in four drainages in central and eastern Grand Canyon. Samples for palynology were taken from shale intervals on average one every 7 m (23 ft) through one of those stratigraphic sections, while elsewhere spot samples were taken. They reported that the palynomorphs recovered from their samples did not match exactly any stratigraphically younger assemblages. They broadly classified the palynomorphs into three palynofacies. Type A represents primary-sourced organic matter that was dominated by cryptospores and non-marine algal cell clusters. Metazoan fragments were rare or missing, but overall preservation was excellent. Type B contained a more mixed assemblage that included thinner-walled cells and cell clusters with relatively fewer thicker-walled (cryptospore) forms. That assemblage contained noticeable fragments of metazoan origin (cuticles and structural elements) and may have contained larger leiospheres that could be protoctist or metazoan derived. Preservation was mixed. Type C represented a degraded assemblage that contained significant metazoan remains dominating primary photosynthetic biota and algal debris.

Baldwin et al. (2004) also reported an additional distinctive assemblage they recovered from samples immediately adjacent to an outcropping erosional "hill" of Proterozoic strata (presumably Hakatai Shale) in the drainage of Red Canyon (river mile 77.3). These samples were characterized by excellent preservation of large tissue fragments and "leiospheres" in addition to pervasive non-marine cryptospores and terrestrially-derived algal cell clusters. Additionally, mats of filaments, similar to the tissues that comprise the Silurian terrestrial plant *Nematothallus,* were found in these samples. However, because this assemblage was not characteristic of palynomorphs from the other stratigraphic sections they sampled, they did not discuss it further. Yet the finding of mats of filaments similar to those of a land plant much higher in the stratigraphic record is surely very significant.

Subsequently, Taylor and Strother (2008) investigated the ultrastructure of these Bright Angel Formation palynomorphs and found they had complex resistant walls. They typically preserved both a primary wall, and an outer envelope (synoecosporal wall) that enclosed multiple spore-like bodies within. At least three distinct types of primary walls were recognized with the transmission electron microscope (TEM):

(1) a unilaminate wall with a smooth inner surface and a sculptured outer surface,
(2) a wall of three unornamented laminae of very uniform thickness, and
(3) a thicker wall with multiple thin, lightly-staining layers embedded in a darker matrix.

They concluded that because there are no known extant algae that produce spores with walls as thick or as complex as these Cambrian palynomorphs, the latter may be the desiccation-resistant spores of cryptogams belonging to the supposed charophyte–embryophyte evolutionary lineage. Furthermore, they suggested that multilaminate spore walls, which are characteristic of some extant liverworts and Paleozoic cryptospores, may have evolved via the fusion of separate, multiple laminae. Taylor and Strother (2008) suggested this appeared to be the "primitive" plant sporoderm type, but it may have evolved asynchronously with respect to the supposed evolution of the embryophytic development of the sporophyte in land plants such as mosses, liverworts, ferns, club mosses and horsetails (Strother 2000; Strother et al. 2004b). These palynomorphs are

true cryptospores and apparently represent the earliest evidence of land plants in the geologic record (Rose 2006). Acanthomorphic acritarchs, marine phytoplanktonic cysts typical of Cambrian microfloral assemblages elsewhere, appear to be absent in the Bright Angel Formation.

Trace Fossils (Ichnofauna)

Trace fossils are common in all formations of the Tonto Group, particularly the Bright Angel Formation. Martin (1985) recognized a diverse array of ichnofauna (tracks, trails, and burrows) in the formation, including vertical traces on megaripples and the tops of sand sheets, and horizontal crawling and feeding traces, as well as abundant arthropod trackways. He also noted that these ubiquitous trace fossils typically occurred within the silty and muddy inter-sheet areas at the interfaces between sandstone beds and silty mudrocks in the formation (fig. 25). Despite this, the ichnofauna in the Bright Angel Formation has been described in only a few studies (Baldwin et al. 2004; Elliott and Martin 1987b; Lane et al. 2003; Martin 1985; McKee 1932; Resser 1945; Seilacher 1970). Consequently, according to Middleton and Elliott (2003), much remains to be done to establish the taxonomic affinities and the relationships between certain physical processes such as current strengths and substrate stability and the mode of infaunal and epifaunal behavior.

Martin (1985) found that in bed sequences consisting of medium-grained, planar-tabular cross-stratified sandstone, erosively overlain by fine-grained, ripple cross-laminated sandstone, trace fossils are generally absent, with the exception of truncated *Diplocraterion*, indicating that the relatively mobile substrate precluded permanent faunal colonization. In coarsening-upward sequences that are thin and laterally less extensive and contain a greater proportion of silt and fine-grained sand, vertical trace fossil types, such as *Diplocraterion* and *Skolithos*, are rare, probably due to relatively high current velocities and a mobile substrate. In contrast, in fining-upward sequences consisting of a lower erosively-based, normally-graded or cross-stratified conglomeratic sandstone bed overlain by interbedded, thin fine-grained sandstone lenses and green fissile shale, the presence of complete traces, including funnels and complete burrows of *Diplocraterion*, indicates that the surface was rapidly recolonized after deposition of sediment but that subsequent deposition of mud and silt forced the organisms to evacuate (or they were swept away) to relocate their burrows (Elliott and Martin 1987b).

Martin (1985) found U-shaped *Diplocraterion* burrows perpendicular to bedding. This is the only common trace fossil in the fine- to coarse-grained cross-stratified sandstone beds within the Bright Angel Formation. These tubes appear as paired holes on bedding planes or as concave-upward scours, where they have been eroded to the base of the burrow (Middleton and Elliott 2003). On bedding planes where these U-shaped burrows have been eroded to the bottom end of the U-shape they appear as harrowed out "trails" on the rock surface (McKee 1945; Hereford 1977). These abundant trace fossils were assigned to the ichnogenus *Corophioides* by Hereford (1977) and to *Arenicolites* and *Diplocraterion* by Rose (2006). These traces probably represent dwelling structures of suspension-feeding organisms that occur in shallow-water marine deposits, such as certain groups of annelids (worms), and are common in many modern nearshore deposits (Middleton and Elliott 2003).

Single, unbranched, straight vertical cylindrical burrows assigned to the ichnogenus *Skolithos* (Alpert 1974) are common at many localities in the Bright Angel Formation. These sand-filled burrows tend to occur near the tops of fine-to-medium quartz sandstone beds (Baldwin et al. 2004). They are visible in cross-section and on bed tops where they are found in high abundance as monotaxic occurrences. Burrows of this type probably functioned as dwellings and/or temporary resting structures for suspension feeding organisms, such as annelids (worms) or phoronids (marine horseshoe worms) (Alpert 1974; McKee 1945). These abundant occurrences of *Skolithos* in these fine- to coarse-grained sandstone beds suggested to Middleton and Elliott (2003) deposition of these sandstones occurred in a shallow marine environment characterized by currents capable of active bedload transport. This is further substantiated by their occurrence also in cross-bedded sandstone beds. Similar structures are common in many modern nearshore marine settings.

What Martin (1985) called lenticular heterolithics, essentially mixtures of lithologies, comprise the largest portion of the Bright Angel Formation. They consist primarily of minor sandstone beds within mudstone or sometimes siltstone that are either lenticular and sometimes wavy or flaser bedded, or continuously interbedded. Martin (1985) documented that these lenticular heterolithics are dominated by trace fossils on horizontal interfaces, that is, on the tops of sand beds at interfaces with overlying mud beds. These include *Cruziana* and *Rusophycus* (trilobite trackways), and *Palaeophycus* and *Phycodes* (annelid trails) (fig. 26) [as hypichnia or ridges and grooves found on the soles of the beds of origin at their interfaces with other layers (the opposite of epichnia)—Martinsson (1970)], and *Diplichnites* (trilobite walking traces) and *Scalarituba* (worm trails) (as epichnia or traces that are found wholly

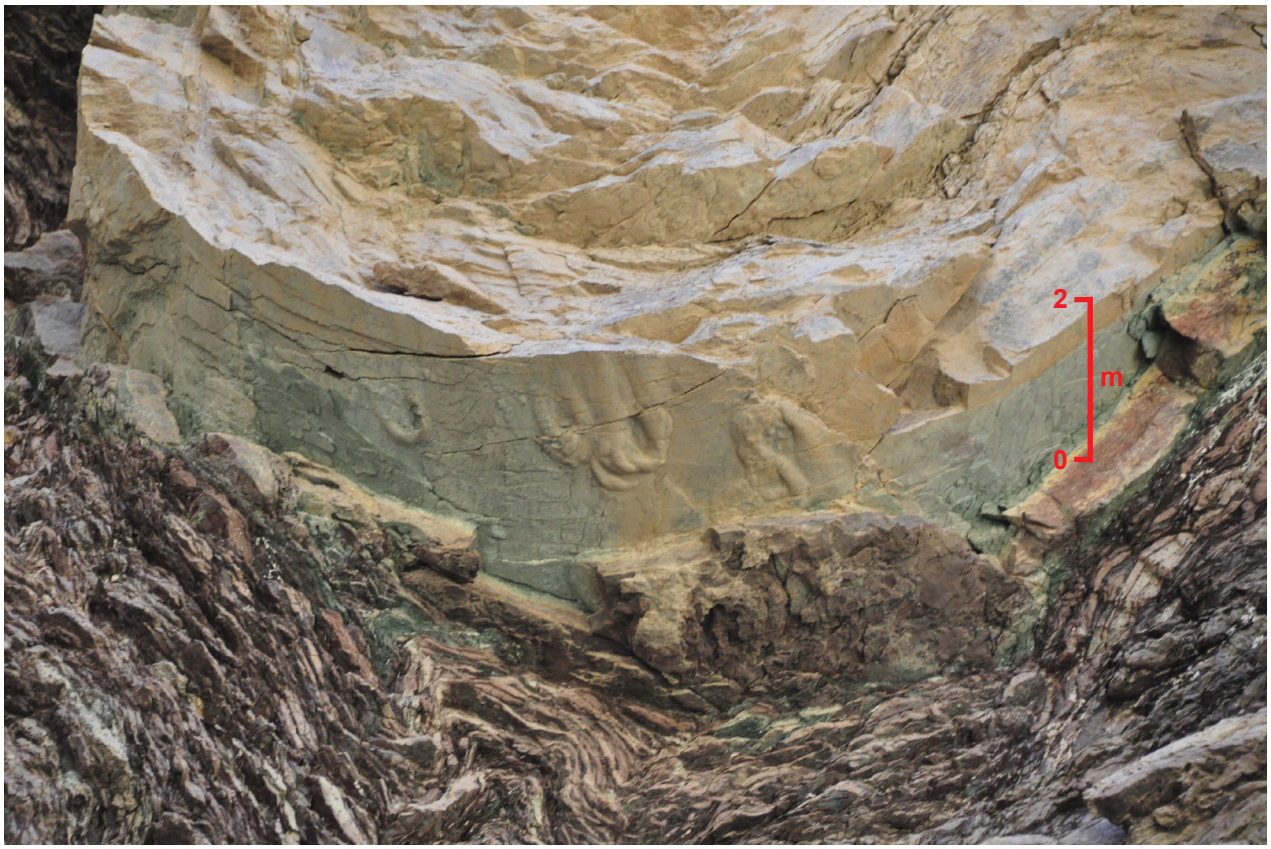

Fig. 25. Looking up to an overhanging ledge of a fine-grained sandstone lens interbedded with underlying thin siltstone and shale laminae (lenticular heterolithics) and with a horizontal trace fossil (probably *Teichichnus*) on the sandstone at the sandstone/shale interface (river mile 187.4). The scale bar to the right is ~2 m (~6.5 ft).

within the casting medium, and therefore can only have been made by an infaunal organism), *Scolicia* (gastropod trails), and *Palaeophycus* and *Teichichnus* (annelid trails) (figs. 25 and 26) (as exichnia or traces that are made of material that is different from the surrounding medium, having either been actively filled by an organism or eroded out and recovered by an alien sediment).

Vertically-oriented, sand-filled cylinders of subequal lengths and widths known as *Bergaueria* found in the lenticular heterolithics were described by Martin (1985) and listed by Lane et al. (2003). The exterior walls are smooth or contain sub-parallel concentric rings (on average <1 mm thick) near the cylinder bases, which are hemi-spherical and flattened or contain a deep central depression (1–2 cm wide). The close resemblance in these shapes to modern actinian (sea anemone) burrow casts described by Frey (1970) suggests that *Bergaueria* likely represents the dwelling burrows of suspension-feeding actinians.

Horizontal traces were first reported by Walcott (1918) in the green fissile shales in the Tonto Group, primarily in the Bright Angel Formation, and then McKee (1932). These traces McKee (1932) called "fucoides." Martin (1985) referred to them as *Palaeophycus, Phycodes* and *Teichichnus* (figs. 25 and 26). These are all smooth-sided curving horizontal casts several inches (up to 10 cm) in length and up to an inch (2–3 cm) thick that typically occur in large numbers often overlapping one another covering entire bedding surfaces of the green fissile shales of the Bright Angel Formation. Presumably, they were formed by detritus-ingesting annelids (worms) moving through the sediment (Middleton and Elliott 2003). They are horizontal burrows with a fairly complicated and distinctive pattern. Along a central, sometimes sinuous, or looping burrow there are successive probes upward through the sediment, generating a trace pattern reminiscent of a fan or twisted rope. Vannier et al. (2010) demonstrated that these horizontal trails are likely the result of burrowing priapulid worms along the sediment surface underwater. Martin (1985) also reported a variety of other horizontal trails and traces such as *Belorhaphe*, *Cochlichnus*, and *Spirophycus*, while Lane et al. (2003) reported *Corophioides* and *Treptichnus* (a central, sometimes sinuous or looping burrow with successive probes also generating a trace pattern reminiscent of a fan or twisted rope), all in the Bright Angel Formation.

Elliott and Martin (1987b) commented that in a general sense the bathymetric model of Seilacher (1964, 1967) could indicate that these horizontal

Fig. 26. Horizontal trace fossils on surfaces of sandstone beds (river mile 170). The lens cap is ~5 cm (~2 in) wide. (a) *Phycodes*. (b) *Palaeophycus*.

trace fossils in the Bright Angel Formation may represent the response of deposit-feeding organisms to nutrient supply on a subtidal shelf under relatively low-energy conditions. They noted, however, that this conclusion apparently contradicts the sedimentologic observations of Martin (1985) which suggested the lenticular heterolithics represented storm-induced deposition of sand, followed by a low-energy period during which traces were formed as mud settled to the bottom. Their resolution was to interpret the natural behavior of the animals that produced these trace fossils in this sedimentological context. Thus, horizontal trace fossils such as *Palaeophycus*, *Phycodes*, and *Teichichnus* were perhaps produced by organisms burrowing completely in mud, or in mud under sand lenses, implying that their movements were largely unrestricted by the physical energy of the overlying water column. Thus, regardless of whether there was supposed fair-weather suspension deposition of mud or storm-induced transport of sand predominated, burrowing was unaffected.

Traces of trilobites crawling (*Cruziana*) and resting (*Rusophycus* and *Isopodichnus*, small <1 cm wide versions of the former*)* occur throughout the Bright Angel Formation, as well as *Diplichnites* [interpreted by Crimes (1970) as trilobite walking traces], *Dimorphichnus* [interpreted by Seilacher (1955) as the sideways grazing motion of trilobites], and *Monomorphichnus* [interpreted by Crimes (1970) as trilobite swimming traces] (Martin 1985; Middleton and Elliott 2003). They were first reported by Walcott (1918) and Gilmore (1928), and then by McKee (1945). Seilacher (1970) provided the first detailed description of *Cruziana arizonensis* traces from the Tapeats Sandstone (see Snelling 2021, 185, fig.17) and Martin (1985) reported the common occurrence of trilobite trace fossils in the interbedded sandstones and mudstones (or lenticular heterolithics) of the Bright Angel Formation. They are thought to result from the digging action of the trilobite's underbody claws sweeping aside the sediment surface underneath the trilobite, creating two adjoining parallel lines of scooped-out burrows or double troughs along the mid-line of the trilobite's underside, as illustrated in Seilacher (1970, fig. 7). What is preserved are molds of the infilled troughs of these burrowing trails.

Elliott and Martin (1987b) noted that *Cruziana* and *Rusophycus* represent hypichnial casts (found on the soles of the beds of origin at their interfaces with other layers) of trilobite crawling and resting or feeding traces that were probably formed on the open muddy sea floor. Because trilobites evidently produced open furrows in mud (Baldwin 1977; Crimes 1975), their movements were restricted by relatively high-energy currents, implying that they furrowed between storms, feeding on nutrients settling to the bottom with mud. During storms, the trilobites were perhaps relatively inactive, forming *Rusophycus* traces. Thus, any *Cruziana* traces formed before a storm might have been filled and preserved by fine-grained sand that was transported offshore by storm-induced currents. Therefore, Elliott and Martin (1987b) suggested that these *Cruziana* traces were formed during fair-weather periods as these arthropods moved across the shelf sediments, whereas the related *Rusophycus* marks formed during storms.

In contrast, Elliott and Martin (1987b) interpreted *Diplichnites* (trilobite walking traces), *Scalarituba* (worm trails), and *Scolicia* (gastropod trails) as representing movements of these organisms across sand lenses under a thin (<1.0 cm) cover of mud that settled after storms. They considered it unlikely these epichnial furrows (found exposed by erosion on the tops of the strata of origin, having been formed by benthic organisms) would have been preserved had they been made as open furrows on sandy lenses. Any slight water movement across the sandy bottom would have partially distorted or destroyed the delicate features Martin (1985) observed on *Scalarituba* in particular. Elliott and Martin (1987b) also reported an unusual distinctive epichnial trackway *Angulichnus*. It consists of a central zigzag furrow bordered by bi-serially opposed alternating tracks. They suggested that though clearly formed by a benthonic arthropod, the trail cannot be attributed to a trilobite and is therefore important as an indicator of the presence of non-trilobite arthropods during deposition of the Bright Angel Formation.

Lane et al. (2003) also reported an unusual trace fossil from the Bright Angel Shale Formation. It consists of two rows of bi-serially opposed circular or oval depressions, with alternating symmetry. They described it as *Bicavichnites*, yet Martin (1985) had also described this same fossil from the same location. Lane et al. (2003) concluded that while specimens of this trace may represent the surface expression of a complex burrow system like *Treptichnus* (probably produced by priapulid worms), it is more likely that they are the walking traces of a bilaterally symmetrical benthic animal. The large variation in external width within the trackways is inconsistent with an arthropod producer. The trackway morphology and presence of limb spur marks suggest that the trace maker may have been a lobopodian, a soft-bodied, worm-like fossil panarthropod with stubby legs.

Baldwin et al. (2004) grouped these trace fossils at a very coarse scale into three associations or ichnoguilds (*sensu* Bromley 1990) based on the deduced general feeding strategies of the organisms (as similarly recognized by Martin 1985):

(1) Sediment feeding, as composed of mostly horizontal furrowing and burrowing ichnogenera such as *Cruziana, Palaeophycus, Phycodes, Rusophycus* (including "dig marks" and other components of obvious arthropodan origin) and *Teichichnus*.
(2) Filter/suspension feeding, composed of vertical and U-shaped burrows assignable to *Arenicolites, Diplocraterion* and *Skolithos*.
(3) Surface feeders are a mix of trail-formers, some of which produce positive relief casts on the upper surfaces of sandstone beds and includes *Palaeophycus* and *Planolites*. This group is often found in association with suspension feeders. This guild contains evidence of shallow-tier burrowing and possibly surficial furrowing or sediment feeding right at the sediment water interface.

Baldwin et al. (2004) base these groupings on the observed distributions and associations of these trace fossils (Droser and Bottjer 1986). They found that in some glauconitic sandstone beds vertical U-shaped and straight burrows extend downwards for a few centimeters. At the tops of these units the cross-bedded sands give way to burrowed and de-stratified units of sand/shale lenticles, plus biogenic pads composed of various *Cruziana*-forming subunits and various superimposed *Arenicolites, Phycodes, Teichichnus* and indeterminate burrow fills. Also, rare but recurrent *Teichichnus* and *Arenicolites* seem particularly large and cut down through multiple laminae and/or multiple sandstone beds. The tops of the numerous magenta arkosic sandstone beds are distinguished by dense packing of *Skolithos* and *Arenicolites* that cross-cut multiple foresets and sometimes penetrate units of climbing ripple cross-lamination, and individual species and superimposed multiple species of epichnial grooves. Other green glauconitic heterolithic units occur above and below the arkosic sandstone beds, where they exhibit almost no penetrative bioturbation or contain small *Phycodes/Teichichnus*-like spreiten (stacked, curved, layered structure) bearing walls that extend from the base of some sandstone beds and are confined to the next adjacent underlying mudstone layer.

Sedimentary Structures

Sedimentary structures are numerous in the coarse-grained lithologies in the Bright Angel Formation throughout the Grand Canyon (Middleton and Elliott 2003). These include horizontal laminations, small- to large-scale planar-tabular and trough cross-stratification (fig. 27), and wavy and lenticular bedding. Locally, structureless and crudely stratified conglomeratic sandstones typically overlie scoured surfaces. Martin (1985) documented a number of coarsening-upward, fining-upward and cross-stratified sequences in the Bright Angel Formation in the central Grand Canyon (figs. 13–15). He also detailed each lithology and its sedimentary structures, measured where possible the paleocurrent indicators and plotted the data on rose diagrams (fig. 28).

The 1.4–18 cm (~0.5–7 in) thick lenticular conglomeratic sandstone beds, which Martin (1985) estimated comprised <5% of the Bright Angel Formation and occur throughout its heterolithic sections, usually have no internal structure, but some exhibit crude trough stratification or normal graded bedding (fig. 15). Some beds consist of amalgamated fining-upward units bounded by low erosion surfaces. Crude cross-stratification exhibits southerly-directed paleocurrent orientations (fig. 28a). These beds are commonly capped by sinuous to straight-crested symmetric ripples (fig. 29a, b) with a wavelength of 20 cm (~8 in) and height of 4 cm (~1.5 in). The ripple crests strike in a pronounced northeast-southwest orientation (fig. 28b). Ripple troughs typically contain lags of pebble-sized sandstone and siltstone clasts. *Diplocraterion* burrows commonly occur along the tops of these conglomeratic sandstone beds, while *Palaeophycus* preserved as hypichnial ridges is common on the bases of the beds. Lower contacts are sharp and planar to scoured, while the upper contacts are typically gradational.

Martin (1985) estimated that the planar-tabular cross-stratified sandstone beds that crop out in the lower half of the Bright Angel Formation comprises about 5% of the formation. Cross-bed foreset laminae are 0.1–1.5 mm thick, typically fine upwards, and dip at 19–25° in pronounced southeast and southwest trends (fig. 28c). Foreset toes are typically tangential and may contain isolated quartz pebbles and mud clasts. All planar-tabular cross-bedded sets contain discrete low angle erosion surfaces that are inclined at angles less than the adjacent lenticular foreset laminae they truncate. Some of these sandstone beds are capped by interference ripples (fig. 29c) with a wavelength of 10 cm (~4 in) and a height of 2–3 cm (~1 in) or by obliquely-oriented, small-scale (<5 cm or 2 in) trough cross-stratification. Vertical *Skolithos* and *Diplocraterion* burrows, and hypichnial ridge and epichnial groove traces, are common. These planar-tabular cross-stratified sandstone beds are laterally discontinuous along outcrops, thus forming tabular sandstone bodies, with sharp or locally erosive lower contacts and upper sharp contacts. Occasionally there are larger-scale planar-tabular cross-stratified sandstone beds up to 2.3 m (~7.5 ft) thick, but they thin to 18 cm (7 in) laterally over 10–65 m (~33–213 ft). They consist of fining-upward foreset laminae inclined from nearly horizontal to 27° dipping southwest.

Fig. 27. Cross-bedding in sandstone beds within the Bright Angel Formation. (a) Normal simple planar-tabular cross-stratification in a sandstone bed ~20 cm (~8 in) thick (river mile 187.6). (b) Faint complex trough cross-stratification (fingers for scale) (river mile 167.9).

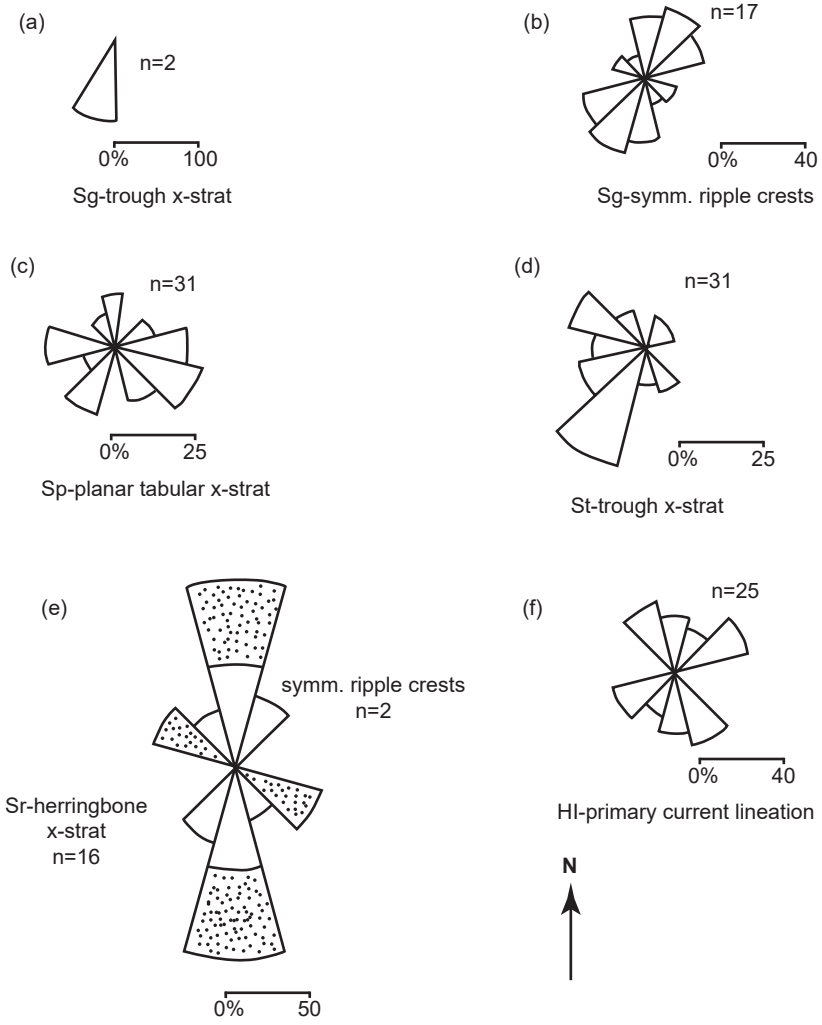

Fig. 28. Paleocurrent data rose diagrams (after Martin 1985, 178, fig.29). (a) Trough cross-stratification orientations in thick lenticular conglomeratic sandstone beds. (b) Symmetrical ripple crest strike orientations in thick lenticular conglomeratic sandstone beds. (c) Cross-bed foreset laminae orientations in planar-tabular cross-stratified sandstone beds. (d) Foreset laminae orientations in trough cross-stratified sandstone beds. (e) Ripple crest and foreset laminae orientations in herringbone cross-stratified sandstone beds. (f) Current lineation orientations in sandstone lenses interbedded with shales (heterolithics).

In contrast, Martin (1985) estimated that trough cross-stratified sandstone beds comprise 15–20% of the Bright Angel Formation, but they vary in set thickness and bed geometry. Single cross-set thicknesses are 3–32 cm (~1–13 in) thick and amalgamated sequences of cross-sets are up to 1.1 m (~3.6 ft) thick. Foreset laminae fine upwards, occasionally are lenticular and dip at 20–25° to the southwest and northwest (fig. 28d). Basal low-angle erosion surfaces are common, and foreset toes are tangential, occasionally containing isolated quartz pebbles and sandstone and siltstone granules. U-shaped *Diplocraterion* burrows are common, as are horizontal hypichnial ridge and epichnial groove traces. Single cross-sets are lenticular to tabular, and pinch and swell along outcrops, while amalgamated sequences are tabular in form. Lower contacts are sharp or locally erosive, and upper contacts are sharp or gradational. Similar tabular sandstone beds are composed of single, crudely trough cross-stratified sets and typically exhibit normal grading. Poorly- to moderately-sorted brachiopod shell fragments and granular to pebble-sized clasts of sandstone, siltstone and shale are concentrated along foresets. Foreset laminae are commonly convoluted and over-steepened. Lower contacts are erosive and upper contacts gradational.

What Martin (1985) claimed to be herringbone cross-stratified sandstone beds are present throughout the Bright Angel Formation and comprise about 30% of the trough cross-stratified sandstone beds. Alternately, these may be sets of cross-beds dipping in different directions, one on top of another, as true herringbone cross-stratification is rare and probably could only be preserved under a rapidly subsiding tidal basin. Composed of quartzose

and glauconitic sandstone with up to 25% brachiopod shell fragments, these beds typically occur as amalgamated units consisting of single oppositely-directed cross-sets separated by sub-horizontal erosion surfaces. These claimed herringbone cross-sets are often capped by straight-crested or interference ripples (fig. 29b, c) with a wavelength of 3 cm (~1 in) and a height of 0.2 cm (~0.2 in). Ripple crests trend northwest-southeast and north-south (fig. 28e). Foreset laminae exhibit normal grading, foreset toes are tangential, and foreset dips exhibit a bipolar-bimodal pronounced north-south trend with minor northeast-southwest and northwest-southeast trends (fig. 28e). *Cruziana* preserved in the shales between the cross-sets and *Palaeophycus* in hypichnial ridge preservation are common in these sandstone beds which also exhibit sheet geometry. The larger beds are up to 2.5 m (~8 ft) thick and can be traced laterally up to 23 km (14 mi). Thinner beds are <20 cm (~8 in) thick and are lenticular. Lower contacts are gradational or locally erosive, while upper contacts are sharp but may be overlain by a quartz pebble conglomerate veneer with sandstone and siltstone intraclasts.

Hummocky cross-stratified quartzose and glauconitic sandstone beds comprise <1% of the Bright Angel Formation (Martin 1985). They consist of a series of fining-upward units approximately 10 cm (~4 in) thick, each being similar to the idealized hummocky cross-stratified sequences documented by Dott and Bourgeois (1982) (fig. 30a). Some fining-upward units are capped by a 1–5 mm (~0.04–0.2 in) thick shale or mudstone drape, or by a 3–4 cm (~1.2–1.6 in) thick wavy-bedded unit (fig. 30b) (using the terminology of Reineck and Wunderlich 1968). Each fining-upward unit structurally consists of an undulating erosive base followed upward by hummocky cross-stratification or trough cross-stratification (fig. 30b), horizontal lamination, small-scale cross-stratification or ripple cross-lamination (fig. 30c), and a mudstone or shale drape (fig. 30a, b). *Cruziana* and *Rusophycus* are common in the mudstone or shale drapes separating the hummocky cross-stratified sandstone beds, while hypichnial ridge *Palaeophycus* and epichnial groove traces are common within the latter. The hummocky cross-stratified sandstone beds pinch and swell along outcrop, grade laterally into herringbone cross-stratification beds, and both their lower and upper contacts are sharp or erosive.

Martin (1985) estimated that hematitic oolitic sandstone beds, which are composed of grain-supported hematitic ooids, comprise <2% of the Bright Angel Formation. These beds are predominantly structureless, although some exhibit small-scale trough cross-stratification that is <5 cm (~2 in) thick. Rose (2003) called this same unit the magenta sandstone beds. He reported the orientations of ripple crests on rippled surfaces within them, including those that are laterally persistent, and they revealed no particular dominance of flow direction (fig. 31). Martin (1985) found that these sandstone beds remain nearly constant in thickness along outcrop, but within any one vertical section range in thickness from 1–2 cm (~0.4–0.8 in) where associated with mottled siltstone beds and up to 22 cm (~8.7 in) where associated with heterolithics. Contacts are gradational or locally sharp.

Massive bioturbated sandstone beds comprise <5% of the Bright Angel Formation and occur predominantly in the upper half of the formation (Martin 1985). They contain low-angle erosion surfaces that are typically overlain by mudstone, shale or siltstone layers <1 mm thick. Vertically continuous bioturbation of *Diplocraterion* has obliterated any trace of internal structure in these beds, except where the low-angle erosion surfaces truncate protrusive forms of *Diplocraterion*. *Palaeophycus* in hypichnial ridge preservation is profuse. These beds are lenticular and thicknesses within any one section range from 0.8 cm (~0.3 in) to 1.9 m (~6 ft). Lower contacts are gradational while upper contacts are gradational to sharp.

Martin (1985) found that mottled siltstone beds occurred at all localities because it comprises approximately 30% of the Bright Angel Formation. They are composed of structureless, highly bioturbated, hematitic micaceous siltstone that is enriched in K-feldspar, schist fragments and muscovite. The hematite content typically increases upward in these beds, particularly where they are associated with hematitic oolitic sandstone beds. The trace fossil assemblage is non-descript due to the profusion of endichnial burrows (that is, traces that are found wholly within the casting medium, and therefore can only have been made by an infaunal organism). These mottled siltstone beds weather to a recessive, slope-forming profile, have a sheet-like geometry, and range in thickness from 3 cm (~1.2 in) to 5.23 m (~17 ft). Contacts are typically gradational.

Martin (1985) used the term heterolithics to describe a mixture of lithologies that collectively comprise the majority of the Bright Angel Formation. The heterolithics consists of several types of bedding with respect to the different lithologies—sandstone beds, interstratified with dominant fissile shales and siltstones. The heterolithics exhibit the most diverse and abundant trace fossil assemblage in the Bright Angel Formation. Most traces occur at the shale-sandstone interfaces, and include *Palaeophycus*, *Teichichnus*, *Cruziana*, *Rusophycus*, and *Phycodes*.


(a)


(b)
0
5
cm

Fig. 29. **(a) and (b) page 344.** Ripple marks on bedding surfaces of sandstone beds in the Bright Angel Formation (river mile 167.9). (a) Sinuous-crested ripples (fingers for scale). (b) Straight-crested ripples. Scale bar is ~5 cm (~2 in). (c) Interference ripples (fingers for scale).

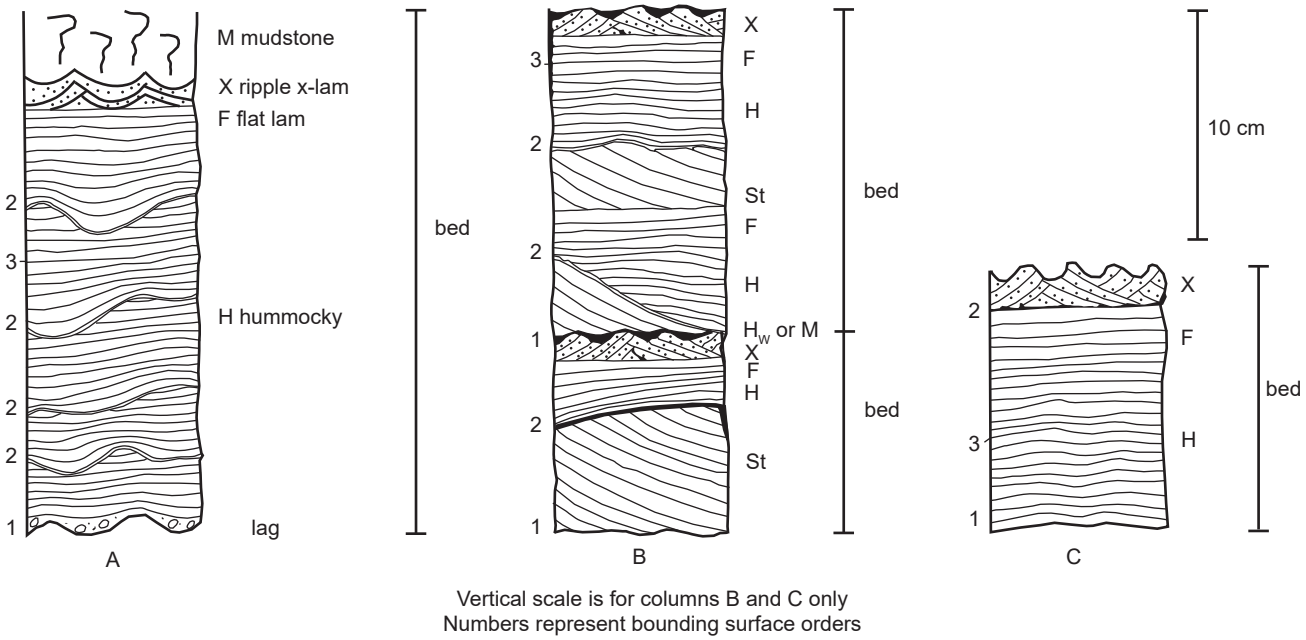

Fig. 30. Hummocky cross-stratified sandstone beds with scale bar (upper right) (after Martin 1985, 190, fig. 38). Numbers represent boundary orders—1 for first-order boundaries representing bottom erosion during initiation of storm episodes; 2 for second-order boundaries representing fluctuations in the intensity of water disturbance; and 3 for third-order boundaries representing deposition of individual laminae. (a) Idealized hummocky cross-stratified sandstone sequence in which each bed is composed of an erosive base, hummocky cross-stratification (H), flat lamination (F), ripple cross-lamination (X) and mudstone (M). (b) Diagrammatic stratigraphic section of a fining-upward hummocky cross-stratified sequence at Horn Creek (river mile 90.8). (c) Diagrammatic stratigraphic section of a single hummocky cross-stratified sequence at Horn Creek (river mile 90.8).

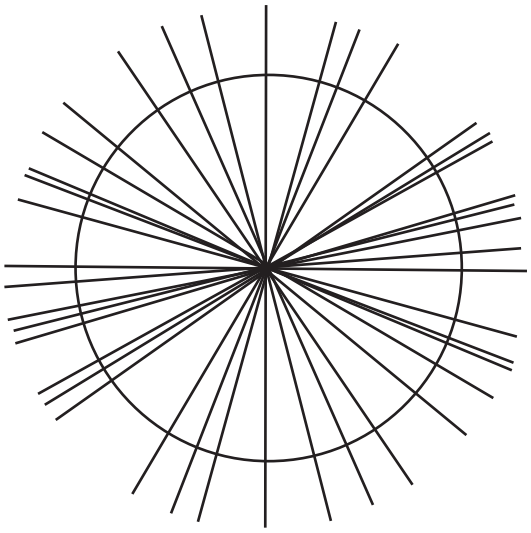

Fig. 31. Star diagram of 21 measurements of the orientations of two-dimensional ripple crests on magenta (hematitic) sandstone beds (after Rose 2003, 194, fig. 105).

Lenticular bedding (using the terminology of Reineck and Wunderlich 1968) is volumetrically the most abundant type and comprises 75% of the heterolithics. The lenticular beds are composed of feldspathic sandstone lenses within green fissile micaceous shale. Individual sandstone lenses range in thickness from 0.1cm (~0.04in) to 8cm (~3in) and exhibit normal grading beginning with granular bases (Martin 1985). Load casts up to 11cm (~4.3in) wide, synaeresis cracks, tool marks and flute casts are common on the bases of these sandstone lenses. Most of the sandstone lenses have undulatory bases and are horizontally stratified. Some exhibit primary current lineation that has a polymodal paleocurrent distribution with pronounced northeast-southwest and northwest-southeast trends (fig. 28f). Horizontal stratification typically grades upward into form-discordant ripple cross-lamination (fig. 32). Interference or straight-crested symmetric ripples with a wavelength of 4cm (~1.6in) and height of 0.7cm (~0.3in) commonly cap the sandstone lenses. These sandstones contain a few *Skolithos* and *Diplocraterion*, and profuse hypichnial ridge *Palaeophycus* and epichnial groove horizontal traces. The interstratified green to gray laminated shales (or mudstones) exhibit papery to fissile parting and are typically well-indurated. They contain passively and actively filled horizontal epichnial burrows, typically *Palaeophycus* and *Teichichnus*. Lower contacts are sharp and upper contacts are gradational to sharp.

The second type of bedding within the heterolithics are graded rhythmites (a term used by Reineck and Singh 1972), which gradationally overlie the massive and crudely trough cross-stratified conglomeratic sandstone beds (Martin 1985). The quartzose sandstone lenses within these graded rhythmites are 1–5cm (~0.4–2in) thick and occur as single or connected lenses that pinch and swell. The interstratified green fissile micaceous shales or mudstones contain small exichnial horizontal traces (traces that are made of material that is different from the surrounding medium, having either been actively filled by an organism or eroded out and re-covered by an alien sediment) of *Palaeophycus* and *Teichichnus*.

The third type of bedding in the heterolithics and the next most abundant consists of laterally continuous quartzose sandstone beds interbedded with sheet siltstone, shales and mudstones. The sandstone beds contain occasional pebble-sized sandstone and siltstone clasts and brachiopod shell fragments and may exhibit normal or reverse grading or be ungraded. Some are bounded by low angle erosion surfaces and comprise amalgamated sequences. Profuse bioturbation has obliterated most of the primary sedimentary structures. The siltstone, mudstone and shale interbeds are massive, and contain abundant exichnial horizontal traces of *Palaeophycus* and *Teichichnus*.

The least abundant type of bedding in the heterolithics is bifurcated wavy and flaser bedding

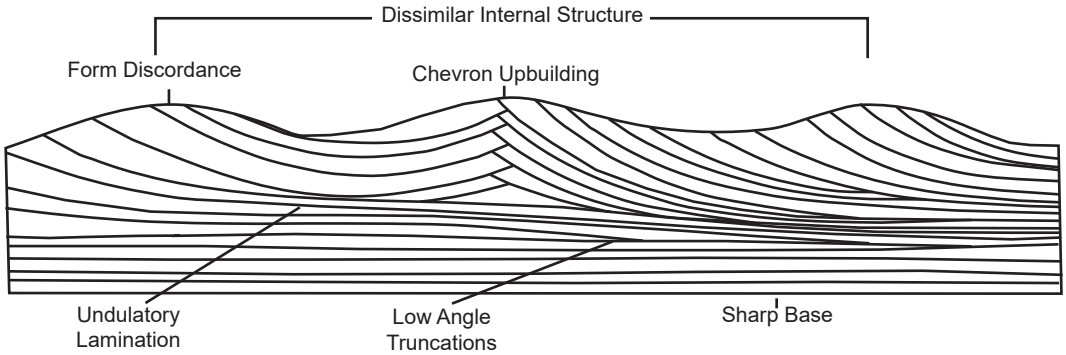

Fig. 32. Diagrammatic cross-section of a typical lens in the lenticular heterolithics (after Martin 1985,197, fig.43). The internal structure consists of horizontal and undulatory laminations, commonly overlain by form-discordant symmetric ripple cross-lamination. Chevron upbuilding is common.

(terminology used by Reineck and Wunderlich 1968). Quartzose sandstone beds exhibit form-discordant ripple cross-lamination with a wavelength of 4 cm (~1.6 in) and height of 1 cm (~0.4 in). Large *Palaeophycus* and *Teichichnus* in exichnial and hypichnial preservation and small *Cruziana* and *Rusophycus* are common. Sheet siltstones, shales and mudstones are interbedded between these sandstone beds.

Horizontally-stratified, laterally-continuous sandstone beds 7–15.5 cm (~2.8–6 in) thick are interbedded throughout the heterolithics and are constant in thickness for up to 100 m (~328 ft). Consisting of quartz fragments, they exhibit slight normal grading and sharp planar bases. Individual laminae can be traced for tens of meters. Synaeresis cracks are common. One of these beds shows primary current lineations with predominantly east-west and north-south trends. These sandstone beds commonly contain *Scalarituba* and horizontal epichnial groove traces. Lower contacts are sharp and upper contacts are gradational.

Martin (1985) also investigated whether there were repeated patterns in the sequences of lithologies, and thus he determined that there were coarsening-upward and fining-upward sequences (figs. 13 and 15). Rose (2003) also recognized what he termed parasequences due to the stacking patterns of the different lithologies evident throughout the Bright Angel Formation. He defined a parasequence as "a relatively conformable succession of genetically related beds or bedsets bounded by marine flooding surfaces and their correlative surfaces" (Van Wagoner et al. 1988), where marine flooding surfaces contain evidence of an abrupt increase in water depth. Thus, Rose (2003) described a shale-siltstone-magenta (hematitic) sandstone parasequence (fig. 19), the equivalent of Martin's (1985) coarsening-upward sequence. And whereas Martin (1985) focused his study on the Bright Angel Formation only in central and eastern Grand Canyon, Rose's (2003) study also encompassed western Grand Canyon. Like Elston (1989), he thus recognized that the rusty brown dolostone "tongues" identified by McKee (1945) and assigned to the Muav Formation are instead part of the Bright Angel Formation (fig. 16) and are carbonate-capped parasequences (fig. 20) able to be correlated with the hematitic magenta sandstone capped parasequences of central and eastern Grand Canyon (fig. 19).

Conventional Age of the Bright Angel Formation

The body fossils found within the transition zone of the Tapeats Sandstone with the overlying Bright Angel Formation establish a conventional late Early Cambrian age for the upper parts of the Tapeats Sandstone in the Grand Wash Cliffs at the western end of the Canyon and an early Middle Cambrian age for the formation in the eastern Canyon (Middleton and Elliott 2003). These ages are based on trilobite assemblages (*Ollenellus-Antagmus*) in the overlying Bright Angel Formation (McKee 1945) (fig. 5). This supposed diachroneity, in which the Bright Angel Formation crosses timelines and becomes younger from west to east, is claimed to be due to the west-to-east sense of the depositional strandline migration. Whereas, in western Grand Canyon the base of the formation lies below the *Olenellus-Antagmus* fossil assemblage zone and hence is designated as late Early Cambrian, in eastern Grand Canyon the upper two-thirds of the formation lies above the *Alokistocare-Glossopleura* fossil assemblage zone and thus is designated as Middle Cambrian (fig. 5).

Matthews, Guest, and Madronich (2018) analyzed samples of the underlying Tapeats Sandstone from East Verde River, central Arizona and Frenchman Mountain, southern Nevada and found they contained abundant middle Cambrian detrital zircons. Eight measurements from the central Arizona sample and seven measurements from the southern Nevada sample yielded concordant $^{206}Pb/^{238}U$ ages of 502.8±8.1 Ma and 504.8±8.2 Ma, respectively (2σ including all sources of random and systematic uncertainty). Thus, these U-Pb dates for zircon grains within the underlying Tapeats Sandstone constrain the conventional age of the Bright Angel Formation to probably <502 Ma.

Similarly, Karlstrom et al. (2018) U-Pb dated zircon grains from three Tapeats Sandstone samples, two of the three being from those same locations sampled by Matthews, Guest, and Madronich (2018). The youngest zircon grains in a coarse sandstone sample from 2 m (6.6 ft) above the base of the Tapeats Sandstone in Hermit Creek in Grand Canyon yielded a weighted mean LA-ICP-MS (laser-ablation–inductively coupled plasma–mass spectrometry) maximum age of 505.4±8.0 Ma (n=12). The youngest zircon grain population in a sample from the coarse-grained cross-bedded sandstone 30 m (98 ft) above the base of the unit in the westernmost limit of Tapeats exposures at Frenchman Mountain near Las Vegas, Nevada, yielded an age of 504.7±2.1 Ma (n=28). And the youngest grains in a sample from the coarse-grained, pebbly cross-bedded sandstone ~19 m (62 ft) above the unconformity with the granitic basement at the southeastern limit of Tapeats exposures along the East Verde River in central Arizona yielded a weighted mean maximum depositional age of 501.4±3.8 Ma (n=19). Again, therefore, these further U-Pb dates for zircon grains within the underlying Tapeats Sandstone constrain the conventional age of the Bright Angel Formation to probably <502 Ma.

In interpreting all these ages, Karlstrom et al. (2018) noted that the Tapeats Sandstone and Bright Angel Formation sections in western Grand Canyon that contain *Olenellus* Zone trilobites are thus probably older than 509Ma (Peng, Babcock, and Cooper 2012). Yet these western Grand Canyon and Lake Mead region trilobites correspond to the upper half of Stage 4 of Cambrian Series 2 (Sundberg 2011), whereas *Glossopleura walcotti* Zone trilobites of the overlying Bright Angel Formation in eastern Grand Canyon (Foster 2011) correlate with Stage 5 of Cambrian Series 3. While a numerical age for the boundary between Cambrian Stages 4 and 5 has not yet been firmly established by the International Union of Geological Sciences, the International Commission on Stratigraphy (2021) has designated an age of ~509Ma. Furthermore, the ages of fossils from these successions have been constrained by correlation of North American trilobite zones to trilobite provinces from other continents and by integrating recalibrated ages of Stages 3–5 ashes globally (Schmitz 2012) with revised fossil zonation (Sundberg et al. 2016) and chemostratigraphic and magnetostratigraphic correlation (Peng, Babcock, and Cooper 2012). Similarly, the *Peachella iddingsi* to *Bolbolenellus euparyia* Zone trilobites from upper Tapeats exposures near Las Vegas are probably 508.1–503.8Ma. Thus, it can be concluded that conventionally the Tapeats Sandstone must have been deposited between 510Ma and 500Ma and the overlying Bright Angel Formation within the same timeframe or very soon thereafter, with younging of both formations from west to east.

Finally, Karlstrom et al. (2020) tandem U-Pb dated detrital zircons from the same samples of the Tapeats Sandstone and the locally underlying Sixtymile Formation (in eastern Grand Canyon) as used in the Karlstrom et al. (2018) study. That involved both LA-ICP-MS analyses followed by CA-ID-TIMS (chemical abrasion–isotope dilution–thermal ionization mass spectrometry) analyses of the youngest grains plucked from the LA-ICP-MS epoxy mounts in order to obtain precise maximum depositional ages for those two units based on the youngest zircon grains. For the Tapeats Sandstone the resultant depositional ages were ≤508.19±0.39Ma in eastern Grand Canyon, ≤507.68±0.36Ma in Nevada, and ≤506.64±0.32Ma in central Arizona. And because the locally conformable underlying Sixtymile Formation had a similar maximum depositional age of ≤508.6±0.8Ma they added it to the Tonto Group, as well as adding the Frenchman Mountain Dolostone, which conformably overlies the Muav Formation (fig. 33). They then combined these depositional ages with the biostratigraphy of trilobite biozones in the Tonto Group based on available precisely-dated regional and global sections (Schmitz 2012; Sundberg et al. 2016, 2020), tied to U-Pb zircon dated Cambrian marker beds elsewhere (Landing et al. 2015; Peng, Babcock, and Cooper 2012), to conclude that the Tapeats Sandstone is ~507–508Ma.

Karlstrom et al. (2020) also confirmed that the long-proposed time transgressive nature of the Tonto Group is supported because the trilobite *Olenellus* is found in western, but not eastern, Grand Canyon (fig. 33). They determined that the Bright Angel Formation which contains the *Olenellus*, *Glossopleura* and *Ehmaniella* biozones is ~502–507Ma, and the conventional timeframe for deposition of the initial sheet Tapeats sands and Bright Angel muds, silts and sands of the Tonto Group transgression likely took place in less than ~4Ma (~504–508Ma) rather than the 40–60Ma proposed by McKee (1945) and Resser (1945).

Provenance of the Bright Angel Formation

Only one study to-date has U-Pb dated detrital zircons recovered from the Bright Angel Formation to determine the provenance of its sediment. Gehrels et al. (2011) collected samples of fine-grained sandstone from three ~50cm (1.6ft) thick horizons within the Bright Angel Formation that were representative in terms of grain size and composition. The three sandstone samples were from 1m (~3.3ft) above the base of the formation at about river mile 58.5 (near Malagosa Canyon), from 5m (~16.4ft) below the top of the formation at about river mile 51.5 (just above Little Nankoweap Creek), and from 3m (~9.8ft) below

Fig. 33 (page 349). Diagrammatic cross-section of the Tonto Group re-defining it across Arizona and through the Grand Canyon, from Karlstrom et al. (2020, 428, fig.3) but modified from McKee (1945, 14, fig.1). The vertical scale is time and the red scale bars show approximate thicknesses at each margin of the cross-section. The biochronology shown to the left is their working hypothesis, that could be refined with additional precise U-Pb detrital zircon (DZ) bracketing dates. The lower Tonto Group is in the subsurface in the central part of the transect, making correlations tentative. The sub-Tonto Group angular Great Unconformity has a variety of different-age Precambrian rocks beneath it, and hence a variable hiatus. Above the unconformity in the eastern part of the transect, islands (monadnocks) of tilted Unkar Group strata (resistant Shinumo Sandstone) created up to 200m (~656ft) of relief and were only covered by the Bright Angel Formation. Tonto Group biozones mentioned are: OL–*Olenellus*; Pd–*Poliela denticulata*; M–*Mexicella mexicana*; G–*Glossopleura walcotti*; Eh–*Ehmaniella*; Bo–*Bolaspidella*; Ce–*Cedaria*; Cr–*Crepicephalus*. GSSP–global stratotype section and point; CA-IDTIMS–chemical abrasion–isotope dilution thermal ionization mass spectrometry; LAD—last appearance datum; Terr.–Terreneuvian; Delam.–Delamaran; Top.–Topazan; Q.–Quartz; F–Feldspar; and G–Glauconite.

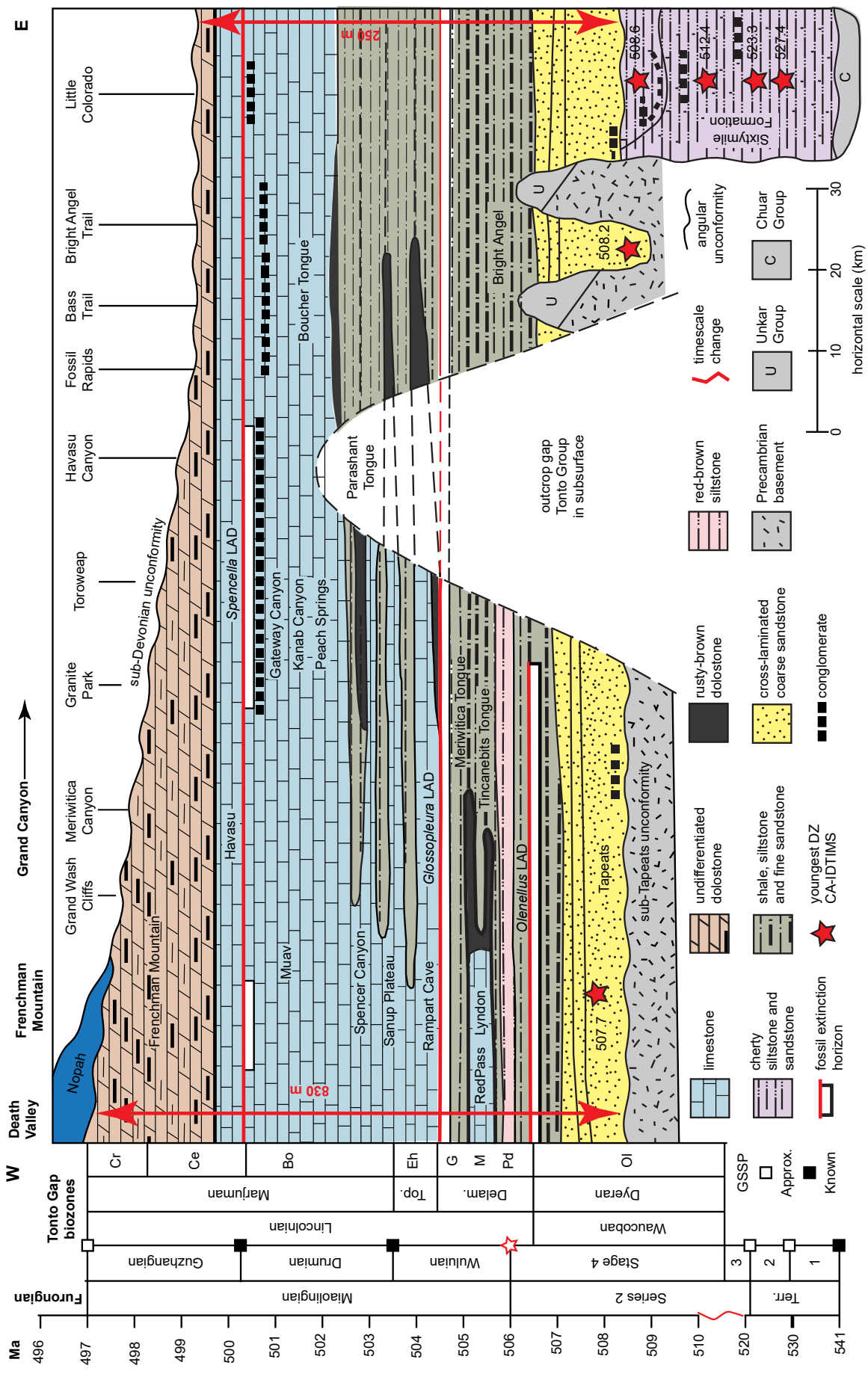
W
E
Death Valley
Frenchman Mountain
Grand Canyon
Nopah
Frenchman Mountain
Grand Wash Cliffs
Meriwitica Canyon
Granite Park
Toroweap
Havasu Canyon
Fossil Rapids
Bass Trail
Bright Angel Trail
Little Colorado
sub-Devonian unconformity
Havasu
Spencella LAD
Muav
Gateway Canyon
Kanab Canyon
Peach Springs
Boucher Tongue
Parashant Tongue
Bright Angel
Spencer Canyon
Sanup Plateau
Rampart Cave
Glossopleura LAD
Meriwitica Tongue
Tincanebits Tongue
RedPass
Lyndon
Olenellus LAD
sub-Tapeats unconformity
Tapeats
507.7
508.2
508.6
512.4
523.3
527.4
Sixtymile Formation
C
830 m
250 m
outcrop gap Tonto Group in subsurface
timescale change
angular unconformity
red-brown siltstone
Precambrian basement
Unkar Group
Chuar Group
horizontal scale (km)
0
10
20
30
limestone
undifferentiated dolostone
rusty-brown dolostone
cherty siltstone and sandstone
shale, siltstone and fine sandstone
cross-laminated coarse sandstone
fossil extinction horizon
youngest DZ CA-IDTIMS
conglomerate
Tonto Gap biozones
Furongian
Cambrian
Ma
Cr
Ce
Bo
Eh
G
M
Pd
Ol
Marjuman
Top.
Delam.
Dyeran
Lincolnian
Waucobian
Guzhangian
Drumian
Wuliuan
Stage 4
Miaolingian
Series 2
Terr.
GSSP
Approx.
Known
1
2
3
496
497
498
499
500
501
502
503
504
505
506
507
508
509
510
520
530
541

the top of the formation at about river mile 49. Some of the separated zircon grains were selected for U-Pb dating analyses using laser-ablation-multicollector-inductively coupled plasma-mass spectrometry (LA-MC-ICP-MS) after vetting for zonation using cathodoluminescence imaging to ensure only homogenous zones were spot analyzed—91, 105, and 86 grains, respectively.

Gehrels et al. (2011) found that the zircon grains within the samples were very small (<100 µm in length), euhedral to only slightly rounded, and generally colorless to light pinkish. The ages obtained were plotted on U-Pb concordia diagrams and the Pb-Pb ages were listed as the "best ages." The three samples yielded very similar age clusters, the main groups peaking around ca. 1.03 Ga (very minor), 1.45 Ga (secondary) and 1.71 Ga (primary). With all three samples combined, the primary age peaks were at 1026 Ma (n=12), 1457 Ma (n=63), and 1712 Ma (n=113). The statistical analysis used by Gehrels et al. (2011) confirmed that there was very good agreement between the three Bright Angel Formation samples of these age peaks.

These U-Pb ages for detrital zircon grains from the Bright Angel Formation are very similar to those they obtained for the underlying Tapeats Sandstone, with the statistical comparison confirming very good agreement. This was to be expected, as the Tapeats Sandstone and Bright Angel Formation were part of the same Sauk megasequence transgression that eroded and transported these sediments from the same source areas. Thus, the provenance interpretations are accordingly similar. Gehrels et al. (2011) concluded that most of the detritus deposited in the Bright Angel Formation was shed from the southwestern United States crystalline basement, with a much lesser contribution from the Grenville orogen to the south or far east. Of the crystalline basement contribution, much of that was likely local from the underlying Yavapai (1.70–1.80 Ga) and Mazatzal (1.62–1.70 Ga) provinces (Karlstrom et al. 2003). Furthermore, they concluded that the slightly greater proportion of 1.62–1.70 Ga (Mazatzal) grains (35%) over 1.70–1.80 Ga (Yavapai) grains (65%) may reflect cratonward migration of the source regions during the Sauk transgression.

Interpreted Depositional Setting of the Bright Angel Formation

The Bright Angel Formation comprises a variety of lithologies and sedimentary and biogenic structures that have been interpreted to indicate its deposition in open shelf marine environments (Middleton and Elliott 2003). McKee (1945) concluded that in his deepening seas depositional model the Bright Angel Formation accumulated in waters below wave base at depths intermediate between the shallow water of the Tapeats Sandstone and the deeper waters of the Muav Formation. More recent work by Wanless (1973a, b, 1975, 1981), Martin (1985), Martin, Middleton, and Elliott (1986), Elliott and Martin (1987b), Rose, Middleton, and Elliott (1998), Rose (2003, 2006, 2011) and Baldwin et al. (2004) has provided new data that they are argue potentially permit more precise uniformitarian environmental reconstructions. Although generally supporting the conclusions of McKee (1945), these later workers have documented various features that they have interpreted as produced in shallow-water deposits of the Bright Angel Formation, as well as providing important information on the possible roles of fair-weather and storm-related processes in controlling depositional patterns in the Bright Angel Formation.

As summarized earlier, Martin (1985) recognized eight facies of sandstone beds, siltstones and shales in the Bright Angel Formation and grouped them into what he regarded as three genetically significant facies sequences. These include cross-stratified sandstone beds in coarsening-upward (fig. 13), and fining-upward sequences (fig. 15), and in a heterolithic sequence consisting of interbedded sandstone and mudstone (fig. 14). He maintained that these facies sequences reflect deposition in subtidal areas influenced by tidal and storm and fair-weather processes, and that they also aid in tracking transgressive and regressive strandline movements.

Coarsening-upward sequences (fig. 13) are up to 8 m (25 ft) thick and typically can be traced for several tens of kilometers. The lower parts of these sequences are characterized by laminated, bioturbated mudstones that conventionally have been interpreted as requiring deposition by fair-weather suspension settling of silt and clay. On the other hand, the coarser-grained portions likely accumulated as sand waves, dunes and ripples that migrated over rapidly accumulating sand sheets. These portions are characterized by thick sets of planar-tabular cross-stratification (Middleton 1989). The presence of reactivation surfaces and abrupt changes in the dip of many foresets indicates periodic movement of these large bedforms, many of which are palimpsest or relict. These also may indicate lee-side erosion during tidal reversals and/or storms. Deposition appears to have been entirely in subtidal areas, although the upper portions of many of these sequences were likely deposited in relatively shallow waters, as evidenced by eroded burrows of *Diplocraterion* (Elliott and Martin 1987b).

Sequences that fine upwards (fig. 15) are common and consist of a lower, normally-graded small-pebble conglomerate or sandstone overlying an erosive base. This, in turn, is overlain by interbedded and fine-

grained sandstone and mudstone. The basal coarse-grained facies likely represent deposition from high-energy storm-induced currents that transported coarse materials from nearshore areas. The tops of these sequences contain symmetrical ripples, as well as appreciable amounts of laminated mudstone probably deposited from waning flows following the passage of storms. These beds are very similar to those reported from both modern and ancient storm deposits. Complete vertical and horizontal fossil traces occur at the tops of many beds, possibly indicating that the substrate was recolonized soon after deposition (Elliott and Martin 1987b).

Lenticular beds of interbedded sandstone and mudstone (fig. 14) constitute the majority of the Bright Angel Formation. This heterolithic association comprises very fine-grained sandstone lenses and micaceous shale. Most beds are graded normally and contain an abundant and diverse trace fossil assemblage (Martin 1985; Elliott and Martin 1987b). Conventionally these heterolithic deposits possibly represent high-energy storm-induced deposition of sand, followed by a low-energy post-storm suspension settling of muds and sands—and possibly remobilization during the fair-weather periods during which traces were formed as mud settled to the bottom. *Cruziana* and *Rusophycus* indicate a substrate inhabited by trilobites. Other trace fossils also indicate a relatively stable substrate colonized by a variety of infaunal and epifaunal organisms.

Martin, Middleton, and Elliott (1986) and Rose, Middleton, and Elliott (1998) summarized Martin's (1985) depositional model for the Bright Angel Formation as a classic example of subtidal siliciclastic marine deposition on a shallow marine shelf that experienced numerous transgressive-regressive cycles. The large-scale cross-stratified sandstones up to 4 m (~13 ft) thick (fig. 14) that occur throughout the formation were the product of subtidal sand wave migration across a tide-dominated coast, with the migration of two and three dimensional megaripples during periodic storm-induced sand transport and deposition and superimposed ripples in response to fair-weather tidal currents. The scoured surfaces and low-angle truncation surfaces in these sandstones are evidence of those storm-influenced events in which these offshore palimpsest sand bodies were periodically mobilized during transgressions and subsequently modified by storms, as indicated by the hummocky and other cross-stratification. Then during subordinate regressive episodes these sand sheets attained maximum size and thickness. However, the majority of the Bright Angel Formation being comprised of fine-grained siliciclastics was deposited under low energy conditions, as indicated by the repetitive laminated beds and the plethora of bedding-parallel trace fossil assemblages. Thus, they concluded that the sedimentation on the inner and outer shelf was consistently affected by storms yet dominated by tide-influenced and fair-weather processes in transgressive-regressive cycles controlled by sea-floor spreading rates during plate tectonic movements, coastal morphology and meteorologic events.

Rose (2003) contrasted the McKee (1945) deepening seas depositional model with the subtidal sand-wave complex depositional model of Martin (1985) (fig. 34). But he claimed to have identified sub-aerial features in the Bright Angel Formation that required supra-tidal and tidal flat depositional environments,

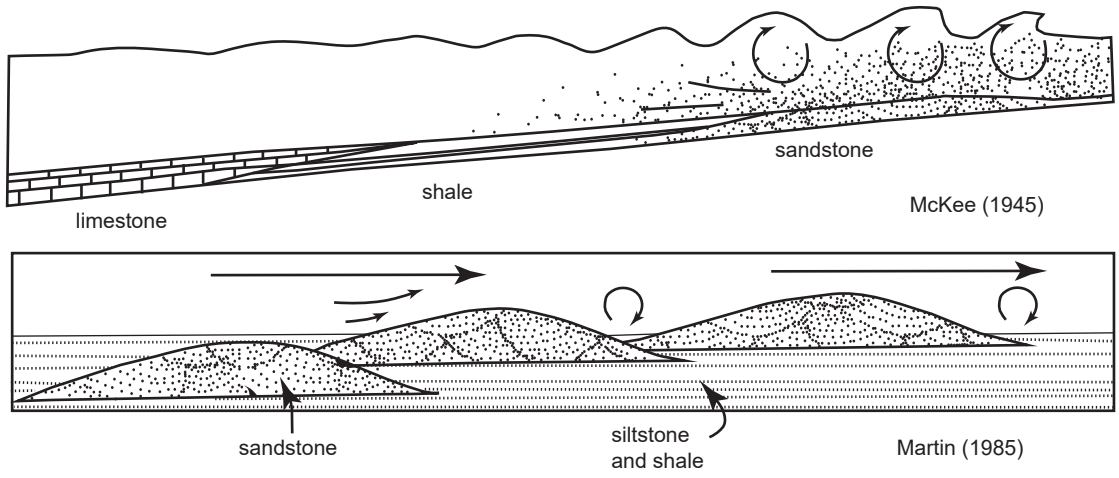

Fig. 34. Diagrammatic representations of two depositional models for the Bright Angel Formation (after Rose 2003, 161, fig.91). The McKee (1945) model (top) explains facies differences in terms of grain size gradient related to proximality/distality with higher energy waves at the shoreface. The Martin (1985) model is that of a sand-wave complex in which large relict sand bodies partition current strength into dune zones of high flow energy sand wave migration and downflow "shadows" of lower energy fine-grained settling.

adjacent to his claimed fluvial depositional environment for some of the Tapeats Sandstone. As evidence, Rose (2003, 2006) and Baldwin et al. (2004) highlighted the ostensibly marine signatures in the Bright Angel Formation, represented by sparse and fragmentary trilobite fossils and the abundant bedding plane trace fossils, closely associated with the non-marine signatures represented by the non-marine palynoflora, the absence of marine acritarchs, the clay mineral assemblages, and the alternating highly oxidized (hematitic) and reduced (glauconitic and gray) sandstone and shale beds, respectively.

In particular, Rose (2006) focused on the highly oxidized hematitic magenta sandstone beds which form thick resistant ledges within otherwise slope-forming green and grayish-green shales. He maintained that these magenta sandstone beds tend to erosively cap parasequences that in various combinations form the dominant facies stacking architecture of the Bright Angel Formation (fig. 19). Those parasequences are characterized by basal green fissile shales and fine sandstone beds interbedded at cm-scale. Furthermore, the cyclic thickening and thinning of these interbedded sandstones at a few localities hints at tidal bundling (Tessier, 1998), while abundant wrinkle structures, ripple lamination, and ladderback ripple marks appear to be consistent with a tidal flat depositional model for these shales and sandstones.

Exquisite preservation of bedding-plane trace fossils indicated to Rose (2006) that consistently high short-term depositional rates were necessary for these interbedded sandstones and shales despite their fine grain-size. He recognized that the timeframe between the animals burrowing into and moving across sediment surfaces and the burial of their traces would range from seconds to days at most. He argued that to achieve the high rates of settling of clay particles to rapidly bury and preserve the traces required flocculation of the clay minerals which is an active process in estuarine environments. Such flocculation of clay minerals has been confirmed in experiments by Schieber, Southard, and Thaisen (2007). Added to that, the millimeter- to meter-scale alternation between reduced and highly oxidized mudstone horizons indicated to Rose (2006) that during deposition of these muds they were potentially exposed to dramatic shifts in redox conditions at or near the sediment surface, which to him indicated a tidal estuarine depositional environment.

Rose (2006) also observed that commonly the magenta sandstone beds and the parasequences they cap are sharply bounded at their upper surfaces with herringbone cross-stratification or cm-scale festoon cross-bedding, and with 1–3 cm (~0.4–1.2 in) amplitude two-dimensional ripple marks with ripple crests spaced 7–13 cm (~2.8–5 in) apart. In some instances, these ripple crests are beveled, possibly indicating subaerial erosion of ripple crests while the water-filled ripple troughs remained structurally intact. In the few instances where the overlying sediment is preserved, it is fine-grained mudstone that appears to drape over both the ripples and beveled tops as a flaser, that is poorly lithified, and that is a gray or greenish-gray color.

In summary, Rose (2006) proposed what he called an expansive epicratonic estuary as the depositional environment for the Bright Angel Formation, which was marginally marine due to tidal flats but dominated by the freshwater estuary. Yet in his estuary model he did not account for the extensive beds that can be traced throughout the Grand Canyon region. Instead, he pictured this depositional environment as an expanded low-lying area of "pre-vegetated epicratonic regolith" that was shallowly flooded during transgression but which experienced sufficient rainfall or other freshwater influx. He suggested that the tidal reach had to extend far enough into the cratonic interior to prevent complete exchange of well-mixed marine water, and the coverage had to be over a wide enough area with low relief (because of the claim that this Cambrian transgression was an historic maximum) so that direct rainfall could be a significant freshwater source (as may be implicated by the widespread, "shelf-scale dolomitization," a reference to the many dolostone units in the Bright Angel Formation and in the two Tonto Group formations above it).

Petrography of the Bright Angel Formation

Previous Studies

As petrographic methods were not routinely practiced until later in the 1950s, McKee (1945) did not undertake a detailed petrographic investigation of the Bright Angel Formation. But he did publish several black and white photomicrographs of "glauconite-iron" sandstones from the upper Bright Angel Formation, one containing angular quartz grains and another containing rounded quartz grains. He also provided an outcrop photograph of "brown-spotted" siltstone from the Bright Angel Formation, as well as photographs of trace fossils and probable scour or drag marks on surfaces of two of the formation's sandstone outcrops.

However, Martin (1985) investigated more closely the sandstones within the Bright Angel Formation. He performed point counting of thin sections of 30 sandstone samples to determine their modal compositions, as well as visually estimating grain sizes, roundness and sorting using the scales of Wentworth (1922), Powers (1953), and Folk (1968) respectively. He also noted the type and percent of

cement, alteration and matrix for the purpose of classification, and used the sandstone classification of McBride (1963). Furthermore, he also provided seven photomicrographs to illustrate selected features in his sandstone samples.

Martin (1985) reported that his 30 selected Bright Angel Formation sandstone samples were composed volumetrically of predominantly monocrystalline quartz and subordinate glauconite grains (47–82% of the grains). In order of decreasing abundance, other grains included K-feldspar, siltstone clasts, brachiopod fragments, polycrystalline quartz, hematitic ooids, and schist fragments. When plotted on a ternary quartz-feldspar-glauconite diagram (fig. 35), the quartz sand-dominated sandstones plotted predominantly as expected in the quartz-rich and glauconite-rich fields, whereas the fine-grained mottled siltstones and sandstones in the heterolithics plotted in the feldspar-rich field. He also found that the sandstones classified as quartz arenites were from the stratigraphically lower half of the Bright Angel Formation, while the sub-glauconitic, feldspathic, and glauconitic sub-feldspathic sandstones and the greensands were from the stratigraphically upper half of the Bright Angel Formation.

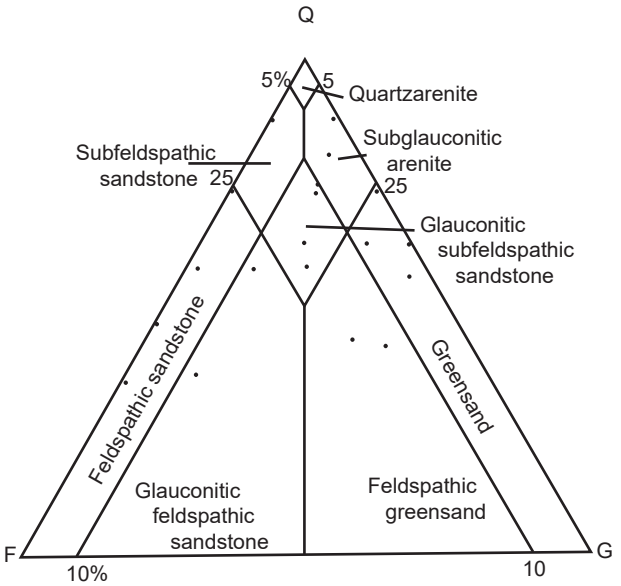

Fig. 35. Composition of selected sandstone samples from the Bright Angel Formation plotted on a ternary diagram (after Martin 1985, 36, fig. 8a), using the classification of McBride (1963). Q = quartz; F = feldspar; G = glauconite.

Martin (1985) determined that the grain sizes, varied from fine silt size to very coarse sand size, but medium sand size predominated, followed by fine and very fine sand size (fig. 36a). Typically sorting varied from poorly-sorted to very well-sorted, while most sandstones were moderately-sorted to very well-sorted (fig. 36b). However, some sandstones had a bi-modal grain-size distribution. Grains were typically rounded to well-rounded (fig. 36c). He found that the very well-sorted, well-rounded, medium-grained sandstones are typically quartzose, whereas the fine-grained sandstones and siltstones are feldspathic. Furthermore, the coarser sandstones are commonly greensands and litharenites. With the exception of silt-sized quartz grains, the matrix percent was negligible, while the cements comprising 13–53% of the sandstones consisted of silica, hematite, calcite and dolomite.

Martin (1985) also described the various grains, beginning with the most abundant, monocrystalline quartz grains. He found that sub-angular, undulose, monocrystalline quartz grains (fig. 36d) range from fine to very coarse sand-size and comprise up to 25% of the quartz grain population. Strongly undulose monocrystalline quartz grains are commonly sub-rounded and may have a bi-modal size distribution, with medium sand-sized quartz grains set in medium silt-sized quartz grain matrix. On the other hand, non-undulose, monocrystalline quartz grains which constitute ~70% of the quartz grains are well-rounded. Some quartz grains contain vacuoles, clear bubble trains, and acicular inclusions of tourmaline and perhaps sillimanite. Dust rims and secondary quartz overgrowths are common. Furthermore, rounded to well-rounded, fine- to medium-grained polycrystalline quartz and chert grains comprise ~4% of the quartz grain population. The polycrystalline quartz grains consist of three or more sub-grains which exhibit weakly sutured contacts, and commonly contain vacuoles and clear bubble trains. Chert grains constitute < 1% of the total quartz grain population and are commonly well-rounded and fine sand-sized grains.

Glauconite, what Martin (1985) called peloids, constitute ~12% of the total grain population. They are, as expected, very well-rounded (except where he observed them to be deformed ductilely) and are well-sorted. Their sizes vary considerably from fine to very coarse-grained, but they are typically slightly larger than associated quartz grains. Many glauconitic peloids contain up to 20% sub-angular to sub-rounded quartz or K-feldspar grains as nuclei, some of the enclosed quartz grains even exhibiting hematitic dust rims and secondary quartz overgrowths.

K-feldspar grains constitute 10% of the total grain population (Martin 1985). Most were identified as orthoclase grains and are typically well-sorted, sub-rounded to rounded and fine-grained. He also found that optically continuous euhedral overgrowths are common, with both the detrital core and overgrowths exhibiting various degrees of vacuolization and sericitization. Approximately 1% of the K-feldspar grains are microcline, while perthite is rare. Rounded

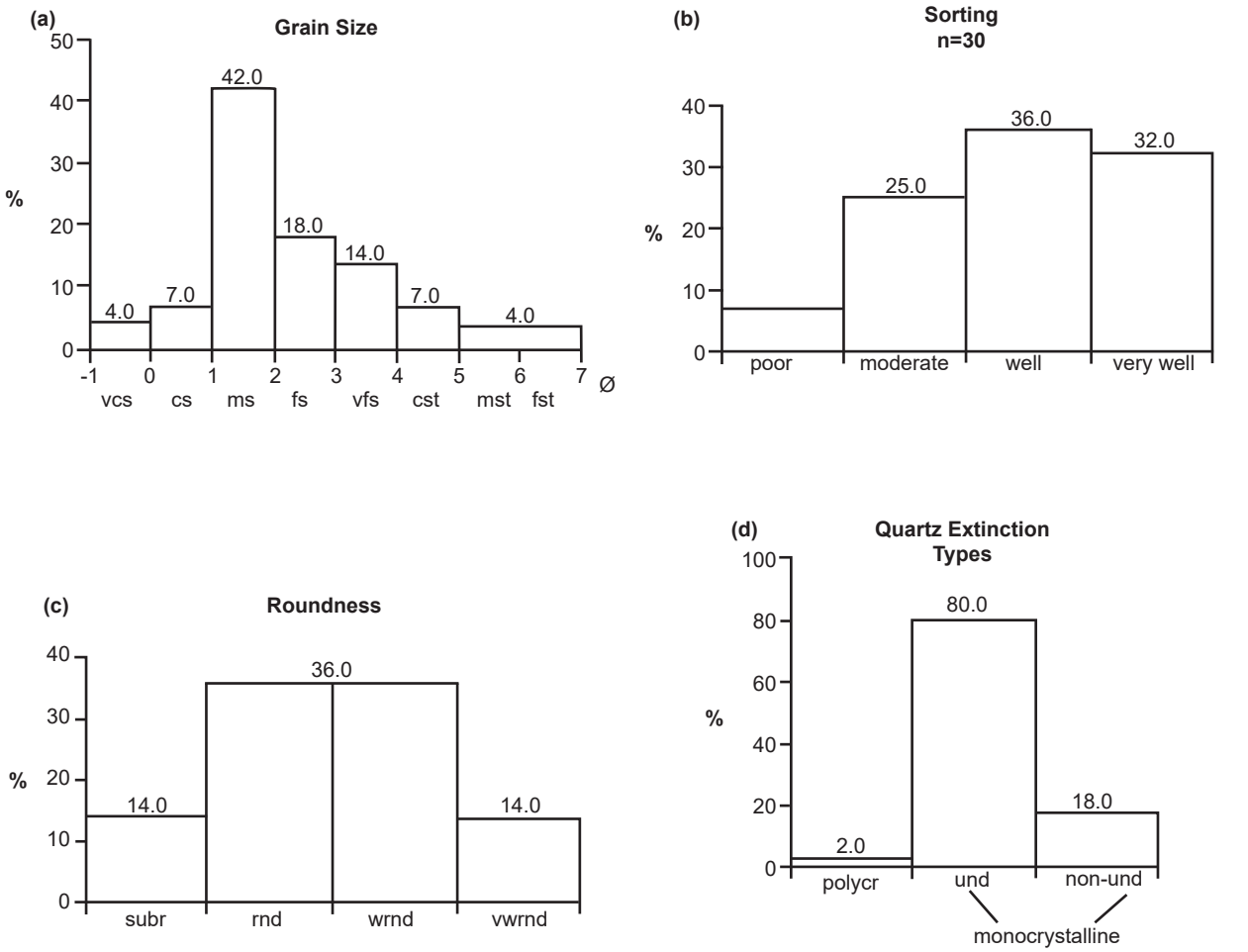

Fig. 36. Grain parameters of selected sandstone samples from the Bright Angel Formation plotted on histograms (after Martin 1985, 38, fig. 9). (a) Grain size in phi (ϕ) units: vcs=very coarse sand, cs=coarse sand, ms=medium sand, fs=fine sand, vfs=very fine sand, cst=coarse silt, mst=medium silt, fst=fine silt. (b) Grain sorting. (c) Grain roundness: subr=sub-rounded, rnd=rounded, wrnd=well rounded, vwrnd=very well rounded. (d) Types of extinction of quartz grains—polycrystalline, undulose, non-undulose.

to well-rounded microcline grains commonly occur in the very fine-grained sandstones.

Martin (1985) found that sub-angular to rounded, moderately-sorted siltstone clasts constitute 7% of the total grain population, with sizes of 0.5–6.0 mm. He noted that some sandstones containing sand-sized siltstone clasts exhibit a bi-modal size distribution, with fine- to coarse-grained siltstone clasts and very coarse silt-sized to very fine sand-sized quartz grains. The siltstone clasts are composed of angular to sub-rounded, poorly- to moderately-sorted quartz and orthoclase grains, brachiopod fragments and glauconitic peloids floating in either a massive hematitic cement or a very fine-grained, gray cherty or clay cement.

Martin (1985) determined the inarticulate brachiopod shell fragments constitute 1.5% of the total grain population. He recognized shell fragments of two genera, *Lingulella* and *Obolus*, with shell thicknesses consistently measuring 0.1 mm and shell fragment lengths commonly being up to 2 mm. Typically the shell fragments are composed of collophane (cryptocrystalline apatite), often as five or six internal layers parallel to the shell surface. Shell fragments are oriented sub-parallel to the bedding, and most fragments are brittlely deformed, the resulting cracks being commonly filled with secondary silica and carbonate cements.

Martin (1985) also recognized sub-rounded to well-rounded and well-sorted hematitic ooids which constituted 1% of the total grain population in his samples. These 0.2–0.6 mm sized ooids were concentrated in a well-sorted, non-graded, structureless, hematite-cemented sandstone. Most of them contained detrital grains as nuclei, which constitute up to 80% of the ooids and consist of sub-rounded to rounded, poorly-sorted quartz or orthoclase grains, schist clasts, brachiopod shell fragments or glauconitic peloids. The hematitic rims consist of concentric layers of hematite and siderite. Some ooids are slightly ellipsoidal in cross-section, probably due to compaction, and most ooids are

slightly larger than associated quartz grains.

The miscellaneous rock and mineral fragments, which Martin (1985) estimated as 2.5% of the total grain population, include detrital schist, chlorite, shale, muscovite, biotite, echinoid fragments, and heavy minerals. The schist, chlorite and muscovite fragments are commonly sub-rounded or acicular, exhibit poor to moderate sorting and are oriented parallel to the bedding. The schist and chlorite fragments vary in size from fine- to medium-grained, and he found them in all the samples he analyzed. Additionally, muscovite and biotite fragments typically occur in the silty matrix of some sandstones. Echinoid spines are rare, and zircon and tourmaline constitute the majority of the heavy minerals he observed.

Martin (1985) also qualitatively determined the clay minerology of randomly selected shale/mudrock samples from four of his measured stratigraphic sections of the Bright Angel Formation. He found that these shale samples contained three clay minerals—illite, kaolinite, and chlorite. The clay mineral distribution and relative abundances of his samples in their approximate stratigraphic positions in his four measured stratigraphic sections is shown in fig. 37. Martin (1985) also found a disordered mixed-layer phase present involving illite and concluded it was an illite mixture with ~10% expandable smectite layers that was indicative of glauconite (Hower 1961). Furthermore, since his shale samples contained abundant muscovite flakes and his sandstone samples often contained glauconite peloids, he concluded that the illite comprised a mixture of detrital and diagenetic illite polytypes and glauconite. The kaolinite peak in his XRD (x-ray diffraction) spectra suggested a relatively well-crystallized kaolinite phase in his shale samples, so he concluded that the burial depth of up to 2 km (6,560 ft) would have produced the temperatures necessary to support such a moderately well-crystallized kaolinite phase. He also determined that the chlorite in his shale samples was dominantly iron-rich and that the polytypes detected were indicative of detrital chlorites and potentially of short transport and rapid burial. Furthermore, the temperatures generated by a maximum burial depth of 2 km (6,560 ft) for the Bright Angel Formation would have been insufficient to diagenetically produce a different chlorite polytype (Hayes 1970), nor would such chlorite have survived extended periods of marine transport.

Martin (1985) admitted that without more precise characterization of the clay mineral types in his shale samples from the Bright Angel Formation as either detrital or diagenetic, their environmental specificity could not be delineated (Keller 1956). However, he concluded that his XRD data pointed to a mixed detrital and diagenetic clay mineral assemblage, primarily because of the ubiquitous occurrence of detrital muscovite in his shale samples, the occasional sharp, steep basal illite XRD reflections indicative of some detrital illite, and the occurrence of occasional broad, shallow basal illite XRD reflections and the

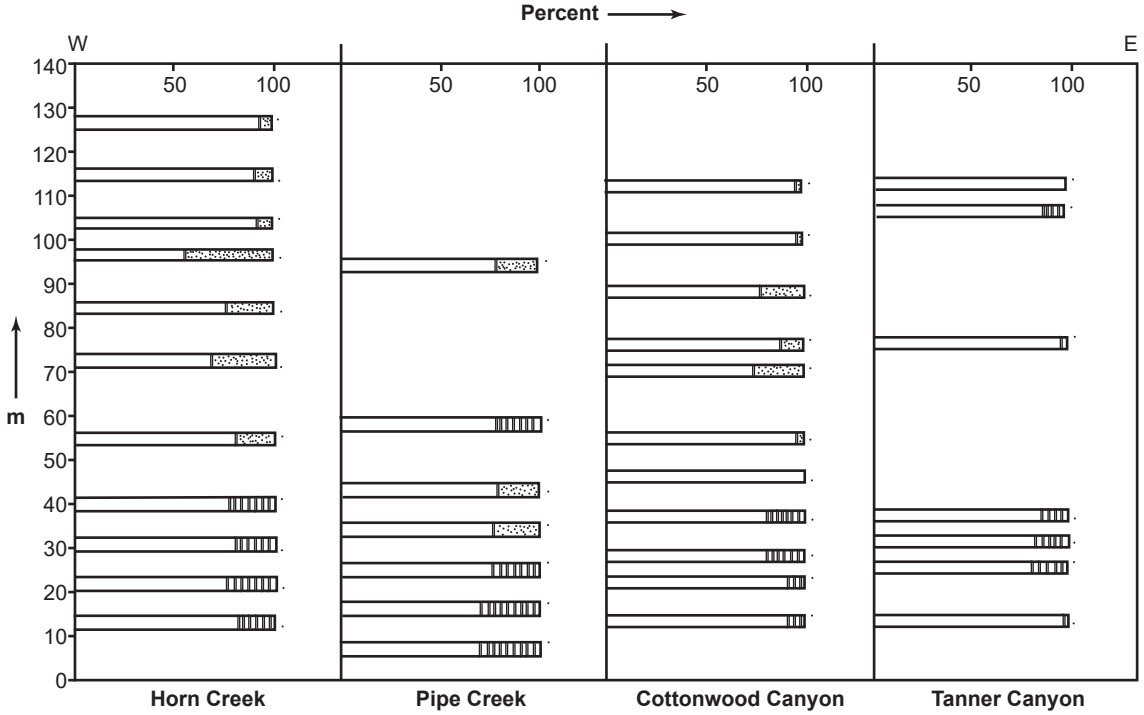

Fig. 37. Clay mineralogy of selected shale/mudstone samples from four measured sections through the Bright Angel Formation (after Martin 1985, 51, fig. 18). The samples are plotted as bar scales at their approximate vertical stratigraphic positions in these sections. Clear=illite, striped=kaolinte, stippled=chlorite.

mixed-layer smectite phase indicative of diagenetic illite/smectite. He also noted kaolinite is generally restricted to the lower portions of the Bright Angel Formation, whereas chlorite predominates over kaolinite in the upper portions but is still subordinate to illite (fig. 37). Furthermore, even though it is not possible to conclusively characterize whether the kaolinite and chlorite are detrital or diagenetic, he concluded that the progressive upward stratigraphic change in the clay mineral assemblage in the Bright Angel Formation evident in fig. 37 could reflect the spatial deposition of the clay minerals or post-depositional diagenetic trends.

Rose (2003) contributed little to the further petrographic description of the Bright Angel Formation. He noted that muscovite flakes were visibly common in thin silty sandstone lenses composed of poorly-sorted fine-grained sandstone and siltstone with small pebble-sized siltstone and sandstone clasts. He also reported that glauconitic peloids occur both as isolated grains within bioturbated and non-bioturbated siltstone beds, as well as in concentrated cross-bedded greensand horizons that are often associated with the bioturbated green crumbly siltstones, which is indicative of the glauconite peloids being detrital (Amorosi 1997). He then extensively discussed how the mineral assemblages present in the Bright Angel Formation could be compared against the theoretical products of diagenesis to limit the range of possible diagenetic pathways from a generic admixture of detrital kaolinite, micas (biotite, muscovite and chlorite), and smectite eroded and deposited from the weathered Precambrian basement schists, gneisses and granites.

However, Rose (2003) only undertook XRD analyses of the clay minerals in a select few of his own samples and published four photomicrographs of the mineral assemblages in the hematitic sandstones he called the magenta or M beds. He showed via his photomicrographs that most of the hematite in them occurs as simple non-concentric grain coatings and void filling cement, and that these sandstones are texturally and compositionally immature due to both unaltered K-feldspar and dolomite being present among abundant quartz grains and variously altered glauconite peloids. And he noted that the dolomite rhombs are fabric-displacive, which he interpreted as indicating the dolomite represented a later replacement of calcite.

Finally, it should be noted that in none of these detailed studies of the petrology of the Bright Angel Formation (Martin 1985; McKee 1945; Rose 2003) is any mention made of either macroscopic or microscope evidence of any metamorphic effects on the sandstones, siltstones and shales, or their constituent mineral grains. Even the slightly elevated temperatures of low-grade metamorphism would have substantially affected the quartz and K-feldspar grains, which are the dominant minerals in these rocks, and affected the textures in their rock fabrics. All previous workers agreed that the Bright Angel Formation is unmetamorphosed in all places where it was examined in Grand Canyon.

Results of the Present Mineralogic Study

During an investigation of four folds in Grand Canyon, ten samples of the Bright Angel Formation were collected from the Whitmore helipad fold (fig. 3), and two samples from outcrops along the Colorado River corridor distant from that fold (fig. 1). The purpose was to compare the samples from that fold with the distal samples to ascertain what effects the folding had on the shale, siltstone and sandstone beds of the Bright Angel Formation and thus determine the conditions during, and the timing of, the folding relative to the conditions and timing of the deposition and subsequent lithification (cementation) of the Bright Angel Formation. Details of the locations of these samples are provided in Appendix D (in the Supplementary material) and in fig. 1 and table 2. All samples were sent to Calgary Rock and Materials Services, Inc. (Calgary, Canada) for thin sectioning and for x-ray diffraction (XRD) analyses.

XRD Results

Calgary Rock and Materials Services, Inc., dried the samples overnight at 60°C, and selected 5–10 grams of each sample to grind for ten minutes in a pulverizing mill to obtain homogeneous powders. These powders were then packed in powder mounts against a glass surface before being mounted in the goniometer of a Rigaku Miniflex II x-ray diffractometer in which a copper source tube is used to provide the incident beam of monochromatic x-rays with a wavelength of 1.541874Å. Samples were typically scanned from 4 to 60° 2θ (two theta) to obtain the XRD spectra. The raw data provided in a specific form by the x-ray computer were imported into the x-ray analysis software (Jade 2010), where peak positions, areas and heights were calculated. The software then provided the most likely matches of minerals for each spectrum generated, from a database of over 100,000 compounds. The Rietveld Refinement Method was then used to determine the percentages of the minerals in the samples.

The results of the bulk rock XRD analyses are in Table 3. Quartz is, of course, the dominant mineral in the Bright Angel Formation samples, but it varies between 25.4% and 86.8% in them. K-feldspar features prominently in all samples, and ranges from 11.0% to 46.9%. Only three of the samples contain

Table 2. Locations and stratigraphic details of the Bright Angel Formation samples examined in this study.

Sample	Location	Location Coordinates	Stratigraphic Position	Notes
BAS-01	River Mile 167.9	N 36° 15.322' W 112° 54.439'	Sandstone relatively high in the Bright Angel Formation stratigraphic section	River right between National and Fern Glen Canyons (closer to latter)
BAS-02	River Mile 167.9	N 36° 15.322' W 112° 54.439'	Sandstone relatively high in the Bright Angel Formation stratigraphic section	River right between National and Fern Glen Canyons (closer to latter)
HF-01	Whitmore helipad fold River Mile 187.4	N 36° 9.250' W 113° 11.400'	Heterolithic sequence horizon near the base of the stratigraphic section	River left, cliff behind the scrub-covered slope up from the river-bank
HF-02	Whitmore helipad fold River Mile 187.4	N 36° 9.250' W 113° 11.400'	Heterolithic sequence horizon near the base of the stratigraphic section	River left, cliff behind the scrub-covered slope up from the river-bank
HF-03	Whitmore helipad fold River Mile 187.4	N 36° 9.250' W 113° 11.400'	Heterolithic sequence horizon near the base of the stratigraphic section	River left, cliff behind the scrub-covered slope up from the river-bank
HF-04	Whitmore helipad fold River Mile 187.4	N 36° 9.250' W 113° 11.400'	Heterolithic sequence horizon near the base of the stratigraphic section	River left, cliff behind the scrub-covered slope up from the river-bank
HF-05	Whitmore helipad fold River Mile 187.4	N 36° 9.250' W 113° 11.400'	Heterolithic sequence horizon near the base of the stratigraphic section	River left, cliff behind the scrub-covered slope up from the river-bank
HF-06	Whitmore helipad fold River Mile 187.4	N 36° 9.250' W 113° 11.400'	Heterolithic sequence horizon near the base of the stratigraphic section	River left, cliff behind the scrub-covered slope up from the river-bank
HF-07	Whitmore helipad fold River Mile 187.4	N 36° 9.250' W 113° 11.400'	Heterolithic sequence horizon near the base of the stratigraphic section	River left, cliff behind the scrub-covered slope up from the river-bank
HF-08	Whitmore helipad fold River Mile 187.4	N 36° 9.250' W 113° 11.400'	Heterolithic sequence horizon near the base of the stratigraphic section	River left, cliff behind the scrub-covered slope up from the river-bank
HF-09	Whitmore helipad fold River Mile 187.4	N 36° 9.250' W 113° 11.400'	Heterolithic sequence horizon near the base of the stratigraphic section	River left, cliff behind the scrub-covered slope up from the river-bank
HF-10	Whitmore helipad fold River Mile 187.4	N 36° 9.250' W 113° 11.400'	Heterolithic sequence horizon near the base of the stratigraphic section	River left, cliff behind the scrub-covered slope up from the river-bank

Table 3. Mineral compositions of the Bright Angel Formation samples from x-ray diffraction (XRD) analyses, courtesy of Ray Strom, Calgary Rock and Materials Services, Inc., Canada.

Sample	Lithology	Quartz	K-Feldspar	Calcite	Dolomite	Ankerite	Siderite	Illite	Kaolinite	Pyrite	Total
BAS-01	sandstone	74.3%	21.7%	1.8%	1.2%	-	-	0.5%	0.5%	-	100.0%
BAS-02	sandstone	33.7%	19.6%	32.4%	9.2%	-	-	2.3%	-	2.8%	100.0%
HF-01	sandstone	57.3%	28.7%	3.4%	3.2%	6.8%	-	0.6%	-	-	100.0%
HF-02	shale	33.8%	43.1%	-	-	2.9%	-	20.2%	-	-	100.0%
HF-03	shale	25.4%	36.7%	-	-	3.7%	-	34.2%	-	-	100.0%
HF-04	sandstone	46.5%	33.5%	-	-	17.6%	-	2.4%	-	-	100.0%
HF-05	siltstone	31.1%	46.9%	-	-	3.3%	-	18.7%	-	-	100.0%
HF-06	sandstone	86.8%	11.0%	-	2.2%	-	-	-	-	-	100.0%
HF-07	siltstone	29.6%	32.4%	-	11.9%	-	8.6%	17.5%	-	-	100.0%
HF-08	sandstone	47.6%	42.2%	-	7.9%	-	-	2.3%	-	-	100.0%
HF-09	siltstone	27.3%	45.1%	-	5.3%	-	-	22.3%	-	-	100.0%
HF-10	sandstone	42.6%	45.3%	-	9.1%	-	-	2.5%	-	0.5%	100.0%

significant amounts of calcite, varying from 1.8% to a dominant 32.4%, yet the same three samples contain between 1.2% and 9.2% dolomite while one of them also contains 6.8% ankerite. Indeed, as many as eight of the twelve samples contain between 1.2% and 11.9% dolomite, five samples contain between 2.9% and 17.6% ankerite, and one sample contains 8.6% siderite. Illite is the most ubiquitous clay mineral, which is present in eleven of the samples from 0.5% to 34.2% and probably also reflects the glauconite and muscovite contents, while one sample also contains 0.5% kaolinite. Two samples contain 0.5% and 2.8% pyrite.

The results of the clay fraction XRD analyses are in table 4. In most samples clay minerals occur in significant amounts. The clay mineral present in all samples is illite, varying from 23.0% to 95.2%, and dominates in all but one sample. Additionally, mixed-layered illite/smectite is present in all samples, ranging from 4.8% to 25.5%, and likely is a measure of the glauconite content. Kaolinite is the dominant clay mineral in one sample at 57.1% and is present in three other samples in much smaller amounts ranging from 1.4% to 5.6%. Chlorite is also present at 9.1% in the sample dominated by kaolinite.

Thin Section Examination

The thin sections for this study were all mounted on standard glass microscope slides. Before the slices were cut from the rock samples using a diamond saw, the rock samples were impregnated under confining pressure with epoxy resin that contained a blue dye. This ensured that grains did not get dislocated or the rock fabrics get distorted during the sawing of the slices. However, this process left the thin sections with a blue dye staining as the surrounding background and in any holes or pores within the rock fabrics. Before cover slips were added, the thin sections were stained so as to make the K-feldspar and calcite in the rock fabrics more easily distinguished. Thus, the K-feldspar grains have a distinctive yellow color and the calcite is pinkish in plane polarized light.

Petrographic descriptions of all samples from extensive thin section examination are provided in Appendix D (in the Supplementary material), along with photographs of the whole thin sections (as in fig. 38) from which the descriptions were derived. Of the twelve samples, eight of them are fine-grained sandstones, one is a siltstone and three are shales or mudstones. The thin sections of all the samples are shown in fig. 38, while a representative set of photomicrographs in fig. 39 show typical textures within each of the samples. It should be noted that in these thin sections there is often a blue dye staining between the grains, and sometimes encroaching on the grain edges or even across grain surfaces. This blue dye is associated with the epoxy that the samples were impregnated with prior to the preparation of the thin sections. Thus, some patches of blue dye mark the occasional pore spaces.

In the thin sections, the fine-grained sandstones are generally massive and well-sorted, sometimes laminated parallel to the bedding or sometimes with a hint of being partially cross-laminated. They are usually dominated by angular, and even euhedral, to sub-rounded quartz grains ranging in size from medium to coarse silt to very fine and fine sand and very occasional medium sand, using the standard definitions and terminologies for sorting of Folk (1966, 1980) and Pettijohn, Potter, and Siever (1973), for shape of Powers (1953) and Folk (1955), and for size of Udden (1914) and Wentworth (1922). Usually, coarse silt to fine sand-size, sub-angular to sub-rounded K-feldspar grains, and sometimes even sub-euhedral laths, are subordinate to the quartz grains, but occasionally the K-feldspar grains predominate. Most of the sandstones contain small oval-shaped olive green-brown glauconite pellets or sub-angular to sub-rounded grains. Scattered muscovite flakes are usually sub-parallel to the bedding or occasional laminae, and there are occasional brachiopod shell fragments (distinguished by their thick internal structure and composition). Generally, there are virtually no original pore spaces remaining because they were filled with quartz (silica) cement, usually as overgrowths around the detrital quartz grains, which are occasionally outlined by the original iron oxide coatings, so that many grains now meet at triple points. In finer-grained rocks the grain radii are smaller than the microscope slide thickness and thus the grains stack up on each other, obscuring the porosity. So, there still may be just a few very small pore spaces that are difficult to see. Alteration is marked by carbonates (calcite, dolomite and/or ankerite) or clay minerals (predominantly illite), often accompanied by iron oxides filling former pores, replacing K-feldspar grains, or filling fractures. So, these are glauconitic sub-arkosic quartz arenites according to the classifications of Dott (1964), Folk (1980), McBride (1963) Pettijohn (1954, 1957), Pettijohn, Potter, and Siever (1972), Scholle (1979) and Ulmer-Scholle et al. (2015), and some are even glauconitic arkoses where the K-feldspar contents are greater than 25%.

In thin section, the siltstone is very similar to the sandstones except that the grain sizes are smaller and dominantly in the silt-size range. In fact, it is difficult to distinguish the siltstone from the fine-grained sandstones because the latter also contain some silt-sized grains, and some of the shales have selvages or laminae of siltstone (figs. 38d, j, and 39h, i). The siltstone is an interlocking mosaic of tiny to very

Table 4. Clay mineral fraction compositions of the Bright Angel Formation samples from x-ray diffraction (XRD) analyses, courtesy of Ray Strom, Calgary Rock and Materials Services, Inc., Canada.

Sample	Lithology	Illite	Illite/Smectite	Kaolinite	Chlorite	Total
BAS-01	sandstone	23.0%	10.2%	57.7%	9.1%	100.0%
BAS-02	sandstone	71.5%	22.9%	5.6%	-	100.0%
HF-01	sandstone	81.8%	18.2%	-	-	100.0%
HF-02	shale	87.9%	10.7%	1.4%	-	100.0%
HF-03	shale	90.2%	8.2%	1.6%	-	100.0%
HF-04	sandstone	79.5%	20.5%	-	-	100.0%
HF-05	siltstone	85.0%	15.0%	-	-	100.0%
HF-06	sandstone	94.0%	6.0%	-	-	100.0%
HF-07	siltstone	87.4%	12.6%	-	-	100.0%
HF-08	sandstone	81.0%	19.0%	-	-	100.0%
HF-09	siltstone	95.2%	4.8%	-	-	100.0%
HF-10	sandstone	74.5%	25.5%	-	-	100.0%

small, angular to sub-rounded quartz and K-feldspar grains with subordinate sub-euhedral, angular and sub-rounded to rounded greenish glauconite grains and fragments, numerous muscovite flakes at various angles but sometimes parallel to the bedding, and occasional brachiopod shell fragments. However, there are also brown patches in the rock fabric (fig. 38k) dominated by very small, sub-angular to sub-rounded, iron-oxide-stained carbonate grains and rhombs (dolomite, siderite and calcite), some of which may be detrital, and there is illite alteration of some K-feldspar grains. Some of these may even be carbonate clasts. While there is some silica cement apparent, likely as overgrowths on the original detrital quartz grains, much of the mosaic is now cemented by a combination of illite and carbonates, some of which is iron-oxide-coated, so there are virtually no pore spaces remaining (although the tight stacking of many of the very small grains may obscure any trivial pore spaces). If the same sandstone classification criteria are applied, the siltstone would likewise have originally been a glauconitic arkose.

The shales or mudstones in the thin sections consist of alternating thin bands or laminae and selvages of "softer" predominantly iron-oxide-stained yellow-brown very fine-grained illite and "harder" laminae and "augen"-like bands or "eyes" of siltstone consisting of a "clean" fine-grained mosaic of quartz and K-feldspar grains (figs. 38d, j, l, and 39g-i, p). According to the classification scheme for shales of Ulmer-Scholle et al. (2015, 183, fig. 8.1), given the large amounts of quartz and K-feldspar in these shales (table 3) they would be termed "siliceous mudstones." The illite-dominated laminae appear to be primarily due to alteration of tiny K-feldspar grains because there are tiny remnant K-feldspar grains and residual tiny irregularly-shaped quartz grains scattered through the rock fabric. There are also numerous tiny muscovite flakes at various angles but mostly inclined parallel to the bedding, some tiny irregularly-shaped blotches of greenish glauconite, and many scattered very tiny-tiny specks, blotches and streaks of heavy iron oxide, as well as the pervasive iron oxide staining. There are virtually no pores as the original mosaic was already tightly fitted and the pervasive illite alteration is now the predominating cement, perhaps along with the occasional patches of heavy iron oxide. The siltstone bands and "eyes" consist of the same mineral grains but they are slightly larger silt-sized and are often dominated by quartz, though K-feldspar is still present, as well as the greenish glauconite grains, and numerous muscovite flakes often parallel the borders of the bands, laminae, and "eyes." Some tiny carbonate grains are sometimes present, often accompanied by iron oxides and clumped together in brown patches (fig. 39f, o). Some trivial pores may also still be present. It is to be expected that the shales would have a similar mineral composition to that of the interbedded siltstones and sandstones, their segregation being due to sorting of grain sizes during deposition.

Quartz

Under the microscope, quartz grains are invariably in tightly-packed interlocking mosaics with the other mineral grains with virtually no pore spaces remaining (fig. 40). Depending on whether the rock is a sandstone, siltstone, or shale, the quartz grains in each are in narrow size ranges corresponding to fine to coarse silt (0.01–0.06 mm, ϕ=+6.72 –+4.05) and very fine and fine sand (0.07–0.25 mm, ϕ=+3.77 –+2.00), so each rock fabric appears well-sorted. The quartz grains are sometimes irregularly-shaped angular (sometimes elongated parallel to the bedding), but invariably are euhedral and sub-angular to sub-

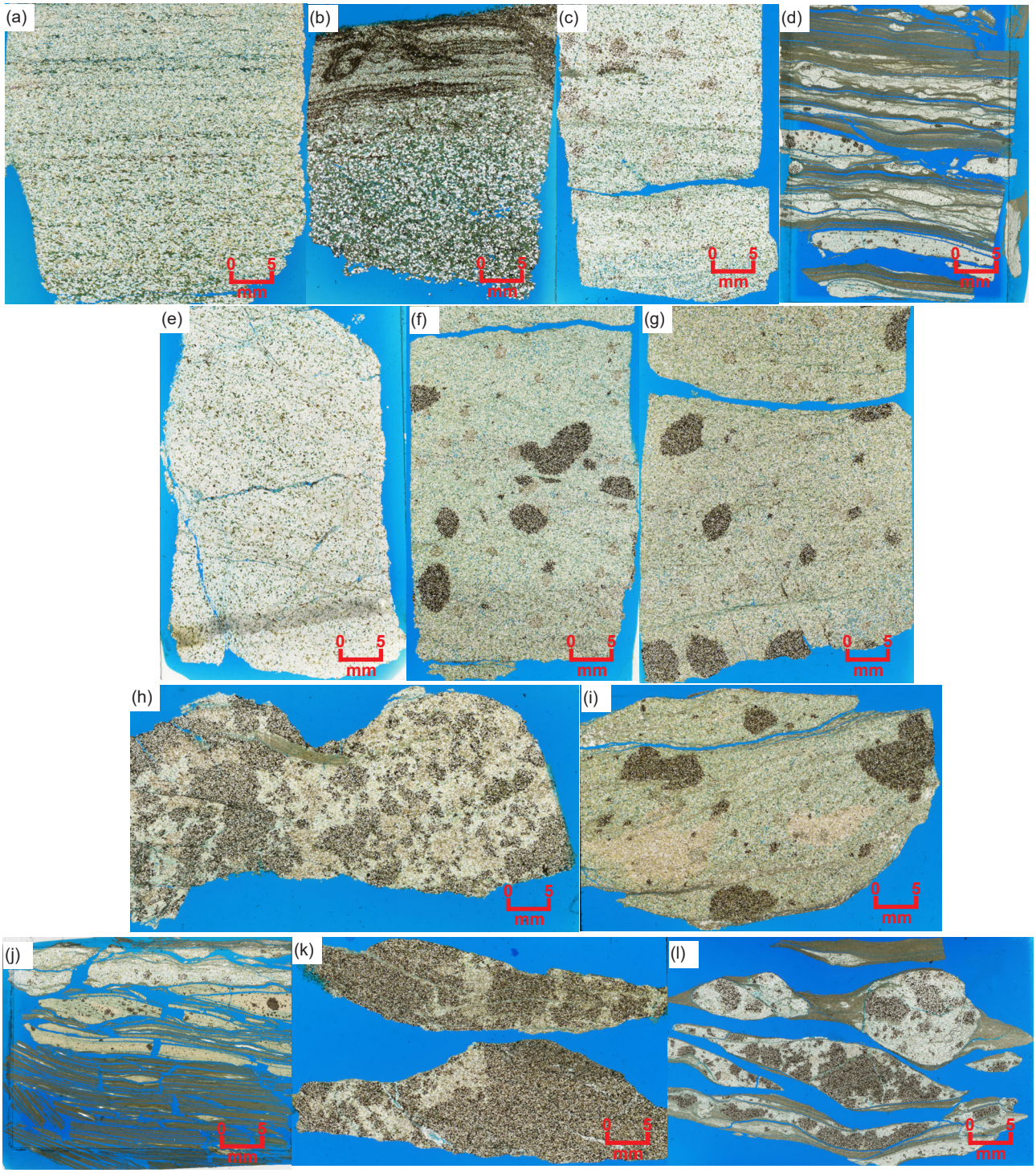

Fig. 38. The thin sections of all twelve Bright Angel Formation samples at normal hand specimen scale (scale bars indicate ~5 mm), orientated so that the bedding is across the image and the upside is to the top. (a) BAS-01, ((b) BAS-02, (c) HF-01, (d) HF-03, (e) HF-06, (f) HF-08, (g) HF-10, (h) HF-04, (i) HF-05, (j) HF-02, (k) HF-07, and (l) HF-09.

rounded, some with internal iron oxide "ghost" outlines of the original sub-rounded detrital grains with the overgrowths in optical continuity so the grains meet at triple points (fig. 40p). In some places this quartz cementation infilling between the quartz grains in optical continuity is so complete with the original grain boundaries so indistinct that the fabric looks like a solid mass of quartz. The quartz cementation clearly had to have occurred early as in some places the quartz grains are dominantly euhedral and angular due to the overgrowths being in optical continuity and not always discernible, while in other places there are quartz grains that are molded around other grains so the quartz cement must have overgrown the detrital grains in optical continuity.

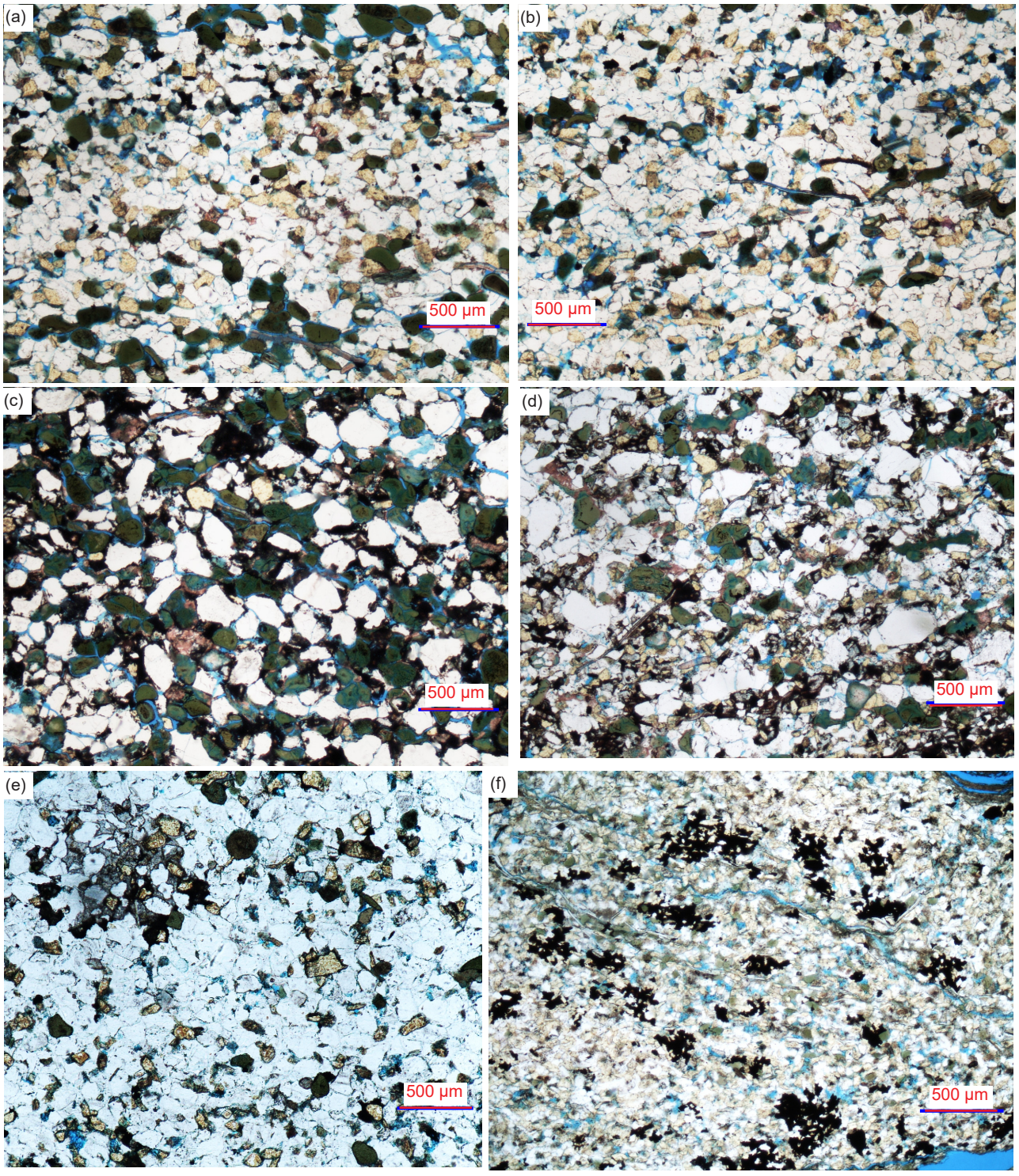
(a)
500 µm
(b)
500 µm
(c)
500 µm
(d)
500 µm
(e)
500 µm
(f)
500 µm

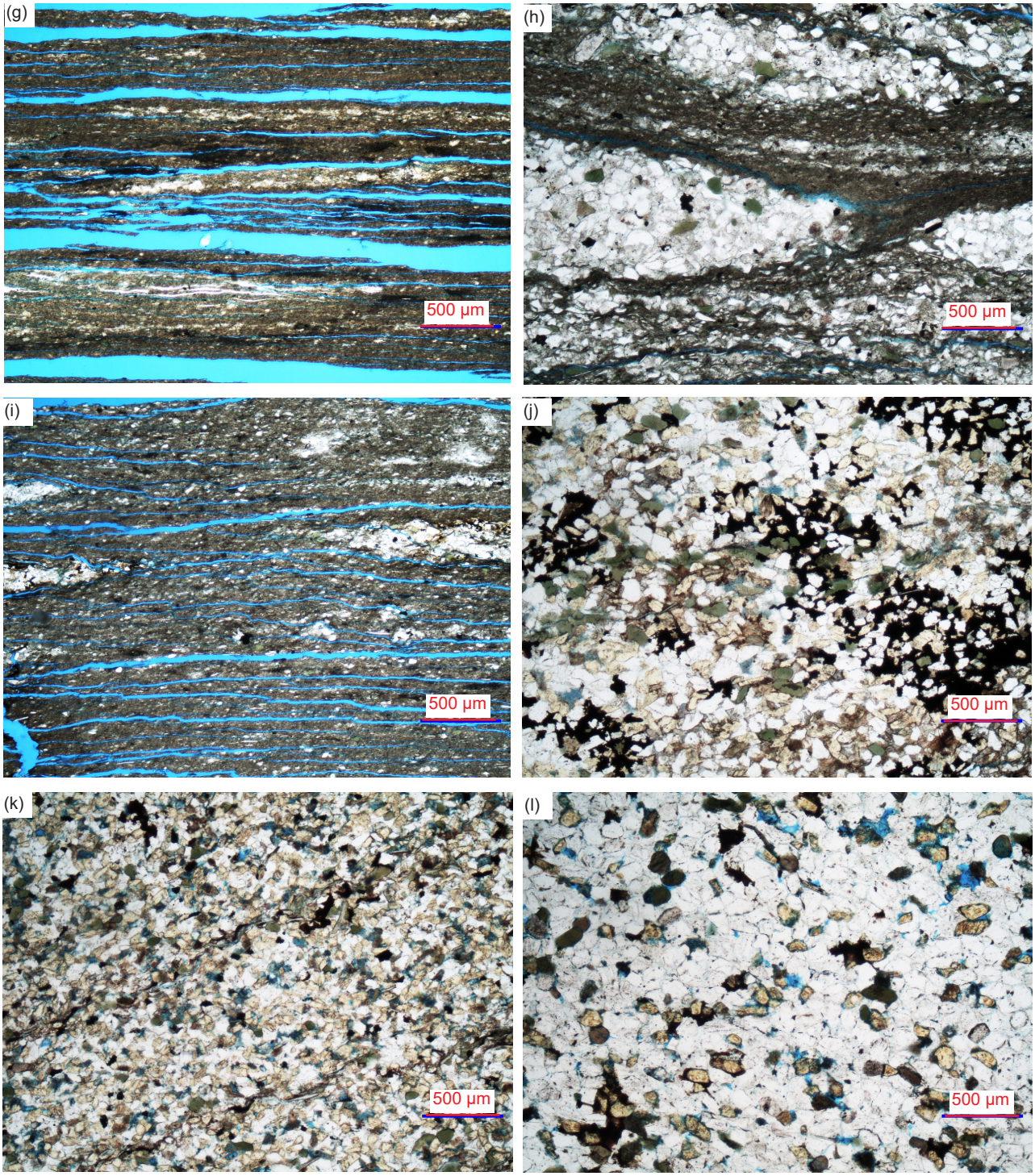
(g)
500 µm
(h)
500 µm
(i)
500 µm
(j)
500 µm
(k)
500 µm
(l)
500 µm

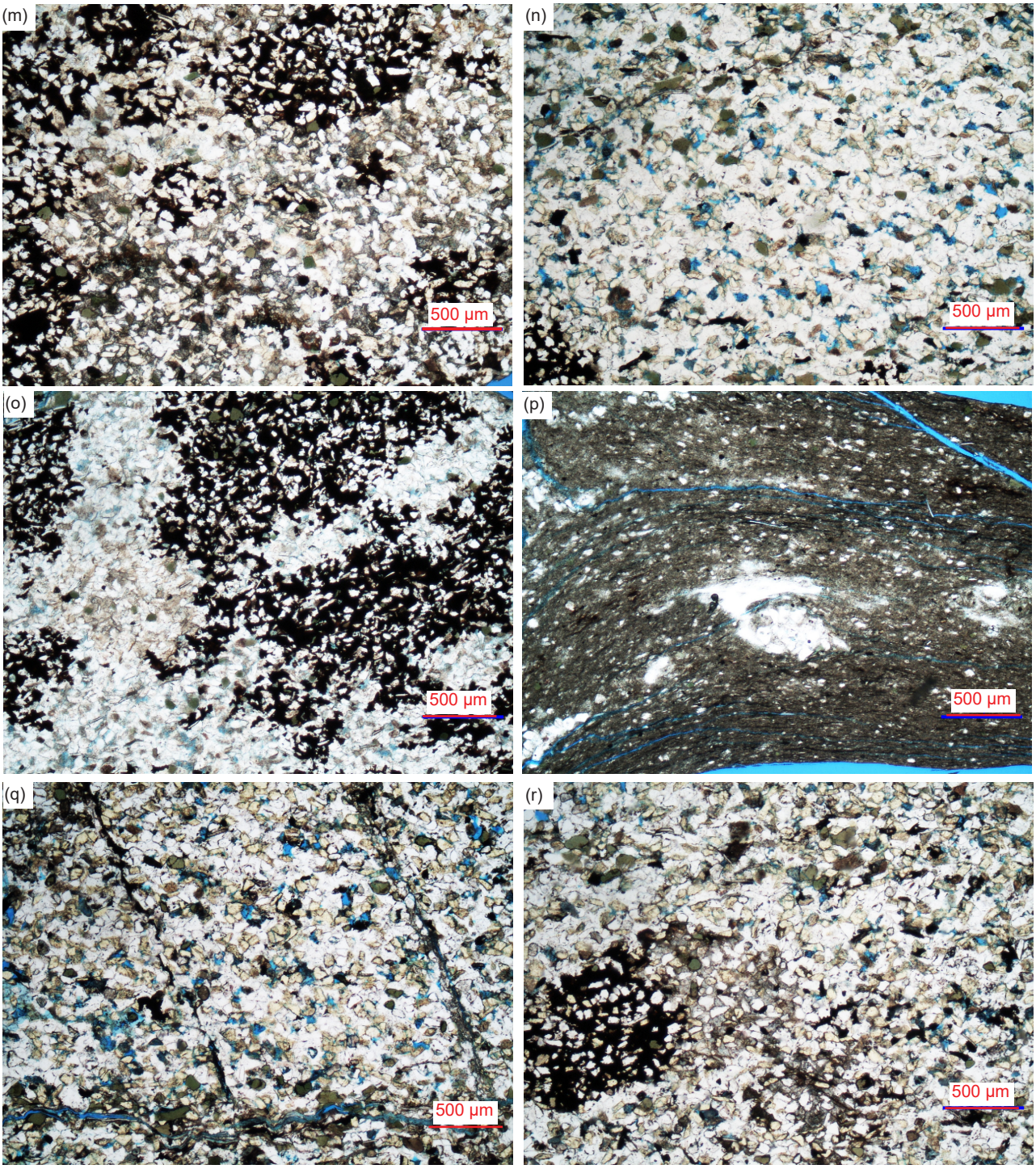

Fig. 39 (pages 362, 363, and 364). A representative set of photomicrographs at the same scale (as indicated) showing the variations in textures in the samples from the Bright Angel Formation. Note the variations in grain sizes from shales to siltstones and sandstones, the grain shapes and sorting, and the almost universal presence of K-feldspar grains. Most samples have some residual pore spaces (usually highlighted by the blue dye), but most pores have been infilled with quartz cement (as overgrowths), or in a few places by illite, carbonates and/or iron oxides. (a), (b) BAS-01, (c), (d) BAS-02, (e) HF-01, (f), (g) HF-02, (h), (i) HF-03, (j) HF-04, (k) HF-05, (l) HF-06, (m) HF-07, (n) HF-08, (o), (p) HF-09, and (q), (r) HF-10.

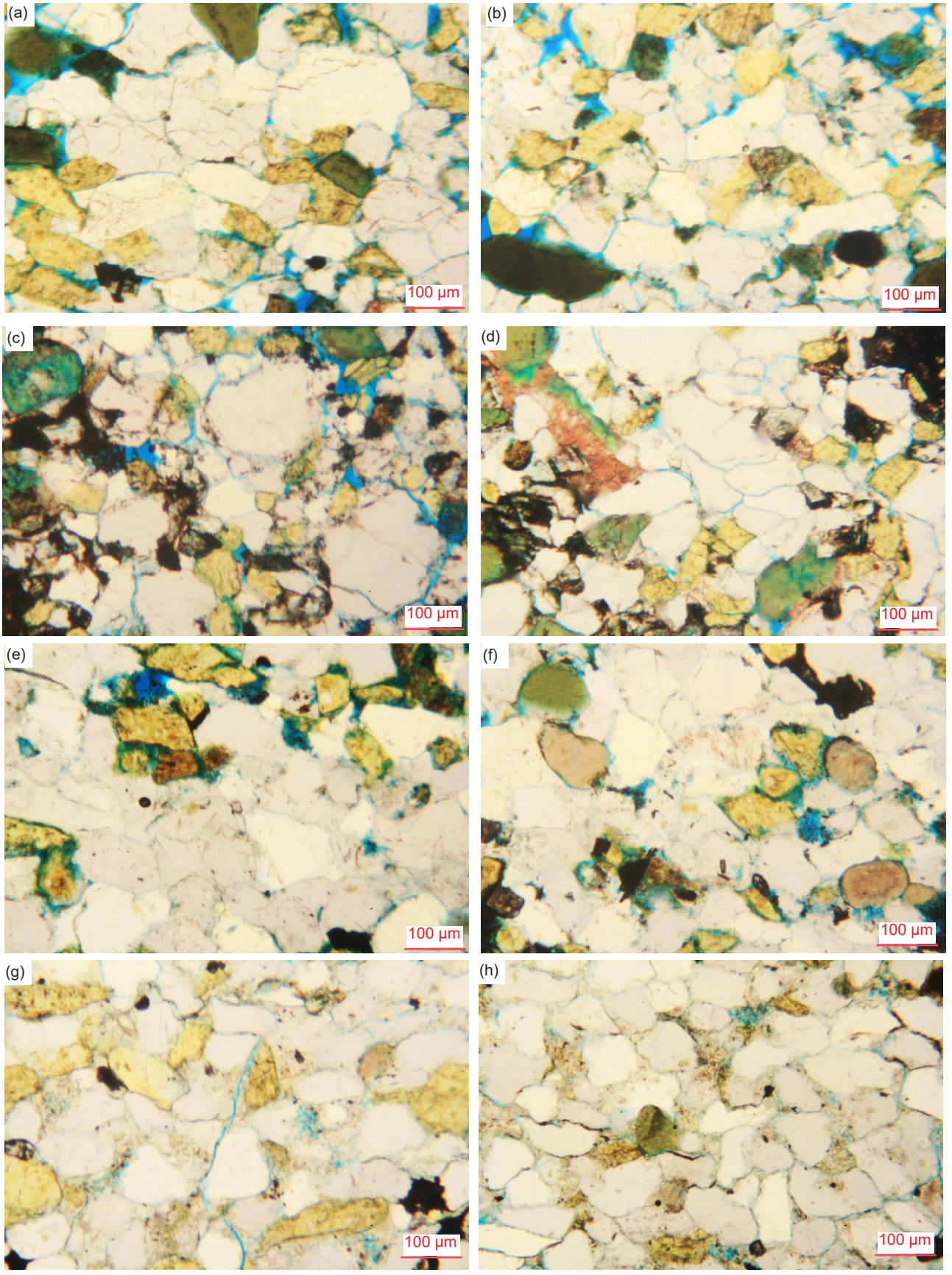
(a)
100 µm
(b)
100 µm
(c)
100 µm
(d)
100 µm
(e)
100 µm
(f)
100 µm
(g)
100 µm
(h)
100 µm

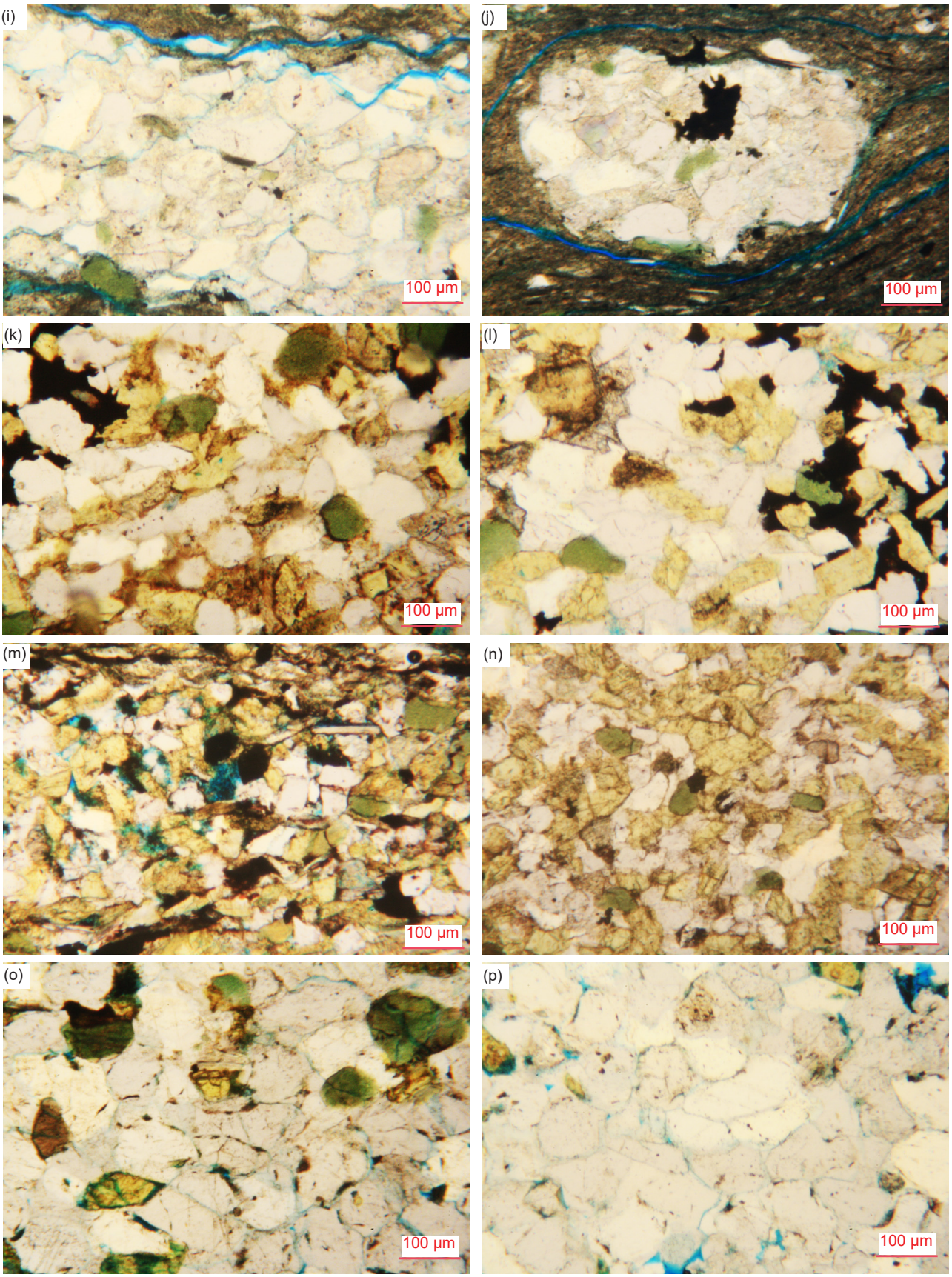
(i)
100 μm
(j)
100 μm
(k)
100 μm
(l)
100 μm
(m)
100 μm
(n)
100 μm
(o)
100 μm
(p)
100 μm

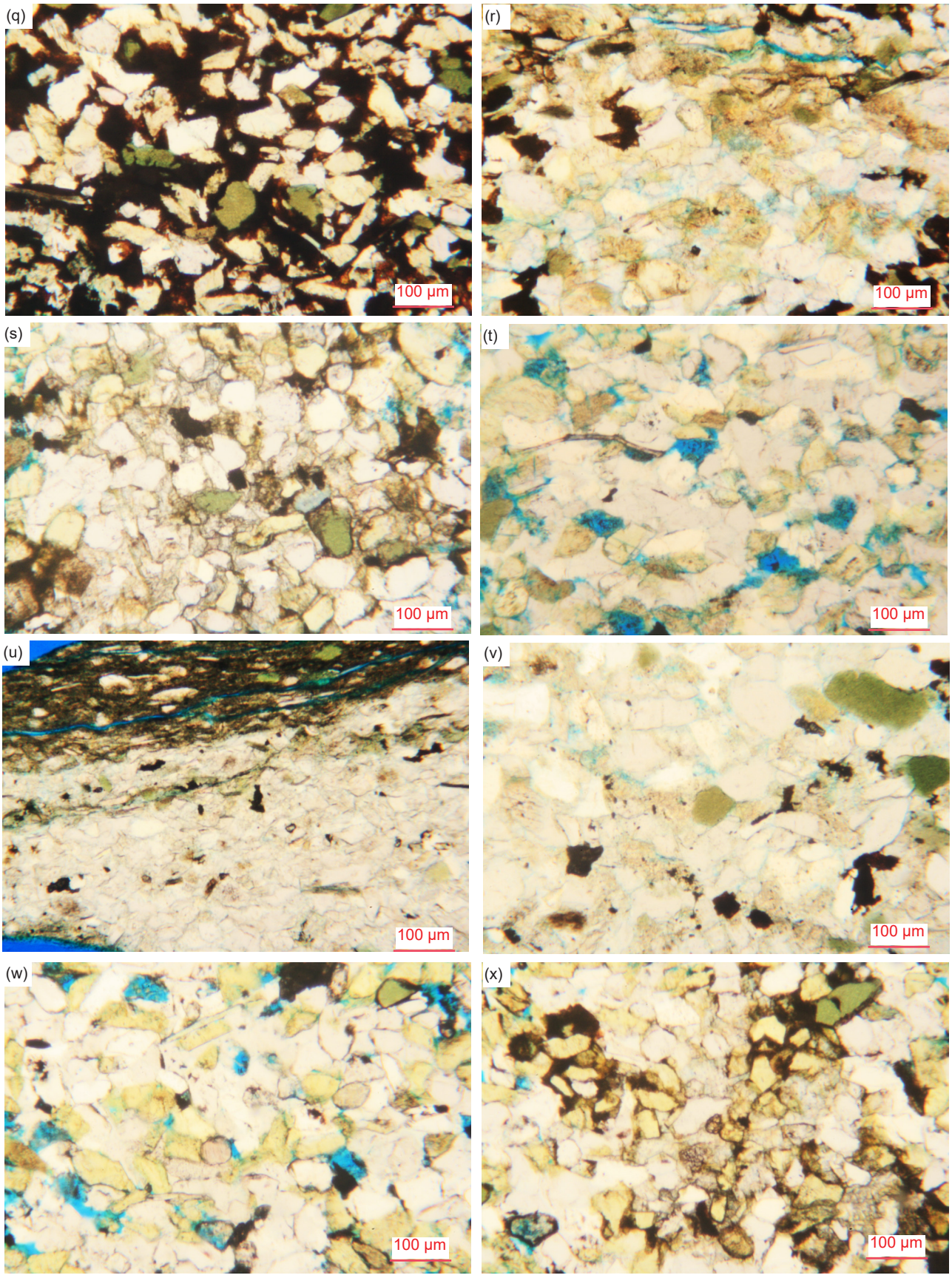
(q)
100 µm
(r)
100 µm
(s)
100 µm
(t)
100 µm
(u)
100 µm
(v)
100 µm
(w)
100 µm
(x)
100 µm

Fig. 40 (pages 365, 366, and 367). A representative set of photomicrographs at various scales (as indicated) showing the quartz grains and various cements in the Bright Angel Formation samples. Note the variations in grain sizes, shapes, inclusions and sorting. Most samples have very few residual pore spaces (usually highlighted by the blue dye), and most pores have been infilled with quartz cement (as overgrowths), or in many places by carbonates, illite (often after K-feldspar) and/or iron oxides, which gives the appearance of the close packing, indicating the degree of the compaction of the sediments. (a), (b) BAS-01, (c), (d) BAS-02, (e), (f) HF-01, (g), (h) HF-02, (i), (j) HF-03, (k), (l) HF-04, (m), (n) HF-05, (o), (p) HF-06, (q), (r) HF-07, (s), (t) HF-08, (u), (v) HF-09, and (w), (x) HF-10.

In places, there are several medium-sized quartz grains together surrounded by smaller quartz grains. Larger quartz grains consist of very small irregularly-shaped sub-domains, or sometimes sub-grains, with different extinction angles and some quartz grains display undulose extinction (particularly near fracture planes and zones). Some of these quartz grains could be derived from metamorphic schists. Other quartz grains have straight edges and are more euhedral to polygonal due to their overgrowths. Some quartz grains are cracked (fig. 40a), often with faint iron oxide staining the cracks, and some quartz grains with irregular edges look like broken fragments, occasionally being somewhat elongated. Where illite alteration is present between the quartz grains, particularly in the shales but also in some sandstones, they sometimes have fuzzy and/or irregular edges due probably to resorption of silica during encroaching illite alteration, and sometimes such quartz grains are together in "clumps" in which they meet at triple points. A few quartz grains appear to have very tiny inclusions within them, while other quartz grains contain tiny K-feldspar grains or tiny muscovite flakes.

In one sandstone sample from near the hinge zone of the Whitmore helipad fold, where there is also a minor fault with trivial offset, there are linear zones of variable thickness where there has been fracturing, and recementing with a mosaic of tiny angular quartz grains, often with lots of iron oxide staining. In several places, blocks of the regular mosaic of small quartz grains have been offset along fracture planes, some quartz grains having also been fractured and slightly offset. In other places, small patches of a mosaic of tiny quartz grains, often lightly dusted with iron oxides, are between the quartz grains in the regular mosaic, although some of those quartz grains are fractured and/or exhibit undulose extinction, and others are remnants with fuzzy (resorbed?) edges, indicating the effects of the fracturing and recementing.

K-Feldspar

K-feldspar grains and former laths are ubiquitous in all samples, usually being subordinate to quartz grains, but sometimes are more abundant and thus are the dominant component (fig. 41). Most K-feldspar grains are very small (0.02–0.06 mm, ϕ=+5.71 –+4.05) and small (0.07–0.24 mm, ϕ=+3.77 –+2.06), depending on whether the rock is a sandstone, siltstone or shale. In the sandstones, sometimes there are also some medium (0.25–0.47 mm, ϕ=+2.00 –+1.09) grains and laths. Some K-feldspar grains are angular or euhedral and some are rounded, but the majority are sub-angular, irregularly-shaped to sub-rounded. The former laths are tabular and elongated, some being long and relatively thin. Often the K-feldspar grains and laths tend to clump together. Occasionally there are very small and small, irregularly-shaped, angular or broken fragments of K-feldspar grains and former laths. All these grains, former laths and fragments are wedged in the tightly-fitted, interlocking, sometimes laminated, mosaics with the other mineral grains, particularly quartz grains.

Some K-feldspar grains, former laths and even fragments exhibit pseudo or partial multiple twinning and some display cross-hatched twinning (indicative of microcline) under crossed polars, and in some the cleavage is still evident. It is possible a few fresh-looking stained grains that exhibit full multiple twinning under crossed polars may be plagioclase. Many K-feldspar grains and laths are dusted with iron oxide specks and streaks, and most mosaic grains have their edges outlined by iron oxide. Some K-feldspar grains seem to have "ghost" outlines marked by iron oxides within them, perhaps suggesting there have been overgrowths of K-feldspar, although the latter have different extinction angles. However, the dominant quartz cement has clearly grown around the original detrital quartz grains and between the K-feldspar grains to bind together the mosaics.

Some K-feldspar grains appear to be partially, variably and even highly altered to illite, perhaps best evident under crossed polars because in plane polarized light they have retained their K-feldspar habit and appearance. The impregnation of the samples has caused blue dye staining of some altered K-feldspar grains, making them look greenish (like glauconite), while others are also heavily iron oxide stained making them also brownish. Within the brown patches in some sandstone samples the edges of K-feldspar grains are ill-defined due to encroachment on them of the siderite and iron-oxide-covered dolomite cement.

In the shales, the dark yellow-brown laminae consist of iron-oxide-stained illite alteration, which

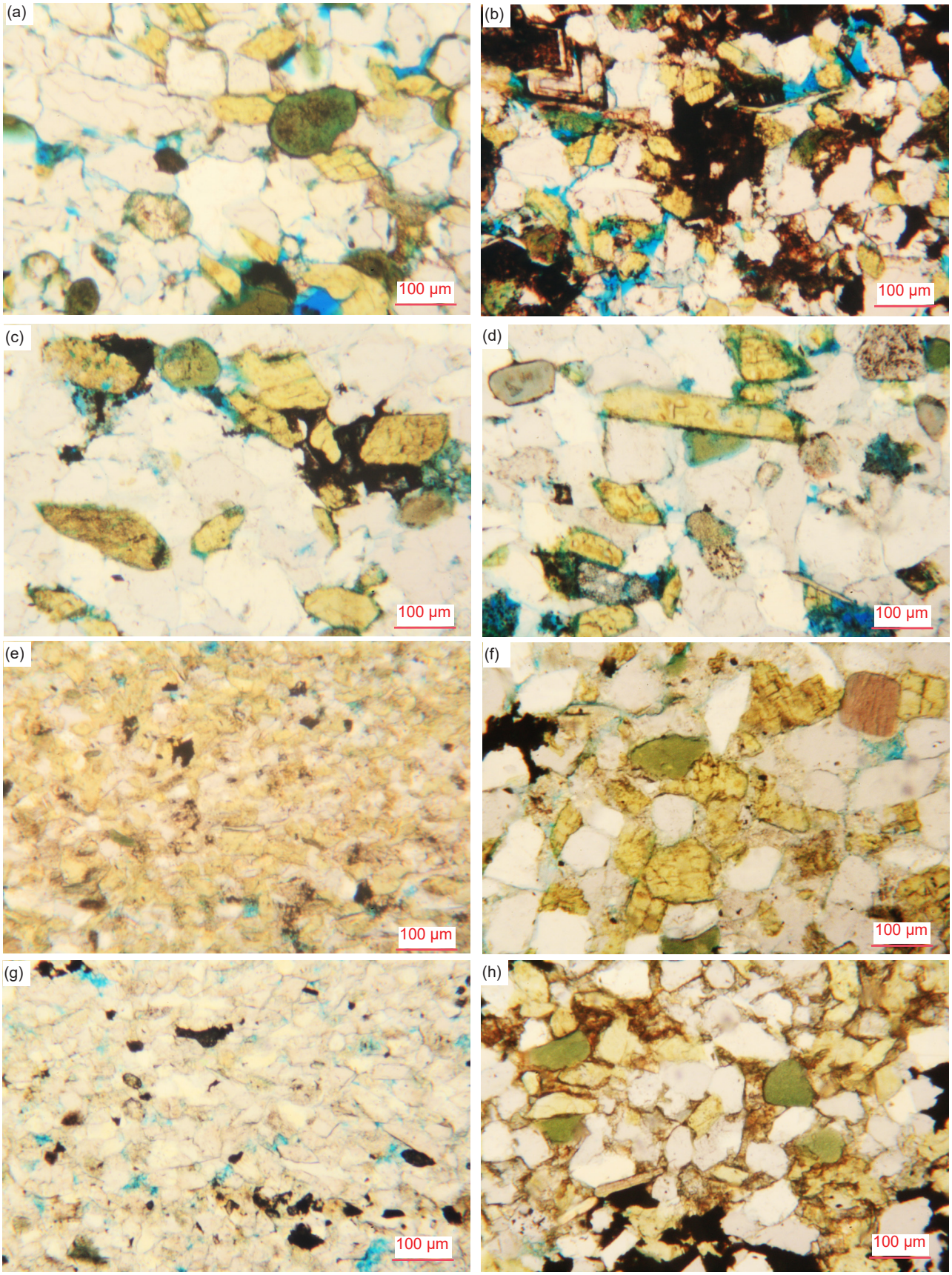
(a)
100 µm
(b)
100 µm
(c)
100 µm
(d)
100 µm
(e)
100 µm
(f)
100 µm
(g)
100 µm
(h)
100 µm

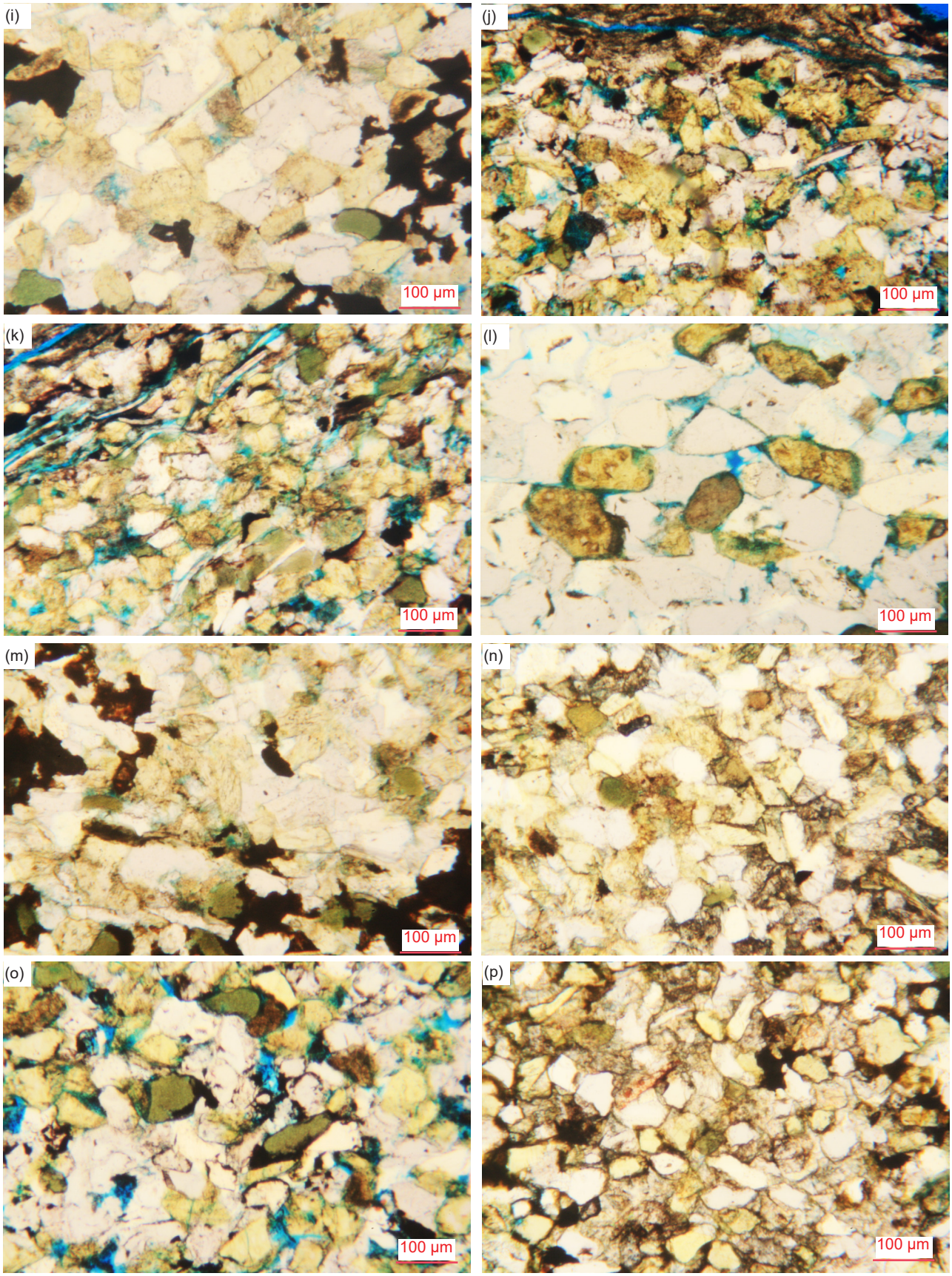
(i)
100 μm
(j)
100 μm
(k)
100 μm
(l)
100 μm
(m)
100 μm
(n)
100 μm
(o)
100 μm
(p)
100 μm

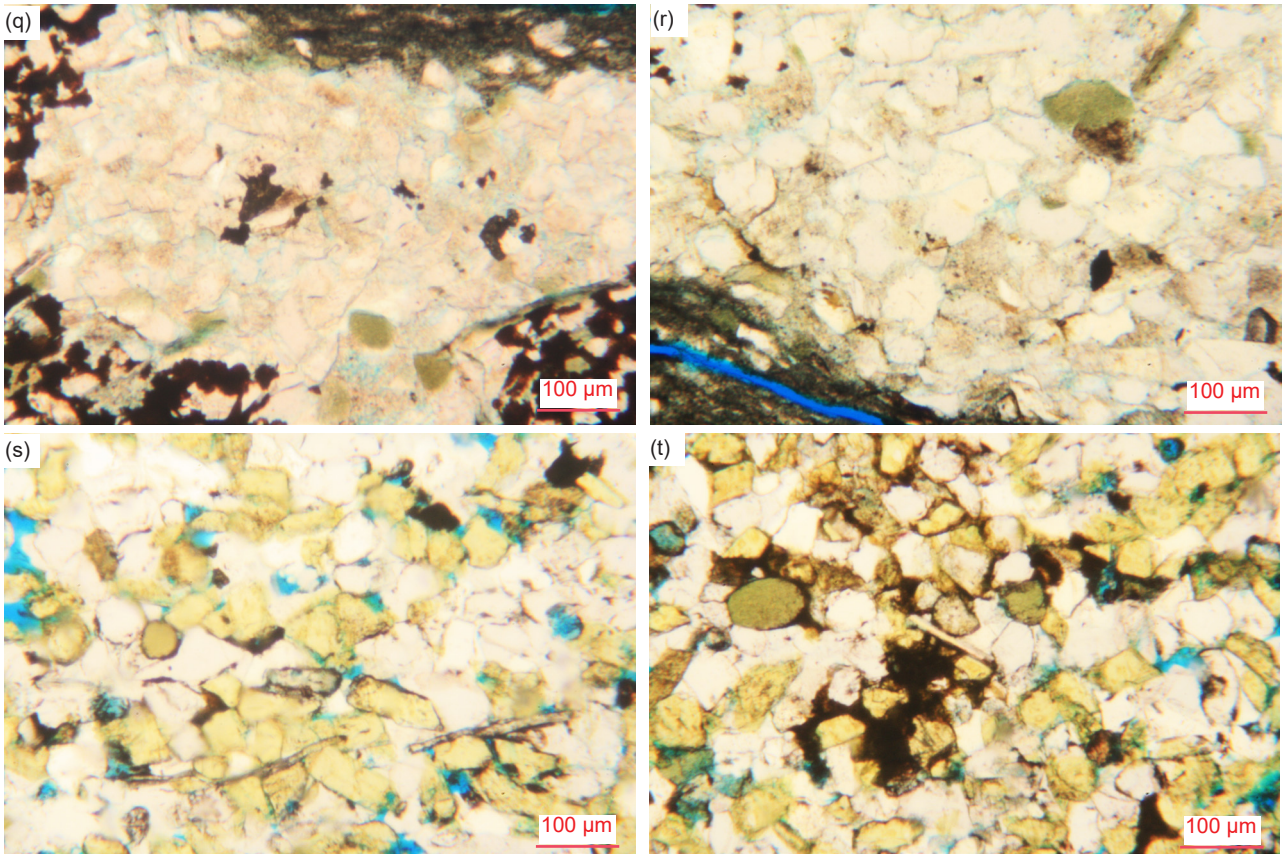

Fig. 41 (pages 369, 370, and 371). A representative set of photomicrographs at various scales (as indicated) showing the K-feldspar grains of various sizes, shapes and states of alteration in the Bright Angel Formation samples. While most are rounded, many have retained their original lath shape, also with the cleavage still evident. (a) BAS-01, (b) BAS-02, (c), (d) HF-01, (e), (f) HF-02, (g) HF-03, (h), (i) HF-04, (j), (k) HF-05, (l) HF-06, (m), (n) HF-07, (o), (p) HF-08, (q), (r) HF-09, and (s), (t) HF-10.

is pervasive and overwhelms the fabric, with only remnants of tiny irregularly-shaped quartz and K-feldspar grains. It is easily discerned that the tiny K-feldspar grains were originally the dominant mineral present in these laminae, but subsequently were mostly altered to illite, which at the same time left many quartz grains with fuzzy edges. Interbedded between these laminae are prominent harder "augen"-like non-iron-oxide-stained bands and "eyes" that consist of a tightly-fitted mosaic of very small-small, and a few medium, irregularly-shaped angular to tabular, mostly sub-angular to sub-rounded and partly altered (to illite) K-feldspar grains and quartz grains often meeting at triple points.

Glauconite

Most of the sandstones contain numerous, subordinate, very small (0.03–0.06 mm, ϕ=+5.01 –+4.05), small (0.07–0.19 mm, ϕ=+3.77–+2.40), and occasionally small-medium (0.20–0.33 mm, ϕ=+2.33 –+1.60), olive green-brown, sub-rounded to rounded oval-shaped (and sometimes elongated and sometimes also curved, and parallel to the bedding) glauconite pellets and sub-angular fragments of glauconite pellets that are also tightly fitted with the other mineral grains within the mosaic (fig. 42). Some of the glauconite pellets have clearly grown with concentric zoning around very small quartz fragments or small quartz grains, and also possibly small K-feldspar grains or tiny fragments (fig. 42a-c). Some glauconite pellets have concentric zoning around their edges, their cores often marked by iron oxide staining as well as their outer edges. Other glauconite pellets are also elongated and curved, and some appear to be broken-edged fragments of rounded oval-shaped pellets. Even the glauconite pellets when sub-euhedral and clumped display a tight molded fit with the mosaic quartz grains, often with all edges meeting at triple points. Thus, the glauconite pellets appear to be detrital.

However, some glauconite even appears to be the product of illite alteration of K-feldspar. And the greenish color can sometimes be accentuated by the blue dye staining of the impregnated resin. There is some evidence for some K-feldspar grains being altered by illite to form the glauconite, such as apparent glauconite alteration along fractures in K-feldspar grains, and some cleaved K-feldspar grains (with iron oxide along the cleavages) with the same alteration as seen under crossed polars as

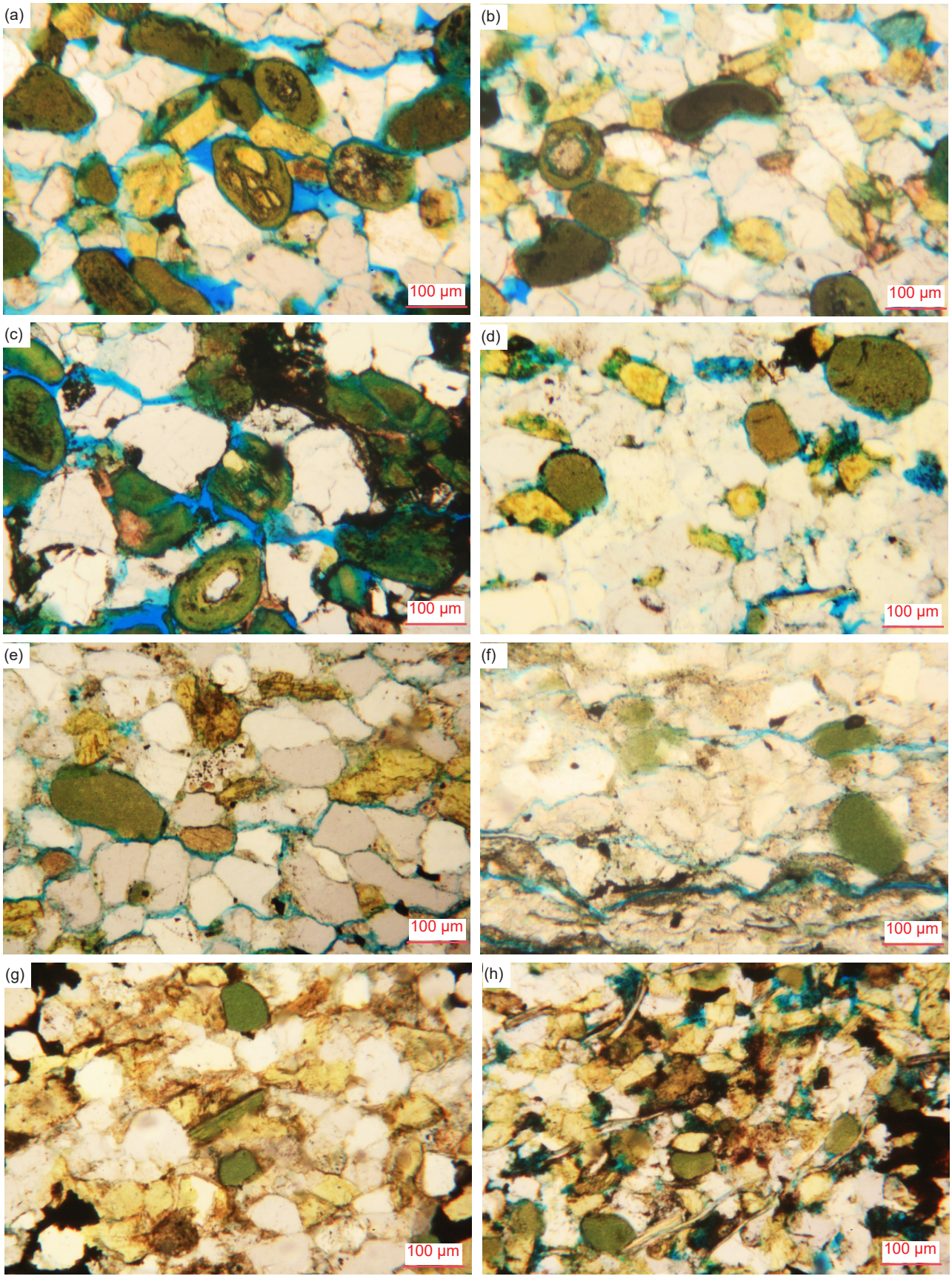
(a)
100 μm
(b)
100 μm
(c)
100 μm
(d)
100 μm
(e)
100 μm
(f)
100 μm
(g)
100 μm
(h)
100 μm

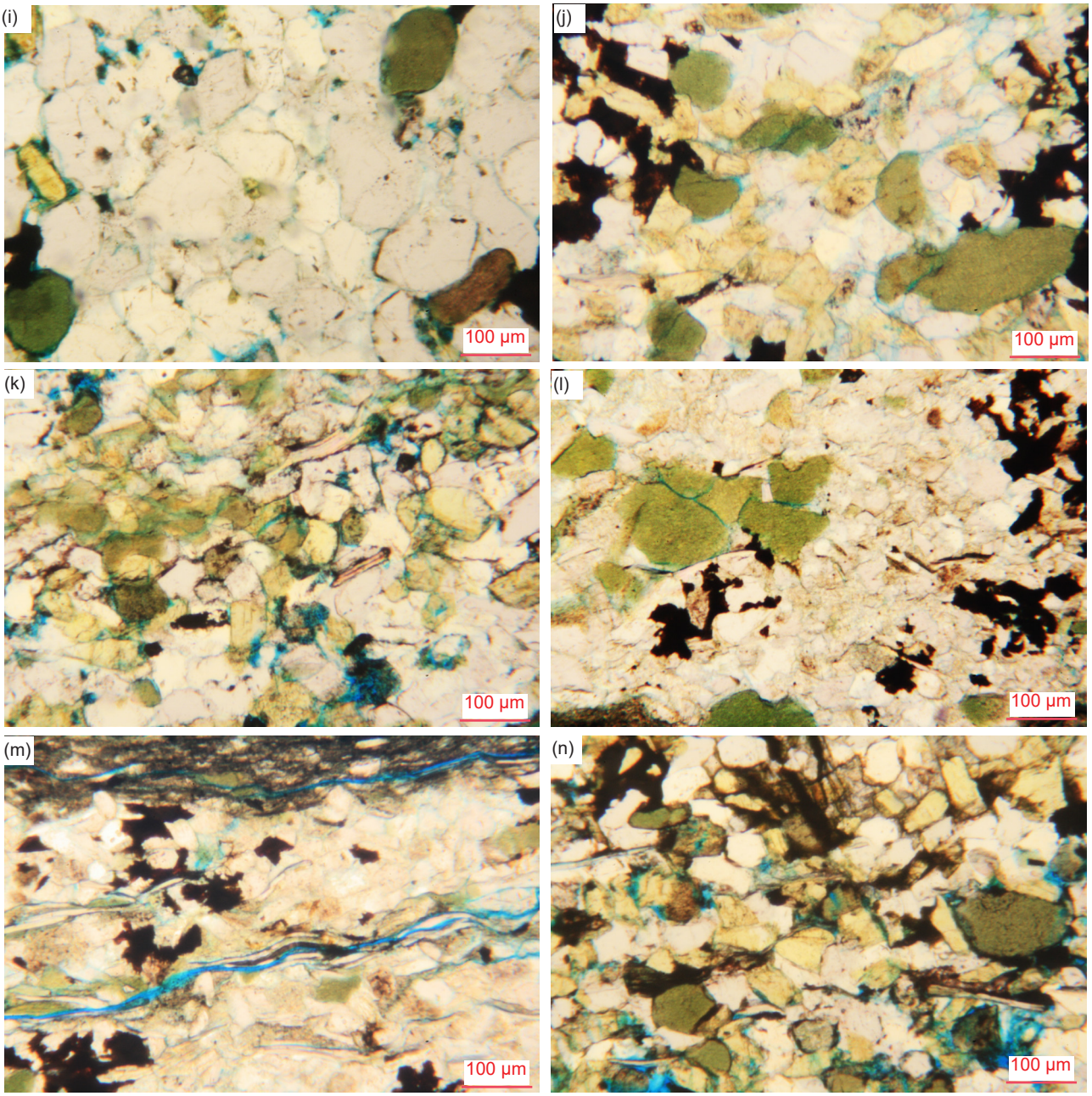

Fig. 42 (pages 372 and 373). A representative set of photomicrographs at various scales (as indicated) showing the mostly rounded glauconite grains and pellets or peloids in the Bright Angel Formation samples. Those that have quartz or K-feldspar grains or fragments at their centers, it appears the glaucontie has grown around those, whereas other grains are uniform and appear to have resulted from alteration of K-feldspar grains. (a), (b) BAS-01, (c) BAS-02, (d) HF-01, (e) HF-02 (f) HF-03, (g) HF-04, (h) HF-05, (i) HF-06, (j) HF-07, (k), (l) HF-08, (m) HF-09, and (n) HF-10.

glauconite. The K-feldspar remnants in glauconite pellets can appear to be residual to illite alteration of K-feldspar grains, and illite or glauconite alteration of some muscovite has resulted in heavily-degraded edge-on "books" of flakes. There are some tiny irregularly-shaped patches or blotches of greenish glauconite as a product of that illite alteration in some laminae in shales that consist of iron-oxide-stained illite alteration. Sometimes these patches have iron oxides outlining them and appear to be very fine-grained illite (glauconite?) alteration of K-feldspar. Sometimes sub-angular to sub-rounded greenish glauconite grains occur in the siltstone bands and "augen" interbedded with those shale laminae, indicating the glauconite may have been originally detrital.

Muscovite

All samples, whether sandstone, siltstone or shale contained many tiny, very small, small, medium or

long-very long (0.02–0.89 mm, ϕ=+5.71–+0.17), thin (some thicker), edge-on muscovite flakes (fig. 43), some with one end frayed, very frayed or split apart (one with the frayed end also curled) (fig. 43a, b, d, o), wedged tightly in the mosaic between quartz, K-feldspar and glauconite grains and often parallel or sub-parallel to the bedding. Some muscovite flakes are bent around and between the various mosaic grains, usually parallel to the bedding (fig. 43c, e, j, k, o), while a few have been broken and others are at various angles oblique to the bedding (Fig. 43e, m, t). One long (0.45 mm, ϕ=+1.15) thin edge-on muscovite flake is bent multiple times as it weaves parallel to the bedding between various other mosaic grains and ends with a frayed end, while another (0.39 mm, ϕ=+1.36) is at a steep angle to the bedding wedged between mosaic and is broken at right angles as it weaves between other mosaic grains (fig. 43e). In several instances, a few flakes are stacked together and offset from one another parallel to the bedding. In another instance, two stacked very long, thin edge-on muscovite flakes diverged as they bend and weave their separate ways between mosaic grains, one of them broken at one point. Elsewhere, a small-medium thin flake is partially wrapped around two adjoining glauconite pellets. Several tiny-small thin edge-on muscovite flakes are included in quartz grains, accompanied in one instance by a tiny K-feldspar grain. And many small irregularly-shaped face-on muscovite flakes are usually inclined slightly from bedding surfaces.

Some muscovite flakes have been variously altered. For example, two longer thick, broken and bent flakes are partially altered to/replaced by calcite, while two other very thick flakes (0.10–0.14 mm long, ϕ=+3.32 –+2.84, by 0.05–0.11 mm thick) were altered and expanded, and several 0.11 mm wide (ϕ=+3.19) and 0.11 mm thick, edge-on muscovite "books" are heavily altered to illite with their constituent sheets likewise expanded and splayed. Such edge-on muscovite "books" are sub-rounded and tabular and are wedged tightly in the mosaic with triple point junctions with surrounding grains. One small edge-on muscovite flake appears to be totally covered with, or altered to, iron oxide. In one sample, quite a few small edge-on flakes may possibly be biotite but are more likely iron-oxide-coated altered muscovite flakes because they are wedged in the mosaic between what are clearly small edge-on muscovite flakes. In another, several small thin edge-on muscovite flakes are stacked on top of one another along with a parallel band of iron oxide between two of them. Sometimes there has apparently been growth of quartz cement against the edge-on muscovite flakes.

In illite-altered shale laminae, numerous tiny-small thin edge-on muscovite flakes occur at various angles but most are inclined parallel to the bedding (fig. 43g, h, l, p, r). In the interbedded siltstone augen are numerous tiny-small and a few long-very long, thin edge-on muscovite flakes (sometimes altered or sometimes expanded with frayed ends) at various angles but usually inclined close to being parallel to the bedding and sometimes bent between and around mosaic grains (fig. 43q, r). In places within some samples, the thin edge-on muscovite flakes are at the same angle effectively cross-cutting through the rock fabric aligned along what thus became planes of weakness that have facilitated fractures. Similarly, a thin long edge-on muscovite flake is sharply bent and broken, weaved around and between blocks of mosaic grains almost parallel to the bedding in what became fracture zones due to the muscovite flakes that provided planes of weakness.

Brachiopod Shell Fragments

Nine of the twelve samples contain at least one edge-on brachiopod shell fragment, while some samples contain several (fig. 44). They are easily confused with edge-on muscovite flakes but are distinctive because they are thicker and composed of collophane, a birefringent cryptocrystalline form of apatite. They also often exhibit a two-layered internal structure of the shell wall (fig. 44e–h). These fragments are small to medium length to very long, ranging in length from 0.06 mm to 0.77 mm (ϕ=+4.05 –+0.38). Some are very thick and appear altered (fig. 44a, b, d). They are often broken into shorter segments and are tightly wedged and/or bent between the various other grains in the mosaics, often parallel to the bedding (fig. 44a–d).

Carbonates

The XRD analyses (table 2) indicate that there are various carbonate minerals present in all samples—calcite [$CaCO_3$], dolomite [$CaMg(CO_3)_2$], ankerite [$Ca(Fe, Mg, Mn)(CO_3)_2$] or siderite [$FeCO_3$]. Dolomite is the most prevalent, being present in eight of the samples, whereas ankerite solely dominates in several samples.

Typically, dolomite is easily recognized when it occurs as rhomboidal crystals, many small (0.07–0.23 mm, ϕ=+3.77–+2.13) but some quite large (0.38 mm, ϕ=+1.39), with concentric growth zones marked by iron-oxide staining (fig. 45b, c). A large dolomite rhomb has a medium-sized, rounded oval-shaped "dirty" core. Otherwise, dolomite often occurs as occasional small (0.04–0.23 mm, ϕ=+4.64–+2.13) sub-angular to rounded "dirty" (iron-oxide-stained) grains, elongated clear fragments or irregularly-shaped patches, which usually are wedged within the mosaic as part of it and sometimes with euhedral edges meeting other mosaic grains at triple points.

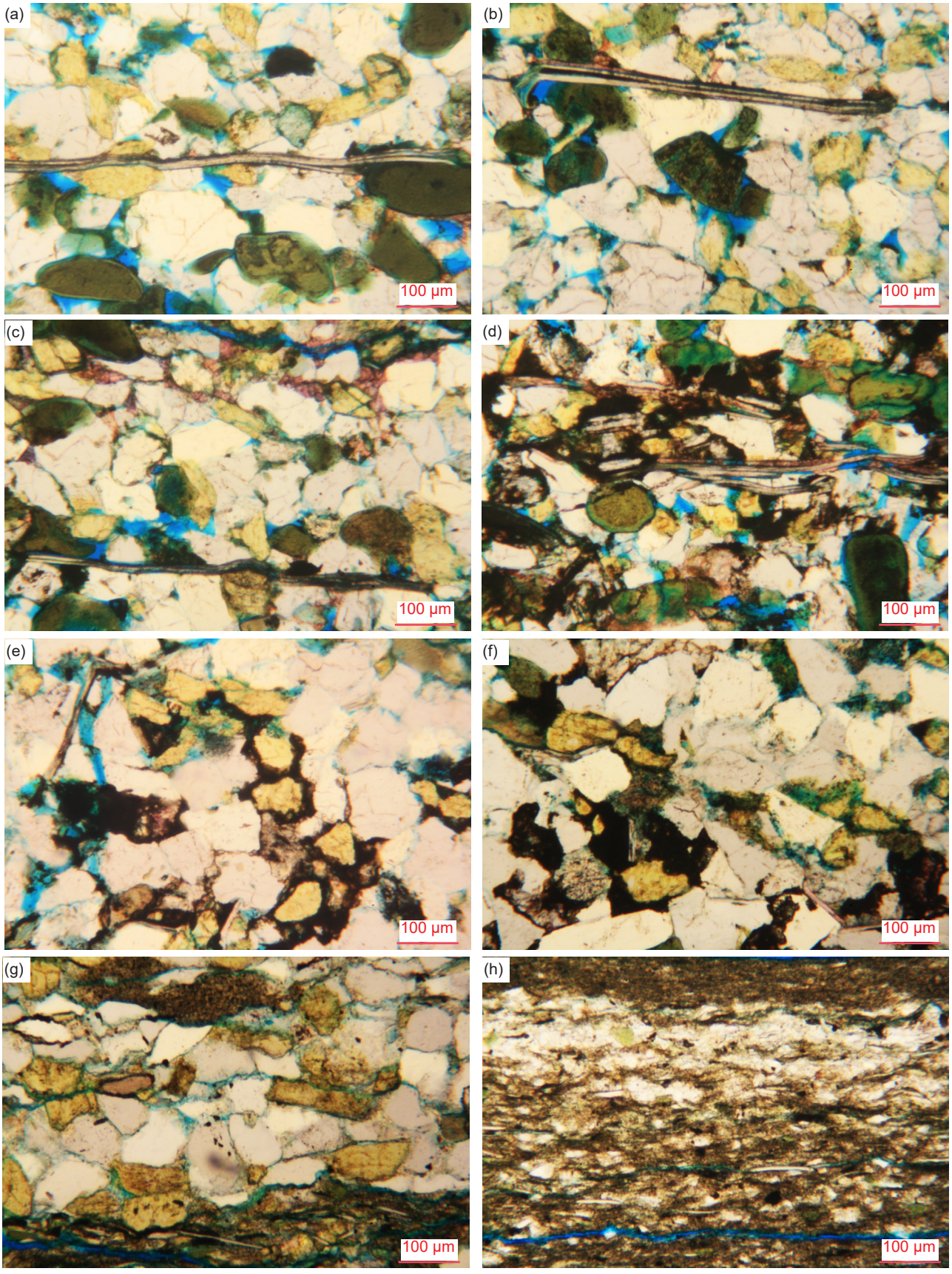
(a)
100 µm
(b)
100 µm
(c)
100 µm
(d)
100 µm
(e)
100 µm
(f)
100 µm
(g)
100 µm
(h)
100 µm

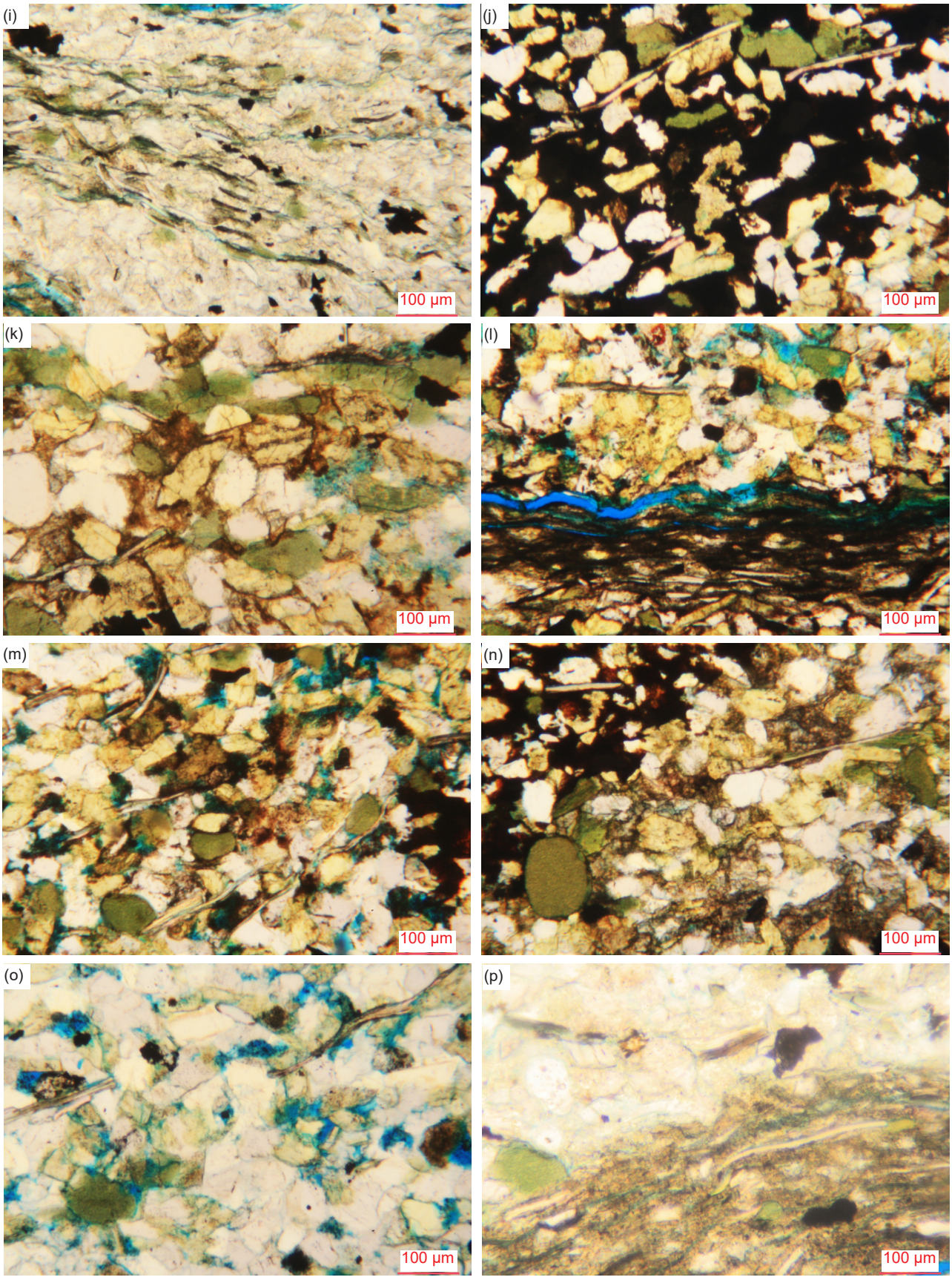
(i)
100 μm
(j)
100 μm
(k)
100 μm
(l)
100 μm
(m)
100 μm
(n)
100 μm
(o)
100 μm
(p)
100 μm

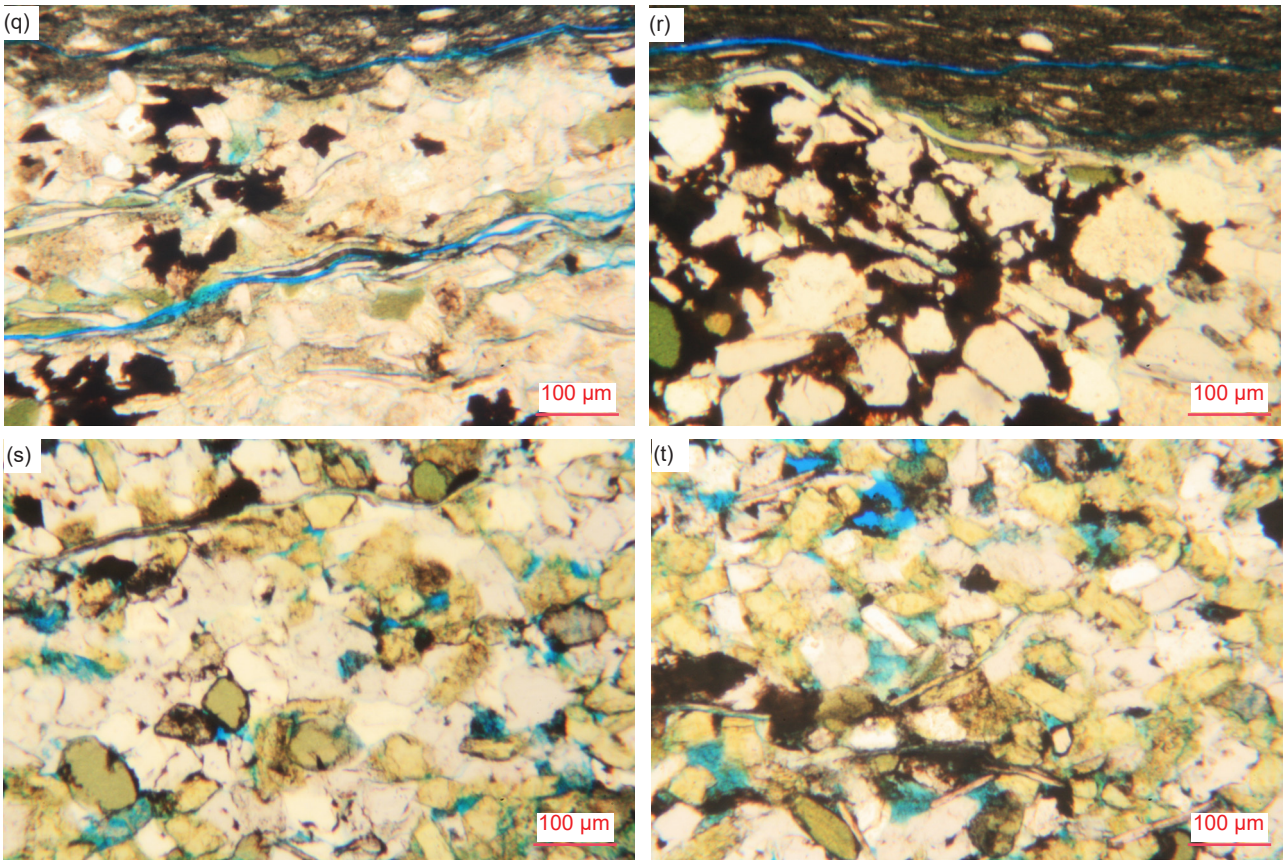

Fig. 43 (pages 375, 376, and 377). A representative set of photomicrographs at various scales (as indicated) showing typical edge-on muscovite flakes in the Bright Angel Formation samples with features such as frayed or flayed ends and/or bent around quartz and K-feldspar grains indicating they are detrital grains, while some have expanded due to alteration. (a), (b), (c) BAS-01, (d) BAS-02, (e), (f) HF-01, (g) HF-02, (h), (i) HF-03, (j), (k) HF-04, (l), (m) HF-05, (n) HF-07, (o) HF-08, (p), (q), (r) HF-09, and (s), (t) HF-10.

In places, the small scattered dolomite grains infill between mosaic grains as cement, probably infilling former pores, but may replace some K-feldspar mosaic grains, especially where quartz grains predominate. In one place, iron-oxide-stained dolomite cements a large clump of quartz and K-feldspar grains together with a degraded edge-on muscovite flake. In other places, large areas of irregularly-shaped small iron-oxide-stained dolomite grains coalesce to form a network of widespread cement between scattered quartz, K-feldspar, glauconite and muscovite mosaic grains, often encroaching on those grains' edges and over the grains themselves. Sometimes the dolomite cement grains are small, scattered, irregularly shaped and not stained by iron oxide. Some dolomite may be replacing calcite because of the visible calcite remnants within the dolomite rhombs, while some dolomite may instead have been partially replaced by calcite. In one sample, thin veins of dolomite partially coated with, and accompanied by, heavy iron oxide cross-cut the mosaic almost perpendicular to the bedding.

Calcite is usually recognizable as pink because of the stain applied to the thin sections during their preparation. However, it is harder to recognize when it too is iron-oxide-stained. Some calcite infilling spaces between mosaic grains acts as the cement (significantly in a few places), and even coats some grain edges or partly replaces or veins K-feldspar, quartz or muscovite grains/flakes. In one instance, calcite replaces the core of a glauconite pellet in patches or along fractures in that grain. And in one location, a large area of calcite infills a former pore. In some places, very small calcite grains appear to be a replacement or more likely calcite cement, sometimes iron-oxide-coated. One former small-medium K-feldspar lath appears to have been replaced by calcite. However, calcite also occurs as many small and medium (0.05–0.40 mm, ϕ=+4.23 –+1.32), sometimes iron-oxide-coated, sub-angular to sub-rounded and rounded (oval) grains (sometimes several clumped together) wedged in the mosaic as apparent detrital grains similar to the quartz and K-feldspar grains.

Ankerite is harder to recognize, though it is usually reddish-brown due to being iron-oxide-stained. Many very small to small-medium (0.03–0.23 mm, ϕ=+5.01–+2.13) sub-angular to sub-rounded and

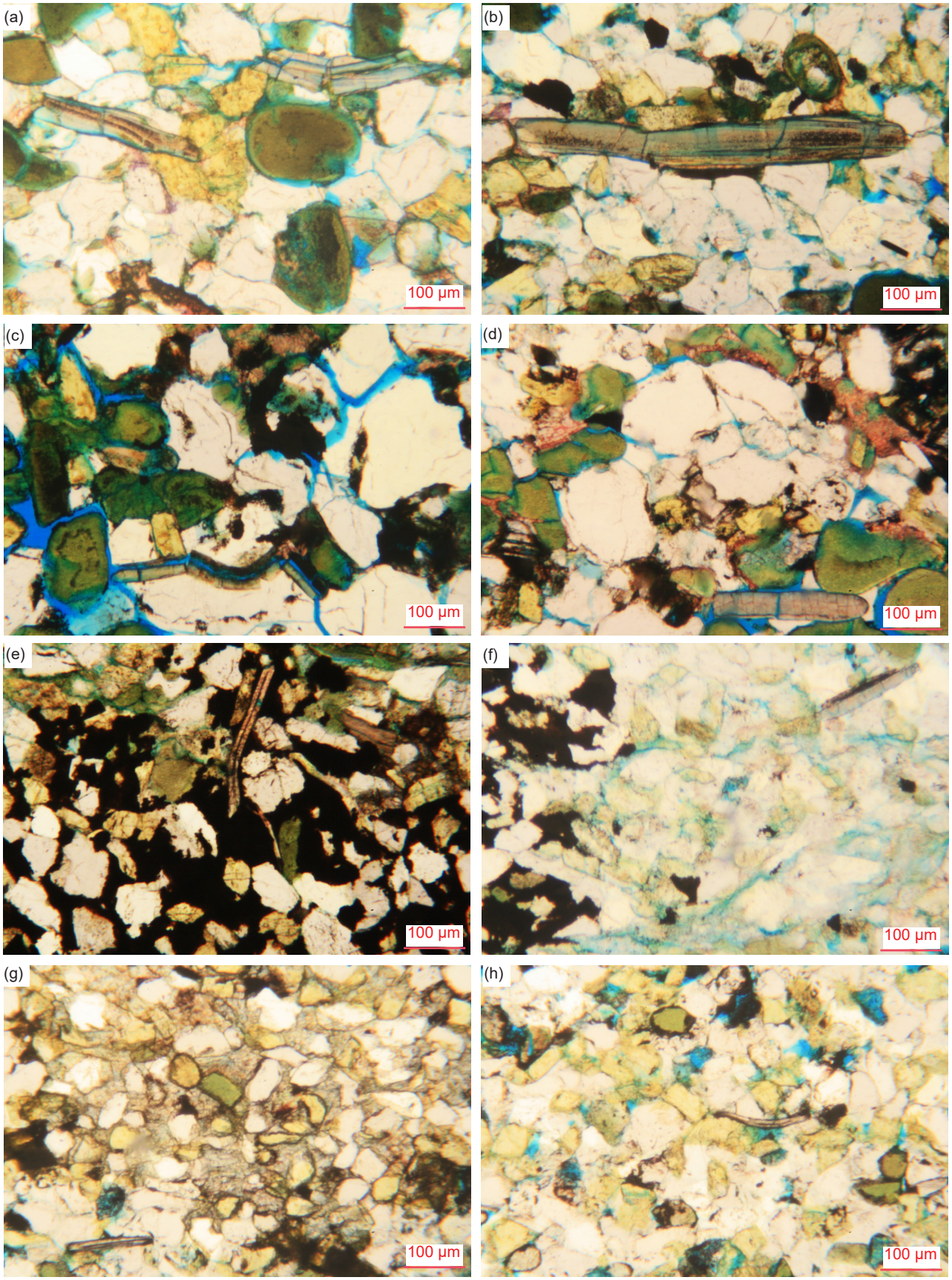

Fig. 44. Representative edge-on brachiopod shell fragments found in many samples from the Bright Angel Formation, evident from their thickness and layered wall structure, as well as their birefringence due to consisting of collophane (cryptocrystalline apatite) (scale as indicated). (a), (b) BAS-01, (c), (d) BAS-02, (e) HF-04, (f) HF-08, and (g), (h) HF-10.

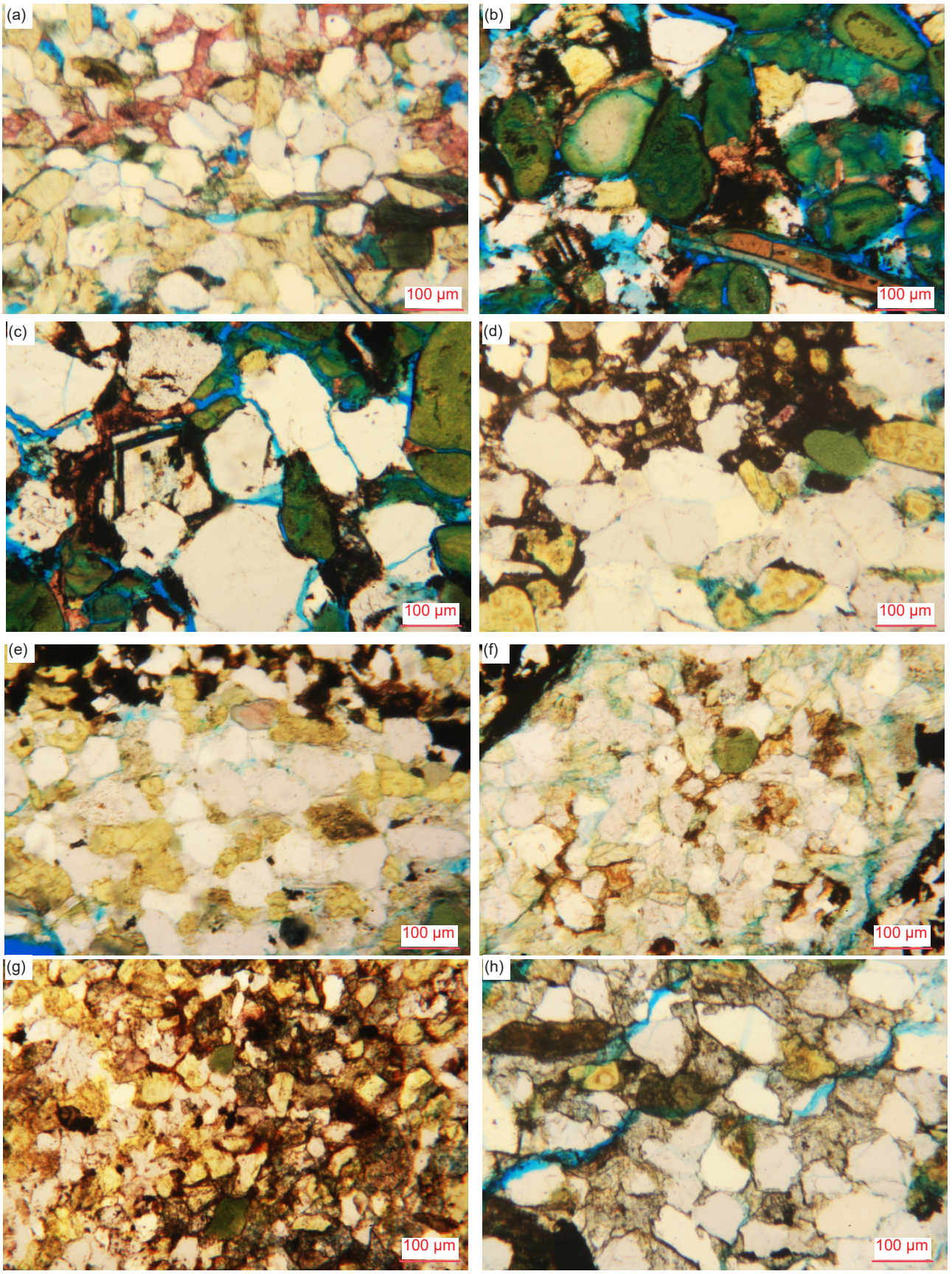
(a)
100 µm
(b)
100 µm
(c)
100 µm
(d)
100 µm
(e)
100 µm
(f)
100 µm
(g)
100 µm
(h)
100 µm

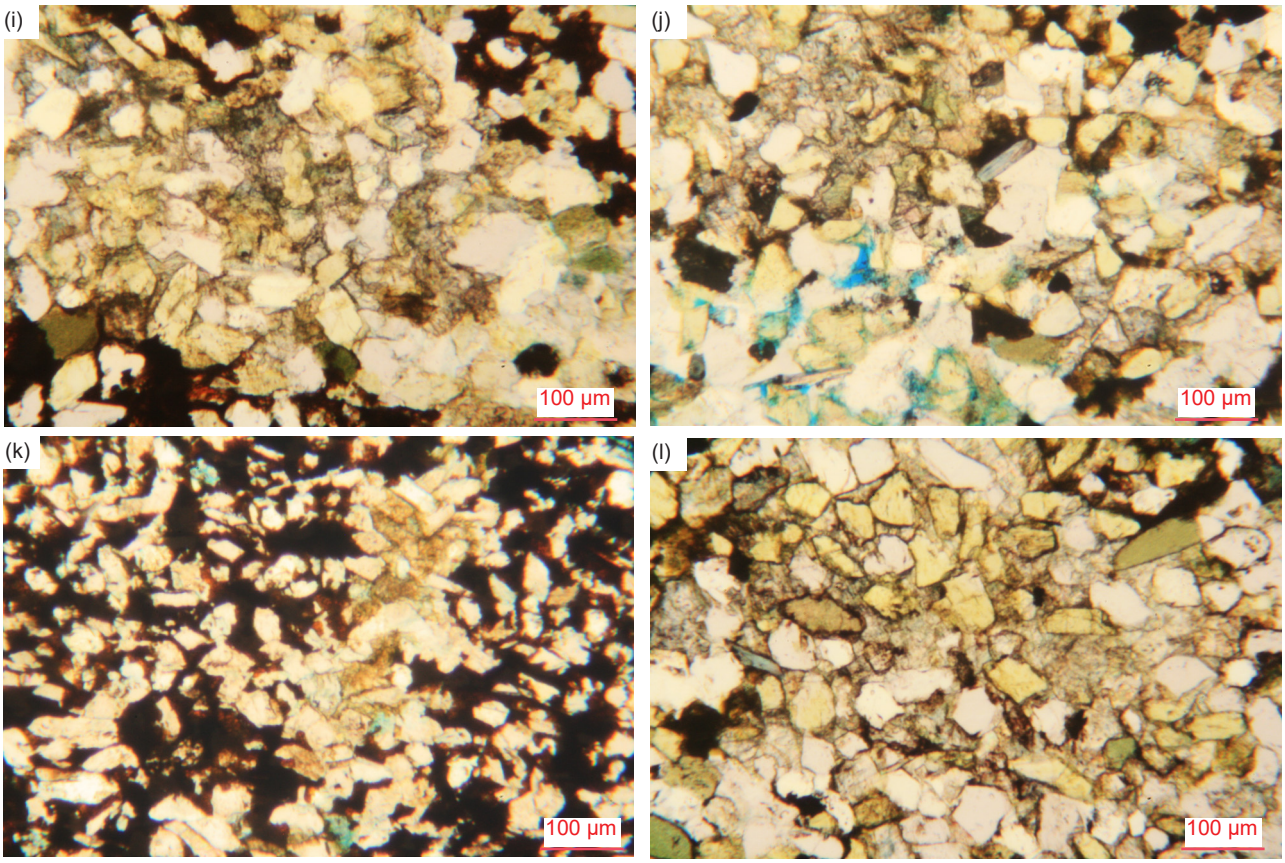

Fig. 45 (pages 379 and 380). A representative set of photomicrographs at various scales (as indicated) showing the various carbonates in the Bright Angel Formation samples, which are generally later introduced alteration, but occasionally may be primary (detrital) grains. Calcite usually shows as pink due to an applied stain to the thin sections, while dolomite sometimes occurs as rhomboid crystals with growth bands marked by iron oxides. Most of the dark coloration is due to iron oxides staining and/or covering the carbonate minerals. (a) Calcite BAS-01, (b), (c) Calcite and dolomite BAS-02, (d) Calcite and dolomite HF-01, (e) Ankerite HF-02, (f) Ankerite HF-04, (g) Ankerite HF-05, (h) Dolomite HF-06, (i) Dolomite and siderite HF-07, (j) Dolomite HF-08, (k) Dolomite HF-09, and (l) Dolomite HF-10.

rounded ankerite grains, some being rhombs with the characteristic cleavage evident, while others are oval-shaped and elongated, are scattered through and wedged in the mosaic similar to the other detrital grains and thus some may be detrital. There are later pervasive small scattered or large extensive areas/patches of very small sub-angular ankerite grains infilling as cement between scattered quartz and K-feldspar grains, encroaching on their edges and perhaps replacing some K-feldspar grains and laths (due to "ghost" cleavages and lath shapes as well as the apparent K-feldspar grain remnants). In one location, a small thin carbonate (ankerite?) veinlet cross-cuts the mosaic, some grains and the iron-oxide-stained ankerite cement at a steep angle for a short distance.

Siderite is also difficult to recognize from iron-oxide-coated dolomite. It is unclear in the one sample in which it occurs (table 3) whether any of the small (0.06–0.27 mm, ϕ=+4.05–+1.90) siderite grains might also be detrital since the siderite may have resulted from replacement of dolomite. Most of the mosaic in that sample is cemented with a combination of illite alteration and siderite (or dolomite partially covered with iron oxide), that is in patches consisting of a tightly-interlocking mosaic of tiny siderite grains between the quartz and K-feldspar grains. In several areas, not coated and obscured by iron oxide, there are abundant small sub-angular to sub-rounded dolomite and/or siderite grains and cement areas (with streaks and light dustings of iron oxide) between the scattered quartz, K-feldspar and greenish illite after K-feldspar grains. The siderite (and maybe some iron-oxide-covered dolomite) cement can sometimes encroach on mosaic grains.

Zircon

Eleven of the twelve samples each contain at least one zircon grain and some samples contain three or four zircon grains (fig. 46). They are easily distinguished by their high relief and high birefringence. They are invariably very small (0.03–0.08 mm, ϕ=+5.01–+3.64) and often are partially coated with iron oxides. While most are sub-angular

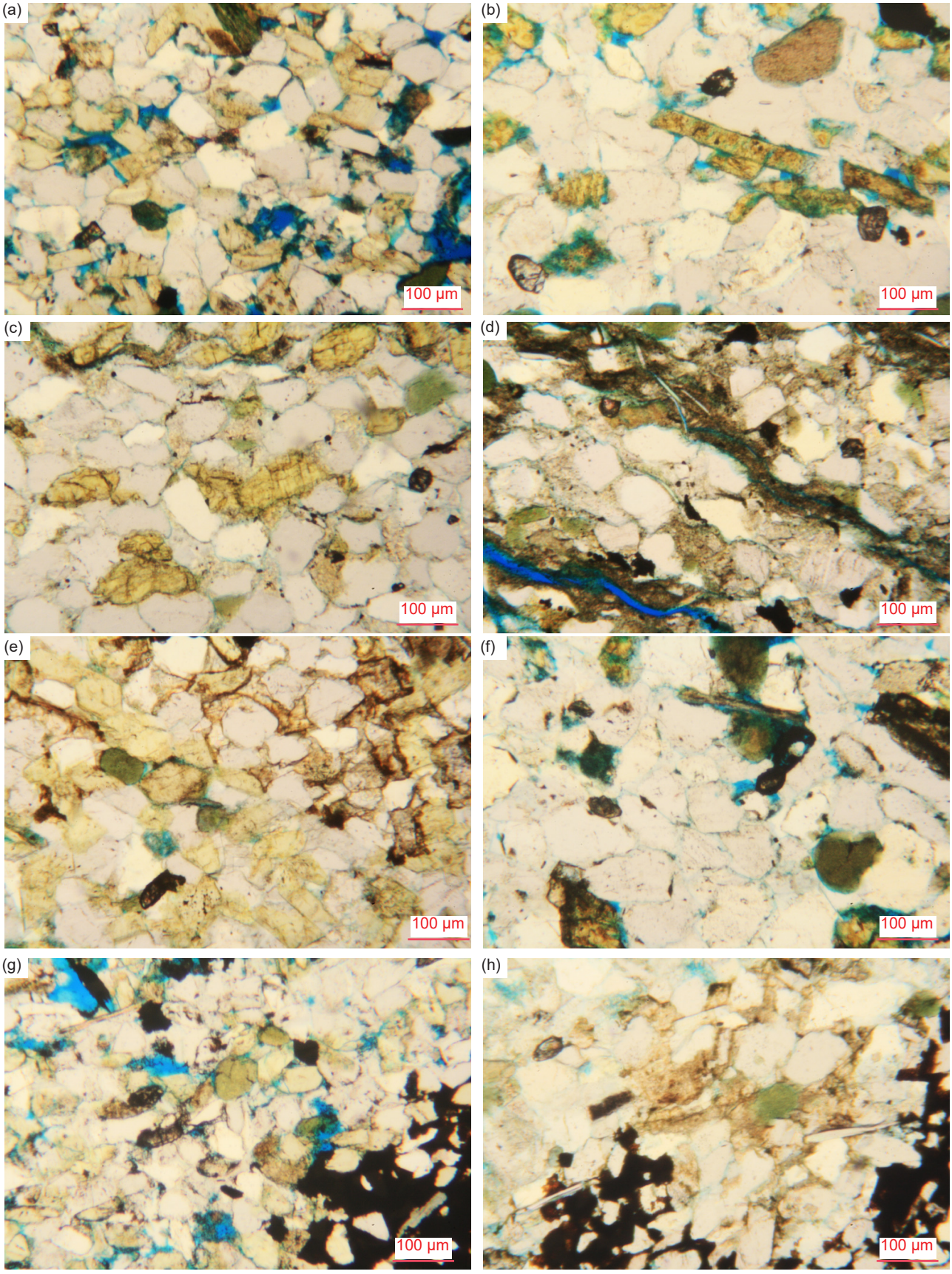

Fig. 46. Representative zircon crystals, evident from their high relief and high birefringence, as well as their mostly tabular habit, found in many samples from the Bright Angel Formation (scale as indicated). (a) BAS-01, (b) HF-01, (c) HF-02, (d) HF-03, (e) HF-04, (f) HF-06, (g) HF-08, and (h) HF-09.

to sub-rounded, some are rounded or oval-shaped, and others are tabular (which is their usual crystal habit). They are typically wedged between other grains in the mosaic.

Clay Minerals

Clay minerals occur in all samples as determined by XRD analyses (tables 3 and 4) and are dominated by illite with subordinate illite/smectite. In only one sample is there more kaolinite. The most obvious occurrence of illite and illite/smectite is that which constitutes the glauconite (McRae 1972; Thompson and Hower 1975) easily recognized in most samples (fig. 42). Otherwise, the clay minerals are not always so easily recognized, except under crossed polars. For example, under crossed polars it is immediately evident when K-feldspar grains have been totally altered to illite.

The shales exhibit laminae and bands that are predominantly illite alteration, mainly of K-feldspar grains and laths of which there are tiny, barely-distinguishable blurred/fuzzy remnants, and are pervasively stained yellow-brown by accompanying iron oxides (fig. 47e, h, o). Indeed, these selvages or laminae of intense illite alteration are evident from the heavy dusting of iron oxides associated with it that also covers the remnant mosaic grains, primarily quartz grains, as it appears that the K-feldspar grains have been altered to illite. As in these laminae, large areas in other samples of almost total illite alteration have remnant resorbed tiny-very small, irregularly-shaped quartz grains with fuzzy edges. Other areas of illite alteration are less dusted with iron oxide and the illite alteration can be seen to be after K-feldspar grains.

In the interbedded clear patches or bands the mosaic has scattered thin brown-stained illite alteration (probably primarily after K-feldspar), clearly with remnants of K-feldspar and quartz grains similar to those in the illite-alteration-dominated shale laminae.

In the sandstones and siltstones, many of the glauconite grains look like pellets, especially where they exhibit concentric growth zones surrounding tiny "seed" grains or fragments of quartz or K-feldspar, and thus they are likely detrital. In some of the samples the greenish grains look definitely more like illite alteration of former K-feldspar grains and laths. In other areas, the illite alteration has extended beyond the green glauconite grains (after K-feldspar) to infill between them and between some of the mosaic quartz grains so that the pervasive illite alteration is now the predominating cement, along with the occasional patches of heavy iron oxides. In other samples, most of the mosaic is cemented with a combination of illite alteration and dolomite partially covered with iron oxide and/or siderite, that is between, and sometimes in patches between, the quartz and K-feldspar grains. Elsewhere the mosaic has been cemented by the pervasive illite alteration but with occasional small angular to sub-rounded green glauconite (illite) grains, so that the rock is now dominated by the illite alteration of K-feldspar and occasional dolomite forming the cement/matrix.

Where there is extensive illite alteration between the mosaic grains, it would appear that it has facilitated some fracturing and possible shearing of some mosaic grains along linear zones. For example, in one sample an obliquely cross-cutting linear zone appears to be a fracture with fractured mosaic grains and abundant illite alteration. In another sample the illite alteration and many linearly-aligned edge-on muscovite flakes have produced linear weaknesses in the rock fabric that have facilitated fractures, but no obvious shearing or fracturing of mosaic grains is evident so no movement has occurred.

Iron Oxides

Iron oxides are ubiquitous in all samples. Due to their opaqueness they always appear to be black, even in thin sections (fig. 48). They most commonly occur in these samples as minor tiny spots and streaks on some quartz, K-feldspar and glauconite pellets and small blotches/patches or edge linings between mosaic grains. The iron oxides appear to preferentially coat the K-feldspar grains, perhaps accompanying illite alteration of them, but sometimes just encroach on the edges of the quartz and K-feldspar grains. Iron oxides also preferentially coat dolomite and ankerite rhombs, grains and cement. Tiny to small irregular blotches of heavy iron oxide are also scattered within the mosaic between and encroaching on the edges of some grains or almost completely covering some grains. Where there are discreet solid black grains with well-defined edges in two samples, they may instead be pyrite (table 3). Some iron oxide linings around some grains appear to act like a cement, and some areas are more heavily iron-oxide-stained with most grains iron-oxide-coated and perhaps also cemented together. Large patches of heavy iron oxide spread around and between many mosaic grains and in many places are inclined close to being parallel to the bedding. Where the shale fabric's alternating bands or laminae and selvages have been heavily altered to illite, they are generally lightly stained with iron oxide to make it colored yellow-brown, though there are also occasional tiny to very small heavy iron oxide specks and blotches (sometimes appearing to be possibly replacing or coating edge-on muscovite flakes) between and on the edges of the residual mosaic grains. In a few places, in some samples the mosaic is so heavily coated with iron oxide that all mosaic grains and the cement are either totally covered

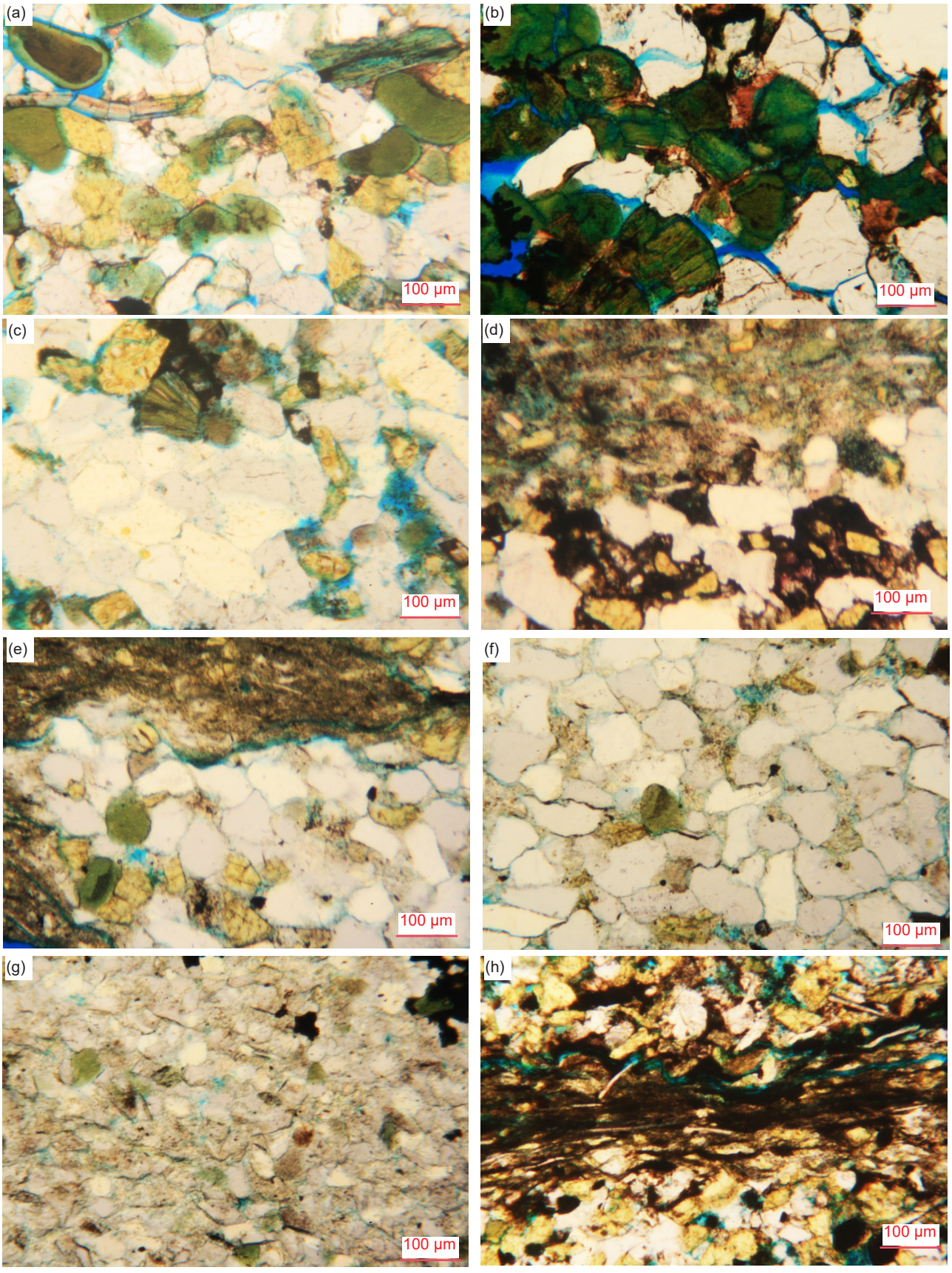
(a)
100 µm
(b)
100 µm
(c)
100 µm
(d)
100 µm
(e)
100 µm
(f)
100 µm
(g)
100 µm
(h)
100 µm

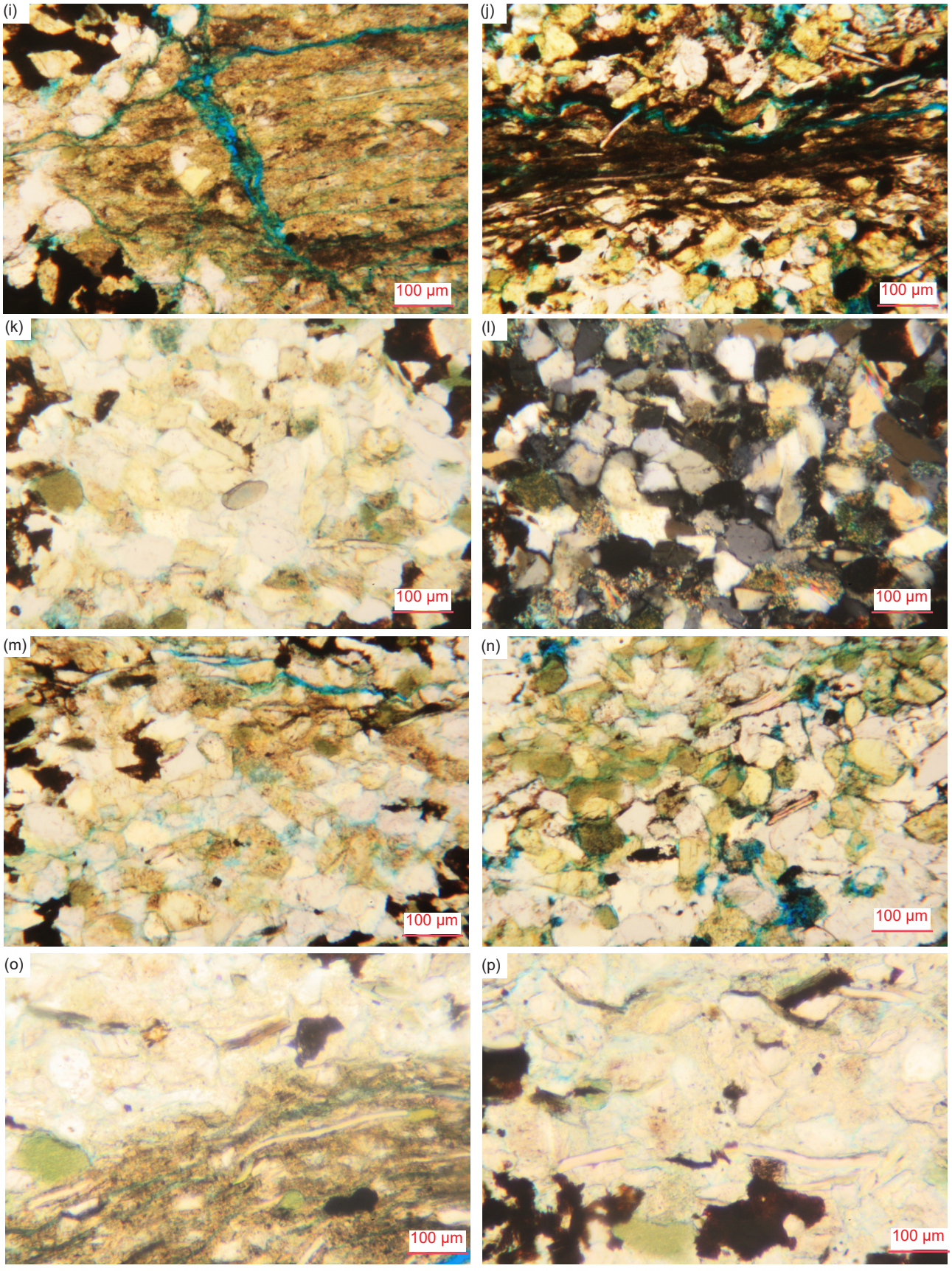
(i)
100 µm
(j)
100 µm
(k)
100 µm
(l)
100 µm
(m)
100 µm
(n)
100 µm
(o)
100 µm
(p)
100 µm

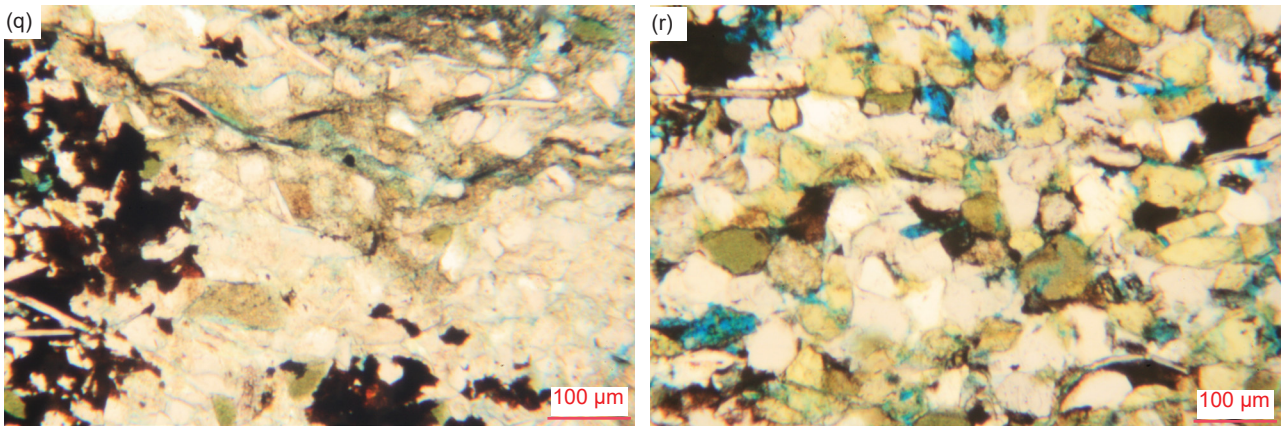

Fig. 47 (pages 383, 384, and 385). A representative set of photomicrographs at various scales (as indicated) showing typical clay minerals, primarily illite, as diagenetic alteration in the Bright Angel Formation samples. While some of the illite is interstitial, it is often partially replacing some K-feldspar grains, sometimes replaces "books" of muscovite flakes, and constitutes the primary clay mineral in the glauconite grains. It also dominates in the mudstone/shale laminae where it is most likely replacing very small K-feldspar grains. (a) BAS-01, (b) BAS-02, (c), (d) HF-01, (e), (f) HF-02, (g), (h) HF-03, (i) HF-04, (j) HF-05, (k) HF-07 (plane polarized light), (l) HF-07 (crossed polarized light), (m) HF-07, (n) HF-08, (o), (p), (q) HF-09, and (r) HF-10.

or have their edges covered, giving them irregular shapes, or even partially covered making the grains red-brown so that it is difficult to discern whether they are quartz (which is most likely), ankerite or dolomite. Sometimes the iron oxide patches are somewhat aligned and even form a vein cross-cutting the mosaic, and in one sample thin veins of dolomite partially coated with, and accompanied by, heavy iron oxides cross-cut the mosaic almost perpendicular to the bedding (fig. 48m).

Lithic Fragments

Clasts consisting of other rock (lithic) fragments are exceedingly rare in these samples, although they can be difficult to identify. Two classes of lithic fragments are observed in these sandstone samples, those that are likely siltstone and those that are definitely shale (mudstone rip-up clasts) (fig. 49). For example, in one sandstone there are two small-medium rounded "dirty" rock fragments that would appear to be siltstone (fig. 49a), and in another are two small rounded grains consisting of extremely tiny quartz sub-domains, one speckled with iron oxide, that appear to be possible siltstone fragments. (fig. 49c). A huge (8.75 mm, ϕ=-2.79), thick and long, curvilinear area in the overall fabric in another sandstone sample appears to be a rip-up shale/mudstone clast (figs. 38h, 49b). It consists of iron-oxide-stained brown intense illite alteration permeated through a mosaic of tiny angular to sub-rounded quartz grains and remnants of altered K-feldspar grains with very thin but long edge-on muscovite flakes parallel to the strong laminations which are parallel to the long axis of the clast. A very much smaller but identical example is evident in the siltstone bands between shale laminae in a dominantly shale sample (fig. 49d).

Pores

In most samples there are virtually no pores remaining in the rock fabric, whether sandstones, siltstone or shale, just a lot of cracking between grains and rare tiny and very small pores, some likely due to the forced impregnation with blue dye staining prior to the thin sections being cut (fig. 39). This is not just due to the original quartz cementation of the mosaic grains infilling the original pores, but also to the subsequent additional cementation by illite alteration and apparent carbonate infiltration and alteration, both accompanied by iron oxides. However, in a few samples there are a few pore spaces left in the rock fabric, but again, the blue dye that accompanied the resin used under pressure to impregnate the samples before the thin sections were cut has stained between the grains and encroached on some of them, sometimes covering grains and thus distorting their colors, which can make some look like pore spaces. It should again be noted that in these fine-grained rocks the very small grain radii are smaller than the microscope slide thickness and thus the tight stacking of the grains may obscure any residual tiny pores.

Finally, during extensive petrographic examination of these twelve samples of the Bright Angel Formation no macroscopic or microscopic evidence was found of any metamorphic effects on the sandstones, siltstones, or shales or their constituent mineral grains. This includes the ten samples from the one fold, as well as the two samples distant from that fold selected for comparison. Not only have the quartz grains maintained their detrital characteristics, but the ubiquitous K-feldspar grains and the muscovite flakes have also, some of the latter having been bent around the quartz grains

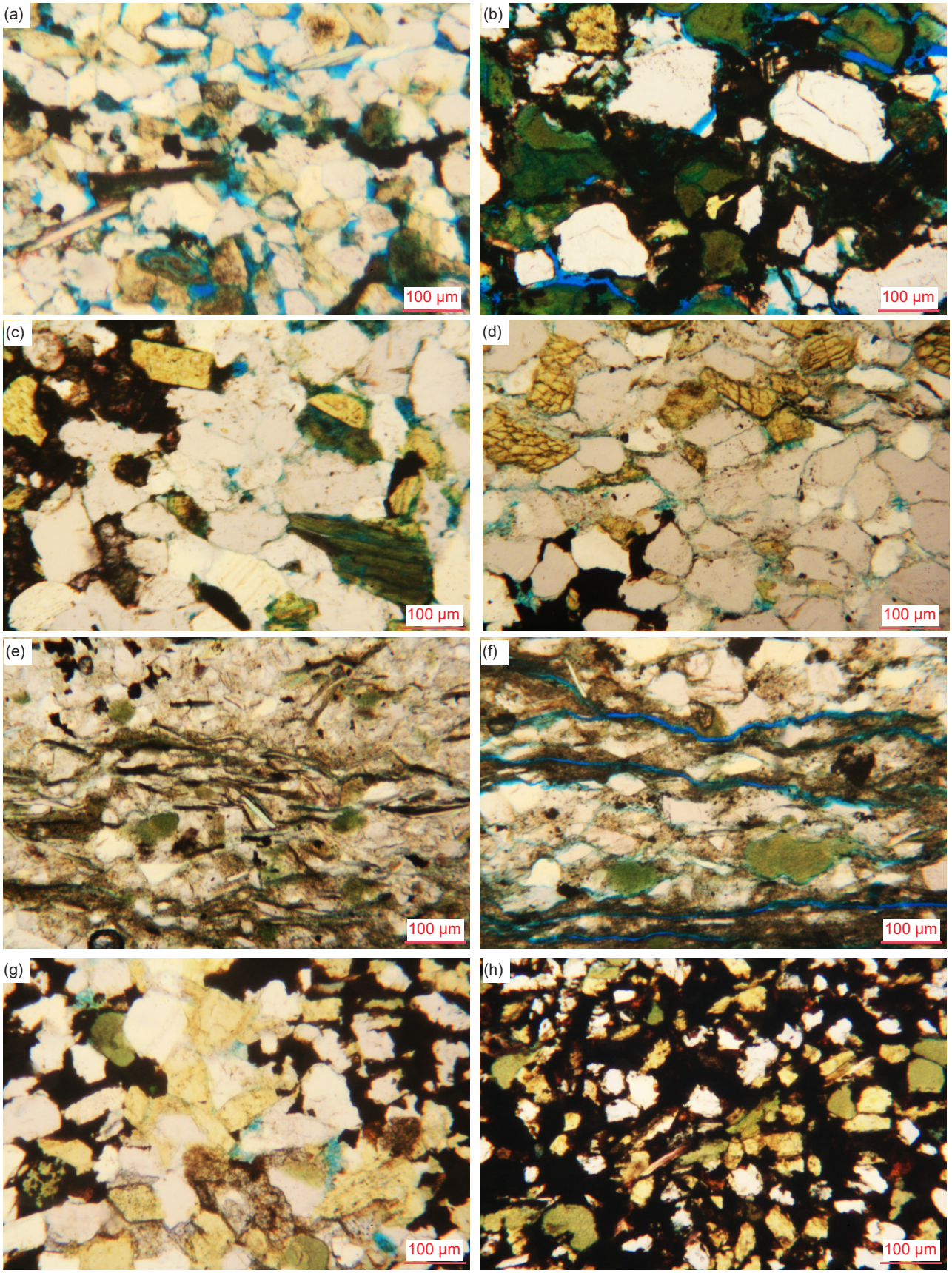
(a)
100 μm
(b)
100 μm
(c)
100 μm
(d)
100 μm
(e)
100 μm
(f)
100 μm
(g)
100 μm
(h)
100 μm

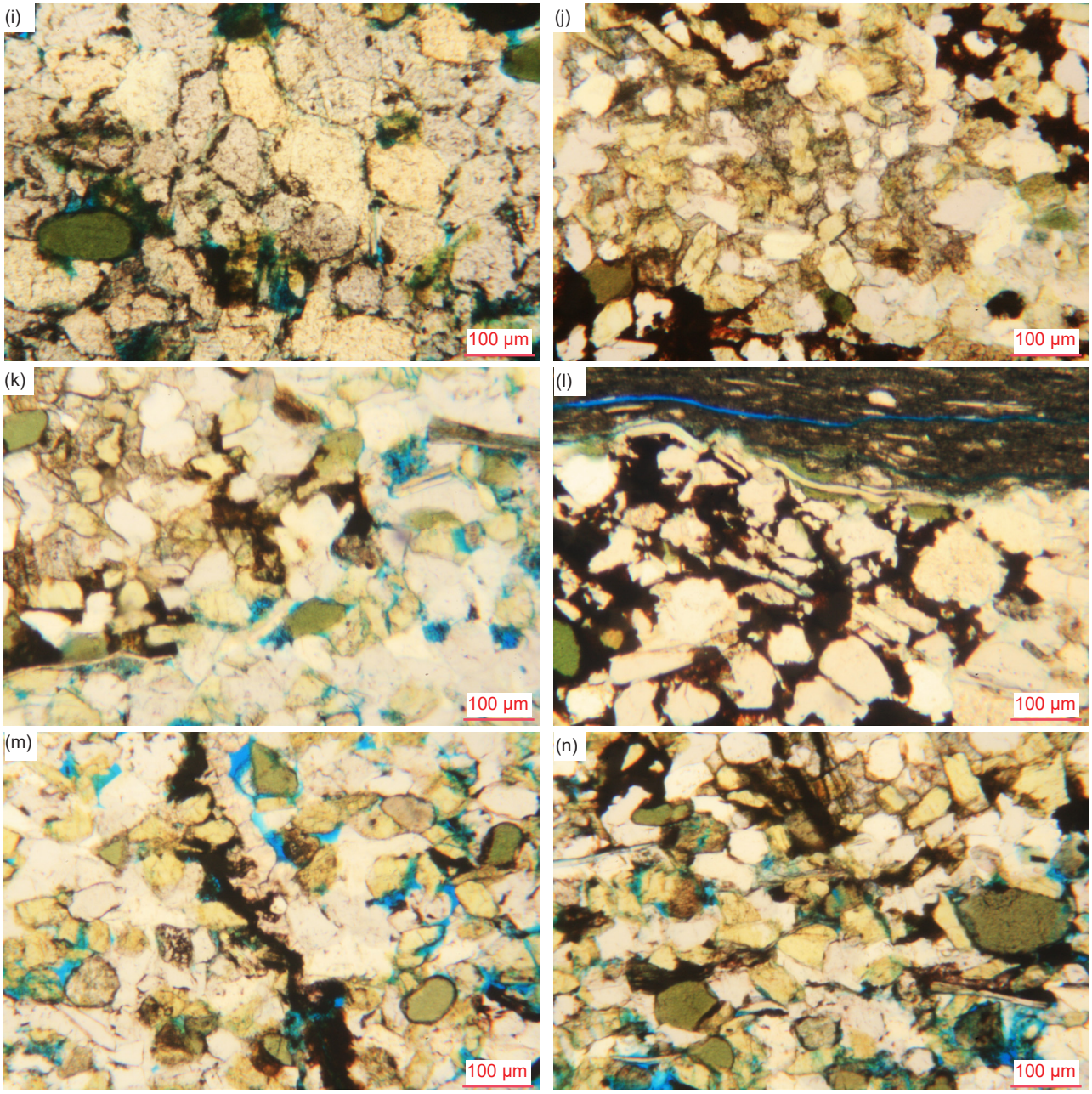

Fig. 48 (pages 386 and 387). A representative set of photomicrographs at various scales (as indicated) showing typical iron oxides present in the Bright Angel Formation samples. These iron oxides typically coat grains as alteration products or are deposited on them either as dustings or fuller coverings, most often on carbonates and clay minerals, but sometimes on muscovite and glauconite. They also fill the interstitial spaces between grains and/or are on their edges, and sometimes fill fractures as veins. (a) BAS-01, (b) BAS-02, (c) HF-01, (d) HF-02, (e), (f) HF-03, (g) HF-04, (h) HF-05, (i) HF-06, (j) HF-07, (k) HF-8, (l) HF-09, and (m), (n) HF-10.

they are wedged between and some having frayed or split ends caused by abrasion during deposition. Even slightly elevated temperatures from low-grade metamorphism would have substantially affected the quartz and K-feldspar grains, which usually dominate in these rocks, as well as affecting the textures in the rock fabric. Clay minerals which are ubiquitous and still present due to post-depositional diagenesis would not have survived such metamorphism but would have been transformed into other minerals, such as metamorphic muscovite. Thus, it is likewise concluded that the Bright Angel Formation is unmetamorphosed in all places where it was examined in Grand Canyon.

Discussion

Details gleaned from this intensive petrographic examination of these Bright Angel Formation samples in conjunction with previous field and other studies enable various relevant conclusions to be drawn.

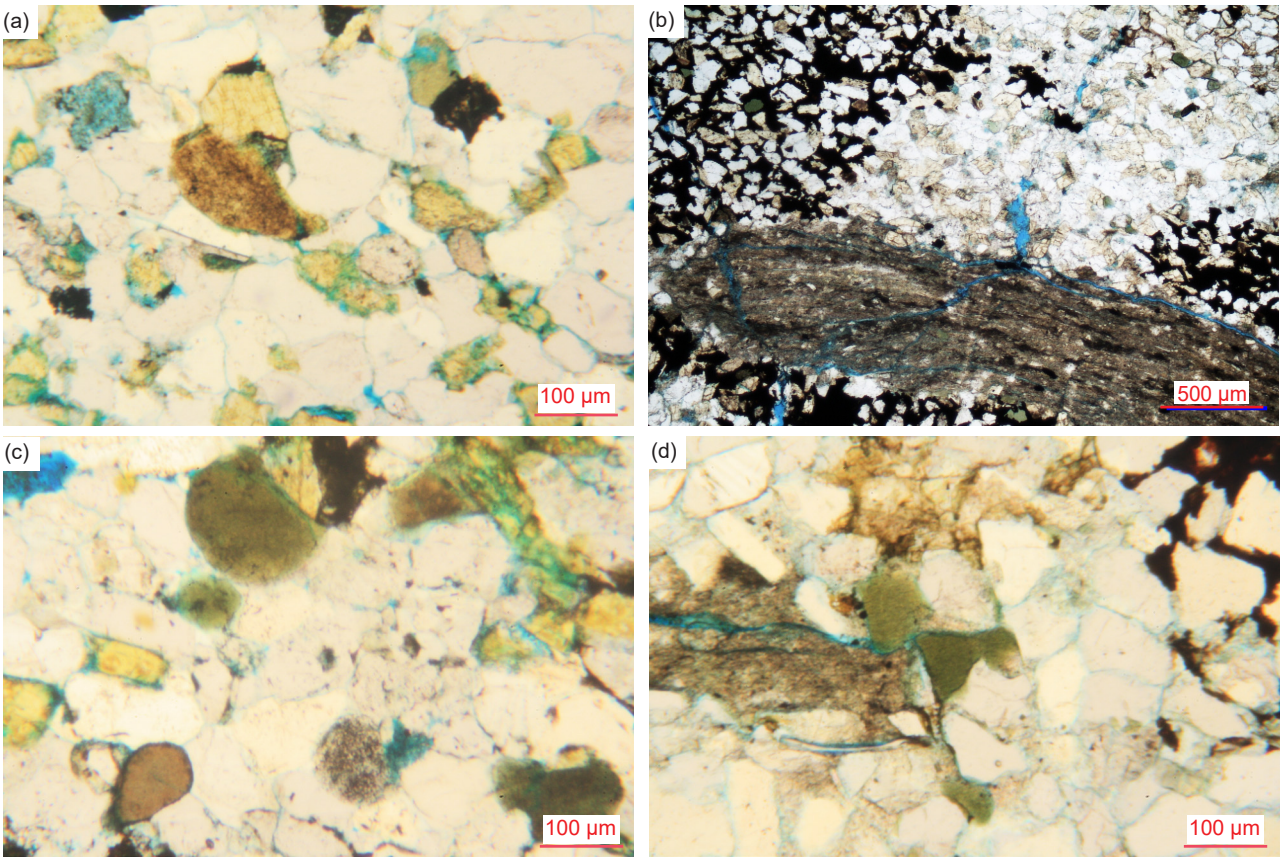

Fig. 49. Several rock (lithic) fragments in the Bright Angel Formation samples in photomicrographs at various scales (as indicated). These are rare, probably due to the difficulty of recognizing and identifying them. (a) Siltstone HF-01, (b) Shale HF-04, (c) Siltstone HF-06, and (d) Shale HF-09.

Mineralogical Composition Indicates Nearby Sediment Provenance

Quartz is the most abundant mineral in terrigenous sedimentary rocks, including in the sandstones, siltstones and shales of the Bright Angel Formation, because it is exceedingly durable due to often surviving multiple generations of weathering and deposition (Ulmer-Scholle et al. 2015). Quartz can occur as single crystals or polycrystalline aggregates that may provide clues to the provenance of the grains, but quartz is common to most rock types, though rare in basalts. Semi-composite and polycrystalline quartz is found in metamorphic and plutonic rocks as well as hydrothermal vein deposits and fractures. In metamorphic rocks, the size of the quartz crystals may represent increasing metamorphic grade, larger crystals forming under higher temperatures and pressures.

Grain size can make provenance determination more difficult (Ulmer-Scholle et al. 2015). With the smaller grain sizes in siltstones and especially shales, the ability to see undulatory quartz or polycrystalline/composite grains becomes more difficult. Since crystal sizes within polycrystalline grains may be large, grains formed from their breakdown may not exhibit polycrystallinity or undulatory extinction. According to Krynine (1946) and Folk (1980), straight to slightly undulose extinction in quartz is characteristic of plutonic igneous and schistose metamorphic rocks. They also noted that whereas plutonic igneous rocks generally have subequant to xenomorphic quartz grains (that is, they did not develop their otherwise typical external form because of late crystallization as the matrix between earlier formed crystals), schistose metamorphic rocks generally have elongate composite quartz grains with straight borders and commonly have mica inclusions.

Feldspars are far less resistant than quartz to chemical and physical destruction, although they can survive some aqueous transport with only a relatively small reduction in grain size, but not angularity (Garzanti et al. 2012, 2015). However, they are altered or removed by weathering, transport, and diagenesis yielding secondary pores or alteration products such as illite, white mica/sericite, albite or kaolinite (Ulmer-Scholle et al. 2015). Almost all detrital feldspars are igneous or metamorphic in origin, with the K-feldspars orthoclase and microcline being the most common. Na-rich plagioclase, the next most common feldspar, is usually from volcanic rocks. Sanidine, from high-temperature felsic volcanic rocks, and Ca-rich plagioclase, from mafic to intermediate igneous rocks, are relatively uncommon.

Detrital micas are rarely mentioned or discussed as being present in any sandstones, siltstones and especially shales, except when they are present in rock fragments (Ulmer-Scholle et al. 2015). However, standard petrography textbooks suggest that detrital micas should be found in subaqueous sediments, but not eolian ones (Hallam 1981, 20; Moorhouse 1959, 343, Tucker 1981, 45). This notion is so entrenched in the minds of some geologists that they proclaim the absence of mica in certain sandstones based only on their assumption that a particular sandstone is eolian, without even doing any petrographic work, for example, the Permian Coconino Sandstone of Grand Canyon region (Young and Stearley 2008, 305). They claim that the less resistant (softer) mica grains and ultra-fine clay particles all should have been abraded to oblivion and/or wafted off site by the wind. Yet sandstones like the Coconino contain abundant detrital mica flakes (Whitmore et al. 2014), as do the sandstones, siltstones, and shales of the Bright Angel Formation as described above, indicating all these sedimentary units are water-deposited.

Rock fragments (also called lithic fragments or composite grains) can be derived from a wide variety of lithotypes and commonly have source-specific textures and compositions that can be recognized in thin section. Because of their multi-crystalline or granular nature, rock fragments obviously tend to be more common in the coarser grain-size modes of clastic terrigenous rocks, primarily sandstones and conglomerates. Rock fragments should be very common in sediments, but many succumb to the effects of weathering, abrasion, or later mechanical or chemical diagenesis. Nevertheless, the surviving rock fragments yield some of the most direct evidence of contributions from igneous, metamorphic, or sedimentary terranes, so it is especially important that such grains be accurately identified.

Sedimentary rock fragments include eroded and transported clasts of siliciclastic rocks (sandstone, siltstone, and claystone or shale), which consist of a variety of mineral particles, but are dominated by quartz, feldspars, heavy minerals, micas, and clays (Ulmer-Scholle et al. 2015). Textures within the clasts sometimes can give clues to their origin. Argillaceous/micaceous metamorphic rock fragments cover a wide spectrum of grain types derived from high- to low-grade metamorphic rocks, which is a function of texture and sheet silicate mineralogy. Common grain types include schist, gneiss, and quartzite clasts, dominated by quartz and sheet silicates (muscovite, biotite, and chlorite), while gneiss fragments also contain feldspar. Metamorphic grains commonly display some foliation or schistosity, and may be composed of polygonal equant crystals, depending on whether they have been annealed. Quartz crystals may display sutured contacts if highly strained. Cemented and compacted sandstones grade into metamorphic quartzite. Quartzite consists of polycrystalline elongated quartz crystals that have undulatory extinction of the individual sub-crystals as well as sutured boundaries.

Because igneous rock fragments can be composed of a number of minerals with a range of sizes, determinations of their mineralogic composition, crystallinity and texture are key to identifying them. Plutonic grains must contain two or more crystals to qualify as a rock fragment, and they must be composed of phaneritic crystals (that is, large enough to be seen with the naked eye). The most common are granitic clasts composed of quartz, feldspar, iron-titanium oxides and mica or hornblende. Component crystals tend to be roughly the same size and commonly are anhedral to subhedral. As with other rock fragments, they are more common in coarser-grained clastic sedimentary rocks.

In the Bright Angel Formation, quartz grains are ubiquitous clasts in the sandstones and siltstones but are less so in the shales where the grain size is very small. Subordinate K-feldspar grains and former laths are common, even being dominant in some instances, especially in the shale laminae where the very small K-feldspar grains have been partially or totally altered to illite. There are also occasional detrital muscovite flakes. The presence of a few possible plagioclase grains and former laths, together with occasional zircon crystals is clearly indicative of an apparent primary sediment source area(s) consisting of granitic plutons and metamorphic rocks, which are of course locally present, exposed in the inner gorges of Grand Canyon. Usually, the Tapeats Sandstone directly overlies those granites and schists, separated by the Great Unconformity erosion surface, but where resistant "hills" or monadnocks of Shinumo Quartzite occur in the paleotopography of the Great Unconformity surface the Bright Angel Formation directly sits unconformably on the tilted Grand Canyon Supergroup sedimentary strata. Consistent with the conclusion that the sediment source of much of the Bright Angel Formation was the granites and schists are the quartz grains which have undulose extinction and the quartz grains with inclusions of muscovite and/or biotite flakes, occasional K-feldspar grains or laths, some possible plagioclase grains, and a few zircon grains. Also, there are occasional K-feldspar grains and former laths with inclusions of quartz or muscovite.

Indeed, some of the quartz and K-feldspar grains with muscovite or biotite inclusions could likely be fragments from the granitic rocks, while other rock fragments may be altered (weathered) schist.

However, the primary identified rock fragments are altered (weathered) siltstone and quartzite, and also "rip-up" clasts of shale, which are all consistent with the rock types in the Grand Canyon Supergroup strata that in some locations within the Grand Canyon corridor unconformably overlie the granitic plutons and metamorphic rocks. Furthermore, some of the large quartz grains that consist of many sub-grains (sometimes as patchworks) with different extinction angles may also be quartzite grains. These would be from the Shinumo Quartzite in the Grand Canyon Supergroup, which is very hard and resistant to erosion.

Strong confirmation of this conclusion about the provenance of many of the sediment grains making up the Bright Angel Formation comes from the U-Pb ages of the detrital zircon grains extracted from it in the study by Gehrels et al. (2011), discussed in detail above. Their Bright Angel Formation sandstone samples yielded detrital zircons overwhelmingly dominated by U-Pb ages of 1.60–1.72 Ga and 1.68–1.80 Ga, consistent with the Mazatzal and Yavapai provinces respectively whose granites and schists crop out in Grand Canyon's inner gorges locally underneath the Bright Angel Formation and Tapeats Sandstone (Karlstrom et al. 2003). There were secondary and very minor clusters of detrital zircon U-Pb ages around 1.45 Ga and 1.03 Ga respectively that might reflect a contribution from local Grand Canyon Supergroup strata and/or from the more distant Grenville orogen to the south or far east. Thus, while not definitive, this combined evidence is certainly consistent with the provenance of the sediment that forms the Bright Angel Formation being local and quite close to where the sandstones, siltstones and shales were deposited and sampled.

However, it is somewhat puzzling that the Bright Angel Formation, at least in Grand Canyon area, seems to contain very few zircon grains from the underlying Grand Canyon Supergroup (Unkar and Chuar Groups). Gehrels et al. (2011) determined the detrital ages of zircons in these locally underlying Grand Canyon Supergroup sedimentary strata and found that little detritus had been recycled from them. Thus, it may well be that the extent of the Grand Canyon Supergroup is limited, because elsewhere across North America underlying the Great Unconformity are invariably Precambrian granites and metamorphics (Peters and Gaines, 2012). Yet this widespread occurrence of underlying Precambrian basement granites and metamorphics with similar zircon and crystalline signatures might suggest at least some detrital grains in the Bright Angel Formation could have been transported longer distances from outside Grand Canyon area, similar to the possible contribution from the more distant Grenville orogen. This would make sense in a global Flood cataclysm model (see below), especially as Gehrels et al. (2011) found that the detrital zircons in higher layers in Grand Canyon Paleozoic sequence had been transported longer distances.

The other major mineralogical component of the Bright Angel Formation that appears to be largely detrital is glauconite, which often occurs as peloids (pellets), apparently grown around nuclei of tiny quartz and/or K-feldspar grains, and fragments of them. Rose (2003) maintained that these glauconite peloids were detrital because in places they were concentrated in cross-bedded greensand horizons often associated with bioturbated green crumbly siltstones (after Amorosi 1997). Glauconite was long accepted as a necessary indicator of low oxygen conditions in a deep marine depositional environment, but that is no longer the case (McRae 1972). However, as a technical term, glauconite cannot be considered a distinct mineral species. As pointed out by Thompson and Hower (1975), the dominant or exclusive mineral in most glauconite pellets is iron-rich interlayered illite-smectite. The term glauconite should thus be strictly used only to denote the morphological occurrence of these clay minerals. Martin (1985) found that the glauconite in the Bright Angel Formation consisted of a disordered mixed layer phase consisting of an illite mixture with ~10% expandable smectite layers (after Hower 1961). Indeed, because from a crystallographic perspective glauconite shares commonality with mixed-layer illite-smectite and micas (which are closely related to illite, the main differences being the amounts of Fe^{3+}, Al^{3+} and K^{+} substitutions in the crystal structures), from a practical standpoint the illite or illite-smectite found in glauconite pellets is indistinguishable from other iron-rich illite or illite-smectite found in other morphologies. That is why in the XRD analyses reported in this study (tables 3 and 4) the glauconite was included in the illite reported at a 2θ angle of 8.9°.

The relevant question now is where was the source of these glauconite peloids? There is petrographic evidence in the thin sections that at least some of the illite forming the glauconite was due to illite alteration of K-feldspar grains. In Figs. 42 and 47 many of the greenish glauconite grains retain the shapes of original K-feldspar grains and appear to be due to illite alteration of them. Even some of the peloids (pellets) have grown around tiny K-feldspar fragments. It is conceivable that the glauconite peloids formed around tiny K-feldspar (and quartz) fragments eroded from the Precambrian basement granites and washed around in the shallow marine waters that possibly covered the Grand Canyon area

in the pre-Flood era prior to deposition of the Tonto Group, as evidenced by the stromatolites and in situ stromatolite reefs found in the Kwagunt Formation of the Grand Canyon Supergroup (Wise and Snelling 2005). Additionally, the many glauconite grains that appear to have formed from K-feldspar grains could be the result of the illite alteration during diagenesis after deposition of the Bright Angel Formation (fig. 47). Indeed, some of the shale laminae appear to consist of tiny illite alteration of tiny former K-feldspar grains, with tiny quartz grains and with detrital muscovite flakes parallel to the laminations (figs. 43 and 47). This suggests that those K-feldspar grains were originally detrital along with the quartz grains and muscovite flakes and were altered to illite during diagenesis subsequent to deposition. If the glauconite peloids and the glauconite are a result of illite alteration during diagenesis of detrital K-feldspar grains, then these scenarios are also consistent with the provenance of the sediment that forms the Bright Angel Formation being local and quite close to where the sandstones, siltstones and shales were deposited and sampled.

Mineralogical and Textural Indicators of Short-Distance Transport and Deposition

Petrographic examination of the Bright Angel Formation samples in this study revealed the fine-grained sandstones to be well-sorted and dominated by medium silt-sized to fine sand sized, angular to sub-rounded quartz grains, with subordinate K-feldspar grains and former laths that are coarse silt-sized to fine sand-sized and sub-angular to sub-rounded. The siltstones are very similar to the fine-grained sandstones except for the angular to sub-rounded quartz and K-feldspar grains being silt-sized. Occasionally K-feldspar grains are more abundant than quartz grains. This is especially the case in the shales with siltstone laminae, the dominant tiny and very small sub-angular K-feldspar grains (respectively) usually being largely altered to illite in the shales (and brown-colored due to iron oxide staining).

There have been several explanations for how sand grains, especially more resistant quartz grains, become rounded (Chandler 1988; Dott 2003; Goudie and Watson 1981):

(1) abrasion of sand grains by wind,
(2) selective transport of better-rounded grains (to the dune) with the more angular ones being left behind in aqueous environments,
(3) recycling of older deposits containing rounded grains, and
(4) intense chemical activity causing sharp corners of grains to be removed.

Of these four suggested mechanisms for how sand grains become rounded, the current consensus appears to be *only* eolian transport, especially for the more mechanically and chemically resistant quartz grains (Chandler 1988; Dott 2003), even though there have been several other explanations for how quartz grains become rounded. Additionally, it should be noted that rounding of sand grains also depends on grain size. Even in eolian settings silt and fine sand-sized grains never get rounded; only the larger grains do. Thus, the mass of the grains in collisions seems to be the major factor in rounding, especially in deserts. Nevertheless, it is inferred that textural and compositional maturity is inherited and usually the result of several sedimentary cycles, with eolian abrasion having happened in at least one of the cycles in the history of the sand grains (Dott 2003; Folk 1978). Chemical activity can also make a sandstone appear more "mature" by removing or altering more soluble grains such as feldspars, especially in wet tropical environments, thus leaving quartz behind. McBride (1985) referred to these as "diagenetic quartz arenites."

In stark contrast, it has been well-known for some time that aqueous transport does not appreciably round quartz or K-feldspar sand grains (Kuenen 1960; Russell and Taylor 1937; Twenhofel 1945). Indeed, it is now undisputed that even energetic aqueous conditions (such as longshore currents and daily tidal currents) are insufficient to round any minerals. It is believed that this is because the differences in rounding between eolian and aqueous environments are due to the ability of water to cushion impacts between grains. A noteworthy study is that of Garzanti et al. (2012; 2015), who investigated sand from the Orange River and Orange River Delta that empties into the Atlantic Ocean in southwestern Africa. Sand from these locations is carried northward along the African coast by continuous longshore currents and tidal activity, some of it for over 1400 km (870 mi). After this great distance of transport and mechanical activity, all of the sand grains are still angular. The angular beach sand grains are then blown inland by southwesterly winds where they are deposited in the dunes of the Namibian Erg. They found that aqueous transport of beach sand grains, along the entire transport distance, fails to make them appreciably rounded compared to the original river and delta sand grains. It is not until the wind picks up the sand grains and blows them into the erg does any appreciable rounding take place. Thus, from that study it can be concluded that rounding appears to happen *only* by eolian transport and not by any other mechanisms. This has been confirmed by Whitmore and Strom (2017a, b, 2018), whose studies demonstrated that feldspar grains can show rounding with as little as a

few 100 m (328 ft) of eolian transport from a beach to a nearby eolian setting.

Thus far, this discussion on rounding has mainly focused on quartz, which is the most common component of most sandstones and siltstones. However, Pye and Tsoar (2009, 72) claim that K-feldspar rounds faster than quartz because of its lower hardness (6.0 on Mohs scale of hardness, compared to 7.0 for quartz). Therefore, it is to be expected that during erosion and transport the softer K-feldspar grains would deteriorate more quickly and, depending on the distance of transport, would likely be totally eliminated by the abrasive action on them by the harder quartz grains. Some theoretical, experimental, and observational rounding data has been collected on K-feldspar grains. Marsland and Woodruff (1937) demonstrated experimentally that K-feldspar rounds slightly faster than quartz. Yet the lack of consensus is probably because the movement of various shapes, sphericities and sizes of grains is a complex process and is highly dependent on various velocity conditions (Morris 1957).

Despite these studies, some have suggested K-feldspar grains can be successfully abraded in aqueous environments. Odom (1975) and Odom, Doe, and Dott (1976) studied a variety of quartz arenites. They observed that K-feldspar content increases with decreasing grain size. In many sandstones with mean grain sizes greater than about 0.177 mm (ϕ=+2.50), K-feldspar is often less than 10% of the rock volume (which defines a quartz arenite or quartz sandstone). With grain sizes less than about 0.125 mm (ϕ=+3.00), K-feldspar is often more abundant (10–25%), a rock which is called a feldspathic arenite (or arkosic sandstone or sub-arkose). Those authors suggested that this trend occurs because K-feldspar grains are abraded more easily in aqueous high energy environments (forming the larger-grained quartz arenites) and conserved in lower energy aqueous environments (forming the smaller-grained feldspathic arenites). This trending relationship certainly appears to apply to the sandstones, siltstones and shales of the Bright Angel Formation, with most of the finer-grained clastic sediments containing more K-feldspar than quartz. While the K-feldspar content varies between 11.0% and 46.9% (table 3) in the siltstone and shale layers in the Whitmore helipad fold, K-feldspar dominates over quartz with contents between 32.4% and 46.9% (table 3 and fig. 3). However, Snelling (2021) found this inverse relationship between K-feldspar grain size and the K-feldspar percentage did not apply to the Tapeats Sandstone, as some of the largest K-feldspar clasts (2.00–4.00 mm, ϕ=-1.00–-2.00, granule size) occur in samples with K-feldspar amounting to 22–33% of the rock volume. This is consistent with rapid transport and deposition of the Tapeats Sandstone over a short distance, which thus also applies to the Bright Angel Formation as representing the finer sediments from the same source and transport and deposition processes (see below).

As already noted, Garzanti et al. (2015) found that angular sand grains of all mineral species changed little from marine and fluvial transport but were only significantly rounded by eolian abrasion. Most detrital mineral grains were still angular to sub-angular after ~2000 km (~1,240 mi) of transport along the Orange River, confirming that fluvial environments are ineffective in rounding sand grains. Roundness changed little in the marine environment even after 300 to 350 km of high-energy littoral transport along the Atlantic shores of the Sperrgebiet. This condition demonstrated that beach action, as any transport in aqueous media, does not have much influence either (Pettijohn 1957) and disproves the long-held idea that beach sand grains are rounded faster than river sand grains because the former grains are rolled back and forth repeatedly on beaches (Folk 1980). This misunderstanding likely occurred because beach pebbles are usually round and flat, so this observation was probably extended to sand grains too.

From their observations Garzanti et al. (2015) also concluded the "relative toughness" or susceptibility of various minerals to rounding. Based on the observed compositional trends and differential rates of increased roundness with transport distance, the following sequence of relative toughness and mechanical durability was established (from "toughest" to "weakest"):

> garnet > quartz > epidote ≥ volcanic rock fragments ≥ feldspars > opaques ≥ pyroxene > amphibole > sedimentary/metasedimentary rock fragments.

However, K-feldspar also cleaves relatively easily compared to the conchoidal fracture of quartz. This perhaps explains why angular and sub-angular K-feldspar grains were found in virtually every Bright Angel Formation sandstone, siltstone and shale thin section examined (see Appendix D in the Supplementary material). Similarly, Whitmore et al. (2014), Whitmore and Garner (2018) and Whitmore and Strom (2018) found angular K-feldspar grains in virtually every sample they examined of the Permian Coconino Sandstone and many other related or correlated sandstones in the western USA, England and Scotland. Indeed, they reported that the angular K-feldspar sand grains were sometimes more angular than the similar-sized quartz grains that surrounded them. Yet many of those same sandstones that have angular K-feldspars also contain angular grains of quartz and mica flakes (mostly muscovite) and are moderately- to poorly-sorted (Borsch et al. 2018; Maithel, Garner, and Whitmore 2015; Whitmore et

al. 2014). In other words, under the microscope these sandstones are not as texturally mature as they might appear to be at the outcrop scale. They thus concluded that the presence of angular K-feldspar grains in ancient sandstones should be a reliable indicator of

(1) a first-order cycle of at least some of the sediment, and
(2) aqueous transport and depositional processes of the sandstone.

This is consistent with the claim of Wanless (1973a, b, 1981) that water transported sands remained sub-arkosic throughout the entire Tonto Group section (defined at that time as just the Tapeats, Bright Angel and Muav). This is also consistent with the petrographic observations of Rose (2003) and Snelling (2021) of the Tapeats Sandstone, and here regarding the sandstones, siltstones, and shales of the Bright Angel Formation. These observations imply the rapid transport and dispersal of the Tonto Group's constituent sandy, silty and muddy units.

Furthermore, micas are much softer on the Mohs scale of hardness (muscovite 2.0-2.5 and biotite 2.5-3.0) and consist of fragile sheets that easily cleave. Therefore, in a sediment dominated by quartz and K-feldspar grains with hardnesses of 7.0 and 6.0 respectively, the micas should be rapidly abraded. Standard petrography textbooks thus suggest micas should only be found in subaqueously transported and deposited sediments (Hallam 1981, 20; Moorhouse 1959, 343; Tucker 1981, 45).

In their studies of sand transport along the southwestern coast of Africa, Garzanti et al. (2012, 2015) found no appreciable change in the composition of the sand transported for hundreds of kilometers along the coastline (which contained micas). However, when the beach sand was picked up by wind and transported to the Namib dunes, all mineral grains became quickly rounded and the mica flakes either disappeared or possibly were never transported to the dunes.

Similarly, Whitmore (2017) and Whitmore and Strom (2017a, b) collected sand samples from beaches along the California and Oregon coastline and compared those samples with coastal dune samples from the same locations. They found that mica flakes were conspicuously absent from dune samples, unless those dunes were in close proximity (less than tens of kilometers) from mica-bearing bedrock, stream (fluvial) sediments or beach sands.

Anderson et al. (2013) and Anderson, Struble, and Whitmore (2017) devised a series of experiments to test the durability of mica flakes in eolian and subaqueous environments. A small amount of muscovite-rich sand was placed in a one-gallon glass jar with an RC airplane propeller attached on the inside of the lid and laid on a rock tumbler assembly, so that the rotation of the jar sustained a lateral dune. The velocity of the propeller was adjusted so that a small "dune" slowly migrated around the bottom of the jar. Surprisingly, after one year of spinning in this water-saturated tumbler (roughly equivalent to transport of 7,500 km or 4,660 mi), not only did the sand still contain an appreciable number of muscovite grains, but they were still large enough to be seen with the naked eye. This is potentially explained by the cushioning effect of the water, which has a much higher viscosity than air and reduces the kinetic energy of grain-grain collisions, thereby preventing the rapid degradation of mica flakes and other softer minerals. The experiments of Marsland and Woodruff (1937) further confirm these observations. Despite the simplicity of these experiments, they confirm field and experimental observations that mica flakes are rare in modern eolian deposits and commonly present in subaqueously deposited sands.

Borsch et al. (2018) emphasized it is important to note that the mica flakes they found in cross-bedded sandstones are detrital (transported) rather than diagenetic (altered from other minerals post-deposition) in character. For example, muscovite can be formed via the following chemical alteration of K-feldspar (orthoclase) in the presence of an acid (H^+):

$$3KAlSi_3O_8 \text{ (orthoclase)} + 2H^+ \rightarrow KAl_3Si_3O_{10}(OH)_2 \text{ (muscovite)} + 6SiO_2 + 2K^+$$

The mica produced in this conversion is sericite, which most often occurs entirely within the host grain, and is visible in thin section as fibrous bundles. Consequently, sericite is generally much smaller than the host grain and randomly oriented. By contrast, many of the mica flakes observed in their study were longer than the matrix grains (size inversion), and the characteristic fibrous textures were not present. Furthermore, in their samples they observed:

(1) thin books of mica bent around other grains (often quartz),
(2) thin contorted mica books with splayed ends,
(3) the mica flakes did not often occupy the fairly common empty spaces of dissolved K-feldspar grains, and
(4) significant amounts of orthoclase (as much as ~8–15%) were often found in the thin sections along with the mica flakes (that is, orthoclase had not been diagenetically altered).

Together, these clearly indicated that the mica flakes they observed are detrital, and thus are part of the original depositional fabric.

The micas observed in every thin section of the Bright Angel Formation in this study are muscovite flakes and have exactly the same characteristics as listed by Borsch et al. (2018). Most of the

muscovite flakes are visible as edge-on stacked sheets in thin books. Because the thin sections were cut perpendicular to the bedding this means those muscovite flakes are parallel, and when at an angle are sub-parallel, to the bedding, a pattern consistent with aqueous deposition of detrital flakes. Furthermore, while the lengths of the flakes are variable, they are often longer than the widths of the surrounding quartz and K-feldspar grains and thus wedged between the quartz and K-feldspar grains (fig. 43). Sometimes they are also bent around the quartz and K-feldspar grains, and occasionally with their ends frayed, split, splayed, and even bent back. In other instances, the long thin books of muscovite have been altered after deposition, probably to illite or illite/smectite, the sheets sometimes expanding to be thicker, but still disposed in the positions in which they were originally deposited as detrital flakes. Furthermore, the muscovite flakes do not occupy empty spaces due to dissolved K-feldspar grains. To the contrary, all twelve samples contain very significant amounts of K-feldspar, primarily orthoclase (11.0–46.9%), along with the muscovite flakes (table 3). Some K-feldspar grains and former laths still display cross-hatched twinning under crossed polars characteristic of microcline and any diagenetic alteration of them is partial and in situ. Therefore, there can be no doubt these muscovite flakes are detrital and were transported and deposited subaqueously.

Finally, there are the occasional grains consisting of rock fragments observed in the Bright Angel Formation sandstones and siltstones. Quartzite fragments are difficult to distinguish because of their similarity to quartz grains containing sub-domains, but they are hard enough (with the 7.0 hardness of quartz) to have easily survived subaqueous transport and deposition and so some may be present in these sandstones and siltstones. In contrast, Ulmer-Scholle et al. (2015) noted that schist fragments tend not to survive extensive transport. During more extensive transport, they reasoned, such grains would probably break down into silt-size fragments or their individual constituent quartz crystals. They suggested that mica-rich schist grains would rarely survive significant transport unless carried in suspension with muddy sediments. Therefore, Ulmer-Scholle et al. (2015) concluded that any surviving mica schist clast was probably deposited in relatively close proximity to its source.

However, no indisputable mica schist clast was observed in the Bright Angel Formation samples in this study, although Martin (1985) reported observing mica schist fragments in his samples. Only several rock fragments were observed in this study and tentatively identified as weathered siltstone (fig. 49). Thus, the observations and conclusions of Ulmer-Scholle et al. (2015) would still seem to apply to the Bright Angel Formation, because both mica schist fragments and even weathered siltstone fragments would seem to be very vulnerable to mechanical breakdown into their constituent grains during sediment transport and deposition unless that transport and deposition was extremely rapid and the transport distance was extremely short. Transport in suspension with the muddy sediments of the Bright Angel Formation would definitely have been a factor. Furthermore, the other identified rock fragments in the Bright Angel Formation are shale-mudstone "rip-up" clasts, one of which is relatively large (figs. 38h, 49b). Their survival during transport among the hard, abrasive quartz and K-feldspar sand and silt grains would also seem to be consistent with extremely rapid transport over an extremely short distance.

In conclusion, the collective evidence suggests a short-distance rapid transport of the sandy, silty and muddy sediments during rapid deposition of the Bright Angel Formation. The transport distance had to be very short, since the source of the sediment has been clearly identified as the underlying Precambrian granitic plutons and schists of the Granite Gorge Metamorphic Suite, with some contributions from the stratigraphically intervening Grand Canyon Supergroup sedimentary strata. These include the shales and siltstones of the Hakatai Shale and very thick Dox Formation (~3,200 ft or 975 m), as well as the quartzite of the Shinumo Quartzite. Thus, erosion of the Great Unconformity was most likely catastrophic to rapidly supply so much sediment locally. And transport and deposition, likewise, was likely rapid and over only a very short distance for detrital muscovite flakes and weathered siltstone, mica schist and shale/mudstone fragments to have survived, and for K-feldspar grains and former laths to be so widely distributed within the full thickness of the Bright Angel Formation. The fact that the Bright Angel Formation consists of predominantly angular to sub-angular quartz and K-feldspar grains is also further confirmation of rapid transport and deposition.

Sedimentary Structures and the Depositional Environment

The above observations and conclusions clearly seem to overturn the uniformitarian interpretation of the Bright Angel Formation being the product of a comparatively tranquil marine transgression lasting several million years involving shallow open shelf marine, subtidal and intertidal sedimentary environments (Baldwin et al. 2004; Elliott and Martin 1987b; Martin 1985; Martin, Middleton, and

Elliott 1986; McKee 1945; Middleton and Elliott 2003; Rose, Middleton and Elliott 1998; Rose 2003, 2006, 2011; Wanless 1973a, b, 1975, 1981). Indeed, Kennedy, Kablanow, and Chadwick (1997) and Chadwick and Kennedy (1998) provided compelling evidence of more catastrophic deep-water deposition of at least some of the Tapeats Sandstone, which implies the Bright Angel Formation was similarly deposited more catastrophically in deeper water. Thus, the sedimentary structures used to identify the Bright Angel Formation as a shallow marine to intertidal facies need to be re-evaluated. If the Bright Angel Formation were instead deposited under the catastrophic conditions of a global flood cataclysm in which the sea level rose rapidly and the resulting "dramatic global marine transgression" (Karlstrom et al. 2018) was exceedingly rapid, then we know of no such processes operating today. Therefore, the slavish commitment to the uniformitarian dogma that "the present is the key to the past" by most past workers researching the Bright Angel Formation is totally unwarranted. Such researchers have tried to interpret the sedimentary structures in the Bright Angel Formation on the basis of those produced in today's relatively slow-and-tranquil shallow marine, intertidal and even fluvial sedimentary environments. Garzanti (2017) has commented that sedimentologists "often resort to mythical thinking in the face of natural phenomena that we hardly understand" and that myths are ideas that owe their popularity to plausible reasoning rather than to observational evidence. It is no wonder that no unified consensus has been reached after over 150 years of investigations. Indeed, since the focus of uniformitarian-thinking investigators has been only on the Bright Angel Formation primarily in Grand Canyon region, they have ignored the global context of this "dramatic global marine transgression" which catastrophically eroded the underlying Precambrian basement rocks and rapidly deposited the Bright Angel Formation as a component of the Sauk megasequence on a global scale.

Therefore, in reevaluating the sedimentary structures in the Bright Angel Formation, the only sedimentary environment today that might be used as a guide to the more catastrophic environmental conditions under which it was deposited would be that produced by severe storms and hurricanes. Yet even that comparison would be deficient, as today severe storms and hurricanes are seasonally intermittent, whereas under the likely catastrophic flooding conditions of a dramatic global marine transgression severe storms and hurricanes would be happening continuously. Thorne et al. (1991) have endeavored to quantify how much of the thicknesses of the beds produced by intermittent storms would be preserved based on the periodicity of the storms and the sediment accumulation rate. They obviously found that the more frequent the severe storms and the more rapid the rate of sediment accumulation, the greater the potential preservation of thicker beds. Also, the greater the water depths, the greater the preservation potential. In their modeling such storm event beds would be up to a meter (~3.3 ft) or so thick, though typically 25–50 cm (~10–20 in) or less, not unlike the 0.3–1.3 m (~1–4.3 ft) thick beds preserved within the Bright Angel Formation (figs. 9–15).

Seilacher and Aigner (1991) and Walker and Plint (1992) identified what would be the distinguishing features of storm deposits, and hummocky cross-stratification was concluded to be a primary feature. As originally defined by Harms et al. (1975), hummocky cross-stratification is low-relief surfaces with overlying parallel to subparallel laminae of slightly variable thickness and scattered dip directions. More recently, Boggs (1995) defined hummocky cross-stratification as characterized by amalgamated undulating sets of cross-laminae that are both concave-up (swales) and convex-up (hummocks), the cross-bed sets being commonly 15–50 cm (~0.5–1.6 ft) thick and cutting gently into each other with curved or wavy basal erosion surfaces. The spacing of the hummocks and swales are typically from 50 cm to several meters (~1.6–13 or so ft). Dott and Bourgeois (1982) noted that hummocky cross-stratification has been identified in the geologic record in transgressive strata up to 175 m (~575 ft) thick and may be interstratified (between storm events) with mudstone, siltstone, sandstone and conglomerate. They also calculated the formation of hummocky beds (storm beds or tempestites) occurred in the upper sheet flow regime with water flow velocities at 80–200 cm/sec (0.8–2 m/sec), with intense oscillatory flow in shallow water depths. Prave and Duke (1990) also argued for upper flow regime sediment transport, but with unidirectional flow. In contrast, Duke (1985) after examining the paleogeographic distribution of 107 occurrences of hummocky cross-stratification in the geologic record spanning the Proterozoic to the Recent had concluded that most occurrences were generated by hurricanes and that hurricane-generated bottom flows tend to be oscillatory- or multi-directionally-dominant.

Ironically, Rose (2003) claimed that hummocky cross-stratification structures widely regarded in the literature as produced by storm-accentuated oscillatory flows have neither been successfully reproduced in controlled laboratory conditions nor observed directly forming from oscillatory flows. Yet when Duke, Arnott, and Cheel (1991) proposed a depositional model for hummocky cross-stratification formation as due to storm transport

of coastal sand to the inner shelf under dominantly oscillatory flow controlled by a very minor component of unidirectional flow, they based it in part on controlled laboratory experiments by Arnott and Southard (1990) and Southard et al. (1990). Those experiments had successfully reproduced hummocky cross-stratification and symmetrical 3D mega-ripples in a long-period purely oscillatory flow and very strong oscillatory-dominant combined flow. Duke, Arnott, and Cheel (1991) also commented that the grain fabric in hummocky sandstones indicates rapid reversals of bed shear stress consistent with deposition due to shore-normal transport of coarse bedload on the inner shelf during storms caused by the interactions of high-speed oscillatory bottom motions and a relatively slow bottom current. DeCelles and Cavazza (1992) likewise invoked high-energy oscillatory flow as the primary entrainment and bedform sculpturing mechanism, followed by a high sediment fallout rate resulting from rapid decay of storm-wave energy. Furthermore, Swift et al. (1983) concluded that hummocky cross-strata sets are due to the action of strong storm-wave surges involving combined-flow currents with sediment deposition throughout much of the storm's duration, while Swift and Thorne (1991) argued that the depositional hydraulic conditions during storms meant sediment accumulation only occurred below storm wave base, which Walker and Plint (1992) estimated was at greater than ~25 m (~82 ft) water depth.

Martin (1985) reported finding hummocky cross-stratified sandstone beds within the Bright Angel Formation comprising <1% of it (fig. 30). They consist of a series of fining-upward units ~10 cm (~4 in) thick, each being similar to the idealized hummocky cross-stratified sequences documented by Dott and Bourgeois (1982), who also reported that hummocky cross-stratification identified in the geologic record may be interstratified (between storm events or surges) with mudstone, siltstone, sandstone and conglomerate. Martin (1985) found that some fining-upward units are capped by a 1–5 mm (~0.04–0.2 in) thick shale or mudstone drape, or by a 3–4 cm (~1.2–1.6 in) thick wavy-bedded unit (using the terminology of Reineck and Wunderlich 1968). Each fining-upward unit structurally consists of an undulating erosive base followed upward by hummocky cross-stratification or trough cross-stratification, horizontal lamination, small-scale cross-stratification or ripple cross-lamination, and a mudstone or shale drape.

Of relevance here is that the reason the overall unit's designation was changed from the Bright Angel Shale to the Bright Angel Formation (Karlstrom et al. 2020; Rose 2011). It is because it does not predominantly consist of shale. Martin (1985) estimated that the formation consists of ~30% sandstone beds (of which ~25% are cross-stratified), another ~30% consists of mottled siltstone beds, and the remainder consists of what he termed lenticular heterolithics, due to being a mixture of lithologies, predominantly interstratified fissile laminae of siltstone and shale with occasional very thin sandstone lenses. Martin (1985) recognized not only the cross-stratified sequences, but both fining-upwards and coarsening-upwards sequences, all separated by erosion surfaces (figs. 13–15). He interpreted each of these sequences as due to the passage of high-energy storms, the sand beds being deposited by sand waves at the heights of the storms and the finer-grained silts and muds deposited in the waxing and waning phases of the passing storms, and during the quieter low-energy times between, the muds settling from suspension. Furthermore, Martin (1985) noted that the allochthonous concentration of brachiopod shell fragments in the sandstone beds of the Bright Angel Formation (as confirmed in this study, see fig. 44) indicates that the shells were perhaps routinely moved about and broken, hydrodynamically sorted, and concentrated in the higher energy coarser-grained sandstone beds.

However, thin-section petrographic examinations reveal that most shales consist of very finely-laminated alternating siltstone and mudstone laminae, the silt laminae sometimes thickening into lenses (Ulmer-Scholle et al. 2015, and in this study, see fig. 39g–i, p). Uniformitarians have traditionally envisaged these being deposited one lamina at a time, the grain sizes deposited according to the variability in the energy of the sedimentation processes. Furthermore, as indicated above, the finer-grained muds are envisaged as settling very slowly out of suspension in the water column in the slackest energy conditions. Such slow-and-gradual depositional processes punctuated by occasional high-energy storms across a shallow shelf marine environment and its intertidal reach is essentially what has been envisaged for deposition of the Bright Angel Formation. However, observations of sedimentation in laboratory experiments in flumes substantiated by observations of the sedimentation resulting from real-world depositional events has resoundingly demonstrated that whole sequences of laminated sediment layers are deposited rapidly all-at-once from heterogranular sediment mixtures, and muds are also deposited rapidly (Schieber, Southard, and Thaisen 2007).

Berthault (1988, 1990), Julien, Lan and Berthault (1994) and Julien, Lan, and Raslan (1998) reported numerous laboratory experiments in which heterogranular mixtures of sediments transported in water or air rapidly deposited in multiple laminae consisting of alternating fine and coarse grains. From

each surging slurry of mixed grain sizes, the motion of the grains plus gravity sorted and separated them during the depositional process so that the resulting alternating fine- and coarse-grained laminae were identical to shales and other laminated sedimentary layers found in the geologic record. Subsequently, Fineberg (1997) and Makse et al. (1997) confirmed those findings from further experiments and referred to this grain-size separation process as spontaneous stratification, substantiating their experimental outcomes with many papers in the literature on the physics involved, including when there are vibrations added to the transport of the heterogranular mixture. Furthermore, that this same spontaneous stratification process does occur in real-world depositional events to produce laminated sedimentary layers has been confirmed by Austin (1986, 2009) and Rowley, Kuntz, and MacLeod (1981). On June 12, 1980, pyroclastic flows generated by the collapse of the eruption plume of heterogranular debris and steam over the Mount St. Helens volcano and travelling at a hurricane velocity of 90 mph (150 kph) deposited stratified layers in total up to ~7.6 m (~25 ft) thick and up to ~2 km (~1.25 mi) wide on the pumice plain to the north of the volcano within three hours. These layers deposited from the slurries consisted of alternating fine- and coarse-grained thin laminae and included graded bedding and cross-bedding.

Uniformitarians have assumed that most mud accumulates directly from suspension in the water column, that mud deposition requires quiet bottom-water conditions, and that hence it takes long periods of time to deposit the great thicknesses of mudstones and shales that make up the majority of the geologic record (Macquaker and Bohacs 2007; Schieber, Southard, and Thaisen 2007). In fact, Moshier, Helble, and Hill (2016, 58–59, 62) specifically state that most grains in shales are composed of clay minerals, that clays settle out of suspension very slowly from relatively still water to accumulate shale layers very slowly, and that shales make up roughly 50 percent of the sedimentary rocks in earth's geologic record, so by implication the Bright Angel "Shale" could not have accumulated in Noah's Flood. Yet they provided no details describing the Bright Angel "Shale" to demonstrate it is composed mostly of clay mineral grains, when it is well documented in the relevant literature that shales often contain large amounts of fine quartz and K-feldspar grains in alternating thin laminae (for example, Ulmer-Scholle et al. 2015), and that the Bright Angel Formation consists of not just shales but the majority of it is sandstones and siltstones (Martin 1985; Middleton and Elliott 2003; Rose 2003, 2006, 2011). Furthermore, thin section examination confirms that the shales of the Bright Angel Formation are actually thin alternating laminae of siltstone and mudstone, and the clay minerals are subordinate in most laminae to very small quartz and K-feldspar grains (table 3 and figs. 38–49).

However, while Schieber, Southard, and Thaisen (2007) admitted it is difficult to reconstruct the complex processes of mud deposition in the laboratory, such as the clumping of particles into floccules, they successfully used flume experiments to investigate the bedload transport and deposition of clay floccules. In fact, they demonstrated that the clumping of clay particles into floccules occurs at flow velocities that transport and deposit sand. First, they found that deposition-prone floccules form over a wide range of experimental conditions, which suggests an underlying universal process. And second, at a critical flow velocity of only 20–25 cm/sec (0.66–0.82 ft/sec) or 0.72–0.90 kph (0.45–0.56 mph) floccule ripples develop into low-angle foresets and mud beds that appear laminated after post-depositional compaction. But the layers retain signs of floccule ripple bedding that would be detectable in the rock record. Schieber, Southard, and Thaisen (2007) concluded that because mudstones were long thought to record low-energy conditions of offshore and deeper water environments, their experimental results call for reevaluation of published interpretations of ancient mudstone successions and derived paleo-oceanographic conditions.

In commenting on these experimental findings, Macquaker and Bohacs (2007) agreed this mechanism for depositing mud is at odds with the perceived (uniformitarian) wisdom that most mud accumulates directly from suspension in the water column requiring quiet bottom-water conditions, and that mudstones containing closely-spaced, parallel laminae represent continuous deposition. They affirmed that, in contrast, Schieber, Southard, and Thaisen (2007) had shown that mud can accumulate as current ripples composed of grain aggregates under currents that can transport very fine sand. Furthermore, their laboratory investigations have now provided direct evidence of advective sediment transport of mud-sized material in floccules, those clay aggregates forming migrating ripples with low crests (2–20 mm or ~0.08–0.80 in)) and very long spacings (300–400 mm or ~11.8–15.7 in) that deposited the sediment in non-parallel inclined laminae that could be easily misinterpreted as parallel-laminated under much higher current velocities than previously assumed.

Macquaker and Bohacs (2007) asserted that the results call for critical reappraisal of all mudstones previously interpreted as having been continuously deposited under still waters. Instead, substantial

volumes of mud can accumulate in higher-energy conditions than most researchers had assumed. Furthermore, these experimental results came at a time when mudstone science was poised for a paradigm shift.

Schieber and Southard (2009) performed additional flume experiments to demonstrate that muds can be transported in bedload as floccule ripples and deposited at current velocities that would suffice to transport and deposit sand. Their further experiments provided firsthand observations of the processes that shape and propagate mud ripples, whose geometries are very similar to those produced in sandy sediments. Thus, there is no excuse for Moshier, Helble, and Hill (2016) ignoring these well-established experimental conclusions in their claims about the slow-and-gradual deposition of shales in Grand Canyon strata, such as those in the Bright Angel Formation.

Therefore, it is abundantly obvious that the same observed sedimentary structures in the Bright Angel Formation are subject to different interpretations based on the bias and experience of the investigators.

Yet the sedimentary structures, as well as the fossils and trace fossils, within the Bright Angel Formation are entirely compatible with its rapid deposition by high-energy, storm-driven water currents in a shallow marine environment. The presence of hummocky cross-stratification and similar bedforms in the sheet sandstone beds would have been produced by storm events such as hurricanes (Boggs 1995; Harms et al. 1975), the erosive bases and tops of the repeated fining-upwards and coarsening-upwards sequences due to successive hurricane-driven storm surges eroded into the sands deposited by preceding storm surges, that is, high-energy oscillatory flows that deposited the sand rapidly (Swift et al. 1983). And because these successive storm beds are well-preserved, the water depths in which this sand deposition occurred must likely have been below the storm wave base. Furthermore, even the fissile shales and inter-stratified siltstones, usually displaying alternating thin mudstone and siltstone laminae, are indicative of the rapid deposition of a rapidly-transported heterogranular sediment mixture resulting in spontaneous stratification, while the mud floccules were deposited as rapidly as the fine sand and silt grains, all likely in the intervals between the storm surges that rapidly deposited the sand beds.

It was noted by Martin (1985) that the vertical traces were preserved on megaripples and the tops of sand sheets, along with horizontal crawling and feeding traces, as well as abundant arthropod trackways. Furthermore, the ubiquitous trace fossils typically occurred within the silty and muddy inter-sheet areas at the interfaces between sandstone beds and silty mudrocks in the formation. Bioturbation requires time for creatures to recolonize bed surfaces after deposition and commence their burrowing activity. Indeed, it has been long recognized that fissility in shales is directly related to not only the parallel orientation of their constituent mineral grains but to a decrease in or absence of bioturbation (Byers 1974). Thus the fissility due to the characteristic pronounced laminae in the Bright Angel Formation's shales and siltstones that make up to 70% of the formation are testimony to the observed lack of bioturbation, which correlates with deposition and accumulation of the muds and silts being so rapid due to continuous spontaneous stratification that there was insufficient time for bioturbation to occur.

However, Martin (1985) found that in sequences consisting of cross-stratified sandstone beds erosively overlain by fine-grained, ripple cross-laminated sandstone, trace fossils are generally absent, with the exception of truncated U-shaped *Diplocraterion*, indicating that the substrate was relatively mobile and thus precluded permanent faunal colonization. These tubes appear as paired holes on bedding planes, or as concave-upward scours where they have been eroded to the bases of the burrows (Hereford 1977; McKee 1945; Middleton and Elliott 2003). Also, in coarsening-upward sequences, vertical trace fossil types, such as *Diplocraterion* and *Skolithos*, are rare, probably also due to relatively high current velocities and a mobile substrate. In contrast, in fining-upward sequences, the presence of complete traces, including funnels and complete burrows of *Diplocraterion*, indicates that the surface was rapidly recolonized after deposition of sediment but that subsequent rapid deposition of mud and silt forced the organisms to evacuate (or they were swept away) to relocate their burrows (Elliott and Martin 1987b). Furthermore, even the massive sandstone beds and mottled siltstones that Martin (1985) described as bioturbated would not have required long time intervals for that bioturbation, given the huge numbers of trace-makers that evidently were active during the rapid deposition of those sediment layers who would otherwise have obliterated their internal structures.

Martin (1985) interpreted the lenticular heterolithics as due to storm-induced deposition of sand followed by lower energy periods during which traces were formed. However, even Rose (2006) conceded that the exquisite preservation of bedding-plane trace fossils required consistently high short-term depositional rates for these interbedded sandstones and shales despite their fine grain-size, and that the timeframe between animals borrowing into and moving across the sediment surfaces and

burial of their traces would range from seconds to days at most. Alternately, it is thus conceivable that surging tsunamis waves would produce similar rapid deposition as there are generally multiple waves from one plate movement, and repeated plate movements as modeled by Baumgardner (2018a, b) would result in a rapid succession of layers. Nevertheless, Martin (1985) regarded the horizontal trace fossils such as *Palaeophycus*, *Phycodes*, and *Teichichnus* as produced by organisms burrowing completely in mud, or in mud under sand lenses, implying that their movements were largely unrestricted by the physical energy of the overlying water column. Likewise, Elliott and Martin (1987b) noted that *Cruziana* and *Rusophycus* which represent trilobites crawling and resting or feeding traces were probably formed on the open muddy sea floor. Because trilobites evidently produced open furrows in mud (Baldwin 1977; Crimes 1975), their movements were restricted by relatively high-energy currents, implying that they furrowed between storms, whereas during storms the trilobites were perhaps relatively inactive, forming *Rusophycus* traces. Furthermore, whereas Pemberton, MacEachern, and Frey (1992) argued that such trails would only be preserved below the minimum wave base, that is, in deeper water, Bromley and Asgaard (1991) warned that trace fossils could be preservational (where they are buried) rather than behavioral (where they lived).

Thus, even the trace fossils are consistent with the rapid deposition of the Bright Angel Formation, with rapid successive hurricane-driven storm surges depositing the sand beds and the interstratified siltstones and shales deposited in the brief lower energy intervals between. Likewise, the invertebrate fossils found in the Bright Angel Formation required rapid burial for their preservation before decay or scavenging in storm events, particularly where there have been larger numbers of trilobites buried together in restricted areas in what are termed lagerstätten (Brett and Seilacher 1991). This required burial below storm wave base, yet the presence of broken brachiopod shell fragments indicates how destructive the stormy conditions must have also been. Similarly, it can be argued that contrary to the claims of Hill and Moshier (2009, 2016) that delicate trace fossils require relatively gentle conditions for their preservation, once the tracks and burrows were made, they needed to be buried rapidly before being obliterated by the stormy conditions and/or by the continuing activity of the trackmakers. Additionally, the hurricane-driven stormy depositional conditions are consistent with the cryptospores from land plants (Baldwin et al. 2004) being wind-blown and thus also found buried with the marine invertebrates and their traces and tracks. Therefore, in conclusion, the sedimentary structures and fossil content within the Bright Angel Formation are entirely compatible with its catastrophically rapid deposition by hurricane-driven storm surges in a shallow marine environment in deeper water below the storm wave base.

"Age" Indicators

The conventional age of the Bright Angel Formation was initially established based on the formation's stratigraphic position relative to two trilobite fossil assemblage zones. However, whereas in western Grand Canyon the base of the formation lies below the *Olenellus-Antagmus* fossil assemblage zone and hence is designated as late Early Cambrian, in eastern Grand Canyon the upper two-thirds of the formation lies above the *Alokistocare-Glossopleura* fossil assemblage zone and thus is designated as Middle Cambrian (fig. 5). The numerical ages of these trilobite zones have subsequently been determined by precisely U-Pb dated zircon grains in regional and global sections (Schmitz 2012; Sundberg et al. 2016, 2020), tied to U-Pb zircon dated Cambrian marker beds elsewhere (Landing et al. 2015; Peng, Babcock, and Cooper 2012) (fig. 33). Karlstrom et al. (2018, 2020) have thus established the conventional age of the Bright Angel Formation at ~502–507Ma based on U-Pb dating of detrital zircons in the underlying Tapeats Sandstone and the now established U-Pb zircon dates of these trilobite fossil zones. But the methodology they all used raises numerous issues and questions, including how reliable is the U-Pb dating method.

In their supplemental data, Karlstrom et al. (2018) tabulated all the U-Pb dating results of every detrital zircon grain from the Tapeats Sandstone that they, Gehrels et al. (2011) and Matthews, Guest, and Madronich (2018) analyzed. They obtained a wide spectrum of U-Pb ages with peaks corresponding to the published ages of the source rocks from which they concluded the zircon grains had been eroded. They, and Karlstrom et al. (2020), then established the age of the Tapeats Sandstone by statistically determining from the spectrum of the lowest detrital zircon U-Pb ages the peak of the "bell-shaped" curve, which at 507–508Ma they called the maximum depositional age. Yet the supplemental data tables listed that many of the detrital zircons yielded U-Pb ages less than that 507–508Ma age for the Tapeats Sandstone—at least 59 spot analyses of zircons from their Hermit Creek sample with the lowest U-Pb age of 407.2Ma, at least 45 spot analyses of zircons from their Frenchman Mountain sample with the lowest U-Pb age of 481.8Ma, and at least 51 spot analyses of zircons from their East Verde River sample with the lowest U-Pb age of 468.0Ma. Karlstrom et al. (2018) do not explain how the supposedly 507–508 million years old Tapeats Sandstone can have included

within it so many detrital zircons with U-Pb ages less than its supposed depositional age, including one as "young" as only 407.2 million years old. Nor do they explain where these "younger" detrital zircons originated from within the Tapeats Sandstone. Indeed, how could the 507–508Ma detrital zircons be incorporated in the Tapeats Sandstone if the underlying rocks that were eroded to provide the sand grains, including the zircon grains, are older than 507–508Ma? This question alone raises serious doubts as to the applicability and reliability of this technique for supposedly quantifying the apparent depositional ages of sedimentary rock units.

Yet not only is their methodology questionable, so must be the U-Pb dating method they used if it produced such illogical ages. Snelling (2000, 2009) has already provided details of numerous problems with the U-Pb dating method that are well-documented in the scientific literature. Furthermore, Snelling (2017a) reviewed all the determinations of the U-Pb decay rates (half-lives) and demonstrated that these crucial parameters are not yet precisely known, while Snelling (2017b, 2018, 2019) highlighted in detail the problems of common Pb, U and Pb mobility, and mass fractionation respectively that plague all efforts to obtain accurate U-Pb age determinations. Nevertheless, Karlstrom et al. (2018, 2020) championed the tandem U-Pb dating procedure they used, that is, LA-ICP-MS (laser-ablation–inductively coupled plasma–mass spectrometry) analyses followed by CA-ID-TIMS (chemical abrasion–isotope dilution–thermal ionization mass spectrometry) analyses. Yet even though it often produced apparently concordant U-Pb dates (essentially matching ^{206}Pb-^{207}Pb, ^{238}U-^{206}Pb and ^{235}U-^{207}Pb ages), there were still so many detrital zircon grains that yielded illogically younger ages than the supposed depositional age of the Tapeats Sandstone. Furthermore, Snelling (2005b) reported CA-ID-TIMS analyses of three zircon grains recovered from a thin tuff bed in the Tapeats Sandstone in the western Grand Canyon that yielded concordant U-Pb ages of 86.2Ma, 98.2Ma, and 90.1Ma. And Snelling (2005b) also obtained single zircon grain fission track ages of 75Ma, 158Ma, and 408Ma that are very much younger than the Karlstrom et al. (2018, 2020) tandem U-Pb ages for deposition of the Tapeats Sandstone. Yet fission tracks are the physical evidence of the quantity of nuclear decay that has actually occurred. These considerations and highly inconsistent results from what is touted as a superior analytical procedure only highlight the unreliability and fallibility of the U-Pb dating method.

However, it could be argued that the accepted radiometric ages of the various Grand Canyon strata, including the basement granites and schists, date those rocks and strata in the correct relative order, and consistently in hundreds of millions to almost two billion years, except for the recent lava flows in western Grand Canyon (Wiens 2016). Vardiman, Snelling, and Chaffin (2005) have demonstrated from six lines of evidence supported by experimental results that the reason for this systematic consistency of radiometric ages in the Grand Canyon stratigraphic sequence is because during a past catastrophic event there was a systematic acceleration of nuclear decay rates, potentially by six orders of magnitude. Three of those six lines of evidence involved experimental results obtained on Grand Canyon samples, namely, discordant radiometric ages obtained from four Precambrian units (the Cardenas Basalt, the Bass Rapids diabase sill, the Elves Chasm Granodiorite and the Brahma Schist amphibolites) (Snelling 2005c), coexisting uranium and polonium radiohalos (Snelling 2005a) and fission tracks in zircons (Snelling 2005b). Critics have pointed to the enormous quantities of heat that apparently would be released by such accelerated nuclear decay (Wiens 2016), yet Vardiman, Snelling, and Chaffin (2005) had already anticipated this criticism and provided plausible possible explanations, including the experimental fact that the radiohalos (which only form below 150°C) would have been annealed if such an enormous heat release had occurred (Snelling 2005a).

In conclusion, there is sufficient overwhelming evidence, also documented in the scientific literature, to question the reliability, and even the validity, of the U-Pb dating method. This is highly evident from so many U-Pb dates for zircons within the Tapeats Sandstone that are markedly younger than the claimed depositional age of that sandstone which directly underlies the Bright Angel Formation. Thus, the U-Pb dating of detrital zircons from the Tapeats Sandstone that was used to obtain a ~502–507Ma age for the Bright Angel Formation (Karlstrom et al. 2018, 2020), coupled with the claimed biostratigraphic age of the Bright Angel Formation (Karlstrom et al. 2020; Sundberg et al. 2020), is not an impediment to explaining the deposition of the Bright Angel Formation in a much more recent catastrophic event, namely, the global Genesis Flood cataclysm. That would be more consistent with the textural and mineralogical evidence for the rapid local erosion and short-distance rapid transport and deposition of its constituent sand, silt and mud.

Initial Flood Catastrophic Erosion and Deposition

Austin (1994) provided a detailed comprehensive description and account of the geological development of Grand Canyon strata in the context of the

global Genesis Flood cataclysm and the Canyon's erosion in the Flood's aftermath. In particular, he described the Tonto Group as being deposited by the Flood waters advancing eastwards onto the western edge of the North American portion of the pre-Flood supercontinent at the initiation of the Flood event with the breaking up of the fountains of the great deep (Genesis 7:11) and the triggering of catastrophic plate tectonics (Austin et al. 1994; Baumgardner 2003). However, before the Bright Angel Formation was deposited there had to be a prolonged period (possibly days or more) in which there was a significant amount of continental-scale erosion to bevel the Precambrian (pre-Flood) land surface to produce the Great Unconformity. In Grand Canyon region, this involved intensive catastrophic erosion removing several thousand meters of Grand Canyon Supergroup strata (which appear to only have survived in several down-faulted blocks) and then beveling of the underlying metamorphic schists and granite plutons. After this period of destructive erosion, and subsequent to the localized deposition of the Sixtymile Formation, the Tapeats Sandstone and the overlying Bright Angel Formation were deposited as the first widespread (continental-scale) deposits of the Tonto Group. That initial brief period of catastrophic erosion may have coincided with the initial rifting ("breaking up") that occurred until significant plate motion began to generate the tsunamis in surges of waves that deposited the Tonto Group strata.

Austin (1994) diagrammatically envisaged a fining upwards model for the time transgressive rapid deposition of the Tonto Group strata as the powerful westward back under-flow of the advancing Flood waters, moving at a water flow speed of >2 m/sec, intensely scoured and catastrophically eroded pre-Flood rocks to produce the Great Unconformity before sequentially depositing their load of sediments as horizontally segregated facies in the vertically stacked Tonto Group strata (fig. 50). In the adjacent shallow-water area, the westwards-flowing, intense bottom-surging current deposited coarse pebbles and sand with lag boulders up to 9 m (30 ft) diameter in flat beds or cross beds to form the base of the Tapeats Sandstone at a water flow speed of 1.5 m/sec. Further westwards in deeper water the central portion (cliff-forming unit) of the Tapeats Sandstone composed of sand waves of coarse sand in thin cross-beds with westerly and south-westerly dips was deposited in a water velocity of about 1 m/sec. Simultaneously, and even further westward, the top of the formation composed of thinner, fine-grained sand and silt beds dominated by plane beds with ripples was deposited by deeper and slower moving waters at 0.5 m/sec, forming a gradational transition into the overlying fine-grained sandstones, siltstones and shales of the Bright Angel Formation. In these deeper and slower-moving waters, the silicate clay-, silt- and fine sand-sized particles accumulated as the graded fine-grained sandstone, siltstone and shale beds of the Bright Angel Formation, these deposits being the residue winnowed from the coarser sands in the more energetic shoreward zones where the Tapeats Sandstone was deposited.

This sedimentation model is consistent with the conventional, classical time-transgressive deepening seas model first advocated by McKee (1945) and the deep-water deposition of the Tapeats Sandstone proposed by Kennedy, Kablanow, and Chadwick (1997), except that the timeframe for simultaneous deposition of the Tapeats Sandstone and the Bright Angel Formation is a mere few days as part of the initial catastrophic erosion and deposition of the global Genesis Flood cataclysm, about 4,350 years ago. This is in stark contrast to the conventional 5 million years of slow deposition of the Bright Angel Formation claimed to have occurred about 502–507 million years ago following almost equally slow deposition of the Tapeats Sandstone (Karlstrom et al. 2020). Yet, Karlstrom et al. (2018) admitted that the Sauk transgression represented by the Tonto Group "was one of the most dramatic global marine transgressions in Earth history." And even Rose (2003) admitted that these lower Paleozoic strata were deposited during higher rates of tectonism and accompanying inertial true polar wander (plate motion) which generated an historic high sea-level rise and abnormally high-frequency sea-level fluctuations. The fact that the Great Unconformity is well recognized and documented as a global stratigraphic surface (Peters and Gaines 2012), and in most regions across the globe separates Precambrian continental crystalline basement rocks from the overlying Cambrian Sauk megasequence shallow marine sedimentary deposits, including the Bright Angel Formation. Furthermore, it is totally consistent with initial catastrophic erosion of local underlying basement rocks and rapid, short-distance transport and deposition at the onset of the global Genesis Flood cataclysm, which would have been accompanied by continuous intensive high-energy storms and surging tsunamis generated by earthquakes due to the hot waters erupting from the breaking up of the fountains of the great deep.

Furthermore, the westward transport of the detritus, depicted by Austin (1994) in fig. 50 as due to the deep back-flowing counter-current, has been confirmed by the documentation of continental-wide paleocurrent direction indicators by Brand, Wang, and Chadwick (2015), who have demonstrated this was a global phenomenon consistent with the

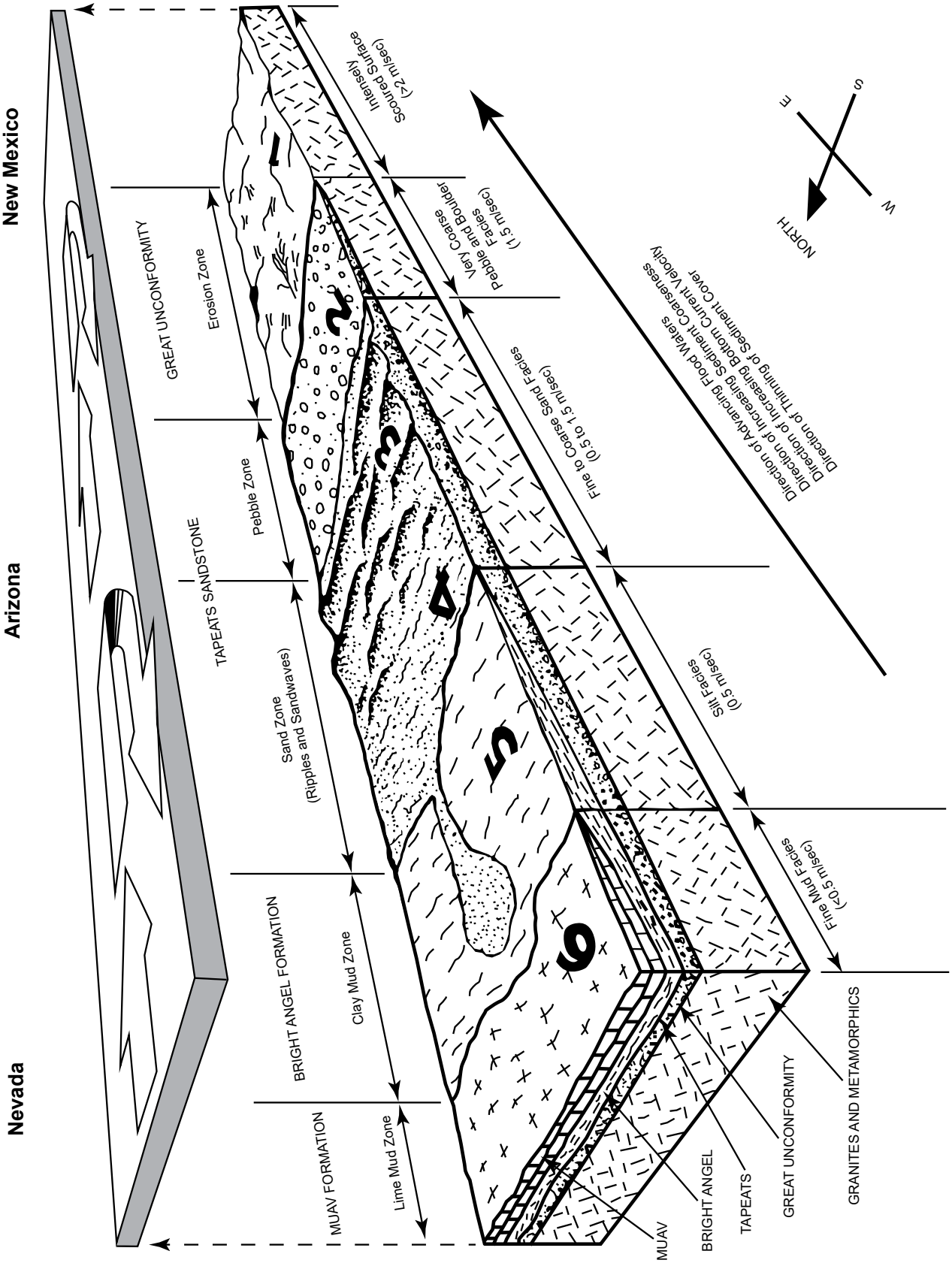
Nevada
Arizona
New Mexico
GREAT UNCONFORMITY
Erosion Zone
TAPEATS SANDSTONE
Pebble Zone
Sand Zone
(Ripples and Sandwaves)
BRIGHT ANGEL FORMATION
Clay Mud Zone
MUAV FORMATION
Lime Mud Zone
Intensely Scoured Surface
(>2 m/sec)
Very Coarse Pebble and Boulder Facies
(1.5 m/sec)
Fine to Coarse Sand Facies
(0.5 to 1.5 m/sec)
Silt Facies
(0.5 m/sec)
Fine Mud Facies
(<0.5 m/sec)
Direction of Advancing Flood Waters
Direction of Increasing Sediment Coarseness
Direction of Increasing Bottom Current Velocity
Direction of Thinning of Sediment Cover
NORTH
W
E
S
1
2
3
4
5
6
MUAV
BRIGHT ANGEL
TAPEATS
GREAT UNCONFORMITY
GRANITES AND METAMORPHICS

Fig. 50 (page 402). A model for the formation of the Tonto Group sedimentary deposits beneath advancing floodwaters across Nevada, Arizona, and New Mexico (after Austin 1994, 69. fig. 4.12). This likely occurred well after the onset of the Flood, as much of the Grand Canyon Supergroup had to first be planed off down to the crystalline basement granites and metamorphics. The water mass advancing eastward over Arizona has been "lifted" off the surface of the earth to reveal, underneath, the erosion and sedimentation that was occurring. The Flood model explains the erosion of the Great Unconformity, and subsequent deposition of the Tapeats Sandstone, Bright Angel Formation (fine-grained sandstone, siltstone and shale), and Muav Formation (limestone). The waters of the Flood advanced eastward through Nevada (lower left of diagram), finally reaching the more elevated area in Arizona and New Mexico (upper right of diagram). As the Flood advanced eastward, it produced horizontally segregated deposits (facies) and vertically stacked sediments (strata).
Zone 1 is the highest elevation area of the continent, where shallow, fast floodwaters are causing intense scouring and erosion of the pre-Flood rocks.
Zone 2 is the adjacent shallow-water area, where coarse pebbles and lag boulders are accumulating at the base of the Tapeats Sandstone. All the finer sand, silt, and mud are being winnowed from Zone 2, and moved westward into Zones 3 and 4 by the intense bottom-surging current (velocity about 1.5 m/sec).
Zone 3 is composed of sand waves forming thinly cross-bedded sands, which compose the middle section of the Tapeats Sandstone (the cliff-forming unit). Here, the water velocity is about 1.0 m/sec.
Zone 4 is plane beds of sand and some silt, with ripples representing the deepest and lowest-velocity waters depositing the uppermost Tapeats Sandstone (the "transitional" unit).
Zone 5 is located in still deeper and slower-moving waters. The silicate clay-, silt- and fine sand-sized particles are accumulating as graded fine sand, silt and clay beds. These deposits are the residue winnowed from Zones 1 through 4 and compose the Bright Angel Formation (principally shale and siltstone but with some fine-grained sandstone beds). Here, the water velocity is about 0.5 m/sec.
Zone 6 is farthest to the west, in the deepest and slowest-moving water, where there is a deficiency of silicate clay- and silt-sized particles. Lime mud, apparently the dominant type of pre-Flood sediment to the west, is accumulating in Zone 6 as rhythmically laminated and bedded flat strata, where the water current velocity is less than 0.5 m/sec. The continuous advance of the Flood over Arizona caused deeper-water, slower-velocity sediment facies to be stacked above the shallower-water, faster-velocity sediment facies. The result is the vertical sequence, consisting of the Great Unconformity, and the Tapeats Sandstone, Bright Angel Formation, and Muav Formation comprising most of the Tonto Group. Each has enormous horizontal extent, which can be measured in hundreds of kilometers.

direction of the global tidal movements in the global Flood cataclysm. Baumgardner (2013, 2018a, b) has made considerable progress with numerical simulations of the catastrophic erosion of bedrock via cavitation to produce the sediments that were rapidly deposited on the continental plates as shallow waters moved rapidly around the surface of the rotating globe. His modeling posits that the dominant means for sediment transport during the Flood was by rapidly-flowing turbulent water, and that water motion was driven by large-amplitude tsunamis that were generated along subduction zone segments as the subducting plate and overriding plate, in a cyclic manner, locked and then suddenly released and slipped rapidly past one another. His calculations show that with plausible parameter choices average erosion and sedimentation rates on the order of 9 m/day (0.38 m/hr) occurred with tsunami-driven pulses of turbulent water that transported the generated sediments vast distances across the continental plate surfaces, sufficient to deposit the Bright Angel Formation within 3–10 days, early during the initial 150-day rising and prevailing waters phase of the Flood (Genesis 7:18–24), and to thus account for the vast majority of the Phanerozoic sediments that blanket the earth's continental surfaces today.

Austin and Wise (1994) described in detail five robust criteria for defining the pre-Flood/Flood boundary and then applied them to the Grand Canyon region. They concluded that the Great Unconformity under the Tapeats Sandstone and occasionally under the locally underlying Sixtymile Formation in eastern Grand Canyon matched all five criteria. Thus, they included the Sixtymile Formation in the Sauk megasequence, which has recently been confirmed by Karlstrom et al (2018, 2020), who have proposed the formation be added to the base of the Tonto Group. Within the Sixtymile Formation, Wise and Snelling (2005) reported large megaclasts of the underlying Kwagunt Formation of the Chuar Group piled up at least three deep and separated by meter-thick pebble to boulder breccia layers, which were first recognized by Elston (1979) and subsequently documented by Karlstrom et al. (2018). Elston (1979) and Elston and McKee (1982) argued that these megaclasts were emplaced by sliding as the Sixtymile Formation was rapidly deposited as a result of more than 2 km of displacement of the adjacent Butte Fault in a sudden tectonic disturbance. Austin and Wise (1994) also correlated these megaclasts and breccias in the Sixtymile Formation with the gigantic breccia clasts, some more than a mile wide, in the Kingston Peak Formation in the eastern Mohave Desert of California, with the tectonic upheaval that marked the initiation of the Flood cataclysm (the breaking up of the fountains of the great deep).

They suggested those gigantic breccia clasts in the Kingston Peak Formation resulted from the collapse of the continental margin westward towards what was the pre-Flood ocean basin. Additionally, Austin (1994) had suggested the Chuar Group underlying the Sixtymile Formation was deposited in latest pre-Flood time, which was confirmed by the identification by Wise and Snelling (2005) of in situ grown stromatolites in an apparent reef structure in the Kwagunt Formation of the Chuar Group, an example of the pre-Flood hydrothermal biome proposed by Wise (2003).

This overall scenario and model for the tectonic upheaval at pre-Flood/Flood boundary and the initial catastrophic Flood deposition of the Tapeats Sandstone and the overlying Bright Angel Formation have also been summarized by Snelling (2009). However, critics have countered with the claimed evidences for slow-and-gradual deposition of the Bright Angel Formation in shallow marine to subtidal and intertidal environments as suggested by Baldwin et al. (2004), Elliott and Martin (1987b), Martin (1985), Martin, Elliott and Middleton (1986), Middleton and Elliott (2003), Rose, Middleton, and Elliott (1998), Rose (2003, 2006, 2011) and Wanless (1973a, 1975). In particular, Hill and Moshier (2009, 2016) have pointed to the marine invertebrate tracks and burrows found throughout much of the Bright Angel Formation, suggesting such delicate trace fossils require relatively gentle conditions for preservation.

However, as already explained above, both the sedimentary structures and fossil content within the Bright Angel Formation are entirely compatible with its catastrophically rapid deposition by hurricane-driven storm surges and very frequent tsunamis. Indeed, whereas Pemberton, MacEachern, and Frey (1992) argued that such trails would only be preserved below the minimum wave base, that is, in deeper water, Bromley and Asgaard (1991) warned that trace fossils could be preservational (where they are buried) rather than behavioral (where they lived). Likewise, the invertebrate fossils found in the Bright Angel Formation required rapid burial for their preservation before decay or scavenging in storm events, particularly where there have been larger numbers of trilobites buried together in restricted areas in what are termed lagerstätten (Brett and Seilacher 1991). This required burial below storm wave base, yet the presence of broken brachiopod shell fragments indicates how destructive the stormy conditions must have also been. And trace fossils are buried within coarse-grained units within the Bright Angel Formation that were deposited in high-energy stormy conditions. These considerations totally debunk the claim of Hill and Moshier (2009, 2016) that delicate trace fossils in the Bright Angel Formation required relatively gentle conditions for preservation. Rather, once the tracks and burrows have been made, they need to be buried rapidly to be preserved before any bioturbation or erosion occurs. Indeed, there are some bioturbated units within the Bright Angel Formation, yet trace fossils have still been preserved within them (Martin 1985), which indicates both the bioturbation and the burial of the traces had to be exceedingly rapid. And all this was happening on a global scale. Thus, the prevalence of these trace fossils in the Bright Angel Formation instead indicates that these invertebrate track and burrow makers were highly active as they tried to survive during the rapid deposition of the Bright Angel Formation soon after the beginning of the global Flood cataclysm, and not in the postulated slow-and-gradual, gentle conditions of the postulated uniformitarian sedimentary environments.

In fact, these trace fossils pose an insurmountable problem for these uniformitarians. Why are only the tracks and burrows made by these invertebrates preserved and fossilized in the Bright Angel Formation, and so few of the bodies of these invertebrates? Trilobite crawling (*Cruziana*) and resting (*Rusophycus*) traces occur throughout the Bright Angel Formation and yet the bodies of the trilobites that made the traces are only found buried and fossilized sparingly at a few locations at a few stratigraphic levels in the Bright Angel Formation, which conventionally was deposited over five million years (Karlstrom et al. 2020). But where are the fossilized remains of the other trail and burrow makers? If the delicate traces of these invertebrates could be fossilized in the high-energy depositional environment of rapid deposition of the Bright Angel Formation, then the bodies of these trace-makers should likewise have been buried and fossilized along with the tracks and traces they made. In fact, the fossilized bodies of most these trace-makers are not even found higher in the local stratigraphic record. The conventional millions of years "offset" between fossilized tracks and the body fossils of the trace-makers has been documented by Brand and Florence (1982) and Brand (1997) as a ubiquitous occurrence throughout the fossil record, among both invertebrates and vertebrates. It does not make any rational sense that over supposed millions of years the bodies of the trace-makers were not even sometimes buried with or near the tracks they made. Instead, this is evidence of rapid burial and preservation of the traces before very soon after (hours to days) the trace-makers were eaten or destroyed or rapidly buried and fossilized higher in the sequence in the ongoing rapid accumulation of the sedimentary strata during the global Flood cataclysm.

Hill and Moshier (2009, 2016) make mention of the fossilized ripple marks in the Bright Angel Formation and provide a photograph for comparison with ripple marks on a sandy sea bottom under about 20 ft (6 m) of water and formed by a current of about 0.5–1.0 mph (0.2–0.4 m/sec), thus again implying those fossilized in the Bright Angel Formation are incompatible with hurricane- and tsunami-driven, rapid sediment transport and deposition during the global Flood cataclysm. However, their photograph of the modern ripple marks is still clearly acknowledging that the Bright Angel Formation ripple marks were formed subaqueously. Furthermore, the ubiquitous small-scale cross-bedding within the storm beds of the Bright Angel Formation has resulted from subaqueous sand waves, even though Hill and Moshier (2009, 2016) do not specifically acknowledge that. Martin (1985) also mentions the megaripples and the ubiquitous cross-bedding in most sandstone beds throughout the Bright Angel Formation. Although much is unknown about the fine-scale structures associated with subaqueous sand waves, some observations have been made using radar and video. Thus, it has been found that small ripples are present on the backs of megaripples which occur on the backs of larger sand waves in Long Island Sound, near New York City (Poppe et al. 2006). Currents flowing over the tops of sand waves should produce lee vortices in much the same way as they are produced in eolian settings, so this could possibly produce subaqueous ripples, depending on current velocity. Houbolt (1968) suggested currents could flow perpendicular to the flanks of large sand ridges on steep foreset slopes.

Thus, none of these apparent objections counter the evidence. All such occurrences can be reconciled with the rapid transport of sand, silt and mud and their rapid deposition as the Bright Angel Formation very soon after the initiation of the global Flood cataclysm. The fact that the Bright Angel Formation was deposited virtually on top of the very source rocks its sediment grains were eroded from indicates a very short transport distance. And the ubiquitous presence of K-feldspar grains and former laths, as well as soft and fragile detrital muscovite flakes, throughout the thickness of the formation, is indicative of rapid transport and deposition. The sedimentary structures within the Bright Angel Formation, particularly the cross-bedding, and the erosion of the tops and bottoms of most of the successive storm bed sequences, are consistent with this rapid transport and deposition. The invertebrates likely caught up in the eroded sand left their traces on transient surfaces on the tops of beds immediately after their deposition as they tried to survive before eventually being overwhelmed. Some trilobites were rapidly buried. Robust simulations of the catastrophic erosion of the underlying basement rocks and rapid deposition of the Bright Angel Formation is consistent with this occurring within days of the global Flood cataclysm being initiated. Once deposited, silica and carbonates dissolved in the connate water trapped between the sediment grains subsequently precipitated to lithify the formation's sandstone, siltstone and shale layers as they dewatered under burial pressures towards the end of the Flood event year when the Flood waters drained off the emergent uplifted Colorado Plateau.

Summary and Conclusions

The Cambrian Bright Angel Formation is the 82–137 m (325–450 ft) thick slope-forming formation that recessively outcrops in the middle of the Tonto Group across ~500 km in the walls of Grand Canyon, Arizona, and beyond. It is usually an integral component of the fining upwards lithologies of the Cambrian Tonto Group, which has been touted conventionally as the classic example of the time-transgressive "deepening seas" sedimentation model. Originally described as the Bright Angel Shale, it has been recently designated to formation status due to it consisting of only ~40% green fissile and strongly laminated shales, with the majority made up of ~30% crumbly and laminated siltstones, and ~30% sandstone beds which are often hard and ledge-forming. The Bright Angel Formation immediately overlies a transitional boundary to the Tapeats Sandstone, which mostly sits directly on a pronounced erosion surface known as the Great Unconformity. The underlying rocks eroded at the Great Unconformity include granitic plutons intruded into the Granite Gorge Metamorphic Suite schists unconformably overlain by the tilted sedimentary strata and basalt layers of the Grand Canyon Supergroup, all dated as Precambrian. Both the correlated equivalents of the Bright Angel Formation and the Great Unconformity have been traced across several continents and around the globe, respectively.

Within the Bright Angel Formation well-preserved trilobites and some brachiopods are found in certain of the green fissile shales in some locations, and also a "hash" of unidentifiable fossil fragments are found concentrated locally elsewhere. In contrast, abundant trace fossils occur throughout the formation, primarily burrows and trails likely left by various worms and other invertebrates, and trails left by trilobites. These are often found on megaripples and the tops of sandstone beds but are ubiquitous within the silty and muddy inter-laminae areas at the interfaces between sandstone beds and laminated silty shales. Abundant cryptospores of land plants and algae are present in the shales in the basal section of the formation, but surprisingly no spores

of marine algae. Some ledge-forming sandstone beds are conglomeratic, while most are variously cross-laminated. The formation itself it well-bedded and the siltstones and shales strongly laminated. Detrital zircon grains extracted from the Tapeats Sandstone have been U-Pb dated to determine the maximum depositional age of the formation and coupled with biostratigraphic trilobite faunal zones correlated globally have constrained the conventional age of the Bright Angel Formation to 502–507Ma (early Middle Cambrian). Additionally, U-Pb dates obtained from detrital zircon grains extracted from the Bright Angel Formation potentially identify the provenance of its sediment grains. U-Pb age peaks among the detrital zircons matched the nearby Paleoproterozoic Yavapai and Mazatzal provinces, indicating the primary source of the sediment grains was the locally underlying granitic plutons and schists, plus a very small portion from the underlying Grand Canyon Supergroup strata (though a long-distance transport of some grains cannot be entirely ruled out). The consensus uniformitarian interpreted depositional environments for accumulation of the Bright Angel Formation are intertidal to subtidal shallow-marine environments, yet it has been described as part of "one of the most dramatic global marine transgressions in Earth history."

Quartz grains are the dominant component of the Bright Angel Formation, but bulk rock XRD analyses of the 12 samples studied demonstrated that K-feldspar features prominently, ranging from 11.0% to 46.9%. Various carbonates are present up to 32.4% and illite is ubiquitous, indicative of glauconite and muscovite. In thin sections, the sandstones are fine-grained and generally massive and well-sorted, dominated by angular to sub-rounded, coarse silt to fine sand-sized quartz grains. Many variously small-sized K-feldspar grains are scattered through the rock fabric, with occasional thin edge-on detrital muscovite flakes wedged between quartz and K-feldspar grains. Most samples contain small glauconite pellets and grains, and a few brachiopod shell fragments. There are virtually no original pores remaining, the rock fabric being cemented by silica as quartz overgrowths. The siltstones are very similar, but their grains are silt-sized and occasional patches are carbonate cemented. The shales consist of alternating thin illite (after K-feldspar) dominated laminae with scattered tiny quartz and K-feldspar grains and muscovite flakes, interstratified with thin laminae and "augen" of siltstone. There is no evidence, macroscopic or microscopic, of any metamorphic changes to the detrital mineral grains or textures.

These mineral constituents of the Bright Angel Formation are consistent with the underlying local basement rocks being the sediment provenance, as indicated by the detrital zircon U-Pb ages. The rare presence of siltstone and shale fragments within the sandstones underscores the conclusion that transport was over a short distance and likely rapid. Indeed, due to the very short-distance rapid transport of the sediment and rapid deposition of the sandstones, siltstones and shales, K-feldspar grains and former laths are scattered randomly through the entire formation and are often angular or sub-angular, while the extremely soft detrital muscovite flakes have survived, sometimes bent with frayed ends. The strongly cross-laminated sandstone beds, including occasional hummocky cross-stratification, and the laminated siltstones and shales are consistent with rapid deposition by high-energy storm-like surges, consistent with observational evidence of spontaneous stratification during rapid deposition of heterogranular sediment mixtures and of mud floccules. Numerous detrital zircon grains in the underlying Tapeats Sandstone yield U-Pb ages that are considerably younger than its designated depositional age. These coupled with the well-documented problems with the many assumptions undergirding the U-Pb dating method, and the evidence of past grossly accelerated nuclear decay rates, totally undermine the validity of the conventional age for the Bright Angel Formation. Instead, when combined, the mineralogical content, textural features, sedimentary structures, the continental-scale deposition, the invertebrate fossils and fragments, and even the tracks and traces of transitory invertebrates that had to be buried and fossilized rapidly, are all consistent with the catastrophic erosion of the Great Unconformity near the onset of the global Genesis Flood cataclysm about 4,350 years ago and the hurricane- and tsunami-driven rapid short-distance transport and deposition of the Bright Angel Formation within the fining upwards Sauk megasequence in the first few days or weeks of that year-long event.

Future Work

As indicated at the outset, the purpose of this study on the petrology of the Bright Angel Formation was to thoroughly describe this rock unit in preparation for detailed studies to determine the nature and timing of the folding of this unit in the Whitmore helipad fold in Grand Canyon. Future work will thus involve closer attention to comparing the petrography of the ten samples from the fold with the two samples distant from the fold, especially with respect to grain boundary relationships and textures, the frequency of remaining pores, the compaction of the sandstone, siltstone and shale, and the nature and timing of the cement between the detrital grains

that produced the lithification of those layers. This will require scanning electron microscope (SEM) imaging of selected samples to closely examine the cement crystals which would show evidence of brittle fracturing and healing if the folding occurred after lithification, but would be still pristine if cementation occurred after soft-sediment deformation and before lithification.

Acknowledgements

All samples were collected under the authority of National Park Service Scientific Research and Sampling Permit # GRCA-2017-SCI-0052 dated June 23, 2017, issued by Grand Canyon National Park's Research Office, and Permit #032767 issued by the Hualapai Department of Natural Resources dated July 27, 2017. The Alliance Defending Freedom (ADF) team led by then Senior Counsel Gary McCaleb is especially thanked for their legal work that led to a successful lawsuit against viewpoint discrimination in the permit application and granting process. Tom Vail, founder of Canyon Ministries who encouraged this research from its start, is also thanked for organizing with Terry Vallely, and assisted by their wives Paula and Kathy, respectively, the August 6–12, 2017, research raft trip down the Colorado River through Grand Canyon to collect the samples, facilitated by Grand Canyon National Park Special Use Permit #GRCA-3701 issued June 26, 2017. Special thanks go to Tom Vail and Dr. John H. Whitmore, Senior Professor of Geology at Cedarville University, Ohio for their invaluable field assistance, without which the samples would not have been collected, especially after I was injured early in the trip. Ray Strom of Calgary Rock and Materials Services, Inc. is thanked for the thin sections he prepared, and for the XRD analyses, as well as for the use of his research microscope for photography. Cedarville University is also thanked for use of their research microscope and Dr. John H. Whitmore for his advice, support, and encouragement. The helpful comments and edits from the kind reviewers were much appreciated. This research was fully funded by many generous donors to Answers in Genesis and has had the full support of the Answers in Genesis leadership team under Ken Ham. Our production assistant Laurel Hemmings is also thanked for her work in preparing this paper for publication. Nevertheless, I take full the responsibility for the content of this paper.

References

Alpert, Stephen P. 1974. "Systematic Review of the Genus *Skolithos*". *Journal of Paleontology* 48, no. 4 (July 1): 661–669.

Amorosi, Alessandro. 1997. "Detecting Compositional, Spatial, and Temporal Attributes of Glaucony: A Tool for Provenance Research." *Sedimentary Geology* 109, nos. 1–2 (March): 135–153.

Anderson, Calvin J., Matthew S. Cheney, Alex Struble, and John H. Whitmore. 2013. "Muscovite Survival in Simulated (Turbulent) Eolian and Subaqueous Conditions." *Journal of Creation Theology and Science Series C: Earth Sciences* 3: 1.

Anderson, Calvin J., Alex Struble, and John H. Whitmore. 2017. "Abrasion Resistance of Muscovite in Aeolian and Subaqueous Transport Experiments." *Aeolian Research* 24 (February): 33–37.

Arnott, R. William, and John B. Southard. 1990. "Exploratory Flow-Duct Experiments on Combined-Flow Bed configurations, and Some Implications for Interpreting Storm-Event Stratification." *Journal of Sedimentary Petrology* 60, no. 2 (March): 211–219.

Austin, Steven A. 1986. "Mount St. Helens and Catastrophism." In *Proceedings of the Third International Conference on Creationism*. Edited by Robert E. Walsh, Christopher L. Brooks, and Richard S. Crowell, Vol. 1, 3–10. Pittsburgh, Pennsylvania: Creation Science Fellowship.

Austin, Steven A., Editor. 1994. *Grand Canyon: Monument to Catastrophe*. Santee, California: Institute for Creation Research.

Austin, Steven A., and Kurt P. Wise. 1994. "The Pre-Flood/Flood Boundary: As Defined in Grand Canyon and East Mojave Desert, California." In *Proceedings of the Third International Conference on Creationism*. Edited by Robert E. Walsh, 37–47. Pittsburgh, Pennsylvania: Creation Science Fellowship.

Austin, Steven A., John R. Baumgardner, D. Russell Humphreys, Andrew A. Snelling, Larry Vardiman, and Kurt P. Wise. 1994. "Catastrophic Plate Tectonics: A Global Flood Model of Earth History." In *Proceedings of the Third international Conference on Creationism*. Edited by Robert E. Walsh, 609–621. Pittsburgh, Pennsylvania: Creation Science Fellowship.

Austin, Steven A. 2009. "The Dynamic Landscape on the North Flank of Mount St. Helens." In *Volcanoes to Vineyards: Geologic Field Trips through the Dynamic Landscape of the Pacific Northwest*. Edited by Jim E. O'Connor, Rebecca J., Dorsey, and Ian P. Madin, 337–344. Boulder, Colorado: Geological Society of America, *Field Guide 15*.

Baldwin, Christopher T. 1977. "Internal Structures of Trilobite Trace Fossils Indicative of an Open Surface Furrow Origin." *Palaeogeography, Palaeoclimatology, Palaeoecology* 21, no. 4 (May): 273–284.

Baldwin, Christopher T., Paul K. Strother, John H. Beck, and Eben Rose. 2004. "Paleoecology of the Bright Angel Shale in the Eastern Grand Canyon, Arizona, USA, Incorporating Sedimentological, Ichnological and Palynological Data." In *The Application of Ichnology to Paleoenvironmental and Stratigraphic Analysis*. Edited by Duncan McIlroy, 213–236. London, United Kingdom: The Geological Society of London, *Special Publication 228*.

Basu, Abhijit. 1981 "Weathering before the Advent of Land Plants: Evidence from Unaltered Detrital K-Feldspars in Cambrian-Ordovician Arenites." *Geology* 9, no. 3 (March 1): 132–133.

Baumgardner, John R. 2003. "Catastrophic Plate Tectonics: The Physics Behind the Genesis Flood." In *Proceedings of the Fifth International Conference on Creationism*. Edited by Robert L. Ivey, Jr., 113–126. Pittsburgh, Pennsylvania: Creation Science Fellowship.

Baumgardner, John R. 2013. "Explaining the Continental Fossil-Bearing Sediment Record in Terms of the Genesis Flood: Insights from Numerical Modeling of Erosion, Sediment Transport, and Deposition Processes on a Global Scale." In *Proceedings of the Seventh International Conference on Creationism*. Edited by Mark Horstemeyer. Pittsburgh, Pennsylvania: Creation Science Fellowship

Baumgardner, John R. 2018a. "Numerical Modeling of the Large-Scale Erosion, Sediment Transport, and Deposition Processes of the Genesis Flood." *Answers Research Journal* 11 (June 27): 149–170. https://answersresearchjournal.org/numerical-modeling-genesis-flood-2/.

Baumgardner, John R. 2018b. "Understanding How the Flood Sediment Record was Formed: The Role of Large Tsunamis." In *Proceedings of the Eighth International Conference on Creationism*. Edited by John H. Whitmore, 287–305. Pittsburgh, Pennsylvania: Creation Science Fellowship.

Berthault, Guy. 1988. "Experiments on Lamination of Sediments." *Ex Nihilo Technical Journal* 3, no. 1 (April): 25–29.

Berthault, Guy. 1990. "Sedimentation of a Heterogranular Mixture: Experimental Lamination in Still and Running Water." *Ex Nihilo Technical Journal* 4, no. 1 (April): 95–102.

Blakey, Ronald C., and Larry T. Middleton. 2012. "Geologic History and Paleogeography of Paleozoic and Early Mesozoic Sedimentary Rocks, Eastern Grand Canyon, Arizona." In *Grand Canyon Geology: Two Billion Years of Earth's History*. Edited by J. Michael Timmons and Karl E. Karlstrom, 81–92. Boulder, Colorado: Geological Society of America, *Special Paper 489*.

Boggs, Samuel, Jr. 1995. *Principles of Sedimentology and Stratigraphy*. 2nd ed., 79-107. Upper Saddle River, New Jersey: Prentice-Hall.

Borsch, K., John H. Whitmore, Raymond Strom, and George Hartree. 2018. "The Significance of Micas in Ancient Cross-Bedded Sandstones." In *Proceedings of the Eighth International Conference on Creationism*. Edited by John H. Whitmore, 306–326. Pittsburgh, Pennsylvania: Creation Science Fellowship.

Brand, Leonard R., and James Florence. 1982. "Stratigraphic Distribution of Vertebrate Fossil Footprints Compared with Body Fossils." *Origins* 9, no. 2 (June 1): 67–74.

Brand, Leonard R. 1997. *Faith, Reason and Earth History*. Berrien Springs, Michigan: Andrews University Press.

Brand, Leonard R, Mingmin Wang, and Arthur V. Chadwick. 2015. "Global Database of Paleocurrent Trends Through the Phanerozoic and Precambrian." *Scientific Data* 2 (9 June): 150025; doi:10.1038/sdata.2015.25.

Brett, Carlton E., and Adolf Seilacher. 1991. "Fossil Lagerstätten: A Taphonomic Consequence of Event Sedimentation." In *Cycles and Events in Stratigraphy*. Edited by Gerhard Einsele, Werner Ricken, and Adolf Seilacher, 283–297. Berlin, Germany: Springer-Verlag.

Bromley, Richard G. 1990. *Trace Fossils: Biology and Taphonomy*. Special Topics in Palaeontology, vol. 3. London, United Kingdom: Unwin.

Bromley, Richard G., and Ulla Asgaard. 1991. "Ichnofacies: A Mixture of Taphofacies and Biofacies." *Lethaia* 24, no. 2 (April): 153–163.

Byers, Charles W. 1974. "Shale Fissility: Relation to Bioturbation." *Sedimentology* 21: 479-482.

Chadwick, Arthur V., and Elaine G. Kennedy. 1998. "Depositional Environment of the Tapeats Sandstone in the Region of Grand Canyon, Arizona, USA." In *15th International Sedimentological Congress* 15: 247–248. Ghent, Belgium: International Association of Sedimentologists.

Chandler, Francis W. 1988. "Quartz Arenites: Review and Interpretation." *Sedimentary Geology* 58, nos. 2–4: 105–126.

Clarey, Timothy L., and Davis J. Werner. 2018. "Global Stratigraphy and the Fossil Record Validate a Flood Origin for the Geologic Column." In *Proceedings of the Eighth International Conference on Creationism*. Edited by John H. Whitmore, 327–350. Pittsburgh, Pennsylvania: Creation Science Fellowship.

Crimes, Thomas P. 1970. "The Significance of Trace Fossils in Sedimentology, Stratigraphy, and Paleoecology with Examples from Lower Paleozoic Strata." In *Trace Fossils*. Edited by Thomas P. Crimes, and J.C. Harper, 101–126. London, United Kingdom: Geological Society of London, *Geological Journal Special Issue 3*.

Crimes, Thomas P. 1975. "The Production and Preservation of Trilobite Resting and Furrowing Traces." *Lethaia* 8, no. 1 (October): 35–48.

DeCelles, Peter G., and William Cavazza. 1992. "Constraints on the Formation of Pliocene Hummocky Cross-Stratification in Calabria (southern Italy) from Consideration of Hydraulic and Dispersive Equivalence, Grain-Flow Theory, and Suspended-Load Fallout Rate." *Journal of Sedimentary Petrology* 62, no. 4 (July 1): 555–568.

Dehler, Carol M., George E. Gehrels, Susannah M. Porter, Matt Heizler, Karl E. Karlstrom, Grant Cox, Laura J. Crossey, and J. Michael Timmons. 2017. "Synthesis of the 780–740Ma Chuar, Uinta Mountain, and Pahrump (ChUMP) Groups, Western USA: Implications for Laurentia-wide Cratonic Marine Basins." *Geological Society of America Bulletin* 129, nos. 5–6 (May 1): 607–624.

Dott, Robert H. 1964. "Wacke, Graywacke and Matrix—What Approach to Immature Sandstone Classification?" *Journal of Sedimentary Petrology* 34, no. 3 (September 1): 625–632.

Dott, Robert H. Jr., and Joanne Bourgeois. 1982. "Hummocky Stratification: Significance of its Variable Bedding Sequences." *Geological Society of America Bulletin* 93, no. 8 (August): 663–680.

Dott, Robert H. Jr. 2003. "The Importance of Eolian Abrasion in Supermature Quartz Sandstones and the Paradox of Weathering on Vegetation-Free Landscapes." *The Journal of Geology* 111, no. 4 (July): 387–405.

Droser, Mary L., and David J. Bottjer. 1986. "A Semiquantitative Field Classification of Ichnofabrics." *Journal of Sedimentary Petrology* 56, no. 4 (July 1): 558–559.

Duke, William L. 1985. "Hummocky Cross-Stratification, Tropical Hurricanes, and Intense Winter Storms." *Sedimentology* 32, no. 2 (April): 167–194.

Duke, William L., R. William C. Arnott, and Richard J. Cheel. 1991. "Shelf Sandstones and Hummocky Cross-Stratification: New Insights on a Stormy Debate." *Geology* 19, no. 6 (June 1): 625–628.

Elliott, David K., and Daryl L. Martin. 1987a. "*Chancelloria*, an Enigmatic Fossil from the Bright Angel Shale (Cambrian) of Grand Canyon, Arizona." *Journal of the Arizona-Nevada Academy of Science* 21, no. 2: 67–72.

Elliott, David K., and Daryl L. Martin. 1987b. "A New Trace Fossil from the Bright Angel Shale (Cambrian) of Grand Canyon." *Journal of Paleontology* 61, no. 4 (July): 641–648.

Elston, Donald P. 1979. *Late Precambrian Sixtymile Formation and Orogeny at Top of the Grand Canyono Supergroup, Northern Arizona*. Washington, D.C.: U.S. Geological Survey, *Professional Paper 1092*.

Elston, Donald P., and Edwin H. McKee. 1982. "Age and Correlation of the Late Proterozoic Grand Canyon Disturbance, Northern Arizona." *Geological Society of America Bulletin* 93, no. 8 (August): 681–699.

Elston, Donald P. 1989. "Correlations and Facies Changes in Lower and Middle Cambrian Tonto Group, Grand Canyon, Arizona." In *Geology of Grand Canyon, Northern Arizona (with Colorado River Guides)*. Edited by Donald P. Elston, George H. Billingsley, and Richard A. Young, 131–136. Washington, DC: American Geophysical Union.

Fineberg, Jay. 1997. "From Cinderella's Dilemma to Rock Slides." *Nature* 386, no. 6623 (27 March): 323–324.

Folk, Robert Louis. 1955. "Student Operator Error in Determination of Roundness, Sphericity, and Grain Size." *Journal of Sedimentary Petrology* 25, no. 4 (December 1): 297–301.

Folk, Robert L. 1966. "A Review of Grain-Size Parameters." *Sedimentology* 6, no. 2 (March): 73–93.

Folk, Robert L. 1968. *Petrology of Sedimentary Rocks*. Austin, Texas: Hemphill Publishing Co.

Folk, Robert L. 1978. "Angularity and Silica Coatings of Simpson Desert Sand Grains, Northern Territory, Australia." *Journal of Sedimentary Petrology* 48, no. 2 (June 1): 611–624.

Folk, Robert L. 1980. *Petrology of Sedimentary Rocks*. 2nd ed. Austin, Texas: Hemphill Publishing Co.

Foster, John R. 2009. "Taphonomic Characteristics of a Quarry in the Bright Angel Shale (Middle Cambrian), Grand Canyon National Park, Arizona: A Preliminary Look." In *Rocky Mountains and the Colorado Plateau: Canyons, Resources and Hazards*. Edited by Edward Baltzer, 77–80. Westminster, Colorado: American Institute of Professional Geologists.

Foster, John R. 2011. "Trilobites and Other Fauna from Two Quarries in the Bright Angel Shale (Middle Cambrian, Series 3, Delamaran), Grand Canyon National Park, Arizona." In *Cambrian Stratigraphy and Paleontology of Northern Arizona and Southern Nevada, The 16th Field Conference of the Cambrian Stage Subdivision Working Group, International Subcommission on Cambrian Stratigraphy*. Edited by J. Stewart Hollingsworth, Frederick A. Sundberg, and John R. Foster, 99–120. Flagstaff, Arizona: Museum of Northern Arizona, *Bulletin 67*.

Frey, Robert W. 1970. "The Lebensspuren of Some Common Marine Invertebrates near Beaufort, North Carolina, II. Anemone Burrows." *Journal of Paleontology* 44, no. 2 (March): 308–311.

Garzanti, Eduardo, Sergio Andò, Giovanni Vezzoli, Michele Lustrino, Maria Boni, and Pieter Vermeesch. 2012. "Petrology of the Namib Sand Sea: Long-Distance Transport and Compositional Variability in the Wind-Displaced Orange Delta." *Earth-Science Reviews* 112, nos. 3–4 (May): 173–189.

Garzanti, Eduardo, Alberto Resentini, Sergio Andò, Giovanni Vezzoli, Alcides Pereira, and Pieter Vermeesch. 2015. "Physical Controls on Sand Composition and Relative Durability of Detrital Minerals during Ultra-Long Distance Littoral and Aeolian Transport (Namibia and Southern Angola)." *Sedimentology* 62, no. 4 (June): 971–996.

Garzanti, Eduardo. 2017. "The Maturity Myth in Sedimentology and Provenance Analysis." *Journal of Sedimentary Research* 87, no. 4 (April): 353–365.

Gehrels, George E., Ronald C. Blakey, Karl E. Karlstrom, J. Michael Timmons, William Dickinson, and Mark Pecha. 2011. "Detrital Zircon U-Pb Geochronology of Paleozoic Strata in the Grand Canyon, Arizona." *Lithosphere* 3, no. 3 (June 1): 183–200.

Gilbert, George K. 1874. "On the Age of the Tonto Sandstone." *Philosophical Society of Washington Bulletin* 1: 109.

Gilbert, George K. 1875. "Report Upon the Geology of Portions of Nevada, Utah, California, and Arizona." *U.S. Geographic and Geologic Surveys West of the 100th Meridian*, Vol. 3, pt. 1, 17–187.

Gilmore, Charles W. 1928. "Fossil Footprints from the Grand Canyon: Third Contribution." *Smithsonian Miscellaneous Collections* 80, no. 8: 1–16.

Goudie, Andrew S., and A. Watson. 1981. "The Shape of Desert Sand Dune Grains." *Journal of Arid Environments* 4, no. 3 (September): 185–190.

Hagadorn, James W., Joseph L. Kirschvink, Timothy D. Raub, and Eben C. Rose. 2011. "Above the Great Unconformity: A Fresh Look at the Tapeats Sandstone, Arizona-Nevada, U.S.A." In *Cambrian Stratigraphy and Paleontology of Northern Arizona and Southern Nevada, The 16th Field Conference of the Cambrian Stage Subdivision Working Group, International Subcommission on Cambrian Stratigraphy*. Edited by J. Stewart Hollingsworth, Frederick A. Sundberg, and John R. Foster, 63–76. Flagstaff, Arizona: Museum of Northern Arizona, *Bulletin 67*.

Hallam, Anthony. 1981. *Facies Interpretation and the Stratigraphic Record*. Oxford, United Kingdom: W. H. Freeman and Company.

Harms, John C., John B. Southard, D. R. Spearing, and Roger G. Walker. 1975. "Depositional Environments as Interpreted from Primary Sedimentary Structures and Stratification Sequences." *Society of Economic Paleontologists and Mineralogists, Short Course 2*. Broken Arrow, Oklahoma: SEPM, the Society for Sedimentary Geology.

Hayes, John B. 1970. "Polytypism in Chlorite in Sedimentary Rocks." *Clays and Clay Minerals* 18, no. 5 (October): 285–306.

Hayes, Philip T., and George C. Cone. 1975. "Cambrian and Ordovician Rocks of Southern Arizona and New Mexico and Westernmost Texas." *US Geological Survey Professional Paper* 873.

Hereford, Richard. 1975. "Chino Valley Formation (Cambrian?) in Northwestern Arizona." *Geological Society of America Bulletin* 86: 677–682.

Hereford, Richard. 1977. "Deposition of the Tapeats Sandstone (Cambrian) in Central Arizona." *Geological Society of America Bulletin* 88: 199–211.

Hill, Carol A., and Stephen O. Moshier. 2009. "Flood Geology and the Grand Canyon: A Critique." *Perspectives in Science and Christian Faith* 61, no. 2 (June): 99–115.

Hill, Carol A. and Stephen O. Moshier. 2016. "Sedimentary Structures: Clues from the Scene of the Crime." In *The Grand Canyon, Monument to an Ancient Earth: Can Noah's Flood Explain the Grand Canyon?* Edited by Carol A. Hill, Gregg Davidson, Tim Helble, and Wayne Ranney. Chapter 6, 66–71. Grand Rapids, Michigan: Kregel Publications.

Houbolt, Jacob J.H.C. 1968. "Recent Sediments in the Southern Bight of the North Sea." *Geologie en Mijnbouw* 47, no. 4: 245–273.

Hower, John. 1961. "Some Factors Concerning the Nature and Origin of Glauconite." *The American Mineralogist* 46 (March–April): 313–334.

Huntoon, Peter W. 1989. "Cambrian Stratigraphic Nomenclature, Grand Canyon, Arizona—Mappers Nightmare." In *Geology of Grand Canyon, Northern Arizona (with Colorado River Guides)*. Edited by Donald P. Elston, George H. Billingsley, and Richard A. Young, 128–129. Washington, D.C.: American Geophysical Union.

Huntoon, Peter W. 2003. "Post-Precambrian Tectonism in the Grand Canyon Region. In *Grand Canyon Geology*. 2nd ed. Edited by Stanley S. Beus and Michael Morales, 222–259. New York: Oxford University Press.

International Commission on Stratigraphy. 2021. *International Chronostratigraphic Chart* v.2021/07. https://stratigraphy.org/ICSchart/ChronostratChart2021-07.pdf.

Jade 2010. "Software for X-Ray Diffraction Analyses." JADE for XRD (materialsdata.com). Livermore, California: Materials Data, Inc.

Julien, Pierre Y., Yongqiang Lan, and Guy Berthault. 1994. "Experiments on Stratification of Heterogeneous Sand Mixtures." *Creation Ex Nihilo Technical Journal* 8, no. 1 (April): 37–50.

Julien, Pierre Y., Yongqiang Lan, and Y. Raslan. 1998. "Experimental Mechanics of Sand Stratification." *Creation Ex Nihilo Technical Journal* 12, no. 2 (August): 218–221.

Karlstrom, Karl E., Samuel A. Bowring, Carol M. Dehler, Andrew H. Knoll, Susannah M. Porter, David J. Des Marais, Arlo B. Weil, Zachary D. Sharp, John W. Geissman, Maya B. Elrick, J. Michael Timmons, Laura J. Crossey, and Kathleen L. Davidek. 2000. "Chuar Group of the Grand Canyon: Record of Breakup of Rodinia, Associated Change in the Global Carbon Cycle, and Ecosystem Expansion by 740 Ma." *Geology* 28, no. 7 (July 1): 619–622.

Karlstrom, Karl E., Bradley R. Ilg, Michael L. Williams, David P. Hawkins, Samuel A. Bowring, and S.J. Seaman. 2003. "Paleoproterozoic Rocks of the Granite Gorges" In *Grand Canyon Geology*. 2nd ed. Edited by Stanley S. Beus, and Michael Morales, 9–38. New York: Oxford University Press.

Karlstrom, Karl E., and J. Michael Timmons. 2012. "Faulting and Uplift in the Grand Canyon Region." In *Grand Canyon Geology: Two Billion Years of Earth's History*. Edited by J. Michael Timmons and Karl E. Karlstrom, 93–107. Boulder, Colorado: Geological Society of America, *Special Paper 489*.

Karlstrom, Karl E., James W. Hagadorn, George E. Gehrels, William Matthews, Mark D. Schmitz, Lauren Madronich, Jacob Mulder, Mark Pecha, Dominique Giesler, and Laura J. Crossey. 2018. "Cambrian Sauk Transgression in the Grand Canyon Region Redefined by Detrital Zircons." *Nature Geoscience* 11: 438–443.

Karlstrom, Karl E., Mike T. Mohr, Mark D. Schmitz, Frederick A. Sundberg, Stephen M. Rowland, Ronald C. Blakey, John R. Foster, Laura J. Crossey, Carol M. Dehler and James W. Hagadorn. 2020. "Redefining the Tonto Group of Grand Canyon and Recalibrating the Cambrian Time Scale." *Geology* 48: 425–430.

Keller, W.D. 1956. "Clay Minerals as Influenced by Environments of their Formation." *American Association of Petroleum Geologists Bulletin* 40, no. 11 (November): 2689–2710.

Kennedy, Elaine G. Ray Kablanow, and Arthur V. Chadwick. 1997. "Evidence for Deep Water Deposition of the Tapeats Sandstone, Grand Canyon, Arizona." In *Proceedings of the Third Biennial Conference of Research on the Colorado Plateau*. Edited by Charles van Riper, III, and Elana T. Deschler, 215–228. Washington, D.C.: U.S. Department of the Interior, National Park Service, Transactions and Proceedings Series NPS/NRNAU/NRTP-97/12.

Kirk, Edwin. 1945. *Eocrinus* (*E. multibrachiatus*). In Charles E. Resser, "Cambrian Fossils of the Grand Canyon: Part II. Cambrian History of the Grand Canyon Region." *Carnegie Institute of Washington Publication* 563, pp. 185–187. Washington, DC: Carnegie Institute of Washington.

Krynine, Paul D. 1946 "Microscopic Morphology of Quartz Types." *Annals of 2nd Pan-American Congress of Mining and Geological Engineers*, 35–49.

Kuenen, Philip H. 1960. "Experimental Abrasion 4: Eolian Action." *The Journal of Geology* 68, no. 4 (July): 427–449.

Landing, Ed, Gerd Geyer, Robert Buchwaldt, and Samuel A. Bowring. 2015. "Geochronology of the Cambrian: A Precise Middle Cambrian U-Pb Zircon Date for the German Margin of West Gondwana." *Geological Magazine* 152, no. 1 (January): 28–40.

Lane, A.A., S.J. Brady, Derek E.G. Briggs, and David K. Elliott. 2003. "A New Trace Fossil from the Middle Cambrian of the Grand Canyon, Arizona, USA." *Palaeontology* 46, no. 5 (September): 987–997.

Larson, Edwin E., Penny E. Patterson, and Felix E. Mutschler. 1994. "Lithology, Chemistry, Age and Origin of the Proterozoic Cardenas Basalt, Grand Canyon, Arizona." *Precambrian Research* 65, nos. 1–4 (January): 255–276.

Lochman-Balk, Christina. 1970. "Upper Cambrian Faunal Patterns on the Craton." *Geological Society of America Bulletin* 81, no. 11 (November 1): 3197–3224.

Lochman-Balk, Christina. 1971. "The Cambrian of the Craton of the United States." In *Cambrian of the New World*. Edited by C.H. Holland, 79–169. New York: John Wiley and Sons.

Macquaker, Joe H.S., and Kevin M. Bohacs. 2007. "On the Accumulation of Mud." *Science* 318, no. 5857 (14 December): 1734–1735.

Maithel, Sarah A., Paul A. Garner, and John H. Whitmore. 2015. "Preliminary Assessment of the Petrology of the Hopeman Sandstone (Permo-Triassic), Moray Firth Basin, Scotland." *Scottish Journal of Geology* 51, no. 2 (November): 177–184.

Marsland, Paul S., and John G. Woodruff. 1937. "A Study of the Effects of Wind Transportation on Grains of Several Minerals." *Journal of Sedimentary Petrology* 7, no. 1 (1 April): 18–30.

Martin, Daryl L. 1985. "Depositional Systems and Ichnology of the Bright Angel Shale (Cambrian), Eastern Grand Canyon, Arizona." M.S. Thesis (unpublished). Flagstaff, Arizona: Northern Arizona University.

Martin, Daryl L., Larry T. Middleton, and David K. Elliott. 1986. "Depositional Systems of the middle Cambrian Bright Angel Shale (Cambrian), Grand Canyon, Arizona." *Geological Society of America Abstracts with Programs* 18: 394.

Martinsson, A. 1970. "Toponomy of Trace Fossils." In *Trace Fossils*. Edited by Thomas P. Crimes, and J.C. Harper, 323–330. London, United Kingdom: Geological Society of London, *Geological Journal Special Issue 3*.

Makse, Hernan A., Shlomo Havlin, Peter R. King, and H. Eugene Stanley. 1997. "Spontaneous Stratification in Granular Mixtures." *Nature* 386, no. 6623 (October): 379–382.

Matthews, William, Bernard Guest, and Lauren Madronich. 2018. "Latest Neoproterozoic to Cambrian Detrital Zircon Facies of Western Laurentia." *Geosphere* 14, no. 1 (December 20): 243–264.

McBride, Earle F. 1963. "A Classification of Common Sandstones." *Journal of Sedimentary Petrology* 33, no. 3 (1 September): 664–669.

McBride, Earle F. 1985. "Diagenetic Processes That Affect Provenance Determinations in Sandstone." In *Provenance of Arenites*. Edited by Gian G. Zuffa, 97–113. Dordrecht, The Netherlands: D. Reidel Publishing Company.

McKee, Edwin D. 1932. "Some Fucoids from the Grand Canyon." *Grand Canyon Study Notes* 8: 58–161.

McKee, Edwin D. 1945. "Stratigraphy and Ecology of the Grand Canyon Cambrian: Part 1. Cambrian History of the Grand Canyon Region." *Carnegie Institute of Washington Publication* 563, 1–168. Washington, DC: Carnegie Institute of Washington.

McRae, Stuart G. 1972. "Glauconite." *Earth-Science Reviews* 8, no. 4 (December): 397–440.

Middleton, Larry T. 1989. "Cambrian and Ordovician Depositional Systems in Arizona." In *Geologic Evolution of Arizona*. Edited by J.P. Jenney, and S.J. Reynolds. *Arizona Geological Society Digest*. Vol. 17, 273–286.

Middleton, Larry T., and David K. Elliott. 2003. "Tonto Group." In *Grand Canyon Geology*. 2nd ed. Edited by Stanley S. Beus, and Michael Morales, 90–106. New York: Oxford University Press.

Moorhouse, Walter W. 1959. *The Study of Rocks in Thin Section*. New York: Harper & Row.

Morris, William Joseph. 1957. "Effects of Sphericity, Roundness, and Velocity on Traction Transportation of Sand Grains." *Journal of Sedimentary Petrology* 27, no. 1 (1 March): 27–31.

Moshier, Stephen O., Tim Helble, and Carol A. Hill. 2016. "Sedimentary Rock Types and How They Form." In *The Grand Canyon, Monument to an Ancient Earth: Can Noah's Flood Explain the Grand Canyon?* Edited by Carol A. Hill, Gregg Davidson, Tim Helble, and Wayne Ranney, chapter 5, 54–65. Grand Rapids, Michigan: Kregel Publications.

Newberry, John S. 1861. "Geological Report." In *Report Upon the Colorado River of the West*, explored in 1857-1858 by Lieut. J.C. Ives, pt. 3, 56. Washington, D.C.: Government Printing Office.

Noble, Levi F. 1914. "The Shinumo Quadrangle, Grand Canyon District, Arizona." *U.S. Geological Survey Bulletin* 549.

Noble, Levi .F. 1922. "A Section of the Paleozoic Formations of the Grand Canyon at the Bass Trail." *U.S. Geological Survey Professional Paper* 131-B: 23–73.

Nummedal, Dag. 1991. "Shallow Marine Storm Sedimentation—The Oceanographic Perspective." In *Cycles and Events in Stratigraphy*. Edited by Gerhard Einsele, Werner Ricken, and Adolf Seilacher, 227–248. Berlin, Germany: Springer-Verlag.

Odom, I. Edgar. 1975. "Feldspar-Grain Size Relations in Cambrian Arenites, Upper Mississippi Valley." *Journal of Sedimentary Petrology* 45, no. 3 (1 September): 636–650.

Odom, I. Edgar, Thomas W. Doe, and Robert H. Dott. 1976. "Nature of Feldspar-Grain Size Relations in Some Quartz-Rich Sandstones." *Journal of Sedimentary Petrology* 46, no. 4 (1 December): 862–870.

Pemberton, S. George, James A. MacEachern, and Robert W. Frey. 1992. "Trace Fossil Facies Models: Environmental and Allostratigraphic Significance." In *Facies Models: Response to Sea Level Change*. Edited by Roger G. Walker, and Noel P. James, 47–72. St. John's, Newfoundland, Canada: Geological Association of Canada.

Peng, Shanchi, Loren E. Babcock, and Roger A. Cooper. 2012. "The Cambrian Period." In *The Geologic Time Scale 2012*. Vol. 2. Edited by Felix M. Gradstein, James G. Ogg, Mark D. Schmitz, and Gabi M. Ogg, 437–488. Amsterdam, The Netherlands: Elsevier.

Peters, Shanan E., and Robert R. Gaines. 2012. "Formation of the 'Great Unconformity' as a Trigger for the Cambrian Explosion." *Nature* 484, no. 7394 (April 18): 363–366.

Pettijohn, Francis J. 1954. "Classification of Sandstones." *The Journal of Geology* 62, no. 4 (July): 360–365.

Pettijohn, Francis J. 1957. *Sedimentary Rocks*. New York: Harper.

Pettijohn, Francis J., Paul E. Potter, and Raymond Siever. 1973. *Sand and Sandstone*. Berlin, Germany: Springer.

Poppe, Larry J., Mary L. DiGiacomo-Cohen, Stephen M. Smith, Harold F. Stewart, and Nicholas A. Forfinski. 2006. "Seafloor Character and Sedimentary Processes in Eastern Long Island Sound and Western Block Island Sound." *Geo-Marine Letters* 26, no. 2 (June): 59–68.

Powell, John W. 1876. *Report on the Geology of the Eastern Portion of the Uinta Mountains and a Region of Country Adjacent Thereto*. Washington D.C.: U.S. Geologic and Geographic Survey of the Territories.

Powell, John W., 1891. *Grand Canyon of the Colorado*. New York: Flood and Vincent.

Powers, Maurice Cary. 1953. "A New Roundness Scale for Sedimentary Particles." *Journal of Sedimentary Petrology* 23. no. 2 (June 1): 117–119.

Prave, Anthony R., and William L. Duke. 1990. "Small-scale Hummocky Cross-Stratification in Turbidites: A Form of Antidune Stratification?" *Sedimentology* 37, no. 3 (June): 531–539.

Pye, Kenneth, and Haim Tsoar. 2009. *Aeolian Sand and Sand Dunes*. Berlin, Germany: Springer-Verlag.

Ramsay, John G. 1967. *Folding Fracturing of Rocks*. New York: McGraw-Hill.

Reineck, Hans-Erich, and Friedrich Wunderlich. 1968. "Classification and Origin of Flaser and Lenticular Bedding." *Sedimentology* 11, nos. 1–2 (October): 99–104.

Reineck, Hans E., and Indra B. Singh. 1972. " Genesis of Laminated Sand and Graded Rhythmites in Storms and Layers of Shelf Mud." *Sedimentology* 18: 123-128.

Resser, Charles E., 1945. "Cambrian Fossils of the Grand Canyon: Part II. Cambrian History of the Grand Canyon

Region." *Carnegie Institute of Washington Publication* 563, 168–232. Washington, DC: Carnegie Institute of Washington.

Rigby, J. Keith. 1976. "Some Observations on Occurrences of Cambrian *Porifera* in Western North America and Their Evolution." In *Paleontology and Depositional Environments: Cambrian of Western North America. Brigham-Young University Geological Studies* 23: 51–60. Edited by Richard A. Robison, and Albert J. Rowell.

Rooney, Alan D., Jacqueline Austermann, Emily F. Smith, Yang Li, David Selby, Carol M. Dehler, Mark D. Schmitz, Karl E. Karlstrom, and Francis A. Macdonald. 2018. "Coupled Re-Os and U-Pb Geochronology of the Tonian Chuar Group, Grand Canyon." *Geological Society of America Bulletin* 130, nos. 7–8 (1 July): 1085–1098.

Rose, Eben C., Larry T. Middleton, and David K. Elliott. 1998. "Storm- and Fair-Weather Controls of Deposition of the Middle Cambrian Bright Angel Shale, Grand Canyon, Arizona: Sedimentologic and Ichnologic Evidence." *Geological Society of America Abstracts with Programs* 30: 35.

Rose, Eben C. 2003. "Depositional Environment and History of the Cambrian Tonto Group, Grand Canyon, Arizona." M.S. Thesis (unpublished). Flagstaff, Arizona: Northern Arizona University.

Rose, Eben C. 2006. "Nonmarine Aspects of the Cambrian Tonto Group of the Grand Canyon, USA, and Broader Implications." *Palaeoworld* 15, nos. 3–4 (August–November): 223–241.

Rose, Eben C. 2011. "Proposed Modification of the Nomenclature and Revised Depositional Model for the Cambrian Tonto Group of the Grand Canyon, Arizona." In *Cambrian Stratigraphy and Paleontology of Northern Arizona and Southern Nevada, The 16th Field Conference of the Cambrian Stage Subdivision Working Group, International Subcommission on Cambrian Stratigraphy*. Edited by J. Stewart Hollingsworth, Frederick A. Sundberg, and John R. Foster, 77–98. Flagstaff, Arizona: Museum of Northern Arizona, *Bulletin 67*.

Rowley, Peter D., Mel A. Kuntz, and Norman S. MacLeod. 1981. "Pyroclastic-Flow Deposits." In *The 1980 Eruptions of Mount St. Helens*. Edited by Peter W. Lipman, and Donal R. Mullineaux, 489–512. Washington, D.C: U.S. Geological Survey, *Professional Paper 1250*.

Russell, R. Dana, and Ralph E. Taylor. 1937. "Roundness and Shape of Mississippi River Sands." *The Journal of Geology* 45, no. 3 (April–May): 225–267.

Schieber, Juergen, John B. Southard, and Kevin Thaisen. 2007. "Accretion of Mudstone Beds from Migrating Floccule Ripples." *Science* 318, no. 5857 (December 14): 1760–1763.

Schieber, Juergen, and John B. Southard. 2009. "Bedload Transport of Mud by Floccule Ripples—Direct Observation of Ripple Migration Processes and Their Implications." *Geology* 37, no. 6 (June): 483–486.

Schmitz, Mark D. 2012. "Radiometric Ages Used in GTS2012." In *The Geologic Time Scale 2012*. Vol. 2. Edited by Felix M. Gradstein, James G. Ogg, Mark D. Schmitz, and Gabi M. Ogg, 1045–1082. Amsterdam, The Netherlands: Elsevier.

Scholle, Peter A. 1979. *A Color Illustrated Guide to Constituents, Textures, Cements, and Porosities of Sandstones and Associated Rocks*. Tulsa, Oklahoma: The American Association of Petroleum Geologists, *Memoir 28*.

Schuchert, Charles. 1918. "The Cambrian of the Grand Canyon of Arizona." *American Journal of Science, 4th Series* 45: 362–369.

Seilacher, Adolf. 1955. "Spuren und Fazies im Unterkambrium." In *Beitrage zur Kenntnis des Kambriums in der Salt Range (Pakistan)*. Edited by Otto H. Schindewolf and Adolf Seilacher. *Akadamie der Wissenschaften Lit Mainz Math-Nat Kl, Abhandlungen* 103: 155–180.

Seilacher, Adolf. 1964. "Biogenic Sedimentary Structures." In *Approaches to Paleoecology*. Edited by John Imbrie and Norman D. Newell, 295–316. New York: John Wiley.

Seilacher, Adolf. 1967. "Bathymetry of Trace Fossils." *Marine Geology* 5, nos. 5–6 (October): 413–429.

Seilacher, Adolf. 1970. "*Cruziana* Stratigraphy of Non-Fossiliferous Paleozoic Sandstones." In *Trace Fossils*. Edited by Thomas P. Crimes, and J.C. Harper, 447–476. London, United Kingdom: Geological Society of London, *Geological Journal Special Issue 3*.

Seilacher, Adolf, and Thomas Aigner. 1991. "Storm Deposition at the Bed, Facies, and Basin Scale: The Geologic Perspective." In *Cycles and Events in Stratigraphy*. Edited by Gerhard Einsele, Werner Ricken, and Adolf Seilacher, 249–267. Berlin, Germany: Springer-Verlag.

Sharp, Robert P. 1940. "Ep-Archean and Ep-Algonkian Erosion Surfaces, Grand Canyon, Arizona." *Geological Society of America Bulletin* 51, no. 8 (August 1): 1235–1270.

Sloss, Laurence L. 1963. "Sequences in the Cratonic Interior of North America." *Geological Society of America Bulletin* 74, no. 2: 93–114.

Snelling, Andrew A. 2000. "Geochemical Processes in the Mantle and Crust." In *Radioisotopes and the Age of the Earth: A Young-Earth Creationist Research Initiative*. Edited by Larry Vardiman, Andrew A. Snelling, and Eugene F. Chaffin, 123–304. El Cajon, California: Institute for Creation Research, and St. Joseph, Missouri: Creation Research Society.

Snelling, Andrew A. 2005a. "Radiohalos in Granites: Evidence of Accelerated Nuclear Decay." In *Radioisotopes and the Age of the Earth: Results of a Young-Earth Creationist Research Initiative*. Edited by Larry Vardiman, Andrew A. Snelling, and Eugene F. Chaffin, pp.101–207. El Cajon, California: Institute for Creation Research, and Chino Valley, Arizona: Creation Research Society.

Snelling, Andrew A. 2005b. "Fission Tracks in Zircons: Evidence for Abundant Nuclear Decay." In *Radioisotopes and the Age of the Earth: Results of a Young-Earth Creationist Research Initiative*. Edited by Larry Vardiman, Andrew A. Snelling, and Eugene F. Chaffin, 209–324. El Cajon, California: Institute for Creation Research, and Chino Valley, Arizona: Creation Research Society.

Snelling, Andrew A. 2005c. "Isochron Discordances and the Role of Mixing and Inheritance of Radioisotopes in the Mantle and Crust." In *Radioisotopes and the Age of the Earth: Results of a Young-Earth Creationist Research Initiative*. Edited by Larry Vardiman, Andrew A. Snelling, and Eugene F. Chaffin, 393–524. El Cajon, California: Institute for Creation Research, and Chino Valley, Arizona: Creation Research Society.

Snelling, Andrew A. 2009. *Earth's Catastrophic Past: Geology Creation and the Flood*. Dallas, Texas: Institute for Creation Research.

Snelling, Andrew A. 2017a. "Determination of the Decay Constants and Half-Lives of Uranium-238 (^{238}U) and Uranium-235 (^{235}U), and the Implications for U-Pb and Pb-Pb Radioisotope Dating Methodologies." *Answers Research Journal* 10 (January 18): 1–38.

Snelling, Andrew A. 2017b. "Problems with the U-Pb Radioisotope Dating Methods—1. Common Pb." *Answers Research Journal* 10 (July 26): 121–167.

Snelling, Andrew A. 2018. "Problems with the U-Pb Radioisotope Dating Methods—2. U and Pb Mobility." *Answers Research Journal* 11 (June 13): 85–140.

Snelling, Andrew A. 2019. "Problems with the U-Pb Radioisotope Dating Methods—3. Mass Fractionation." *Answers Research Journal* 12 (November 13): 355–392.

Snelling, Andrew A. 2021. "The Petrology of the Tapeats Sandstone, Tonto Group, Grand Canyon, Arizona." *Answers Research Journal* 14 (June 13): 159–254.

Southard, John B., John M. Lambie, Dennis C. Federico, Harold T. Pile, and Christopher R. Weidman. 1990. "Experiments on Bed Configurations in Fine Sands Under Bidirectional Purely Oscillatory Flow, and the Origin of Hummocky Cross-Stratification." *Journal of Sedimentary Petrology* 60, no. 1 (1 January): 1–17.

Stewart, John H. 1972. "Initial Deposits in the Cordilleran Geosyncline: Evidence of a Late Precambrian (<850 m.y.) Continental Separation." *Geological Society of America Bulletin* 83, no. 5 (May 1): 1345–1360.

Stewart, John H., and Christopher A. Suczek. 1977. "Cambrian and Latest Precambrian Paleogeography and Tectonics in the Western United States." In *Paleozoic-Paleogeography of the Western United States*. Edited by John H. Stewart, Calvin H. Stevens, and A. Eugene Fritsche, 1–18. Society of Economic Paleontologists and Mineralogists, Pacific Section, *Paleogeography Symposium 1*.

Strother, Paul K., 2000. "Cryptospores: The Origin and Early Evolution of the Terrestrial Flora." In *Phanerozoic Terrestrial Ecosystems*. Edited by Robert A. Gastaldo and William A. DiMichele. *The Paleontological Society Papers* 6: 3–17.

Strother, Paul K., and John H. Beck. 2000. "Spore-like Microfossils from Middle Cambrian Strata: Expanding the Meaning of the Term Cryptospore." In *Pollen and Spores: Morphology and Biology*. Edited by Madeline M. Harley, Cynthia M. Morton, and Stephen Blackmore, 413–424. Kew, United Kingdom: Royal Botanic Gardens.

Strother, Paul K., Christopher T. Baldwin, John H. Beck, and Eben Rose. 2004a. "An Integrated Sedimentological, Ichnological and Palynological Study of the Paeloecology of the Middle Cambrian, Bright Angel Shale, Grand Canyon, Arizona." *Palynology* 28, no. 1: 265.

Strother, Paul K., Wilson A. Taylor, G.D. Wood, and John H. Beck. 2004b. "Middle Cambrian Cryptospores and the Origin of Land Plants." *Memoirs of the Association of Australasian Paleontologists* 29 (January): 99–113.

Sundberg, Frederick A. 1999. "Redescription of *Alokistocare subcoronatum* (Hall and Whitfield, 1877), the Type Species of *Alokistocare*, and the Status of Alokistocaridae Resser, 1939B (Ptychopariida: Trilobita, Middle Cambrian)." *Journal of Paleontology* 73, no. 6 (November): 1126–1143.

Sundberg, Frederick A. 2011. "Cambrian of Peach Springs Canyon, Hualapai Indian Reservation, Arizona." In *Cambrian Stratigraphy and Paleontology of Northern Arizona and Southern Nevada, The 16th Field Conference of the Cambrian Stage Subdivision Working Group, International Subcommission on Cambrian Stratigraphy*. Edited by J. Stewart Hollingsworth, Frederick A. Sundberg, and John R. Foster, 186–190. Flagstaff, Arizona: Museum of Northern Arizona, *Bulletin 67*.

Sundberg, Frederick A., Gerd Geyer, Peter D. Kruse, Linda B. McCollum, Tatyana V. Pegel, Anna Żylińska, and Andrey Y. Zhuravlev. 2016. "International Correlation of the Cambrian Series 2–3, Stages 4–5 Boundary Interval." *Australasian Palaeontological Memoirs* 49: 83–124.

Sundberg, Frederick A., Karl E. Karlstrom, Gerd Geyer, John R. Foster, James W. Hagadorn, M.T. Mohr, Mark D. Schmitz, Carol M. Dehler, and Laura J. Crossey. 2020. "Asynchronous Trilobite Extinctions at the Early to Middle Cambrian Transition." *Geology* 48, no. 5 (1 May): 441–445.

Swift, Donald J. P., Albert G. Figueiredo, Jr., G. L. Freeland, and George F. Oertel. 1983. "Hummocky Cross-Stratification and Megaripples: A Geological Double Standard?" *Journal of Sedimentary Petrology* 53, no. 4 (December 1): 1295–1317.

Swift, Donald J. P., and Julian A. Thorne. 1991. "Sedimentation on Continental Margins, I: A General Model for Shelf Sedimentation." In *Shelf Sand and Sandstone Bodies: Geometry, Facies, and Sequence Stratigraphy*. Edited by Donald J.P. Swift, George F. Oertel, Roderick W. Tillman, and Julian A. Thorne, *International Association of Sedimentologists, Special Publication Number 14*, 3-31. Oxford, United Kingdom: Blackwell Scientific Publications.

Tapp, Bryan, and Ken Wolgemuth. 2016. "Broken and Bent Rock: Fractures, Faults, and Folds". In *The Grand Canyon, Monument to an Ancient Earth; Can Noah's Flood Explain the Grand Canyon?*. Edited by Carol A. Hill, Gregg Davidson, Tim Helble, and Wayne Ranney, chapter 12, 116–127. Grand Rapids, Michigan: Kregel Publications.

Taylor, Wilson A., and Paul K. Strother. 2008. "Ultrastructure of Some Cambrian Palymorphs from the Bright Angel Shale, Arizona, USA." *Review of Palaeobotany and Palynology* 151, nos. 1–2 (July): 41–50.

Tessier, B. 1998. "Tidal Cycles: Annual Versus Semi-Lunar Records." In *Tidalites: Processes and Products*. Edited by Clark R. Alexander, Richard A. Davis, and Vernon J. Henry, 69–74. Tulsa, Oklahoma: Society of Economic Paleontologists and Mineralogists Society, *Special Publication No. 61*.

Thompson, Graham R., and John Hower. 1975. "The Mineralogy of Glauconite." *Clays and Clay Minerals* 23 (1 August): 289–300.

Thorne, Julian A., E. Grace, Donald J.P. Swift, and A Niedoroda. 1991. "Sedimentation on Continental Margins, III: The Depositional Fabric—An Analytical Approach to Stratification and Facies Identification." In *Shelf Sand and Sandstone Bodies: Geometry, Facies, and Sequence Stratigraphy*. Edited by Donald J.P. Swift, George F. Oertel, Roderick W. Tillman, and Julian A. Thorne, *International Association of Sedimentologists, Special Publication Number 14*, 59–87. Oxford, United Kingdom: Blackwell Scientific Publications.

Tucker, Maurice E., 1981. *Sedimentary Petrology: An Introduction*. Oxford, United Kingdom: Blackwell Scientific Publications.

Twenhofel, William Henry. 1945. "The Rounding of Sand Grains." *Journal of Sedimentary Petrology* 15, no. 2 (1 August): 59-71.

Udden, Johan August. 1914 "Mechanical Composition of Clastic Sediments." *Bulletin of the Geological Society of America* 25, no. 1 (January): 655–744.

Ulmer-Scholle, Dana S., Peter A. Scholle, Juergen Schieber, and Robert J. Raine. 2015. *A Color Guide to the Petrography of Sandstones, Siltstones, Shales and Associated Rocks*. Tulsa, Oklahoma: The American Association of Petroleum Geologists, *Memoir 109*.

Van Wagoner, John C., Henry W. Posamentier, R.M. Mitchum Jr., Peter R. Vail, J.F. Sarg, T.S. Loutit, and J. Hardenbol. 1988. "An Overview of the Fundamentals of Sequence Stratigraphy and Key Definitions." In *Sea Level Changes: An Integrated Approach*. Edited by Cheryl K. Wilgus, Bruce S. Hastings, Charles A, Ross, Henry W. Posamentier, John C. Van Wagoner, and Christopher G. St. C. Kendall, 39–45. Tulsa, Oklahoma: Society of Economic Paleontologists and Mineralogists, *Special Publication No. 42*.

Vannier, Jean, Ivan Calandra, Christian Gaillard, and Anna Żylińska. 2010. "Priapulid Worms: Pioneer Horizontal Burrowers at the Precambrian-Cambrian Boundary." *Geology* 38, no. 8 (August): 711–714.

Vardiman, Larry, Andrew A. Snelling, and Eugene F. Chaffin, Editors. 2005. *Radioisotopes and the Age of the Earth: Results of a Young-Earth Creationist Research Initiative*. El Cajon, California: Institute for Creation Research, and Chino Valley, Arizona: Creation Research Society.

Walcott, Charles D. 1880. "The Permian and Other Paleozoic Groups of the Kanab Valley, Arizona." *American Journal of Science, 3rd Series* 20: 221–225.

Walcott, Charles D. 1886. "Second Contribution to the Studies on the Cambrian Faunas of North America." *United States Geological Survey Bulletin* 30: 727–1095.

Walcott, Charles D. 1889. "Description of New Genera and Species of Fossils from the Middle Cambrian." *United States National Museum Proceedings* 11: 441–446.

Walcott, Charles D. 1890. "The Fauna of the Lower Cambrian or *Olenellus* Zone." *U.S. Geological Survey 10th Annual Report*, 509–760.

Walcott, Charles D. 1895. "Algonkian Rocks of the Grand Canyon of the Colorado." *The Journal of Geology* 3, no. 3: 312–330.

Walcott, Charles D. 1898. "Cambrian Brachiopods: *Obolus* and *Lingulella*, with Description of New Species." *Proceedings of the United States National Museum* 21: 385–420.

Walcott, Charles D. 1901. "Cambrian Brachiopods: *Obolella*, subgenus *Glyptias*: *Bicia*: *Obolus*, subgenus *Westonia*; with Descriptions of New Species." *Proceedings of the United States National Museum* 23: 669–695.

Walcott, Charles D. 1910. "Cambrian Geology and Paleontology II: Abrupt Appearance of the Cambrian Fauna on the North American Continent." *Smithsonian Miscellaneous Collections* 57, no. 6: 1–16.

Walcott, Charles D. 1916a. "Cambrian Geology and Paleontology III: No.3. Cambrian Trilobites." *Smithsonian Miscellaneous Collections* 64, no.3: 157-258.

Walcott, Charles D. 1916b. "Cambrian Geology and Paleontology III: No. 5. Cambrian Trilobites." *Smithsonian Miscellaneous Collections* 64, no. 5: 303–456.

Walcott, Charles D. 1918. "Cambrian Geology and Paleontology IV: Appendages of Trilobites." *Smithsonian Miscellaneous Collections* 67, no. 4: 115–216.

Walcott, Charles D. 1920. "Cambrian Geology and Paleontology IV: Middle Cambrian Spongiae." *Smithsonian Miscellaneous Collections* 67, no. 6: 261–364.

Walcott, Charles D. 1924. "Cambrian Geology and Paleontology V: No. 2. Cambrian and Lower Ozarkian Trilobites." *Smithsonian Miscellaneous Collections* 75, no. 2: 53–60.

Walcott, Charles D. 1925. "Cambrian Geology and Paleontology V: No. 3. Cambrian and Lower Ozarkian Trilobites." *Smithsonian Miscellaneous Collections* 75, no. 3: 61–146.

Walker, Roger G., and A. Guy Plint. 1992. "Wave- and Storm-Dominated Shallow Marine Systems." In *Facies Models: Response to Sea Level Change*. Edited by Roger G. Walker and Noel P. James, 219–238. St. John's, Newfoundland, Canada: Geological Association of Canada.

Wanless, Harold R., Jr. 1973a. "Cambrian of the Grand Canyon—A Reevaluation of the Depositional Environment." Ph.D. Thesis (unpublished). Baltimore, Maryland: Johns Hopkins University.

Wanless, Harold R., Jr. 1973b. "Cambrian of the Grand Canyon—A Reevaluation." *American Association of Petroleum Geologists Bulletin* 57, no. 4 (April 1): 810–811.

Wanless, Harold R., Jr. 1975. "Carbonate Tidal Flats of the Grand Canyon Cambrian." In *Tidal Flats—A Casebook of Recent Examples and Fossil Counterparts*. Edited by R.N. Ginsburg, 269–277. New York: Springer-Verlag.

Wanless, Harold R., Jr. 1981. "Environments and Dynamics of Clastic Sediment Dispersal across Cambrian of Grand Canyon." *American Association of Petroleum Geologists Bulletin* 65: 1004–1005.

Wentworth, Chester K. 1922. "A Scale of Grade and Class Terms for Clastic Sediments." *The Journal of Geology* 30, no. 5 (July–August): 377–392.

Wheeler, Russell B., and Albert R. Kerr. 1936. "Preliminary Report on the Tonto Group of the Grand Canyon, Arizona." *Grand Canyon Natural History Association Bulletin* 5: 1–16.

Whitmore, John H., Raymond Strom, Stephen Cheung, and Paul A. Garner. 2014. "The Petrology of the Coconino Sandstone (Permian), Arizona, USA." *Answers Research Journal* 7 (December 10): 499–532.

Whitmore, John H., 2017. "Rapid Rounding of K-feldspar Sand Grains from Beach to Dune Environments and its Significance for Ancient Sandstones." *Journal of Creation Theology and Science Series C: Earth Sciences* 7: 2–3.

Whitmore, John H., and Raymond Strom. 2017a. Rounding of K-feldspar and Quartz Sand Grains from Beach to Dune Environments: Implications for Ancient Sandstones. *Geological Society of America Abstracts with Programs* 49, no. 6: 295-5.

Whitmore, John H., and Raymond Strom. 2017b. "Rounding of Quartz and K-Feldspar Sand from Beach to Dune Settings Along the California and Oregon Coastlines: Implications for Ancient Sandstones." *Answers Research Journal* 10 (November 15): 259–270.

Whitmore, John H., and Paul A. Garner. 2018. "The Coconino Sandstone (Permian, Arizona, USA): Implications for the Origin of Ancient Cross-Bedded Sandstones." In *Proceedings of the Eighth international Conference on Creationism*. Edited by John H. Whitmore, 581–627. Pittsburgh, Pennsylvania: Creation Science Fellowship.

Whitmore, John H., and Raymond Strom. 2018. "The Significance of Angular K-Feldspar Grains in Ancient

Sandstones." In *Proceedings of the Eighth International Conference on Creationism*. Edited by John H. Whitmore, 628–651. Pittsburgh, Pennsylvania: Creation Science Fellowship.

Wiens, Roger. 2016. "So Just How Old is That Rock?" In *The Grand Canyon, Monument to an Ancient Earth; Can Noah's Flood Explain the Grand Canyon?*. Edited by Carol A. Hill, Gregg Davidson, Tim Helble, and Wayne Ranney, chapter 9, 88–97. Grand Rapids, Michigan: Kregel Publications.

Wise, Kurt P. 2003. "Hydrothermal Biome—A Pre-Flood Environment." In *Proceedings of the Fifth International Conference on Creationism*. Edited by Robert L. Ivey, Jr., 359–370. Pittsburgh, Pennsylvania: Creation Science Fellowship.

Wise, Kurt P., and Andrew A. Snelling. 2005. "A Note on the Pre-Flood/Flood Boundary in the Grand Canyon." *Origins* 58 (June 1): 7–29.

Young, David A., and Ralph F. Steearley. 2008. *The Bible, Rocks and Time*. Downers Grove, Illinois: InterVarsity Press.

Supplementary Material

Appendix A—Graphic Stratigraphic Log of the Tonto Group in the Unkar Creek Area (River Mile 73).

Appendix B—Graphic Stratigraphic Log of the Tonto Group in the Blacktail Canyon Area (River Mile 120.5).

Appendix C—Graphic Stratigraphic Log of the Tonto Group in the Diamond Creek Area (River Mile 226).

Appendix D—Locations and Petrographic Descriptions of Bright Angel Formation Samples.

Available in a single pdf file at https://assets.answersingenesis.org/doc/articles/arj/v14/bright-angel-formation-supplement.pdf.